

The
University
Of
Sheffield.

Acetals for adaptable and pH degradable
thermosets and the use of internal acid sources

Josh Hayles

A thesis submitted in partial fulfilment of the requirements for the degree of Doctor of
Philosophy

The University of Sheffield

Faculty of Science

Department of Chemistry

November 2022

Declaration

The work described in this thesis was undertaken at the University of Sheffield under the supervision of Prof. Patrick Fairclough and Dr Sebastian Spain between October 2018 and November 2022 and has not been submitted, either wholly or in part, for this or any other degree. All the work is original work of the author, except where acknowledged.

Signature: _____



Joshua Hayles

November 2022

Abstract

Thermosets are a class of polymers with excellent thermal and mechanical properties, which has prompted their use in a wide range of applications and industries. However, thermosets are inherently infusible and insoluble and consequently their recycling is challenging. To address this an acid cleavable, methacrylate cross-linker bearing two acetal groups was synthesised. and used as a cleavable cross-linker in thermosets. ^1H NMR spectroscopy showed the hydrolysis products were HEMA, tri(ethylene glycol) and acetaldehyde and the extent of hydrolysis increased with lower acid $\text{p}K_{\text{a}}$.

The cross-linker synthesis was then optimised and scaled up for consistency in future thermoset syntheses and mechanical testing, while also improving the sustainability of the process. Acetal-containing methyl methacrylate thermosets formed homogeneous solutions in acidic solvent/ H_2O mixtures. The degradation products were found to be p(methyl methacrylate-co-2-hydroxyethyl methacrylate), tri(ethylene glycol) and acetaldehyde, consistent with acetal hydrolysis. Comparison of the rate of acetaldehyde evolution and gravimetric loss of p(MMA-co-A1) showed the rate of degradation related to a complex pathway involving swelling, hydrolysis, and solvation of p(MMA-co-A1). These results showed that acetal cross-linkers may enable chemical recycling of thermosets.

Acid generators were then investigated as internal acid sources for catalysis of acetal hydrolysis and exchange reactions in covalently adaptable networks. Novel polymeric sulfonate thermal acid generators were synthesised and their thermolysis properties comprehensively characterised *via* thermogravimetric analysis and ^1H NMR spectroscopy. However, upon thermolysis they underwent a cross-linking reaction and consequently are unsuitable for use in degradable thermosets.

Lastly, the cross-linker was used in covalently adaptable networks and exhibited re-processable adhesive behaviour.

Acknowledgements

Finally, a chance to write FREELY, without the irritation of italicising *et al.*, and thank Whoever *et al.* got me here, starting with the makers. To Mum cheers for your patience at parents' evenings, funding early experiments with vinegar, bicarb and my air rifle and giving me a passion for learning new things, unlike previous exams I don't think we can drive home with roof down listening to Shaggy for my *viva*. To Dad, you've taught me to work hard at something you enjoy, question everything, argue that white is black and *vice versa* and most importantly to laugh while you do it. Bumper you've been an inspiration and the gunpowder formulation worked well. My sisters Chloe and Floss sources of irritation, fun and my wonderful nieces and nephews. My brother-in-law Lee who really is the brother I never had and a great role-model, yes this is an entire thing is about 'test-tubing'.

To Bishop and Zac who provided me with coat tails to cling on to throughout uni and who always left early to go to the AJ (£3.20 maaaaaan'). I literally wouldn't have done this without you, and I nearly didn't make it because of that Oven Door sandwich, big up. To Tim Milner who has been with me through thick and thin, you've been with me since the start and I struggle to think of my best memories that you're not a part of, please stop buying shoes without supervision. To Nath and Al who are also present in many of my fondest memories and have been crucial in PhD escapism and chronic hangovers. Brolly, you rock and on behalf of polymer chemists, I apologise for gluten. Huge shout out to the Manny lot, here's to playing out more!

To the lunchtime crew, my CDT cohort and post lab pint partakers in Sheffield, cheers for the laughs and welcome distractions. I feel Xander deserves a medal for my regular and impromptu enquiries about CANS. A special mention to the Spain Group members past and present, particularly Anna, Ellen, Marissa, and Sam who had to endure my patter in the lab, office, group meetings and pub, I can only apologise. To Tom, you were almost a role model,

but then I got to know you, yourself and Jonny are the best findings of my PhD. To everyone at Mimetics cheers for a great placement, despite my role becoming barista, excited to return.

Now for the grownups, to Carl thank you for taking a chance on me, illuminating the creativity and pleasure of research and passing on your enthusiasm, most importantly to read around your subject. To Sebwardo, I'll always think of you opening the Polymer Handbook in meetings, thanks for plugging rabbit holes, supporting my enthusiasm, and having a laugh, I've loved my time in your group. Patrick, you taught me an important lesson that a benzene ring is a nut to an engineer, although you did make me feel physically unwell when you mentioned Fourier transformation in a group meeting, cheers for the support. To Andrew Slark thank you for being approachable and providing some excellent discussions about both research and careers, particularly your honest advice about post-PhD employment. To Dean and Steven at Scott Bader, our meetings always fell in an enthusiasm trough, and I always left them re-enthused from your support, encouragement, and suggestions, thank you! To Paul cheers for showing me it really was time to write up, otherwise I'd probably still be in the lab now.

To Jemma the unsung hero of my PhD and the most caring person I know, a lot has changed in these four years. We've sat on the sofa, climbed a mountain, eaten a variety of beige food and sat on the sofa again. You've witnessed highs, supported lows, and admonished egomania and arrogance. Thanks for doing all those dark drives on Snakes Pass and you were the perfect lockdown companion. I love you, cheers for being there. **This is for you, apologies it is quite dull.**

Table of Contents

1. Chapter 1 - Introduction	1
1.1. Thermosets.....	1
1.1.1. Thermosets, their properties, and synthesis	1
1.1.2. Thermoset properties and application	2
1.1.3. Thermoset Recycling.....	3
1.2. Degradable Thermosets.....	4
1.2.1. Additives	5
1.2.1.1. Thermally expansive microparticles	5
1.2.1.2. Nanoparticle additives.....	7
1.2.2. Chemically Modified Thermosets.....	8
1.2.2.1. Lactone modification.....	8
1.2.2.2. Hindered ureas	9
1.2.2.3. Orthoesters.....	10
1.2.2.4. Hexahydrotriazines	12
1.2.2.5. Diketoenamines	12
1.2.2.6. Imines.....	13
1.3. Covalently Adaptable Networks	14
1.4. Acetals.....	16
1.4.1. Acetal stability	19
1.4.2. Acetals in Polymer Chemistry.....	20
1.5. Green chemistry & sustainable synthesis metrics	21
1.6. Acid Generators.....	24
1.7. Research Aims	29
2. Chapter 2 – Synthesis and Characterisation of Dimethacrylate Acetal Cross-Linker	30
2.1. Introduction.....	30

2.2.	Results and Discussion.....	35
2.2.1.	Synthesis of Acetal Cross Linker & Hydrolysis Experiments.....	35
2.2.1.1.	Synthesis of Acetal Bearing Dimethacrylate Cross-Linker A1.....	35
2.2.1.2.	Hydrolysis of A1	36
2.2.1.3.	Effect of pK_a on Hydrolytic Stability.....	37
2.2.2.	Optimisation and Scale Up of A1 Synthesis	40
2.2.2.1.	Acid Species and Concentration	41
2.2.2.2.	Oligomerisation Side Reactions.....	43
2.2.2.2.1.	pTsOH Catalysed Polymerisation of TEGDVE	46
2.2.2.2.2.	pTsOH Catalysed Copolymerisation of TEGDVE and TEG	48
2.2.2.1.	Effect of TEGDVE Feed Rate on Reaction Kinetics.....	49
2.2.2.2.	Choosing a Solvent	50
2.2.2.3.	Optimisation of reaction work up conditions	52
2.2.2.4.	Scale Up of A1 Synthesis.....	54
2.2.2.5.	Sustainability comparison of start and final protocols of Scaled Up A1 Synthesis	54
2.3.	Conclusions	55
2.4.	Experimental.....	56
2.4.1.	Materials	56
2.4.2.	Instrumentation	56
2.4.3.	Initial Synthesis of A1	57
2.4.4.	Hydrolysis of A1	58
2.4.5.	Effect of acid on scale up	58

2.4.6.	Anhydrous Synthesis of A1	59
2.4.7.	Control Polymerisation of TEGDVE	60
2.4.8.	Control Polymerisation of TEGDVE and TEG	61
2.4.9.	Effect of Addition Rate	63
2.4.10.	Effect of Solvent on Synthesis of A1	63
2.4.11.	Effect of work up	63
2.4.12.	Synthetic scale up	64
2.4.13.	Green Metric Calculations	64
3.	Chapter 3 – Synthesis and Degradation of Acetal Containing Methacrylate Thermosets	67
3.1.	Introduction	67
3.2.	Results and Discussion	74
3.2.1.	Degradable A1 and methyl methacrylate thermosets	74
3.2.1.1.	Synthesis and Thermal Characterisation of p(MMA-co-A1)	74
3.2.1.2.	Effect of Post Curing on glass transition temperature	77
3.2.1.3.	Acid Degradation of p(MMA-co-A1)	80
3.2.1.4.	¹ H NMR Spectroscopic and Gravimetric Study of Thermoset Degradation .	81
3.2.1.5.	Effect of Solvent on Degradation	83
3.2.1.6.	Effect of Solvent/Water Ratio on Degradation	85
3.2.1.7.	Effect of Acid Species on Degradation	86
3.2.2.	Degradation Mechanism	88
3.3.	Conclusions	90
3.4.	Experimental	91

3.4.1.	Materials	91
3.4.2.	Instrumentation	91
3.4.3.	Model Adhesive Synthesis	91
3.4.4.	Adhesive Degradation Study	92
3.4.5.	¹ H NMR spectroscopy kinetic study of bulk polymerisation of p(MMA)	92
3.4.6.	Post-curing study of p(MMA)	92
3.4.7.	Synthesis and post curing of p(MMA-co-A1)	93
3.4.8.	¹ H NMR spectroscopy study of p(MMA-co-A1) degradation	93
3.4.9.	Gravimetric degradation study of p(MMA-co-A1)	93
3.4.10.	Degradation Studies.....	94
3.4.11.	Determination of swelling ratios.....	94
3.4.12.	Determination of gel content.....	94
4.	Chapter 4 – Acid Generators.....	95
4.1.	Introduction.....	95
4.2.	Results and Discussion.....	99
4.2.1.	Preliminary Investigations of Acid Generations.....	99
4.2.2.	TGA Analysis of Acid Generators	101
4.2.3.	Addition of TAGs to Networks	102
4.2.4.	HPMA and HEMA Tosylates	103
4.2.5.	Thermal Characterisation of HEMA Tosylate.....	104
4.2.6.	Optimisation and Scale Up of HPMA and HEMA Tosylate Syntheses	105
4.2.7.	FRP Polymerisation of HPMAtos and HEMAtos	108
4.2.8.	Thermolysis of p(HPMAtos) and p(HEMAtos).....	109

4.2.9.	HPMAtos and HEMAtos Model Adhesives	112
4.2.10.	Isothermal TGA Characterisation of p(HPMAtos)	118
4.2.11.	Variable Temperature NMR Spectroscopy Study of p(HEMAtos) and p(HPMAtos) E _i Mechanism	122
4.2.12.	Variable Temperature ¹ H NMR Spectroscopy Study of p(HPMA-tos) and p(HEMA-tos) E _i	128
4.2.13.	The Effect of the R Group and the determination of the E _i Mechanism.....	130
4.2.14.	p(HEMAtos) solid state E _i ¹ H NMR spectroscopy study.....	133
4.3.	Conclusions	138
4.4.	Experimental.....	139
4.4.1.	Materials	139
4.4.2.	Instrumentation	139
4.4.3.	Synthesis of 2-nitrobenzyl tosylate ¹³⁰	139
4.4.4.	Synthesis of <i>N</i> -hydroxy-1,8-naphthalimide ²⁰⁹	139
4.4.5.	Synthesis of <i>N</i> -hydroxytosylate-1,8-naphthalimide	140
4.4.6.	General procedure for synthesis of TAG doped adhesives.....	140
4.4.7.	Tosylation of HEMA and HPMA	141
4.4.8.	Synthesis of HPMAtos Method Development Experiments.....	142
4.4.9.	Reactive Workup of HPMAtos Synthesis.....	143
4.4.10.	Optimised Synthesis of HPMAtos.....	143
4.4.11.	Free radical polymerization of HEMAtos.....	144
4.4.12.	Free radical polymerization of HPMAtos.....	145
4.4.13.	Synthesis of Model Networks	146

4.4.14.	Heating of A1/MMA/HPMAtos networks	147
4.4.15.	Heating and Soxhlet extraction of A1/HPMAtos.....	147
4.4.16.	Isothermal TGA characterisation of p(HPMAtos) and p(HEMAtos)	147
4.4.17.	¹ H vtNMR spectroscopy studies of p(HPMAtos) and p(HEMAtos)	148
4.4.18.	p(HEMAtos) solid state E _i ¹ H NMR spectroscopy study.....	148
5.	Chapter 5 – Acetal Methacrylate CANS.....	149
5.1.	Introduction.....	149
5.2.	Results and Discussion.....	152
5.2.1.	Lap shears and repressing.....	152
5.2.2.	Casting panels and cubes	154
5.2.3.	TGA Analysis	156
5.2.4.	Reprocessing by Vacuum Compression Moulding and Hot Press	157
5.2.5.	Potential Issues with A1/MMA and A1/HEMA/MMA Networks.....	158
5.3.	Conclusions	162
5.4.	Experimental.....	163
5.4.1.	Materials	163
5.4.2.	Instrumentation	163
5.4.3.	Etching aluminium substrates.....	163
5.4.4.	Synthesis of Lap Shears	164
5.4.5.	Synthesis of Panels.....	164
6.	Chapter 6 - Concluding Remarks	166
7.	References	169
8.	Appendices.....	203

List of Figures

Figure 1-1 - Structures of common thermosets classified by their curing mechanism.....	2
Figure 1-2 - Mechanism of thermal expansion of microparticles that leads to physical rupturing of thermosets.	6
Figure 1-3 - Examples of onium ions used in ionic acid generators.	24
Figure 1-4 - Acrylate and methacrylate cross-linkers possessing acetal links and the acid generator NITf used to catalyse their hydrolysis.....	27
Figure 2-1 - ^1H NMR (CDCl_3) spectra of A1 a), b) A1 hydrolysis reaction mixture showing formation of HEMA and c) magnified peaks from hydrolysis spectra showing acetaldehyde after six hours at $50\text{ }^\circ\text{C}$	37
Figure 2-2 - $\text{p}K_a$ of carboxylic and sulfonic acids in H_2O	39
Figure 2-3 - Effect of acid concentration on conversion of HEMA to A1 as determined by ^1H NMR spectroscopy.....	42
Figure 2-4 – (a) HPLC-MS chromatogram showing distribution of products and (b) mass spectrum of chromatogram peak at 10.2 min of the crude reaction mixture of the A1 synthesis.	45
Figure 2-5 - Effect of TEGDVE feed rate on kinetics of A1 synthesis measured by ^1H NMR spectroscopy.....	49
Figure 2-6 – ^1H NMR Spectra (CDCl_3) of reaction products of control polymerisation of TEGDVE.....	61
Figure 2-7 - ^1H NMR spectra (CDCl_3) of poly(acetal) synthesised from TEGDVE and TEG.	62
Figure 3-1 TGA thermogram of A1 cross-linked MMA model adhesive.	76
Figure 3-2 DSC thermogram of A1 cross-linked MMA model adhesive, $20\text{ }^\circ\text{C}/\text{min}$ from -40 - $150\text{ }^\circ\text{C}$	76

Figure 3-3 - Conversion of MMA during p(MMA) model thermoset synthesis determined by ¹ H NMR.	78
Figure 3-4 Effect of post-cure temperature and time on the T_g of p(MMA).....	79
Figure 3-5 TGA thermogram (N ₂ , 20 °C/min) of p(MMA-co-A1) cured using optimised conditions.....	80
Figure 3-6 Evolution of acetaldehyde during the degradation of p(MMA-co-A1) networks in acetone-d ₆ /D ₂ O (9/1 v/v) pTsOH (0.15 M) solutions measured by ¹ H NMR spectroscopy. ..	82
Figure 3-7 Degradation kinetics of p(MMA-co-A1) thermoset in acetone/H ₂ O (9/1 v/v) pTsOH (0.15 M) at 50 °C for 6 hours.....	83
Figure 3-8 Degradation of p(MMA-co-A1) thermosets in different solvent/H ₂ O (9/1 v/v) pTsOH (0.15 M) solutions.	84
Figure 3-9 Swelling ratio of p(MMA-co-A1) in different solvents.	84
Figure 3-10 Degradation of p(MMA-co-A1) in acetone/H ₂ O pTsOH (0.15 M) solutions at 50 °C.	85
Figure 3-11 Effect of acetone/H ₂ O ratio of swelling ratio of p(MMA-co-A1) (left) and remaining mass after exposure to different acetone/H ₂ O pTsOH (0.15 M) solutions (right).....	86
Figure 3-12 Effect of acid on degradation of p(MMA-co-A1).....	87
Figure 3-13 Residual weight of p(MMA-co-A1) thermosets after degradation in acetone/H ₂ O (9/1) acid (0.15 M) solutions.....	87
Figure 3-14 Proposed mechanism of p(MMA-co-A1) degradation.....	89
Figure 4-1 – 8-quinolyl and 2-pyridyl sulfonates and their elimination temperatures. ¹⁹⁴	96
Figure 4-2 – Cyclohexyl sulfonates. ¹²³	97
Figure 4-3 – Thermally cleavable sulfonate-based epoxide cross-linkers. ²⁰⁵	97
Figure 4-4 – p(styrene sulfonates) synthesised and their T_{Ei} determined <i>via</i> temperature sweep TGA. ²⁰⁶	98
Figure 4-5 - TGA thermograms (N ₂ , 20 °C/min) of NHTN and hydroxyethyl ammonium nitrate.	101

Figure 4-6 - Inverted vials of adhesives doped with 2-NBT, free flowing fluids suggested poor curing.....	102
Figure 4-7 – Vials of NHTN (left) and 2-hydroxyethyl ammonium nitrate (right) doped p(MMA-co-MAA-co-A1) adhesives prior to curing.....	103
Figure 4-8 – a) DSC (25-200 °C at 10 °C/min) of HEMA _{tos} showing exotherm that was attributed to homopolymerisation. b) TGA (25-400 °C at 20 °C/min, N ₂) of HEMA _{tos} monomer showing wt % didn't follow expected pattern.	105
Figure 4-9 – a) DSC and TGA thermograms of p(HPMA _{tos}), b) DSC and TGA thermograms of p(HEMA _{tos}) and c) TGA thermograms of p(HEMA _{tos}), p(HPMA _{tos}) and p(MMA-co-A1).	109
Figure 4-10 - ¹ H NMR (DMSO-d ₆) spectrum of a) p(HEMA _{tos}) and b) p(HPMA _{tos}) DSC pan extract, showing heating liberates pTsOH.....	111
Figure 4-11 – TGA thermogram of HPMA _{tos} network and no HPMA _{tos} control.....	113
Figure 4-12 – IR spectra of A1/MMA/HPMA _{tos} networks.....	116
Figure 4-13 – TGA thermogram of A1/MMA/HPMA _{tos} networks obtained <i>via</i> heating from 25-180 °C at 20 °C/min, with an isothermal step at 180 °C for 3 h and heating to 800 °C at 20 °C/min.....	116
Figure 4-14 – Isothermal TGA thermogram of p(HPMA _{tos}) at 140-180 °C.....	118
Figure 4-15 – First order kinetic plots of isothermal TGA of p(HPMA _{tos}), where x is the fractional conversion determined from mass loss.....	120
Figure 4-16 – Second order kinetic plots of isothermal TGA of p(HPMA _{tos}), where x is the fractional conversion determined from mass loss.....	121
Figure 4-17 – Comparison TGA thermograms of p(HPMA _{tos}) and pTsOH monohydrate..	122
Figure 4-18 – a) 5-membered transition state E _i pathway and b) 6-membered transition state E _i pathway of p(HEMA _{tos}).	122
Figure 4-19 – Conversion of tosylate to pTsOH versus time of a) p(HEMA _{tos}) and b) p(HPMA _{tos}) v ^t NMR spectroscopy at 50, 70 or 90 °C in DMSO-d ₆	129

Figure 4-20 – First order kinetic plots of conversion of tosylate to pTsOH at 50 °C, 70 °C, and 90 °C of a) p(HEMATos) and b) p(HPMATos) obtained <i>via</i> vtNMR spectroscopy (DMSO-d ₆).	129
Figure 4-21 – Arrhenius plots of a) p(HEMATos) and b) p(HPMATos).....	130
Figure 4-22 – Conformational analysis of p(HEMATos) E _i 6-membered transition states. ..	131
Figure 4-23 Conformational analysis of p(HPMATos) majority isomer E _i 6-membered transition states.	133
Figure 4-24 Conformational analysis of p(HPMATos) minority isomer E _i 6-membered transition states.	133
Figure 4-25 – ¹ H NMR (DMSO-d ₆) spectra of residue extracts after heating.	135
Figure 4-26 - ¹ H NMR spectrum (CDCl ₃) of p(HEMATos).	144
Figure 4-27 - ¹ H NMR spectrum (CDCl ₃) of p(HPMATos).	145
Figure 5-1 - Bond strength data of lap shear testing of a) A1 cross-linked and b) EGDMA crosslinked MMA networks before and after repressing.	153
Figure 5-2 - Bond strength of A1/MAA/MMA network after lap shear testing and repressing.	154
Figure 5-3 - Panel casting setup (a), imperfect panel (b) and damaged tensile samples (c).	156
Figure 5-4 - TGA thermograms of a) A1/MMA and b) A1/HEMA/MMA networks, under N ₂ from 25-600 °C at 20 °C/min.	157
Figure 5-5 - Samples produced from ground network samples by vacuum compression moulding.	158
Figure 5-6 - Grinding and hot-press reforming of A1/HEMA/MMA networks.	158
Figure 8-1 - Mass spectra of A1 hydrolysis products separated <i>via</i> liquid chromatography.	203
Figure 8-2 - Molar mass distributions for poly(acetal) products synthesised from TEGDVE at different pTsOH loadings.	204

Figure 8-3 - Molar mass distributions for poly(acetal) products synthesised from TEGDVE and TEG at different pTsOH loadings.	205
Figure 8-4 - DSC of p(MMA-co-A1) cured at 100 °C for 48 hours.....	205
Figure 8-5 - ¹ H NMR spectra (acetone-d ₆ /D ₂ O) of p(MMA-co-A1) degradation supernatant.	206
Figure 8-6 - ¹ H NMR (CDCl ₃) spectrum of <i>ortho</i> -nitrobenzyl tosylate.....	206
Figure 8-7 - ¹ H NMR (DMSO-d ₆) spectrum of N-hydroxy-1,8-naphthalimide.	207
Figure 8-8 - IR spectrum of N-hydroxy-1,8-naphthalimide.	207
Figure 8-9 - ¹ H NMR (CDCl ₃) spectrum of NHTN.	208
Figure 8-10 - IR spectrum of NHTN.....	208
Figure 8-11 - ¹ H NMR (CDCl ₃) spectrum of HEMAtos.	209
Figure 8-12 - IR spectrum of HEMAtos.....	209
Figure 8-13 - ¹ H NMR (CDCl ₃) spectrum of HPMAtos isomers.	210
Figure 8-14 - IR spectrum of HPMAtos.....	210
Figure 8-15 - ¹ H NMR (CDCl ₃) spectrum of HPMA, showing the vinyl peaks at 6.13 ppm and 6.11 ppm used to determine the ratio of the regioisomers.....	211
Figure 8-16 - ¹ H NMR (CDCl ₃) spectrum of HPMA tosylation reaction mixture after 3 hrs, using NEt ₃ as the base and the following reagent ratios [OH]:[pTsCl]:[Base] – 1:1.5:1.5. Highlighted vinylic protons were used to monitor the conversion of different HPMA regioisomers.	211
Figure 8-17 - ¹ H NMR (CDCl ₃) spectrum of HPMA tosylation reaction mixture after w3 hrs, using NEt ₃ as the base and the following reagent ratios [OH]:[pTsCl]:[Base] – 1:1.5:1.5. Highlighted vinylic protons were used to monitor the conversion of different HPMA regioisomers.	212
Figure 8-18 - ¹ H NMR (CDCl ₃) spectrum of HPMA tosylation reaction mixture after 27 hrs, using NEt ₃ as the base and the following reagent ratios [OH]:[pTsCl]:[Base] – 1:1.5:1.5. Highlighted vinylic protons were used to monitor the conversion of different HPMA regioisomers.	212

Figure 8-19 - ^1H NMR (CDCl_3) spectrum of HPMA tosylation reaction mixture after 72 hrs, using NEt_3 as the base and the following reagent ratios $[\text{OH}]:[\text{pTsCl}]:[\text{Base}] - 1:1.5:1.5$. Highlighted vinylic protons were used to monitor the conversion of different HPMA regioisomers. 213

Figure 8-20 - ^1H NMR (CDCl_3) spectrum of HPMA tosylation reaction mixture after 3 hrs, using pyridine as the base and the following reagent ratios $[\text{OH}]:[\text{pTsCl}]:[\text{Base}] - 1:1.5:1.5$. Highlighted vinylic protons were used to monitor the conversion of different HPMA regioisomers. 213

Figure 8-21 - ^1H NMR (CDCl_3) spectrum of HPMA tosylation reaction mixture after 23 hrs, using pyridine as the base and the following reagent ratios $[\text{OH}]:[\text{pTsCl}]:[\text{Base}] - 1:1.5:1.5$. Highlighted vinylic protons were used to monitor the conversion of different HPMA regioisomers. 214

Figure 8-22 - ^1H NMR (CDCl_3) spectrum of HPMA tosylation reaction mixture after 27 hrs, using pyridine as the base and the following reagent ratios $[\text{OH}]:[\text{pTsCl}]:[\text{Base}] - 1:1.5:1.5$. Highlighted vinylic protons were used to monitor the conversion of different HPMA regioisomers. 214

Figure 8-23 - ^1H NMR (CDCl_3) spectrum of HPMA tosylation reaction mixture after 72 hrs, using pyridine as the base and the following reagent ratios $[\text{OH}]:[\text{pTsCl}]:[\text{Base}] - 1:1.5:1.5$. Highlighted vinylic protons were used to monitor the conversion of different HPMA regioisomers. 215

Figure 8-24 - ^1H NMR (CDCl_3) spectrum of HPMA tosylation reaction mixture after 3 hrs, using pyridine as the base with DMAP as a catalyst, and the following reagent ratios $[\text{OH}]:[\text{pTsCl}]:[\text{Base}] - 1:1.5:1.5$. Highlighted vinylic protons were used to monitor the conversion of different HPMA regioisomers. 215

Figure 8-25 - ^1H NMR (CDCl_3) spectrum of HPMA tosylation reaction mixture after 27 hrs, using pyridine as the base with DMAP as a catalyst, and the following reagent ratios

[OH]:[pTsCl]:[Base] – 1:1.5:1.5. Highlighted vinylic protons were used to monitor the conversion of different HPMA regioisomers.	216
Figure 8-26 - ¹ H NMR (CDCl ₃) spectrum of HPMA tosylation reaction mixture after 27 hrs, using pyridine as the base with DMAP as a catalyst, and the following reagent ratios [OH]:[pTsCl]:[Base] – 1:1.5:1.5. Highlighted vinylic protons were used to monitor the conversion of different HPMA regioisomers.	216
Figure 8-27 - ¹ H NMR (CDCl ₃) spectrum of HPMA tosylation reaction mixture after 72 hrs, using pyridine as the base with DMAP as a catalyst, and the following reagent ratios [OH]:[pTsCl]:[Base] – 1:1.5:1.5. Highlighted vinylic protons were used to monitor the conversion of different HPMA regioisomers.	217
Figure 8-28 - ¹ H NMR (CDCl ₃) spectrum of HPMA tosylation reaction mixture after 3 hrs, using pyridine as the base and the following reagent ratios [OH]:[pTsCl]:[Base] – 1:2:3. Highlighted vinylic protons were used to monitor the conversion of different HPMA regioisomers.	217
Figure 8-29 - ¹ H NMR (CDCl ₃) spectrum of HPMA tosylation reaction mixture after 23 hrs, using pyridine as the base and the following reagent ratios [OH]:[pTsCl]:[Base] – 1:2:3. Highlighted vinylic protons were used to monitor the conversion of different regioisomers.	218
Figure 8-30 - ¹ H NMR (CDCl ₃) spectrum of HPMA tosylation reaction mixture after 27 hrs, using pyridine as the base and the following reagent ratios [OH]:[pTsCl]:[Base] – 1:2:3. Highlighted vinylic protons were used to monitor the conversion of different regioisomers.	218
Figure 8-31 - SEC chromatograms for p(HPMA-tos) and p(HEMA-tos).....	219
Figure 8-32 - p(HEMATos) DSC pan extract HPLC-MS chromatogram and spectrum.	219
Figure 8-33 - p(HPMATos) DSC pan extract HPLC-MS chromatogram and spectrum.	220
Figure 8-34 - IR spectra of p(HEMATos) before and after heating.....	220
Figure 8-35 - IR spectra of p(HPMATos) before and after heating.....	221
Figure 8-36 - HPLC chromatogram (top) and mass spectrum of 10 wt % HPMATos/A1/MMA network extract before heating.	221

Figure 8-37 - HPLC chromatogram (top) and mass spectrum of 10 wt % HPMAtos/A1/MMA network extract before heating. 222

Figure 8-38 - First order kinetic plot of p(HPMAtos) isothermal TGA. 222

List of Tables

Table 2-1 - Effect of acid pK_a on the extent of A1 hydrolysis in acetone- d_6 /D ₂ O (9/1 v/v) at 50 °C for 5 h.....	40
Table 2-2 - Effect of pTsOH mol % on HEMA conversion during the synthesis of A1 and the formation of acetaldehyde side product.....	43
Table 2-3 - Summary of control poly(acetal) characterisation data.....	47
Table 2-4 - Solvent's properties and effect on conversion of HEMA to A1.....	51
Table 2-5 - Effect of wash volume (%) on yield of A1 synthesised in acetone or ethyl acetate.	53
Table 2-6 - Green metrics for initial and optimised synthesis of A1.	54
Table 2-7 - Effect of pTsOH on A1 synthesis experiment formulations.....	59
Table 2-8 - Control polymerisation of TEGDVE formulations.....	60
Table 2-9 - Control polymerisation of TEGDVE and TEG formulations.....	62
Table 2-10 - Wash formulations and yield of A1 recovered.	64
Table 2-11 – E factor waste data for initial synthesis of A1.	65
Table 2-12 – E factor waste data for optimised A1 synthesis.	65
Table 2-13 - Process mass index data for initial and optimised synthesis of A1.	66
Table 4-1 – Literature conditions of tosylation reactions.....	106
Table 4-2 – Experimental conditions of HPMAtos synthesis optimisation experiments.....	107
Table 4-3 – ¹ H NMR spectroscopy conversion and SEC data for the polymerisations of HPMAtos and HEMAtos.....	108
Table 4-4 – A1/MMA/HPMAtos network formulations.....	115
Table 4-5 – Bases and molar ratios used in method development experiments.	142
Table 4-6 - Quenching agent and amount.....	143
Table 4-7 – Initial A1/MMA/HPMAtos network formulations.....	146
Table 4-8 - A1/HPMAtos and EGDMA/HPMAtos network formulations.	146

Table 4-9 – HAM network formulations.	146
Table 5-1 - Formulation of A1/MMA acetal metathesis networks.	155
Table 5-2 - Formulation of A1/HEMA/MMA transacetalisation networks.	155
Table 5-3 - A1/MMA network formulations.	165
Table 5-4 - A1/HEMA/MMA Network Formulations.	165
Table 8-1 - Reaction products determined <i>via</i> HPLC-MS when synthesising A1 with 0.5 mol % pTsOH.	203

Abbreviations

4-TMA – 4,*N,N*-trimethylaniline

AIBN - 2,2'-azobis(2-methylpropionitrile)

BPO – benzoyl peroxide

CAN – covalently adaptable network

DCA – dichloroacetic acid

DMSO - Dimethyl sulfoxide

DMA – *N,N*-dimethylaniline

DSC – differential scanning calorimetry

EGDMA – ethylene glycol dimethacrylate

E_a – Activation energy

E_i – Intramolecular elimination

HEMA - 2-hydroxyethyl methacrylate

HPLC-MS – high performance liquid chromatography mass spectroscopy

IR – infrared

MAA – methacrylic acid

MCA – monochloroacetic acid

MEK – methyl ethyl ketone

NITf - *N*-hydroxynaphthalimide triflate

NMR – nuclear magnetic resonance

PAG – photoacid generator

pTsCl – *para*-toluene sulfonyl chloride

pTsOH – *para*-toluene sulfonic acid

RAFT - reversible addition-fragmentation chain-transfer

R.T. – room temperature

SEC – size exclusion chromatography

SOE - spiroorthoester

TAG – thermal acid generator

TCA – trichloroacetic acid

T_{Ei} – temperature of intramolecular elimination

TEG – tri(ethylene glycol)

TEGDVE – tri(ethylene glycol)divinyl ether

TFA – trifluoroacetic acid

T_g – glass transition temperature

TGA – thermogravimetric analysis

THF – tetrahydrofuran

TLC – thin layer chromatography

TMA – 4,*N,N*,-trimethylaniline

vtNMR – variable temperature nuclear magnetic resonance

Chapter 1 - Introduction

1.1. Thermosets

1.1.1. Thermosets, their properties, and synthesis

Thermosets are a class of polymer that harden, cure, *via* a chemical reaction involving the chemical cross-linking of chains.^{1,2} The product is an insoluble network of infinite molecular weight, meaning it cannot be measured. The curing process of thermosets may be initiated *via* an external stimulus such as heat or UV and by mixing reactive species such as monomers and a catalyst or monomers and atmospheric moisture. The term curing in the field of thermosets generally refers to polymerisation of a pre-polymer solution. The composition of which can be, polymers, oligomers, mono and multifunctional monomers, and additives such as initiators, antioxidants, and fillers.

At a molecular level the synthesis of thermosets proceeds *via* step or chain growth polymerisation, sometimes both occur simultaneously, for example hybrid cure adhesives.³ A variety of functional groups have been used in thermoset chemistry including poly(urethanes), epoxy resins, poly(benzoxazines), phenolic resins, unsaturated polyesters and (meth)acrylate resins (Figure 1-1).⁴ Collectively, thermosets account for approximately 18 % of all polymers produced⁵ and annual polymer production has increased at a sustained rate since their inception and is expected to continue.⁵⁻⁸

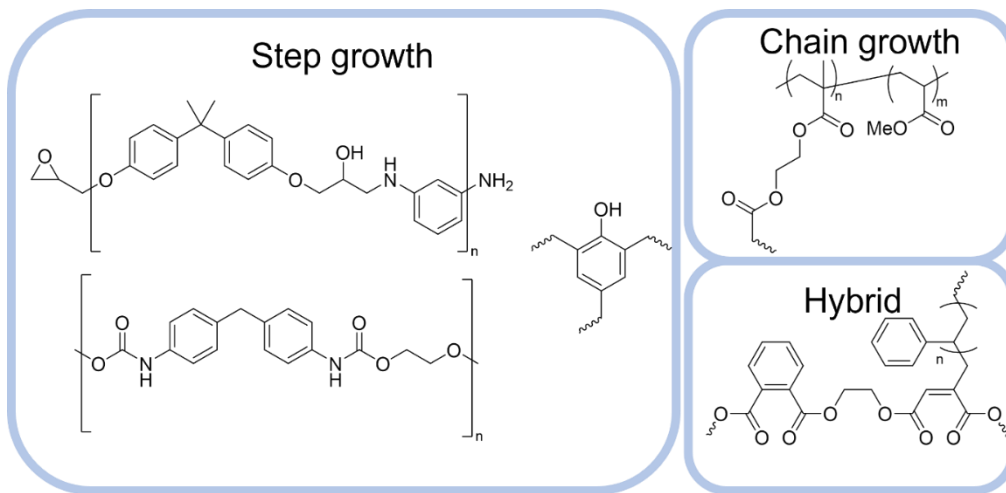


Figure 1-1 - Structures of common thermosets classified by their curing mechanism.

1.1.2. Thermoset properties and application

Thermosets offer excellent thermal stability, good mechanical properties, chemical resistance, and good dimensional stability. This is largely due to the presence of covalent cross-links between polymer chains that form a complex network that is insoluble and cannot be melted. Furthermore, thermosetting polymer synthesis is technically simple and may be used in manufacturing processes unavailable to traditional materials, such as resin vacuum infusion, hand lay-up and pultrusion in composite manufacturing.⁹ The favourable properties of thermosets have enabled their use in a range of applications such as, adhesives, composites and coatings within a range of industries such as, aerospace, construction, electronic and automotive.⁴

Adhesives offer advantages over traditional mechanical fasteners such uniform stress distribution, weight reduction, joining different materials and complex geometries. However, their removal for repairs or at the end of life can be challenging compared to a nut and bolt fastener, separation of adhesively joined components may lead to substrate damage, failure or contamination.^{1,3,7,10,11} For low value substrates this may not be financially damaging but creates recycling challenges and negatively effects the environment. For adhesively joined high value substrates such as anisotropic carbon fibre composites or battery cells in electronic vehicles, damaging these materials is financially and environmentally costly.⁹ This is also true

of thermoset coatings which are applied to an object to give a finish or protection. However, removal or repairs is challenging due to the infusible and insoluble properties of thermosets.

The role of thermosets in composites is to make up the matrix phase within which a reinforcer is dispersed, thermoset-reinforcer composites have unique properties such as excellent mechanical strength while also being lightweight. However, the infusible and insoluble properties of thermosets mean repairs and end of lifecycle disassembly is challenging. Reinforcers such as carbon fibre are valuable, and their production is resource intensive so recovery for reuse is preferable. Technology enabling the repair of glass fibre composite wind turbine blades could increase their operational lifetime and prevent them from entering landfill at their end of life.^{12,13}

1.1.3. Thermoset Recycling

Thermoset recycling is more challenging than their non-covalently cross-linked equivalents, thermoplastics.¹⁴ Current end of life options for thermosets and their composites are landfill disposal, mechanical recycling and thermal treatment. Mechanical recycling of thermosets and composites involves grinding to a fine particulate for use as filler, degrading potentially valuable reinforcers and components. Thermal treatment of thermosets and their composites produces different results depending on whether it is performed under aerobic or anaerobic conditions. Aerobic conditions lead to combustion and the opportunity for energy recovery, usually any reinforcer present is reduced to low quality filler. Anaerobic conditions, often referred to as pyrolysis, allow the transformation of thermosets to fuels and enable reinforcer recovery. The effectiveness of thermal treatment depends on the plant and process emission control technology and energy recovery efficiency.^{5,8,13-16}

Chemical recycling of thermosets, often called solvolysis, involves the reactive dissolution of thermosets with cleavable bonds within their backbone or cross-links. During chemical recycling cleavable bonds react with solvent or other chemical species, breaking them and forming lower molecule weight species. The products may then be separated and collected

via processes such as precipitation or distillation for reprocessing into thermosets if the products are monomers or reactive oligomers and polymers. Chemical recycling is mainly performed on a lab scale and there are concerns over the environmental impact and safety of using hazardous solvents.^{17–22}

1.2. Degradable Thermosets

Despite the excellent properties and usefulness of thermosets, their lack of recyclability is an issue. Common thermosets are fossil fuel derived and follow a linear economy model, whereby resources are extracted and become waste which is environmentally damaging.²³ Their lack of recyclability and reusability creates further consumption of fossil fuels and more pollution. Conventional thermosets do not biodegrade and landfilled thermoset waste slowly breaks down in particulates accumulating in all major ocean basins, freshwater systems and terrestrial habitats.^{5,14} As previously discussed the alternatives are mechanical and thermal recycling, however mechanical recycling is likely to delay the release of thermosets into the environment and thermal recycling can create harmful emissions, while both still further demand for fossil fuels.^{14–18}

One solution is the use of renewable feedstocks such as lignin, hemi-cellulose and cellulose however, life-cycle analysis of bio-derived plastics has shown they can embody more CO₂ equivalents than traditional fossil derived plastics.^{8,14,24} The use of renewable feedstocks doesn't guarantee that these materials won't become pollutants, for example poly(lactic acid) requires collection for industrial composting.²⁵ An alternative is materials that can be degraded in response to a stimulus enabling separation and reuse of components or reinforcers. The degradation products may be designed so that they can be reused in a different application or reprocessed to new thermosets.

Degradable thermosets enable removal of thermoset adhesives and coatings without damaging substrates and facilitate reinforcer recovery in composites. There are two main approaches to achieving degradable thermosets *via* the incorporation of additives that give

physical or chemical degradation or the addition of degradable units to the thermoset). A further category of polymers undergo full depolymerisation to monomers in response to stimuli such as self-immolative polymers^{26,27}, polymers made *via* RAFT polymerisation^{28,29} or in the presence of catalysts or enzymes³⁰⁻³² exists. However, these do not exhibit the mechanical and thermal properties equivalent to conventional thermosets and have been omitted from this introduction.

1.2.1. Additives

Additives may be formulated into thermosets that enable thermoset degradation or component separation. They remain dormant in the network until the joining of substrates is no longer required, upon which a stimulus is applied and debonding achieved. The mechanism of degradation proceeds by a physical change such as rupture, delamination or phase change.^{33,34}

1.2.1.1. Thermally expansive microparticles

Thermally expansive microparticles undergo volumetric expansion when heated. They are composed of a thermoplastic shell, a copolymer of vinylidene chloride, acrylonitrile, methacrylonitrile and methyl methacrylate (MMA), encapsulating a liquid hydrocarbon such as isobutane or isopentane.³⁵ Upon heating two processes occur simultaneously, softening of the thermoplastic shell as it is heated above its T_g and the phase transformation of the liquid hydrocarbon core to a gas, the change in volume is around 50-100 times its original (Figure 1-2).

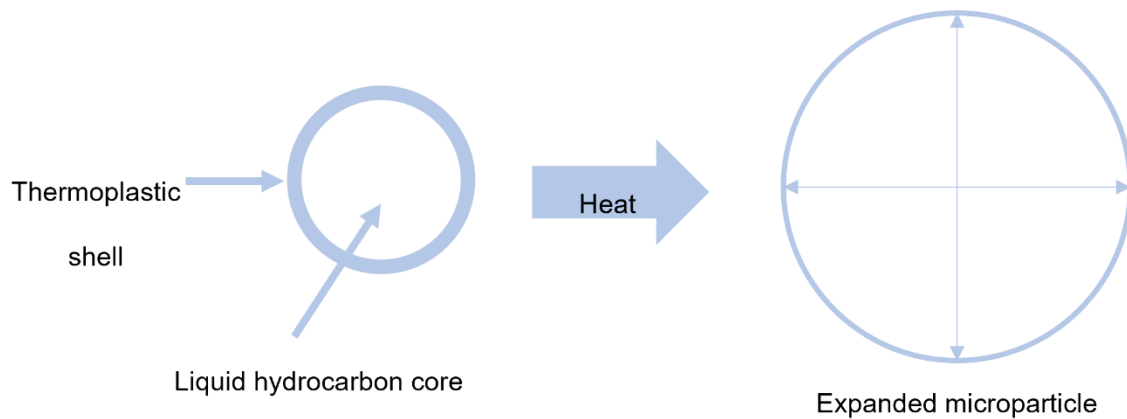


Figure 1-2 - Mechanism of thermal expansion of microparticles that leads to physical rupturing of thermosets.

Upon cooling the thermoplastic core becomes rigid trapping the particle in its expanded state. The overall expansion of a bond joint leads to a reduction in strength and separation.^{33,36,37} Armes *et. al* coated thermally expanding microparticles with poly(pyrrole) which has a known absorption peak in the near infrared region. Subsequent irradiation with an infrared lamp led to expansion of the microparticle removing the need for bulk heating.³⁸ The temperature of expansion varies from 70 to 285 °C.³³

Inorganic thermally expansive microparticles such as graphite, vermiculite, pearlite and mica have been investigated as high temperature alternative to thermoplastic encapsulated hydrocarbons.^{33,34} Kawate and Kanki added expandable graphite microparticles (10-40 wt%) to epoxy resins and observed debonding of substrates after thermal treatment at 250 °C. However, the high wt% used lowered the bonding strength of the epoxy resin.³⁹

Of the additive techniques outlined, thermally expansive microparticles have seen the largest industrial use for mainly non-structural applications.³⁵ Examples of polyurethanes and epoxy-based adhesives utilising thermally expansive microparticles can be found in the literature; however, use of thermally expansive microparticles in (meth)acrylate thermosets are sparse.^{33,34}

1.2.1.2. Nanoparticle additives

Nanoparticles have been used as additives to aid debonding *via* heat generation. Evonik developed MagSilica, a pressure sensitive adhesive containing silicon dioxide encapsulated iron oxide nanoparticles. Upon exposure to external magnetic fields nanoparticles radiate heat aiding disassembly. However, many substrates act as barriers to external magnetic fields decreasing the disassembly efficiency.^{34,40} ElectRelease is a commercially available debondable epoxy adhesive. When a potential difference (10-50 V) is applied debonding is achieved. However, conductive substrates are required limiting the technology.³⁴

1.2.2. Chemically Modified Thermosets

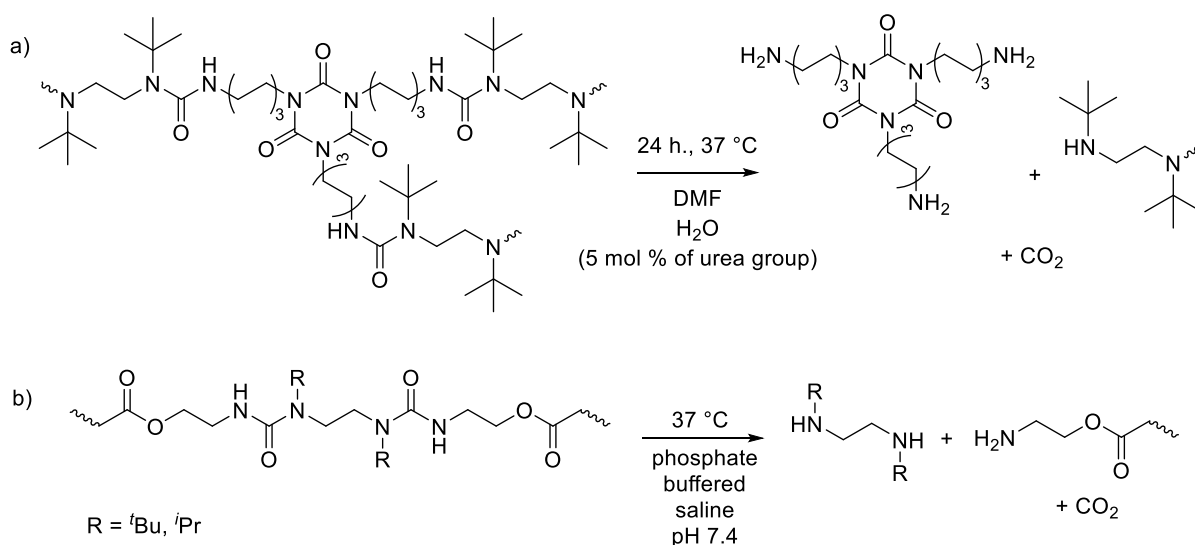
Thermoset degradation can be enabled by chemical modification with groups that respond to stimuli such as temperature, ultraviolet light (UV) and pH.^{1,33} Ultrasonic, near infrared radiation and electrical current are less popular due to the expense of equipment.³⁴ Of these pH degradable thermosets are particularly desirable as the reaction products can be reacted with one another *via* a condensation reaction to yield the original functional group, offering a route to reusable thermosets. pH responsive linkers have been well studied in biomedical polymers^{41–43} such as soft gels, however, their use in degradable thermosets with strong mechanical properties is relatively low and largely confined to epoxy resin chemistry.¹ A brief introduction to functional groups used in degradable thermosets follows; two detailed reviews by Ma and co-workers have recently been published in this area.^{1,15}

1.2.2.1. Lactone modification

Servando *et al.*, Sangermano *et al.* and Tomuta *et al.* copolymerised a modified bisphenol A diglycidyl ether resins to incorporate γ -caprolactone in varying amounts as compostable or alkaline degradable materials.^{44,45} The cross-linked networks were synthesised *via* cationic polymerisation; in all studies the thermal stability was lower than standard epoxy resins. Sangermano *et al.* studied the hydrolysis of networks containing γ -caprolactone at 0, 2, 5 and 10 wt % over 2 months at pH 7.4 in a buffer solution; increasing γ -caprolactone content increased the hydrolytic weight loss to 5 wt%, compared to 0 % weight loss for the sample with no γ -caprolactone.⁴⁴ Tomuta *et al.* synthesised a hyperbranched pre-polymer from 3,5-dihydroxybenzoic acid and γ -caprolactone, which was subsequently polymerised with bisphenol A diglycidyl ether.⁴⁵ The authors used product T_g as an estimate of the extent of hydrolysis in refluxed KOH/EtOH (1 M) solutions; the T_g decreased over time for all networks containing γ -caprolactone segments after 24 hrs. The 10 wt % hyperbranched caprolactone containing sample T_g decreased from 122 to 60 °C. The long degradation times may hinder their use and bisphenol A diglycidyl ether is concerning due to its negative health effects.^{46,47}

1.2.2.2. Hindered ureas

Cheng and co-workers^{48–50} polymerised sterically hindered amines with di- or multifunctional isocyanates, producing sterically hindered poly(ureas) (Scheme 1-1). Traditional ureas are resistant to hydrolysis due to the conjugation within the functional group. However, the presence of steric bulk on the urea bond disrupts conjugation by preventing the orbitals from aligning in a coplanar configuration. Furthermore, the sterically hindered urea bond is dynamic and dissociates to a hindered amine and isocyanate; under aqueous conditions the isocyanate is hydrolysed liberating CO₂ and an amine. The rate of hydrolysis and therefore, thermoset degradation was increased *via* the use of bulkier amines. For example b) in Scheme 1-1b, poly(ureas) synthesised with ⁱPr substituents showed no appreciable degradation when incubated at 37 °C in phosphate buffered saline solution for 200 hrs, whereas the ^tBu bearing poly(urea) fully degraded in 100 hrs.⁴⁹



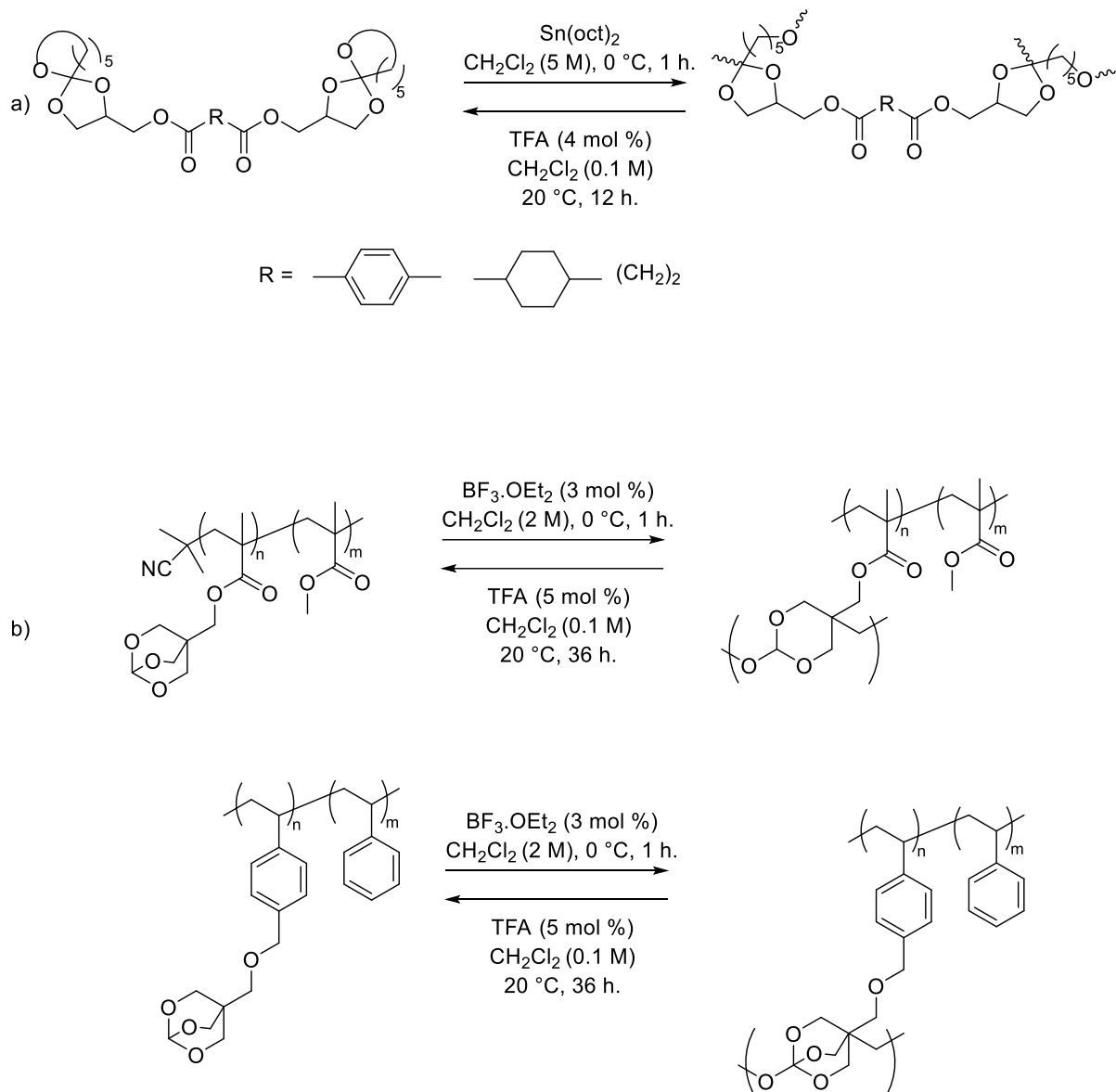
Scheme 1-1 – pH degradable sterically hindered poly(ureas).^{48–50}

Cheng and co-workers then synthesised a thermoset from hexamethylene diisocyanate and 2-(*tert*-butylamino)ethanol which could be hydrolysed in the presence of water or depolymerised in the presence of excess 2-(*tert*-butylamino)ethanol and exhibited covalently adaptable behaviour due to the dynamic nature of the hindered urea bond, see Section 1.3 Covalently Adaptable Networks. The hydrolysis of hindered poly(ureas) offers a route to

simple removal of thermosets; however, their application may be hindered by the use of $\text{Sn}(\text{Oct})_2$ as a polymerisation catalyst and isocyanate monomers, both of which have environmental and health concerns.⁵¹⁻⁵³ Lastly, the materials undergo hydrolytic degradation at neutral pH meaning coatings, adhesives and composites utilising them may undergo premature degradation.

1.2.2.3. Orthoesters

Endo and co-workers developed spiroorthoesters (SOEs) as monomers for pH degradable thermosets synthesised *via* ring opening polymerisation (Scheme 1-2).⁵⁴⁻⁵⁷ Under acidic conditions poly(SOEs) depolymerise to SOE monomers enabling chemical recycling. Initial work developed vinyl functional poly(SOEs) that were cross-linked *via* thiol-ene reactions with dithiols. The corresponding polymers were depolymerised in dichloromethane/trifluoroacetic acid (TFA) (4 mol %) at 20 °C to yield bifunctional SOE monomers in yields >66 %.^{54,55} Endo and co-workers then synthesised poly(SOEs) from SOE derivatives of common diacid monomers (terephthalic acid, succinic acid and 1,4-cyclohexane dicarboxylic acid) aiming to produce chemically recyclable equivalents of commodity polymers (Scheme 1-2a).⁵⁷ However, polymerisation of these reached low conversions and the formation of cross-linked species was not observed.



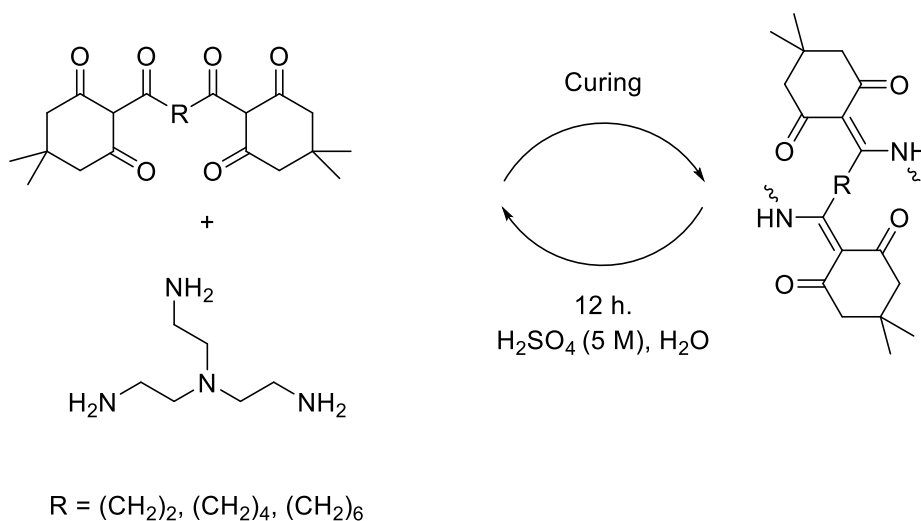
Scheme 1-2 - Examples of spiroorthoester based pH degradable thermosets.^{54,55}

Lastly, Endo and co-workers synthesised SOE functionalised copolymers of methyl methacrylate or styrene which were then cross-linked *via* cationic polymerisation using $\text{BF}_3 \cdot \text{OEt}_2$ to yield poly(SOEs) (Scheme 1-2b). The resultant cross-linked thermosets underwent depolymerisation to the starting SOE functionalised copolymers in solutions of dichloromethane/TFA (5 mol %) at 20 °C after 36 hrs.

1.2.2.4. Hexahydrotriazines

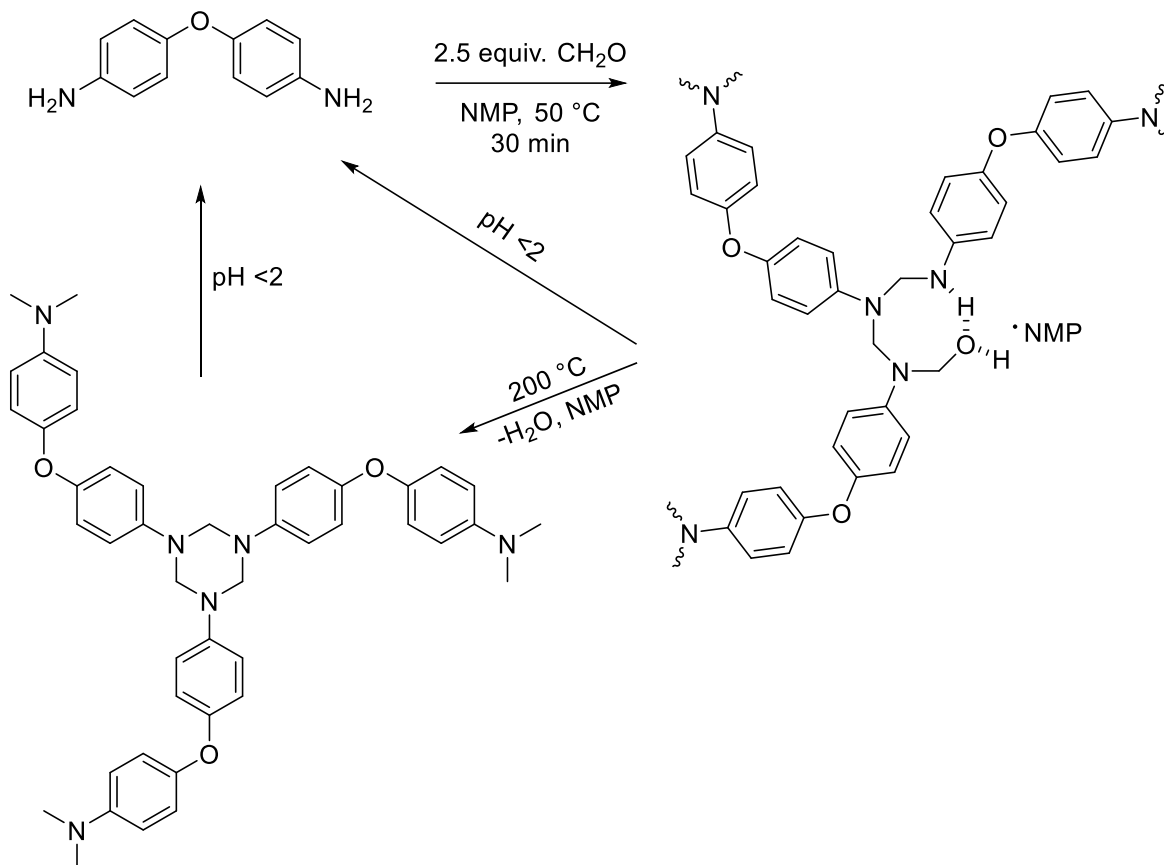
García *et al.*⁵⁸ synthesised degradable thermosets utilising the hexahydrotriazine functional group by the reaction between 4,4'-oxydianiline and paraformaldehyde (Scheme 1-4). The T_g could be tuned between 125-193 °C by changing the equivs. of paraformaldehyde to control the cross-link density. The thermosets were stable in aqueous solutions with a pH >3, whereas in aqueous H₂SO₄ solutions with a pH <2 they underwent full depolymerisation in 56 min.

1.2.2.5. Diketoenamines



Scheme 1-3 - Diketoenamine based degradable thermosets.⁵⁹

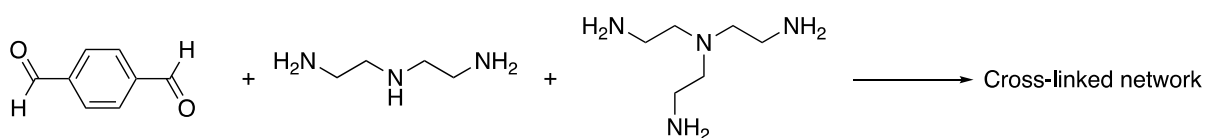
Christensen *et al.*⁵⁹ synthesised three difunctional triketone monomers from adipic, suberic and sebacic acid difunctional triketone that were polymerised with tris(2-aminoethyl)amine producing poly(diketoenamines) (Scheme 1-3). The T_g was between 110-130 °C depending on the equivs. of tris(2-aminoethyl)amine relative to the triketone. The resulting poly(diketoenamines) underwent depolymerisation in H₂SO₄ solutions (5 M) to the corresponding triketone and tris(2-aminoethyl)amine in yields >90 %. Furthermore, the authors demonstrated methodology for separating the triketone monomer from mixed plastic waste streams and recovery of fibres from composites using poly(diketoenamine) as a matrix. Lastly, the authors used recovered triketone monomer to make new thermosets that had near identical mechanical properties to the virgin thermoset.



Scheme 1-4 - Hexahydrotriazine based degradable thermosets.⁵⁸

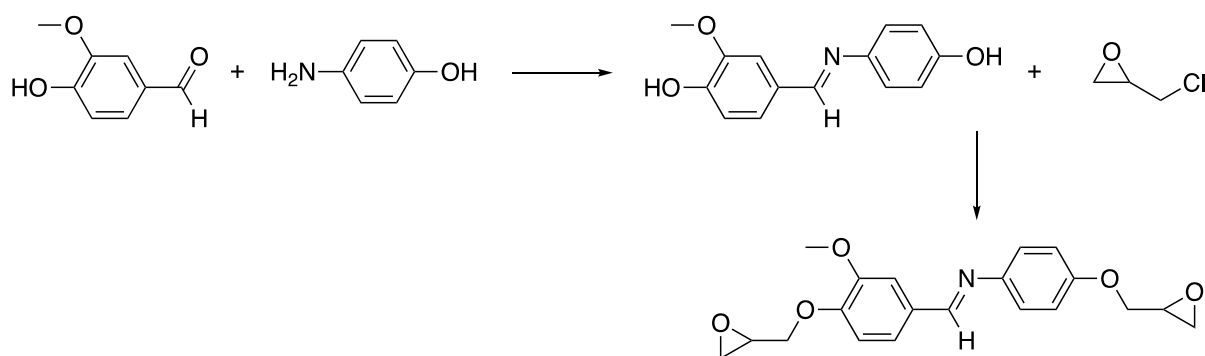
1.2.2.6. Imines

A wide range of multifunctional amines, aldehydes and ketones are commercially available and yield poly(imines) with broad properties.⁶⁰ Taynton *et. al* synthesised poly(imine) thermosets without the use catalysts from terephthalaldehyde, diethylene triamine and triethylene tetramine in organic solvents (Scheme 1-5). The highly cross-linked networks formed were resistant to hydrolysis at up to 90 °C and became malleable and healable; upon loss of water the networks regained rigidity. Carbon fibre reinforced poly(imine) composites could be degraded in acidic solutions and the fibres recovered.⁶⁰⁻⁶³



Scheme 1-5 - Synthesis of cross-linked poly(imine) degradable thermosets.⁶⁰

Lignin is a bio-source of vanillin from which Zhao *et. al* synthesised an imine containing diepoxy cross-linker (Scheme 1-6). An epoxy resin was synthesised from the imine containing diepoxy cross-linker with a diamine hardener and the resin had good mechanical and thermal properties. The resin became malleable under aqueous conditions and was found to solubilise under mildly acidic conditions (0.17 M) in tetrahydrofuran (THF), ethanol, DMF, dimethyl sulfoxide (DMSO) and water. The breaking of imine bonds leads to solubilisation and networks could be recycled by reforming the imine bond.⁶⁴

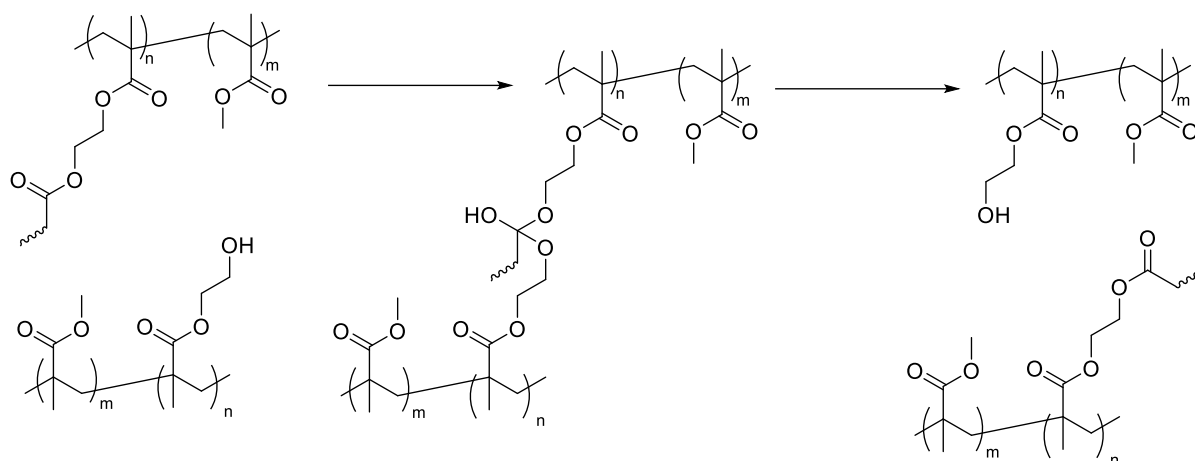


Scheme 1-6 - Synthesis of imine containing bio-based epoxy cross-linker.⁶⁴

1.3. Covalently Adaptable Networks

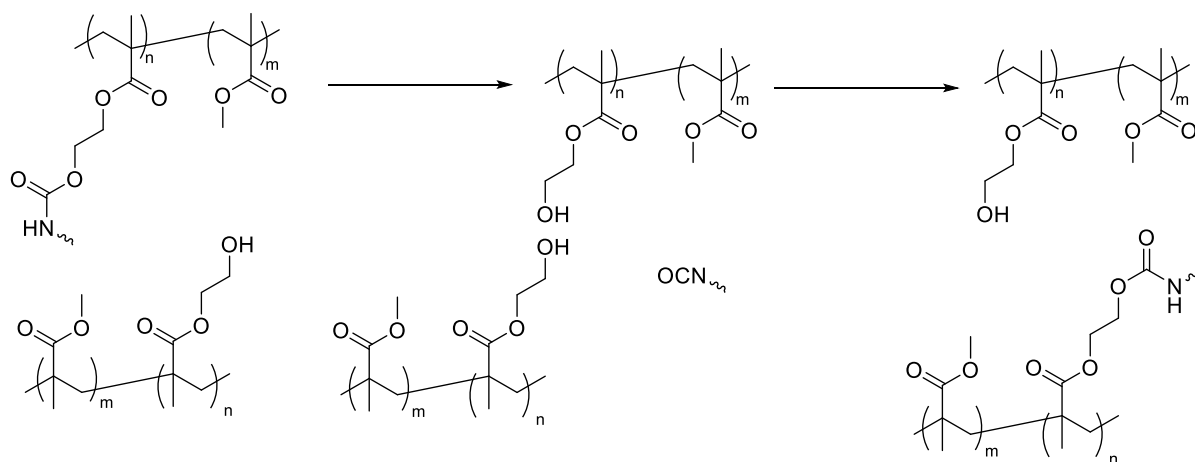
Covalently adaptable networks (CANs) are another solution to the infusible and insoluble properties imparted on thermosets by chemical cross-links. CANs contain exchangeable chemical bonds that undergo exchange reactions. CANs swell in organic solvents like thermosets but flow like thermoplastics when a stimulus is applied, typically heat. The exchange reactions that give CANs this behaviour can follow associative, dissociative, and concerted reaction mechanisms. CANs that react *via* an associative pathway are often called vitrimers as their viscosity is governed by exchange reactions at elevated temperatures following the Arrhenius law.

Associative CANs undergo exchange reactions where a reactive intermediate is formed, and subsequent elimination yields a new cross-link, the networks cross-link density remains constant (Scheme 1-7).



Scheme 1-7 - Associative covalent adaptable network *via* transesterification pathway.

Dissociative exchange reactions proceed by first breaking a cross-link and subsequently forming a new cross-link, as the rate of exchange increases the cross-link density of the CAN decreases (Scheme 1-8). Lastly, the concerted mechanism proceeds in a single step where bonds are formed and broken simultaneously, maintaining a constant cross-link density.⁶⁵



Scheme 1-8 - Disassociative CAN type pathway *via* transcarbamoylation pathway.

The type of exchange reaction impacts the macroscopic properties of CANs *via* the effect on cross-link density. Therefore, the rate of exchange reactions and presence of catalysts and functional group concentration also influences the macroscopic properties of CANs. For example, Leibler and co-workers work on acid-epoxy and anhydride-epoxy resins demonstrated well known epoxy resin thermosets could undergo associative exchange reactions such as transesterification, at $>70\text{ }^{\circ}\text{C}$ in the presence of $\text{Zn}(\text{acac})_2$ or $\text{Zn}(\text{ac})_2$

catalysts. These materials behaved like conventional epoxy resins at room temperature but could be re-molded at elevated temperatures as the rate of exchange increased.⁶⁶ Worrell *et al.* synthesised thiol-thioester associative exchange based CANs that could be reprocessed at 23 °C.⁶⁷

The rate of exchange reaction is one of multiple properties that influence the macroscopic properties of CANs, meaning introduction of a specific dynamic bond to a network will not give the same stress-relaxation behaviour as in other CANs.⁶⁵ The macroscopic properties of CANs depend on a multitude of factors including T_g , cross-link density, chemical composition of the matrix, impurities, catalysts and network stiffness.^{65,68} Dynamic functional groups used in CANs include disulfides, Diels-Alder cycloadditions, transesterification, transcarbonylation, transamidation, transimination, transalkylation, olefin metathesis, transacetalisation and acetal metathesis.^{69–76} Of the aforementioned functional groups, acetals are of particular interest due to their degradable and dynamic properties.

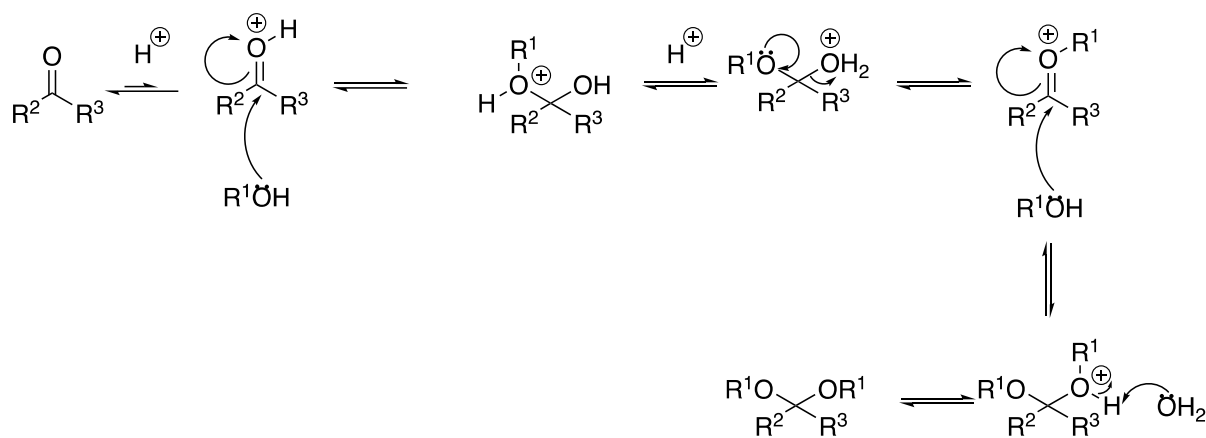
1.4. Acetals

Acetals are commonly used aldehyde and ketone protecting groups in organic synthesis as they can be hydrolysed under acidic conditions.⁷⁷ Their structure is the diether form of geminal diols. Historically the name acetal referred specifically to diethers derived from aldehydes, and ketals was the term for the ketone derivative. However, acetal now refers to both types of geminal diether.⁷⁸

Acetals can be synthesised by the nucleophilic addition of alcohols to an aldehyde or ketone. This produces water which requires removal from the reaction mixture to drive the equilibrium towards acetal formation. Techniques for the removal of formed water include azeotropic distillation with a Dean-Stark apparatus or the use of water scavenging species such as triethyl orthoformate, boron trifluoride-etherate, hydrogen chloride or molecular sieves.^{79,80}

The reaction mechanism proceeds by nucleophilic addition of an alcohol a protonated carbonyl group (Scheme 1-9). Subsequent proton transfer forms a tetrahedral hemiacetal intermediate.

Elimination of water yields an oxonium ion that undergoes a second nucleophilic addition of alcohol and subsequent proton transfer to form an acetal. The formation of the hemiacetal can be performed under basic conditions, but no further reaction takes place as the OH group cannot be turned into a suitable leaving group. Therefore, synthesis of acetals by this route requires acid catalysis to enable the elimination of water.⁷⁷



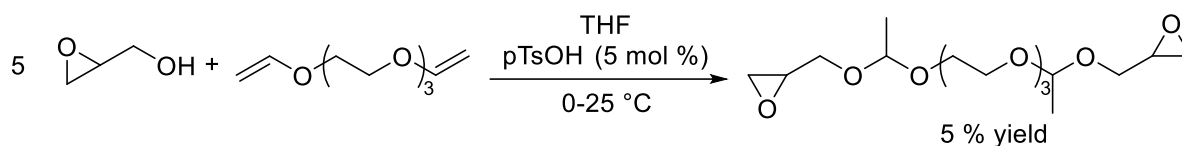
Scheme 1-9 – Acetal synthesis reaction mechanism.

Other synthetic routes to acetals include transacetalisation of an acetal with another alcohol or an aldehyde or ketone with another acetal under acidic conditions.⁸⁰ This is particularly useful for the synthesis of ketone derived acetals, for which the reaction with an alcohol gives poor results.⁸⁰ It is also possible to synthesise mixtures of acetals by an acid-catalysed metathesis reaction between two or more acetals.⁸¹

Acetals can also be synthesised from an alcohol and vinyl ether under acidic conditions and hemiacetal esters *via* the acid-catalysed reaction between a carboxylic acid and vinyl ether.^{1,82,83} This reaction is favourable to those previously mentioned as it does not require the removal of a by-product to drive the reaction to completion and does not produce a mixture of products as with transacetalisation and acetal metathesis methodologies. However, it is limited by the availability of vinyl ethers, specifically divinyl ethers that are required to synthesise monomers bearing multiple polymerizable groups that can serve as chemical cross-links between polymer chains in thermosets. At the time of writing 1,4-butanediol divinyl ether,⁸⁴ 1,4-cyclohexanedimethanol divinyl ether (mixture of isomers),⁸⁵ di(ethylene glycol)

divinyl ether,⁸⁶ poly(ethylene glycol)divinyl ether (M_n 250)⁸⁷ and tri(ethylene glycol)divinyl ether are commercially available,⁸⁸ though there are examples of laboratory scale preparations of novel divinyl ethers *via* a variety of synthetic methodologies.^{89–92}

Nasanit *et al.* synthesised a diepoxy cross-linker from glycidol and tri(ethylene glycol) divinyl ether, however, the yield was 5 % (Scheme 1-10).⁹³ If the low yield can be improved this could provide a synthetic route to meth(acrylate) cross-linkers with cleavable acetal groups by reaction with hydroxyl functionalised monomers such as 2-hydroxyethyl methacrylate and 2-hydroxyethyl acrylates; this is the focus of Chapter 2.

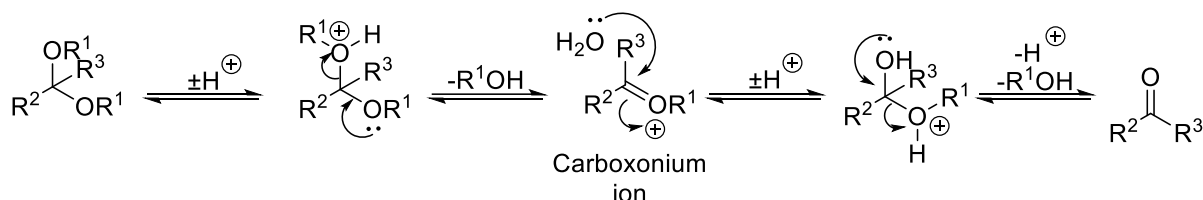


Scheme 1-10 - Synthesis of acetal containing diepoxy cross-linker.⁹³

1.4.1. Acetal stability

It is hypothesised that hydrolysis of acetal groups in cross-links will impart methacrylate thermosets with degradable properties. An understanding of hydrolysis conditions and any structure-property relationships is therefore important. Acetals are stable under basic conditions but undergo hydrolysis in acidic media to form an alcohol and aldehyde or ketone.⁹⁴⁻⁹⁶

Under acidic conditions the acetal oxygen is protonated and subsequently eliminated as an alcohol, forming a carboxonium ion, this is generally rate determining step (Scheme 1-11).⁹⁵ Nucleophilic addition of water forms a hemiacetal which undergoes the same series of reactions to form an aldehyde and two alcohols^{94,96}



Scheme 1-11 - Acetal hydrolysis mechanism.

The specific substituents R^1 , R^2 and R^3 all effect the stability of the intermediate carboxonium ion and therefore the rate of hydrolysis. Liu and Thayumanavan published a comprehensive study of the effect different substituents have on hydrolytic stability of 18 acetal-containing compounds.⁹⁶ They performed hydrolysis experiments in CD_3CN/D_2O /phosphate buffer solutions at pH 5 and monitored them *via in situ* 1H NMR spectroscopy. Several trends were observed. Increasing the distance between R^1 and an electron withdrawing amide group increased the half-life ($t_{1/2}$). The effect of increasing CH_3 substitution at R^2 and R^3 was probed; hydrolysis at pH 5 was only observed when R^2 and $R^3 = CH_3$, due to the electron donating effect of the CH_3 stabilising the carboxonium ion. Acyclic acetals were less stable than 5-membered cyclic acetals, which were then less stable than 6-membered cyclic acetals. Lastly, upon decreasing the pH from 7.4 to 5, the $t_{1/2}$ was found to decrease by two orders of magnitude.

Bulmus *et al.* monitored the hydrolysis of the acetal groups in their benzaldehyde derived cross-linkers *via* UV-spectroscopy in DMF at 37 °C using buffers to maintain solution pH at 4.5, 5.5, 6.5 and 7.4. They found that all cross-linkers were stable at pH 7.4 over 20 hrs. and had $t_{1/2} < 60$ minutes when at pH 5.5. Cross-linkers synthesised from 4-hydroxybenzaldehyde had shorter half-lives than those synthesised from 4-methoxybenzaldehyde due to the electron donating nature of the methoxy group stabilising the carboxonium intermediate.⁹⁷ In summary, electron-donating substituents (R¹, R², R³, Scheme 1-11) will stabilise the carboxonium ion giving rise to faster hydrolysis, meaning there is scope to tune the hydrolysis properties of acetal cross-linkers to an industrially-useful timeframe.

1.4.2. Acetals in Polymer Chemistry

Acetals have been used in a variety of polymer systems as a pH responsive functional group, including drug delivery,⁹⁸ thermoplastics,⁸³ thermosets,¹ and CANs.^{70-76,99-101} Their use in acrylate/methacrylate cross-linkers is covered in Chapter 2, degradable thermosets in Chapter 3 and CANs in Chapter 5. The acetal group is particularly desirable in polymer networks as it is both dynamic and acid degradable. This enables networks to be recycled *via* mechanical and chemical routes. Furthermore, Ma and co-workers have shown that polymeric hydrolysis products containing alcohol groups can be collected and cross-linked *via* reaction with divinyl ethers to yield materials with properties similar to that of the virgin material.^{70,71,99,101}

1.5. Green chemistry & sustainable synthesis metrics

The driving force behind this PhD research is tackling thermosets and their composite's contribution to the global pollution problem. However, designing for degradation is just one of twelve green chemistry principles, first proposed by Anastas and Warner, that chemists can use to design green processes and products.¹⁰² A formal definition of Green Chemistry is the "design of chemical products and processes to reduce or eliminate the use and generation of hazardous substances."^{102,103}

The twelve principles are as follows:^{102,104–106}

1. Prevention of waste – prevention of waste is better than treating waste
2. Atom economy – incorporation of starting materials into products should be maximised
3. Safe synthesis – substances used and produced in syntheses should pose as little toxicity to humans and the environment as possible
4. Safer chemicals – products should maximise function while minimising toxicity
5. Safer solvents and auxiliaries – substances that are used but not incorporated into the final product should either be eliminated from the process or made innocuous
6. Energy efficiency – Energy requirements of chemical processes should be recognised for their environmental and economic impacts and should be minimised. If possible, synthetic methods should be conducted at ambient temperature and pressure
7. Renewable feedstocks – Starting materials and other reagents should be renewable rather than depleting whenever technically and economically practicable
8. Fewer derivatives – The use of derivatisation in a process should be minimised or avoided if possible
9. Catalysis – Catalysts are favourable over stoichiometric reagents and may be recovered and reused
10. Design for degradation – Products should degrade into innocuous by-products in the environment or reusable components for collection

11. Real-time analysis – Real-time monitoring and control of processes can prevent the formation of hazardous substances

12. Safer chemistry for accident prevention – Substances and their form should be chosen to minimise the potential and consequences of chemical accidents

Winterton has added a further twelve principles¹⁰⁵, while Anastas and Zimmerman developed the twelve principles of green engineering.¹⁰⁷ However, quantitatively and qualitatively measuring the greenness of chemical processes is challenging as these are only guidelines.

Some techniques such as life cycle assessment determine a product or process' environmental impact from cradle to grave but require vast amounts of data. This can make the process costly and slow, although there are hybrid systems that look at specific parts of the lifecycle or have lower specificity. However, there are simple metrics available to the synthetic chemist. Three easily calculated metrics are atom economy, E factor, and process mass intensity. Although these do not measure the environmental impact of waste or economic viability of syntheses, they can provide insight into the efficiency and wastefulness of a process.^{106,108}

Atom economy measures the percentage of the reactants incorporated into the product, where a reactant is any building block that forms part of an intermediate or is incorporated into the final product. The atom economy is then calculated using the following equation:

Equation 1-1

atom economy (%)

$$= \frac{\text{molecular weight of product}}{\text{sum of molecular weights of starting materials and byproducts}} \times 100$$

A high atom economy indicates a high amount of incorporation of starting materials in the product. However, the atom economy does not consider the amount of waste generated throughout a process. Therefore, processes with 100% atom economy can be highly wasteful in their use of auxiliaries or through achieving low conversion and selectivity.^{109,110} The E factor

quantifies the amount of waste produced in a chemical process. The ideal E factor is zero. As waste is undesirable in terms of sustainability it provides a more complete quantitative analysis of a process' greenness. E factor is calculated using the following equation:^{108,111,112}

Equation 1-2

$$E \text{ factor} = \frac{\text{mass of waste}}{\text{mass of product}}$$

Lastly, the process mass intensity considers the mass of all materials used in a process that is omitted in the calculation of E factor such as solvent, silica during purification and desiccants during drying. It is calculated using the following equation:

Equation 1-3

$$\text{process mass index} = \frac{\text{Mass used in process}}{\text{Mass of product}}$$

The metrics and twelve principles will be used to guide and quantify the greenness of dimethacrylate acetal containing cross-linkers synthesised in Chapter 2.

1.6. Acid Generators

Acid generators, sometimes referred to as latent acids, is a collective term for molecules that generate an acid upon exposure to an external stimulus such as light, heat or mechanical force. They are often given a prefix relating to the stimuli they respond to such as photoacid, thermal acid or mechanoacid generator; the latter is a relatively new type of acid generator.^{113–115} Within the context of this research they will be investigated as latent degradation and dynamic bond exchange catalysts. Much of the founding work in the field was related to photolithography and utilising the spatial control they give to selectively cleave acid sensitive polymers.^{116,117} Subsequently they have been applied to degradable thermosets¹¹⁸, as latent catalysts in adaptable networks,^{67,119–121} and as latent initiators in acid catalysed polymerisations.^{122,123} Their proposed role in this research is as latent hydrolysis catalysts within degradable thermosets and latent exchange catalysts in adaptable networks. A brief overview of acid generator development, example chemistries, current state of the art and their application in degradable thermosets and CANs will now be given. For more in depth reviews see Shirai and Masahiro¹¹⁶, Martin *et al.*¹²⁴, Zivic *et al.*¹¹⁷ and Tsuchimura.¹²⁵

Early photoacid generators were ionic; such as aryldiazonium, diaryliodonium, triarylsulfonium and triarylphosphonium salts, utilising metal halide counter ions such as BF_4^- , SbF_6^- , AsF_6^- and PF_6^- (Figure 1-3). Upon irradiation with light of a suitable wavelength (200-300 nm), these salts undergo photolysis liberating a free acid. The wavelength of light required can be tuned by incorporating different functionality to the onium component. Onium salts have high thermal stabilities, however, they have low solubilities in organic solvents.^{116,117}

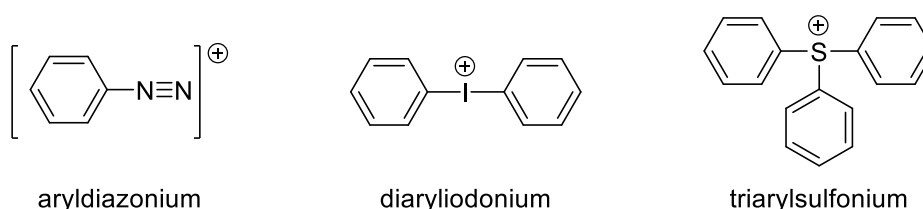
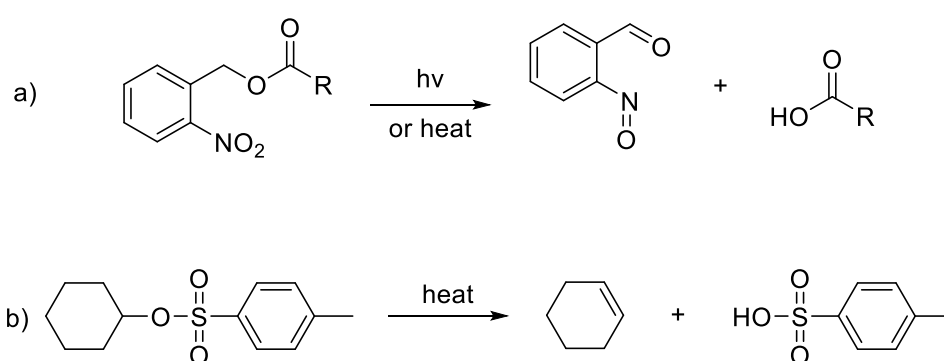


Figure 1-3 - Examples of onium ions used in ionic acid generators.

Alternative non-ionic acid generators were subsequently developed to circumnavigate the low solubility of ionic acid generators. Two categories of ionic acid generators exist, those that require hydrogen donors to generate acids and those that generate acids *via* a unimolecular process. The former includes *para*-nitrobenzyl sulfonates, sulfones, disulfones, *N*-hydroxyimide sulfonates, phenolic sulfonates, diazonaphthoquinones, and imino sulfonates.^{116,125} As the required acid generator will be present in a polymer matrix, the latter type is favoured for simple acid generation. This criterion limits the pool of available acid generators to *ortho*-nitrobenzyl esters and sulfonate esters (Scheme 1-12).



Scheme 1-12 - Nonionic acid generators a) *ortho*-nitrobenzyl esters and an example of a sulfonate b) cyclohexyl tosylate.

Ortho-nitrobenzyl esters of carboxylic and sulfonic acids are thermal and photoacid generators.^{126,127} Upon irradiation with ultraviolet light they undergo a free radical reaction pathway, proceeding *via* the abstraction of a benzylic hydrogen atom *via* a nitro group oxygen atom followed by rearrangement and subsequent elimination of an acid, yielding a nitrosoaldehyde.¹¹⁶ A complication of using light to drive the acid generation within polymer matrices is significant absorption of light by the matrix. To avoid this, the wavelength of light required to drive photolysis can be tuned by substitution on the aromatic ring and acid group.^{126,128} *Ortho*-nitrobenzyl esters are also known to undergo thermal elimination, the temperature of which is controlled by substituent effect. Interestingly the thermolysis temperature has been found to vary within polymer matrices versus the neat acid generator.¹²⁹ Lastly, the syntheses of *ortho*-nitrobenzyl esters is easily achieved *via* the reaction between *ortho*-nitrobenzyl alcohols and acid chlorides.^{127,130}

Sulfonates are known thermal acid generators that undergo an intramolecular elimination reaction to produce an alkene and sulfonic acid.¹³¹ The temperature of acid generation is dependent on substituents enabling the facile synthesis of acid generators with a range of thermolysis temperatures.^{122,123,132,133} Sulfonate acid generators are covered in greater detail in Chapter 4.

Shirai *et. al* have published several examples where thermoset degradation is induced by a photoacid generator (PAG).^{118,134–138} Four (meth)acrylate cross-linkers bearing acetal linkages were synthesised (Figure 1-4). A photo or thermal radical initiator was used to make polymer films. The acetal linkages in films were found to be stable up to 180-240 °C. Films doped with the PAG *N*-hydroxynaphthalimide triflate (NITf) (1 wt%) were irradiated with UV light (366 nm), generating triflic acid, and heated at 100 °C for 10 minutes, after which films were soluble in THF, indicating the degradation of cross-links.¹³⁸ Further work with these monomers, and alternative triflic acid generators, found post baking was not required and films became soluble in methanol upon UV irradiation.¹³⁶ Shirai *et. al* published further work with trifunctional methacrylate acetal cross-linkers that degraded upon acid generation.¹³⁵

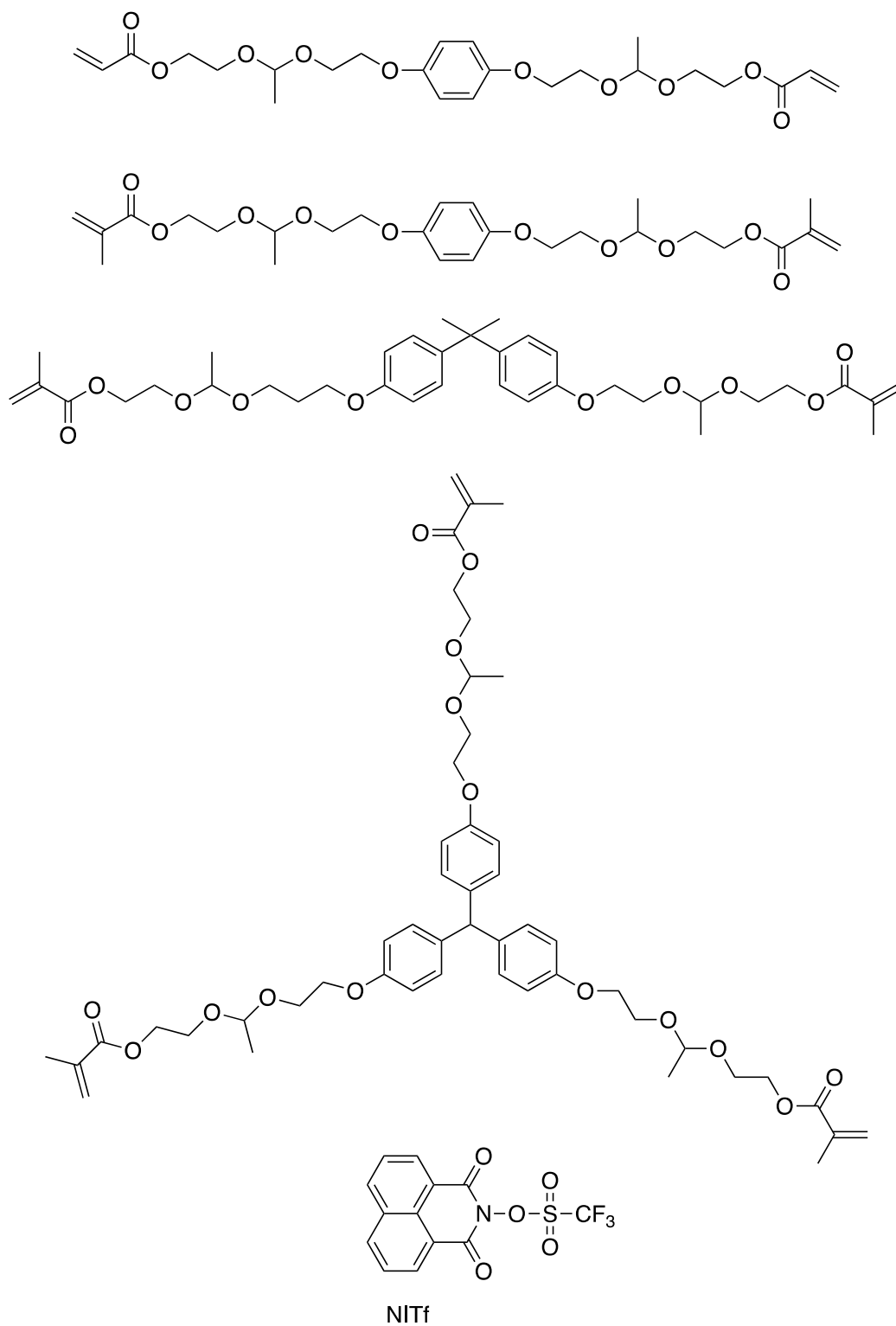
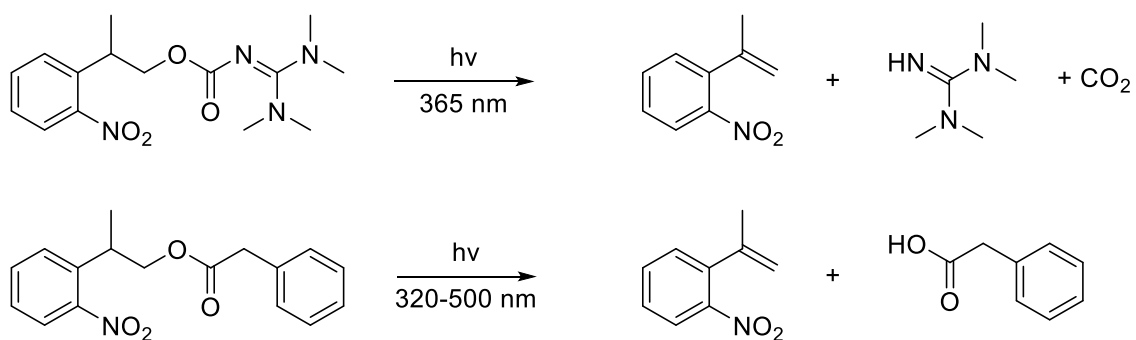


Figure 1-4 - Acrylate and methacrylate cross-linkers possessing acetal links and the acid generator NITf used to catalyse their hydrolysis.

Acid generators have been used to impart CANs with irreversible changes to their dynamic behaviour *via* catalysis. The first example of this methodology was reported by Worrell *et al.* who used photobase generators in thioester/thiol dynamic chemistry-based CANs, whereby

irradiation with light caused an irreversible phase change in the CAN from solid to liquid (Scheme 1-13). Unlike previous CAN systems removal of the stimulus did not return the material to its original state. Furthermore, the spatial control offered by using light as a stimulus enabled them to create distinct regions within the CAN in different physical states. The authors then synthesised networks containing both photoacid and photobase generators, that underwent photolysis at different wavelengths of light. Generation of acid neutralised any free base halting the dynamic bond exchange and returning the network to a solid state.⁶⁷ Schlögl and co-workers have reported further the use of photoacid in thiol-acrylate¹²¹ and photobase generators in thiol-epoxy based CANs^{119,120} to control the rate of bond exchange and therefore the stress-relaxation properties of the networks.



Scheme 1-13 - Photobase and photoacids used by Worrell et al. to impart CANs with lockable phase change behaviour.

1.7. Research Aims

Despite offering excellent mechanical properties, thermosets infusibility and insolubility hinder their recyclability and as legislation on the use and recycling of plastics may ban traditional thermosets, solutions must be found as they are essential to modern life. There are many literature examples of degradable thermosets, however, many require complicated syntheses of novel monomers, post-polymerisation functionalisation and undergo a step-growth type curing mechanism.

The research aims of this project are to assess the viability of acetal chemistry for use in methacrylate-based thermosets that are pH degradable. Methacrylate-based thermosets are of particular interest to Scott Bader, the industrial funders of this research. Their adhesives, coatings and composite product ranges utilise free radical curing techniques that are compatible with methacrylate-based thermosets. Introducing end-of-life recycling options to their product range is of the utmost importance to the business and acetal containing thermosets are hypothesised to enable this.

To achieve this acetal containing cross-linkers will be synthesised from a divinyl ether and hydroxyl functionalised methacrylate, then scaled up to allow characterisation of their degradation and mechanical properties. Furthermore, acetals undergo dynamic exchange reactions and impart networks with adaptable behaviour which will be investigated. Lastly, it is hypothesised that acid generators can be added to acetal containing networks to give hydrolysis on demand properties.

Chapter 2 – Synthesis and Characterisation of Dimethacrylate Acetal Cross-Linker

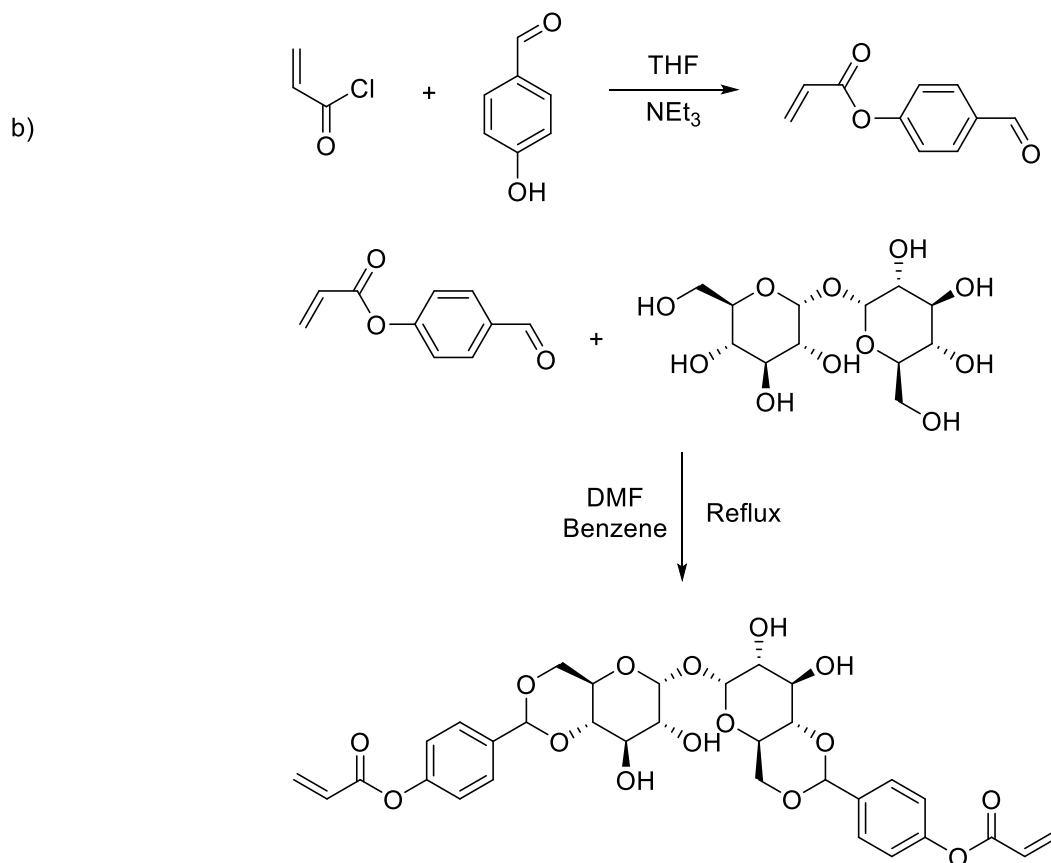
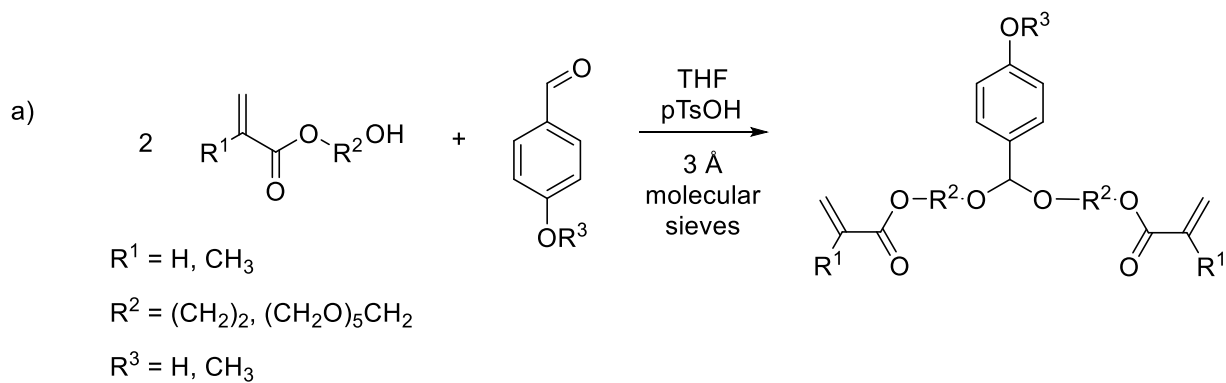
2.1. Introduction

As previously discussed, the starting materials for acetals are an alcohol, a nucleophile, and an electrophile such as an aldehyde, ketone or vinyl ether. Within an industrial context it is desirable for starting materials to be commodity chemicals as these will have an established supply chain and appropriate regulatory status allowing their use. Furthermore, from an industrial and sustainability point of view, multistep reactions are undesirable. Therefore, searching for synthetic routes to methacrylate or acrylate-based acetal cross-linkers was limited to the following nucleophile/electrophile pairs: (meth)acrylates bearing an alcohol and a multifunctional aldehyde, ketone or vinyl ether. Alternatively, the pair could be reversed to meth(acrylates) bearing an aldehyde, ketone or vinyl ether and a diol. Unfortunately in the latter scenario no vinyl ether bearing (meth)acrylates are commercially available and in both scenarios the high temperatures required to synthesise acetals from alcohols and ketones or aldehydes are likely to lead to thermally initiated homopolymerisation of (meth)acrylates.^{139–}
¹⁴¹ Therefore, a route using an alcohol bearing (meth)acrylate and divinyl ether is desirable.

There are few examples of (meth)acrylate cross-linkers containing acetal functional groups in the literature. The majority of examples of degradable thermosets based upon acetal chemistry are epoxy resin materials.^{1,142} Fortunately, acetal chemistry has been utilised in stimuli responsive hydrogels and pH degradable polymers for drug delivery, of these examples all are synthesised from an alcohol and aldehyde or by transacetalisation based syntheses.^{143,144}

Bulmus *et al.* synthesised a library of acetal containing methacrylates and acrylates by the reaction of 2-hydroxyethyl methacrylate (HEMA), 2-hydroxyethyl acrylate and poly(ethylene glycol methacrylate) with 4-methoxybenzaldehyde or 4-hydroxybenzaldehyde (Scheme

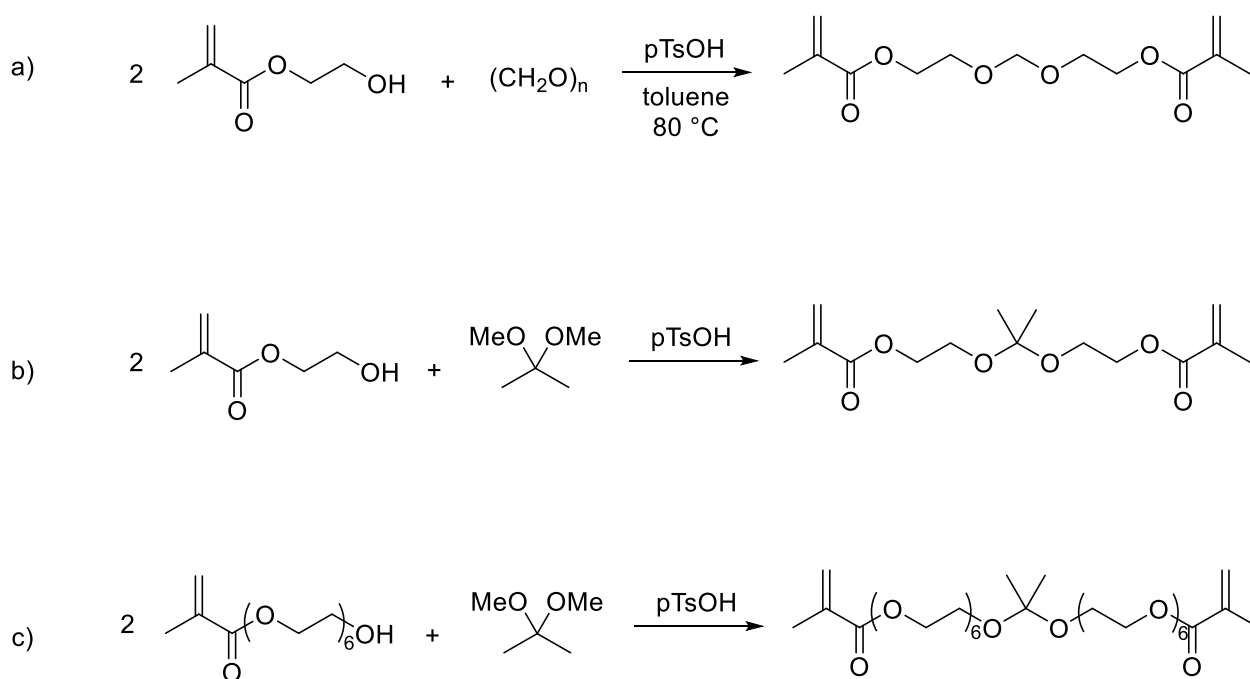
2-1a).^{97,145} Reactions were stirred at 0 °C for 15 hrs using *para*-toluenesulfonic acid (pTsOH) as an acid catalyst and 3 Å molecular sieves as a water trapping agent. Purification was performed *via* basic alumina column chromatography producing the acetals in the yields ranging between 30–70%. Burek *et al.* synthesised a diacrylate cross-linker by a two-step synthetic procedure (Scheme 2-1b).¹⁴⁶ Firstly, acryloyl chloride was reacted with 4-hydroxybenzaldehyde to give an aldehyde functional monomer. The crude product was purified *via* vacuum distillation, and isolated with 81% yield. The aldehyde group was then reacted with trehalose to yield a diacrylate cross-linker bearing two cyclic acetal groups *via* refluxing in DMF and benzene for 16 hrs; water was removed *via* azeotropic distillation. The purification process involved repeated dissolution and precipitation from ethyl acetate and hexane to yield the monomer in 41% yield. Both 4-hydroxybenzaldehyde and trehalose can be sourced from renewable feedstocks.



Scheme 2-1 - Existing synthetic routes to (meth)acrylate cross-linkers containing acetals via reaction of an alcohol and aldehyde by a) Bulmus *et al.* and b) Burek *et al.*^{97,145}

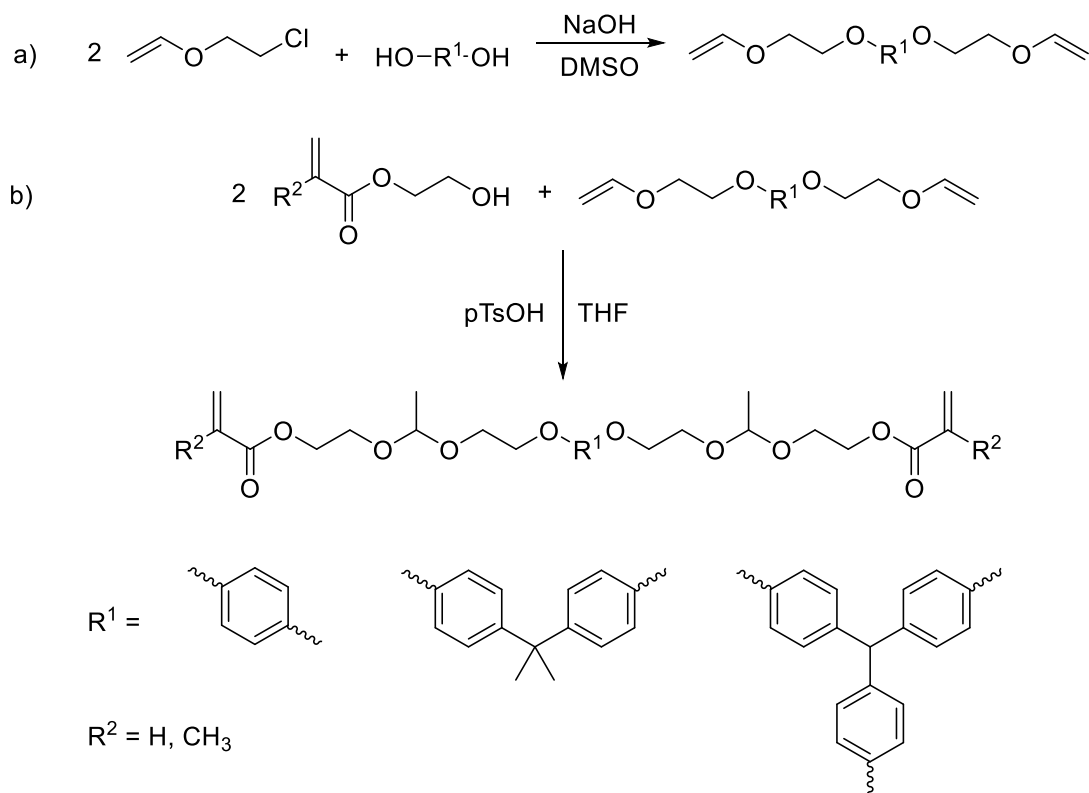
Further examples of dimethacrylate cross-linkers bearing one acetal group were synthesised by Themistou and Patrickios,¹⁴⁸ Heath *et al.*,¹⁴⁹ and Kim *et al.*¹⁵⁰ all *via* transacetalisation reactions (Scheme 2-2). Themistou and Patrickios reacted HEMA with paraformaldehyde using pTsOH as a catalyst in toluene at 80 °C. The crude product was purified *via* column chromatography to give the dimethacrylate with a yield of 15%, which was then further distilled prior to use (Scheme 2-2a). Heath *et al.* prepared a dimethacrylate by the reaction of HEMA

with 2,2-dimethoxypropane using pTsOH as a catalyst in benzene to enable the azeotropic removal of methanol; no yields or purification procedures were reported (Scheme 2-2b). Lastly, Kim *et al.* synthesised a similar dimethacrylate using poly(ethylene glycol) methacrylate (n=6) and 2,2-dimethoxypropane (Scheme 2-2c). Again, pTsOH was the catalyst, however, THF was the solvent and instead of azeotropic distillation, methanol was collected using molecular sieves. No further purification or the yield were described.



Scheme 2-2 - Synthetic routes to (meth)acrylates containing acetal functional groups via transacetalisation.¹⁴⁸⁻¹⁵⁰

Lastly, only one synthetic route to (meth)acrylate cross-linkers utilising the reaction between an alcohol and vinyl ether could be found in the literature (Scheme 2-3). Shirai *et al.* performed a two-step synthetic procedure first reacting a series of aromatic diols with 2-chloroethyl vinyl ether catalysed by NaOH in dimethyl sulfoxide (DMSO) at 75 °C for 14.5 hrs (Scheme 2-3a). The resultant vinyl ethers were purified *via* recrystallisation, or column chromatography when R¹ was the triphenyl group, producing a series of divinyl ethers with yields ranging from 46–79 %. The divinyl ethers were reacted with HEMA or 2-hydroxyethyl acrylate using pTsOH as a catalyst in THF for 25 hours at 0–5 °C (Scheme 2-3b). The monomers were purified *via* column chromatography and isolated in yields ranging 41–72 %.^{118,151}



Scheme 2-3 - Synthetic routes to meth(acrylate) cross-linker containing acetal functional group via reaction of vinyl ether and alcohol.¹¹⁸

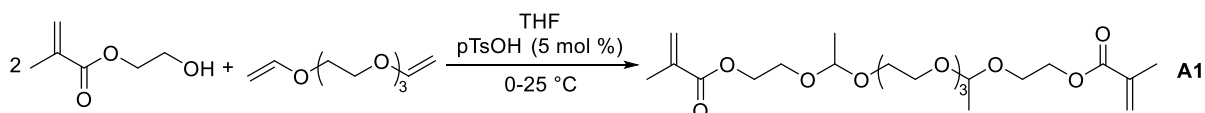
It is clear from the literature a variety of acetals with different substituents can be made, meaning there is scope for tuning their hydrolytic behaviours to those required for degradable thermosets. However, the examples discussed require elevated temperatures, multiple steps or produce waste products such as MeOH or HCl that require removal. Within this chapter research was undertaken to develop a simple synthetic methodology for a dimethacrylate cross-linker containing acetal groups from commercially available starting materials and to characterise its hydrolysis products to guide its application in degradable thermosets.

2.2. Results and Discussion

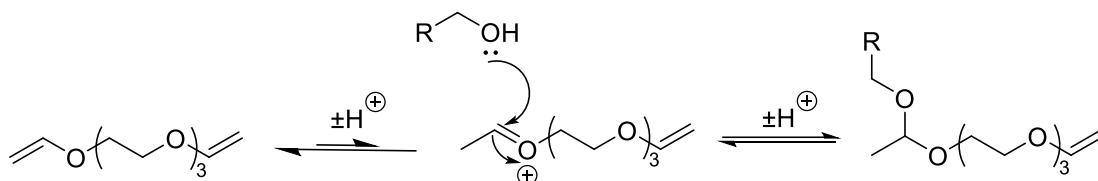
2.2.1. Synthesis of Acetal Cross Linker & Hydrolysis Experiments

2.2.1.1. Synthesis of Acetal Bearing Dimethacrylate Cross-Linker A1

A methacrylate cross-linker bearing two acetal functional groups (A1) was synthesised from tri(ethylene glycol) divinyl ether (TEGDVE) and HEMA using pTsOH as a catalyst (Scheme 2-4) in a process adapted from Nasanit *et al*, by replacing the glycidol with HEMA.⁹³ The proposed mechanism proceeds *via* vinyl ether tautomerisation to an electrophilic oxonium ion and nucleophilic addition by an alcohol followed by proton exchange to yield an acetal (Scheme 2-5).⁷⁷ Thin layer chromatography (TLC) confirmed the reaction was complete in 6 h and the ¹H NMR spectrum of the crude product showed no residual vinyl ether groups were present, suggesting complete formation of the diacetal product. A1 was purified *via* column chromatography and isolated in 75% yield. ¹H NMR spectroscopy revealed the molar ratio of ethylene bridge protons was higher than expected, due to an oligomerisation side reaction (discussed in detail in section 2.2.2.2).



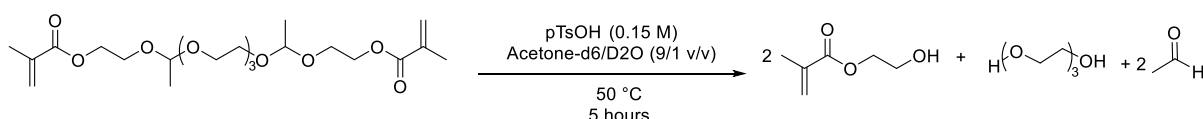
Scheme 2-4 - Synthesis of acetal cross linker.



Scheme 2-5 - Reaction mechanism of acetal formation *via* reaction of alcohol and divinyl ether.

2.2.1.2. Hydrolysis of A1

The acetal groups of A1 were hypothesised to impart acid-degradable behaviour to A1 cross-linked networks by acting as cleavage point between chains. Therefore, an understanding of the hydrolysis behaviour of A1 was required. The hydrolysis kinetics are important as they will contribute to the stability of A1 cross-linked networks and how easily they are removed when desired. Additionally, the hydrolysis products may become environmental pollutants meaning their identification is paramount to understanding the consequences of their release. A1 was added to a 0.15 M solution of pTsOH in acetone-d₆/D₂O (9/1 v/v) and stirred at 50 °C for 5 hrs. (Scheme 2-6), these conditions were selected based on acetal containing epoxy thermoset degradation experiments in the literature where the solvent/water ratio was kept high to maintain product solubility.¹⁵²



Scheme 2-6 - Hydrolysis of A1, yielding HEMA, tri(ethylene glycol) and acetaldehyde.

Comparison of the ¹H NMR spectra of A1 with that of the reaction mixture after 5 hrs. revealed quantitative hydrolysis of the acetal groups, as determined by the disappearance of the CH and CH₃ resonances at 4.80 (m, 2H) and 1.31 (m, 6H) ppm, respectively (Figure 2-1). The literature on acetal hydrolysis states the products should be an alcohol and an aldehyde or ketone.⁹⁴ A1 is unusual as it is an asymmetric acetal, the ether groups on either side are different, often a feature of acetals synthesised from a vinyl ether and alcohol.⁷⁰ It was hypothesised that the hydrolysis of A1 would produce HEMA, tri(ethylene glycol) (TEG) and acetaldehyde. Analysis of the ¹H NMR spectrum of the hydrolysis reaction mixture confirmed the formation of acetaldehyde by the emergence of CH₃C(O)H and CH₃C(O)H peaks at 9.61 (S, 1H) and 2.01 (M, 3 H) ppm, respectively (Figure 2-1). However, the molar ratios of these peaks were lower than expected, this was attributed to acetaldehyde's low boiling point, high volatility, and ability to form hydrates causing difficulty in measurements.¹⁵³

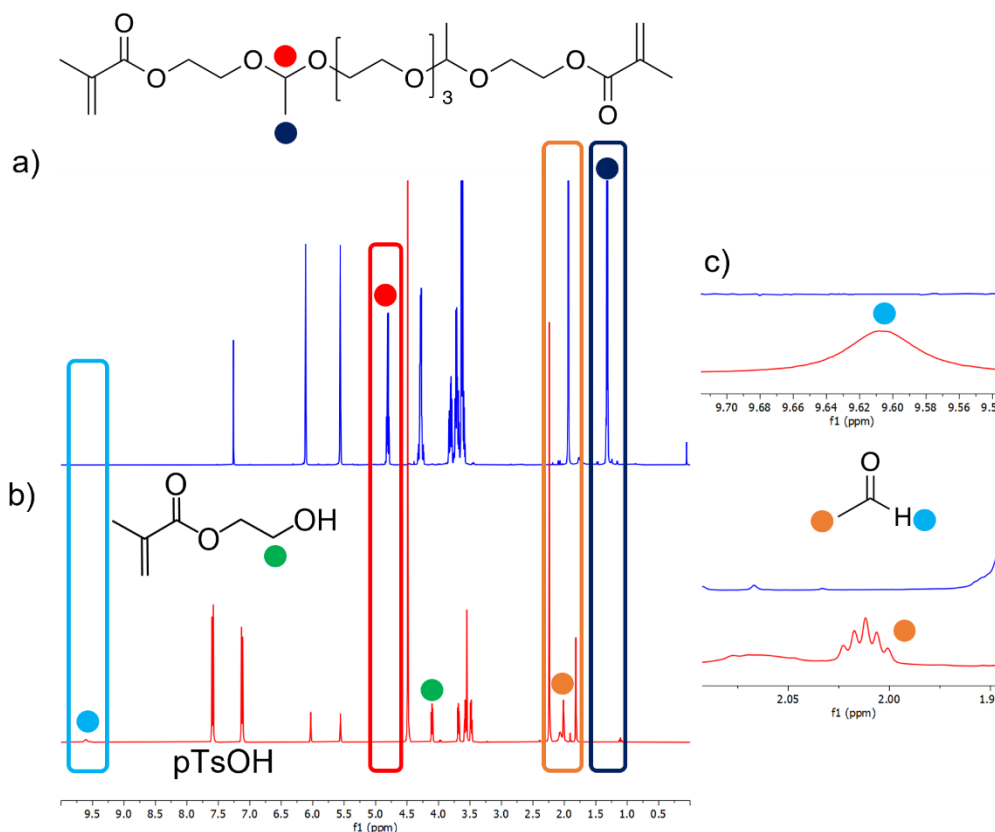


Figure 2-1 - ¹H NMR (CDCl₃) spectra of A1 a), b) A1 hydrolysis reaction mixture showing formation of HEMA and c) magnified peaks from hydrolysis spectra showing acetaldehyde after six hours at 50 °C.

The spectra also showed a shift in the alkene CH peak at 6.11 ppm to 6.03 ppm suggesting the formation of a different methacrylate. The bridging CH₂ peaks in the region 4.25–3.25 ppm were assigned to those in HEMA and TEG but could not be assigned individually due to the similarity in the proton environments. The reaction mixture was also characterised by high pressure liquid chromatography mass spectroscopy (HPLC-MS) which confirmed acetaldehyde, HEMA and TEG were the hydrolysis products (Appendices Figure 8-1).

2.2.1.3. Effect of pK_a on Hydrolytic Stability

With the hydrolysis products of A1 determined, its hydrolytic stability with different strength acids was investigated. As before, hydrolysis experiments were conducted in 0.15 M acid acetone-d₆/D₂O (9/1 v/v) solutions at 50 °C for 5 hrs. Due to the experiments being conducted in organic media, pH could not be used to study the hydrolytic stability, as this is specific to water.¹⁵⁴ The pK_a of various acids in water was used as an empirical measure of acid strength,

as this changes with solvent,¹⁵⁴ to aid with acid selection. pK_a is the negative log of the equilibrium constant of an acid and its conjugate base; lower values indicate a more dissociated and, therefore, stronger acid.¹⁵⁴

It was hypothesised that decreasing pK_a would affect the observed hydrolytic stability of A1. The strength of an acid depends upon the stability of its conjugate base and the HA bond strength. A strong acid may have a stable conjugate base and weak HA bond. Lastly the solvent's ability to stabilise the ions formed upon dissociation is also important.¹⁵⁴ A series of structurally similar acids with pK_a values greater than that of pTsOH (pK_a -2.8)¹⁵⁵ were sought to probe the hydrolytic stability of A1. A variety of sulfonic and carboxylic acids spanning a pK_a range from -2.8 to 4.8 were compiled (Figure 2-2).¹⁵⁶ Notably, only the sulfonic acids had pK_a values below 0. Three series were identified mono, di, and trichloroacetic acid, 2- and 3-furoic acid and 2-, 3-, and 4-nitrobenzoic acid. Of these, monochloroacetic (MCA), dichloroacetic (DCA) and trichloroacetic (TCA), as well as trifluoroacetic (TFA) acid were chosen due to their cost and pK_a values, 2.86, 1.29, 0.65 and 0.23 respectively. pK_a decreases with increasing chlorine substitution in the α position in the chloroacetic acid series, due to the increase in electronegativity weakening the O-H bond *via* the inductive effect. This is also true when comparing TCA and TFA, the CF_3 group is more electronegative weakening the O-H bond.¹⁵⁷

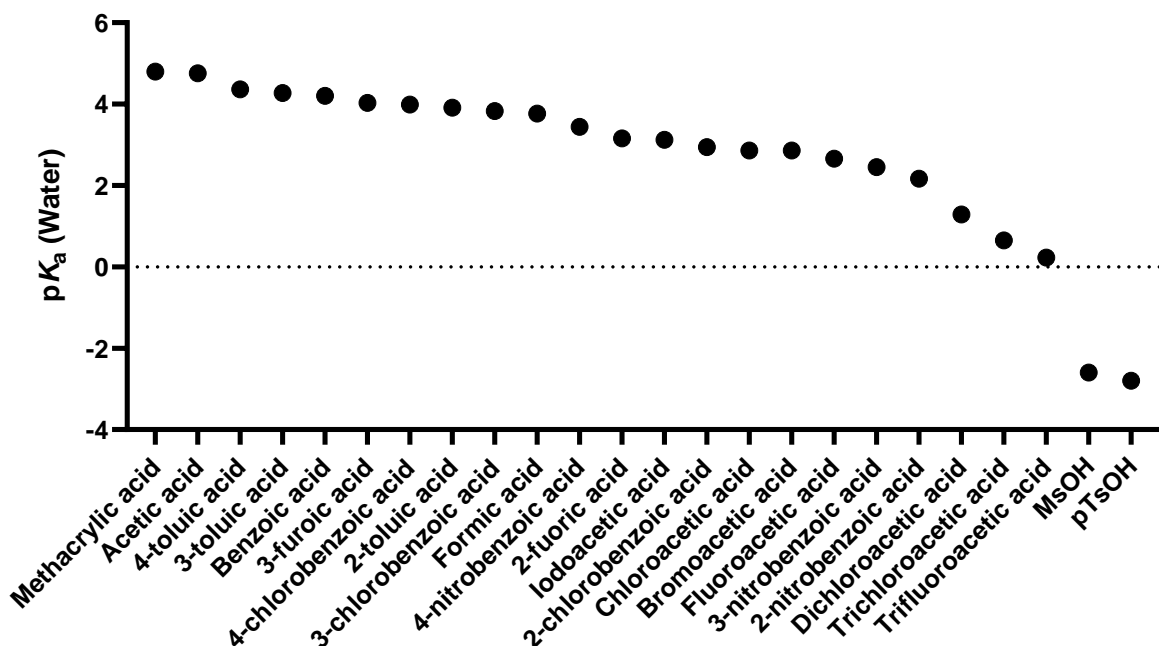
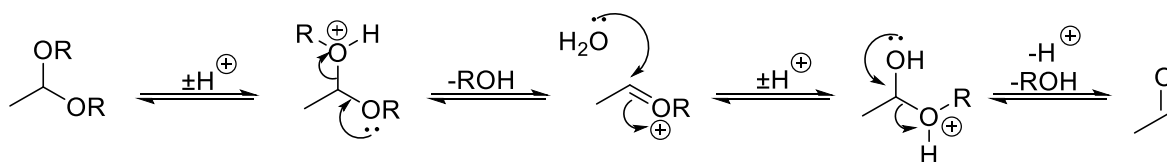


Figure 2-2 - pK_a of carboxylic and sulfonic acids in H₂O.

Acetals are generally stable at basic and neutral pH, but at pH <7 hydrolysis occurs.⁹⁶ Under these acidic conditions the weakly basic acetal oxygen is protonated and subsequently eliminated forming an oxonium ion, this is typically, but not always, the rate determining step (sScheme 2-7).⁹⁵ Nucleophilic addition of water forms a hemiacetal which undergoes the same series of reactions to form an aldehyde and two alcohols^{94,96} pK_a is the pH at which the concentration of acid and its conjugate base are equal,¹⁵⁴ the greater concentration of hydronium ions mean lower pK_a acids should give a greater extent of hydrolysis if the concentrations and time are kept constant. Therefore, it was expected the extent of hydrolysis of A1 would increase in the order MCA, DCA, TCA and TFA.



Scheme 2-7 - Mechanism of acetal hydrolysis.

Table 2-1 - Effect of acid pK_a on the extent of A1 hydrolysis in acetone- d_6 /D $_2$ O (9/1 v/v) at 50 °C for 5 hrs.

Acid	pK_a	Hydrolysed (%) ^a
Monochloroacetic acid	2.86	2
Dichloroacetic acid	1.29	62
Trichloroacetic acid	0.65	100
Trifluoroacetic acid	0.23	100

^aDetermined via 1H NMR spectroscopy

Table 2-1 summarises the extent of A1 hydrolysis after 5 hrs. at 50 °C for the acids MCA, DCA, TCA and TFA. As expected lower pK_a values led to quantitative hydrolysis determined by 1H NMR spectroscopy. It was thought the greater extent of hydrolysis was due to greater acid dissociation giving rise to a higher concentration of hydronium ions capable of catalysing A1 hydrolysis. A1 in solutions of the weaker acids MCA and DCA was only partially hydrolysed, 2 and 62 % respectively. Upon leaving the MCA and DCA samples for 48 hrs at 50 °C the extent of hydrolysis increased to 86 and 31% respectively. This suggests a $pK_a < 1.29$ is desired if A1 hydrolysis is to occur within a useful timeframe, that will vary depending on application.⁷

2.2.2. Optimisation and Scale Up of A1 Synthesis

To further characterise the degradation properties and prepare samples for mechanical testing, large batches of A1 were required to minimise batch-to-batch variation and reduce the time spent repeating small scale syntheses. Furthermore, the scalability of the process is industrially and environmentally relevant. As the application of A1 to thermoset chemistry aims to contribute positively to sustainability, so should the synthetic procedure. To achieve this the synthesis of A1 was scaled up and optimised using the twelve principles of green chemistry, proposed by Anastas and Warner, as a framework for improving the process.¹⁰⁴ Particularly the prevention of waste and using less hazardous materials, safer solvents and catalysis.

Preparation of A1 makes excellent use of TEGDVE and HEMA, as shown by the atom economy of 100%, no side products are produced as it proceeds by proton transfer steps. However, the initial preparation of A1 (Scheme 2-4) used a high pTsOH loading of 5 mol % relative to TEGDVE and tetrahydrofuran (THF) as a reaction solvent, which is expensive, highly flammable and a suspected carcinogen.¹⁵⁸ Furthermore, the work up required back extraction of the product into DCM and subsequent washes, followed by flash column chromatography producing solvent and silica waste. The following parameters were identified for optimisation; acid concentration, solvent, reactant feed rate and the work up procedure.

2.2.2.1. Acid Species and Concentration

To better understand the role of the catalyst pTsOH in synthesising A1 from TEGDVE and HEMA a series of syntheses with varying pTsOH mol % relative to TEGDVE were performed. A solution of TEGDVE and DCM was fed into a reaction vessel containing DCM, pTsOH and HEMA, reagent concentrations and the feed rate were kept constant. The reactions were monitored by ¹H NMR spectroscopy to characterise the effect of catalyst loading on conversion over 300 min. The disappearance of the HEMA vinyl CH peak at 6.13 ppm was used to follow conversion which had very slight overlap with the shoulder of that of A1 at 6.08 ppm. However, the preferred HEMA CH₂ positioned on the β-carbon to the ester at 4.29 pp coalesced with the equivalent protons in A1. Further to this the vinyl ether CH₂ peak at 6.50 ppm could not be used to monitor time conversion as it is susceptible to acid catalysed hydrolysis (see section 2.2.2.2).

The conversion results (Figure 2-3) reveal that the control experiment with no pTsOH did not undergo any reaction during the experiment duration. Interestingly, reducing the pTsOH concentration from 5 to 0.5 and 0.1 mol % led to no observable decrease in conversion during the 2-hour addition of the TEGDVE and DCM solution, meaning the reaction duration can be reduced from 24 to 2 hours. Decreasing pTsOH loading from 5 to 0.1 is a factor of 50 decrease

with no change in the reaction outcome, meaning less catalyst is wasted and subsequently separated from the product.

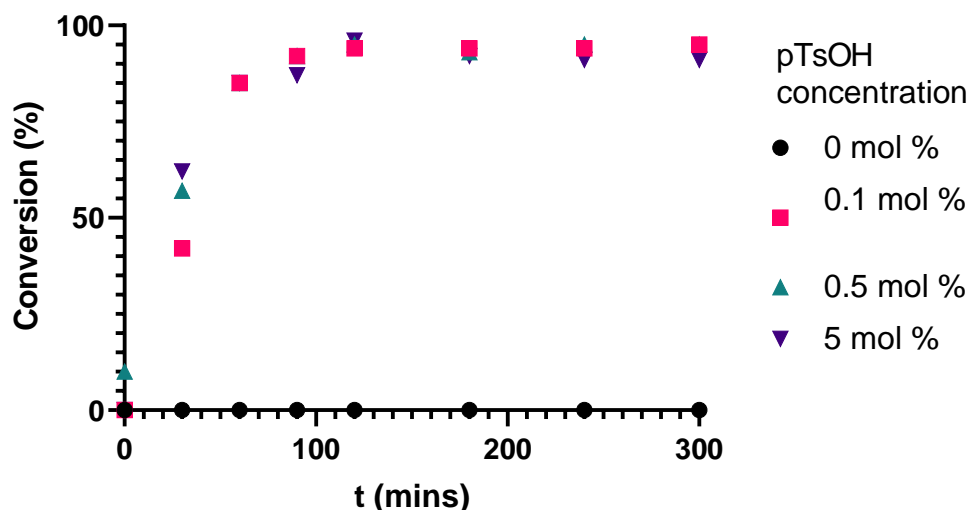


Figure 2-3 - Effect of acid concentration on conversion of HEMA to A1 as determined by ^1H NMR spectroscopy.

Interestingly, no appreciable increase in the conversion of HEMA was observed after 3 hours of stirring when using 0.5 and 0.1 mol % pTsOH suggesting a stoichiometric imbalance arising from experimental error causing the reaction to stall or the possibility of side reactions consuming reactants and preventing the reaction from reaching completion. When using 5 mol % pTsOH a decrease in conversion of HEMA to A1 was observed during the 3 hours stirring which was thought to be due to possible hydrolysis of the acetal product at the higher acid loading. Increasing the pTsOH content would increase the concentration of H_2O in the reaction as pTsOH is supplied as the monohydrate.

Alternative acids may be used that are more suitable for industrial handling, such as methane sulfonic acid and TFA, due to their liquid form. Interestingly when investigating other acids, it was found that using TFA at 0°C gave low conversion that increased to 92 % after removing DCM at 35°C on the rotary evaporator. This may be a useful acid to pursue for larger scale reactions at ambient temperatures. Furthermore, easily removable, and reusable heterogeneous catalysts such as polymer bound pTsOH may be of interest.

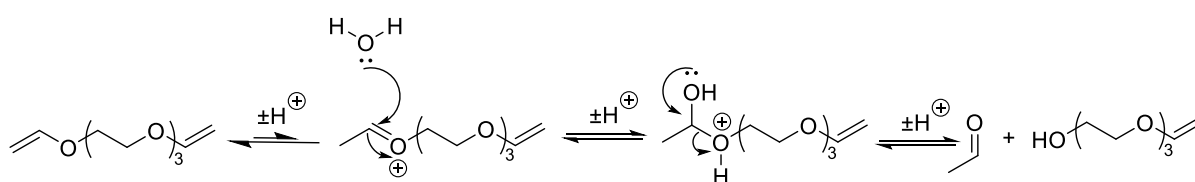
2.2.2.2. Oligomerisation Side Reactions

Table 2-2 - Effect of pTsOH mol % on HEMA conversion during the synthesis of A1 and the formation of acetaldehyde side product.

pTsOH (mol %) ^a	Conversion at 120 mins (%) ^b	Conversion at 300 mins (%) ^b	[Acetaldehyde]:[A1] 300 mins ^b	Methylene CH ₂ Integral ^b
0	0	0	0	
0.1	94	95	1:75	16.78
0.5	95	95	1:47	16.87
5	96	91	1:10	18.33

^a Relative to TEGDVE; ^b determined by ¹H NMR spectroscopy

Upon further examination of the reaction mixture ¹H NMR spectra from reactions performed using different acid concentrations, the emergence of a peak at 9.74 ppm over time was observed. This was assigned as the CH₃C(O)H in acetaldehyde. The difference in shift compared to previous experiments characterising the hydrolysis of A1 was due to the different deuterated solvent systems used.¹⁵⁹ Observing acetaldehyde further supported the hypothesis that hydrolysis of the acetal groups in A1 was occurring during the reaction *via* the previously discussed mechanism. However, TEGDVE may also undergo hydrolysis of the vinyl ether groups producing TEG and 2 equivalents acetaldehyde (Scheme 2-9).¹⁶⁰



Scheme 2-8 - TEGDVE hydrolysis mechanism.

If TEG was being generated *in situ*, it was hypothesised that an oligomerisation side reaction could occur *via* a step growth mechanism generating oligomeric acetal species end-capped with HEMA. TEG is a diol able to undergo polymerisation with TEGDVE *via* addition to the vinyl ether groups to form poly(acetals). A similar reaction was described by Tomlinson *et al.* during the synthesis of polyacetals from poly(ethylene glycol) and TEGDVE. The authors

proposed residual water underwent addition to the vinyl ether group forming a hemiacetal capable of reacting further, creating very hydrolytically unstable diacetal species along the polymer backbone.¹⁶¹ However, there is little evidence in the literature suggesting significant formation of hemiacetals during vinyl ether hydrolysis.^{160,162} The equilibrium favours the formation of an aldehyde and alcohol.¹⁶³ The latter may take part in further reactions with divinyl ethers forming a poly(acetal) under the reaction conditions of A1.

By comparing the ratio of A1 to acetaldehyde in the ¹H NMR spectra of reactions conducted with different pTsOH concentrations it was found that concentrations increased the prevalence of acetaldehyde (Table 2-2). As proton transfer to the methylene group is the rate determining step of vinyl ether hydrolysis,¹⁶² this was indicative of this pathway contributing to a side reaction. Evidence of a step growth oligomerisation was revealed by the integrals of the methylene CH₂. Upon examining the methylene CH₂ shifts in the region 3.40-3.90 ppm the integrals were higher than the expected for A1 relative to the vinyl CH. Higher integrals were observed for higher acid concentrations, suggesting acid catalysis was contributing to the reaction pathway of the side reaction. Furthermore, elemental analysis of the product gave values of carbon 57.11 % and H 8.23 % which differed from the expected values of carbon 59.17% and hydrogen 8.58%, suggesting the molecular composition was different.

HPLC-MS was used to study the product of the 0.5 mol % pTsOH reaction to reveal the true reaction product(s) and therefore, the mechanism (Figure 2-4). The chromatogram revealed a distribution of products of varying polarity, with the largest peak appearing over the retention time range of 8.7-9.3 minutes. The mass spectra revealed structures with higher than expected m/z suggesting the formation of oligomers, the structures of which are shown in Figure 2-4 (full assignments – Appendices Table 8-1). HEMA was identified as the chromatogram peak at 4.2 mins. suggesting the formation of the by-product proceeded *via* vinyl ether hydrolysis as this creates a stoichiometric imbalance that prevents HEMA from reacting. The diol identified at peak 4.8 mins was synthesised by reaction of tri(ethylene glycol) and TEGDVE or tri(ethylene glycol)mono vinyl ether. TEG is synthesised by the hydrolysis of the vinyl ether

groups in TEGDVE; the diol is then created by two possible pathways, addition of TEG to tri(ethylene glycol)monovinyl ether.

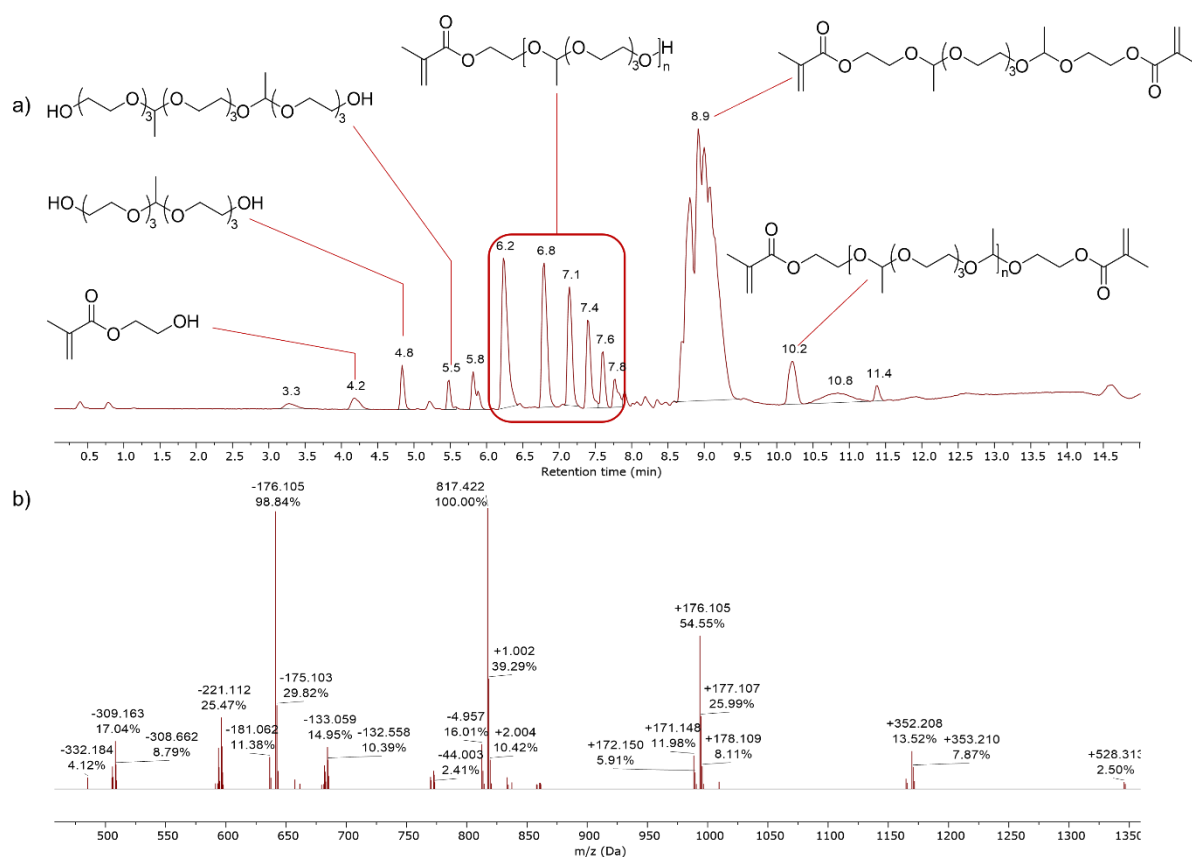


Figure 2-4 – (a) HPLC-MS chromatogram showing distribution of products and (b) mass spectrum of chromatogram peak at 10.2 min of the crude reaction mixture of the A1 synthesis.

The other pathway is the addition of tri(ethylene glycol) to TEGDVE and subsequent hydrolysis of the remaining vinyl ether group. The diol attributed to the peak at 5.5 mins is generated by addition of two tri(ethylene glycol) molecules to TEGDVE. The peaks within the boxed region between 6-7.8 mins. in Figure 2-4 all correspond to structures of the general formula shown. Again these species are generated by a reaction of *in situ* synthesised tri(ethylene glycol) and TEGDVE which are then capped by the reaction of HEMA with a vinyl ether. The degrees of oligomerisation in these species was observed to be up to 6. The peak at 8.9 mins corresponded to the desired product A1, and the peak at 10.8 mins was thought to be oligomeric derivatives of A1. The mass spectrum of the peak at 10.8 is shown in Figure 2-4 with all peaks labelled with their difference in m/z to the base ion peak at 817.422 amu. The

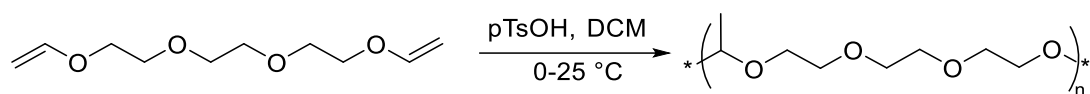
spectrum contains species varying in m/z by ~ 176 amu, this is indicative of molecules of similar polarity varying by a common repeat unit. It was expected that HEMA capped oligomers would vary by an m/z of 150.09 amu or an adduct corresponding to the actual mass of tri(ethylene glycol). However, the closest value to 176 amu was found to be the tri(ethylene glycol) adduct $[M+Na]^+$, 173.09 amu which has a difference of 3 amu units. Therefore, it cannot be definitively stated that these oligomers are similar in structure to A1. This may be resolved by optimising the instrument operating conditions. However, based on the other structures identified and the similarity of these products' proton environments in 1H NMR spectroscopy, the by-products of the reaction between HEMA and TEGDVE, under acidic conditions, are believed to be mono, dimethacrylate or diol oligomers.

2.2.2.2.1. pTsOH Catalysed Polymerisation of TEGDVE

To investigate if hydrolysis was causing the oligomerisation side reaction, the synthesis of A1 was performed under anhydrous conditions. TEGDVE was first purified *via* azeotropic distillation of water with toluene and storing over molecular sieves. HEMA and THF were stored over molecular sieves, and all were stored under nitrogen in Schlenk glassware. The reaction was repeated under anhydrous conditions in Schlenk glassware but unexpectedly high integrals for the methylene CH_2 protons in the region 3.40-3.90 ppm were observed suggesting oligomerisation *via* the previously discussed pathway. The presence of the TEGDVE hydrolysis product acetaldehyde was also observed in the 1H NMR spectrum of the reaction mixture. This suggested oligomerisation was still occurring in the absence of environmental and residual moisture in reagents. It was hypothesised the source of H_2O was pTsOH monohydrate, the catalyst's commercially available form.

A series of control experiments were performed to verify this hypothesis. The synthesis was performed as before without HEMA present and at various acid concentrations. If water from pTsOH monohydrate was hydrolysing TEGDVE to TEG then a poly(acetal) would form (Scheme 2-9). Furthermore, the molecular weight of the resulting poly(acetal) should increase

with pTsOH monohydrate as this leads to an increase in residual water and, therefore, tri(ethylene glycol) reducing the molar ratio of TEGDVE to TEG.



Scheme 2-9 - Synthesis of poly(acetal) *via* the hydrolysis of TEGDVE.

The reactions were performed with acid concentrations of 0.1, 0.5 and 1 mol % relative to the vinyl ether groups. The reaction was quenched 30 minutes after the addition of TEGDVE by addition of Na₂CO₃ to prevent further reaction, and was worked up. When using 0.1 mol % pTsOH, residual TEGDVE was observed in the ¹H NMR spectrum of the products. This was thought to be due to the low acid concentrations reducing the rate of vinyl ether hydrolysis.¹⁶² However, when using 0.5 and 1 mol % no vinyl ether was observed in the products and the integrals of the methylene CH₂ protons in the region 3.40-3.90 ppm were found to increase with acid loading, suggesting the formation of longer chains at higher acid loadings.

Table 2-3 - Summary of control poly(acetal) characterisation data.

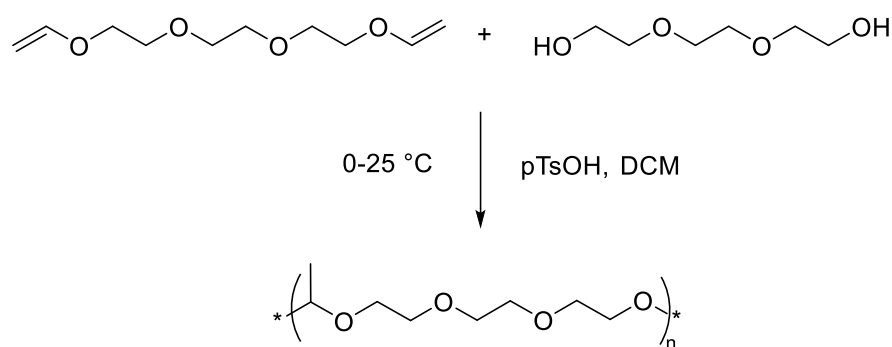
pTsOH mol %	Methylene bridge CH ₂ product ¹ H NMR integral ^a	M _n (g/mol) ^b	M _w (g/mol) ^b
0.1	N/A	1200	1300
0.5	19.12	1500	1900
1	23.15	2400	3300

^aDetermined *via* ¹H NMR spectroscopy (CDCl₃) relative to the acetal CH₃ shift at 1.30 ppm, ^bdetermined by SEC in THF and relative to p(MMA) standards

Furthermore, the molar masses of the reaction products determined by size exclusion chromatography (SEC) were found to increase with acid concentration (Table 2-3 & Appendices Figure 8-2). This supports the hypothesis that pTsOH monohydrate can act as a water source leading to the formation of oligomerisation side products in the synthesis of A1 and therefore, a compromise between rate of reaction and extent of oligomerisation must be reached by selecting a suitable acid concentration.

2.2.2.2.2. pTsOH Catalysed Copolymerisation of TEGDVE and TEG

To further support the formation of poly(acetals) from TEGDVE and TEG formed *in situ*, a final series of control reactions was performed (Scheme 2-10). Poly(acetals) were synthesised directly from TEGDVE and TEG under the same reaction conditions for the synthesis of A1. As before pTsOH concentrations of 0.1, 0.5 and 1 mol % were used to probe the effect on polymerisation and was monitored by product molar mass. Conversely to control polymerisations where only TEGDVE was used, lower catalyst concentrations gave higher molar masses by SEC (Appendices Figure 8-3). As previously discussed, lower catalyst loadings lead to a decreased rate of vinyl ether hydrolysis. In the case of the step growth polymerisation of TEGDVE and TEG this causes a lower stoichiometric imbalance between the A₂ and B₂ type monomers. Stoichiometric imbalance of monomers in step growth polymerisation is known to retard propagation due to the reactive chain ends having no suitable functional group to react with.¹⁶⁴ The result of which is lower than expected molar masses of the polymer products. Therefore, an acid concentration of 0.1 mol % relative to TEGDVE was chosen for future syntheses as it had a lower rate of the competing oligomerisation side reaction and led to no decrease in the rate of conversion of HEMA to A1 over the 6 hrs reaction.



Scheme 2-10 - Synthesis of poly(acetals) from TEGDVE and TEG.

2.2.2.1. Effect of TEGDVE Feed Rate on Reaction Kinetics

The effect of the feed rate of the TEGDVE/solvent solution on reaction kinetics was investigated to reduce the overall reaction time and enable efficiency in later screening of reaction conditions. By increasing the feed rate of TEGDVE the effective concentration is increased which should lead to an increase in the rate of reaction. The feed rate was increased by a factor of 5 from 0.5 mol/hr to 2.5 mol/hr, and the conversion followed at regular time intervals by ^1H NMR spectroscopy (Figure 2-5). At a feed rate of 0.5 mol/hr the conversion reached 94% after 120 min. Upon increasing the feed rate to 2.5 mol/hr, 94% conversion was reached in 20 min enabling faster screening of the effect of solvent on the reaction. Although this increased rate is efficient, it is likely to come with an increased rate of heat evolution that will be unsafe on larger scales due to the decreased rate of heat removal that accompanies reducing the reactor surface area to volume ratio.¹⁶⁵

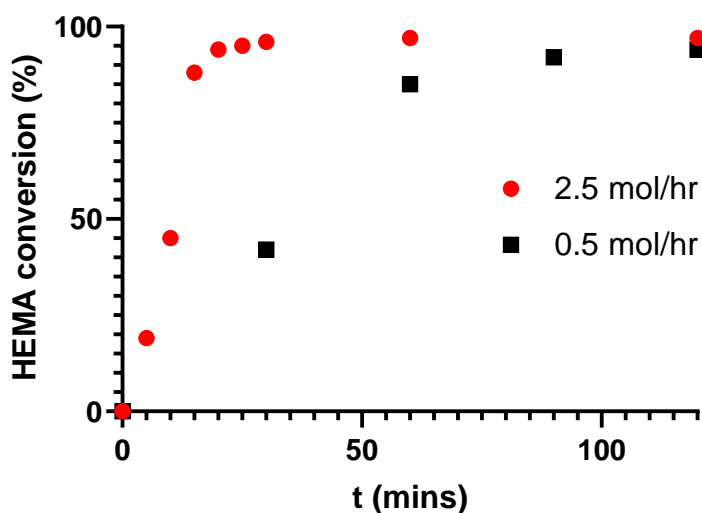


Figure 2-5 - Effect of TEGDVE feed rate on kinetics of A1 synthesis measured by ^1H NMR spectroscopy.

2.2.2.2. Choosing a Solvent

When selecting a reaction solvent, it is often important to consider whether they are required to act as a proton source, their ease of removal and whether it eases separation of products and impurities. Furthermore, when performing large scale reactions, toxicity, physical risks and consequences of environmental release are of importance. Previous syntheses of A1 have utilised THF or DCM as the reaction solvent, both of which are unsuitable on a large scale due to cost, volatility, and their respective hazards.¹⁶⁶ Therefore, an alternative solvent was sought using guidelines available in the literature.^{166–169}

The criteria for selection of the replacement solvents were: no alcohols to prevent reaction with the vinyl ether; suitable polarity to enable charge stabilisation of intermediates; and reduced toxicity relative to THF and DCM. Immiscibility with water was also desirable for ease of purification. Previous reactions had reached near quantitative conversions meaning only catalytic amounts of pTsOH had to be removed. It was hypothesised that this could be achieved by washing with saturated aqueous solutions such as brine. Solvents less dense than water were preferred for ease of separating liquid phases. Lastly, boiling points lower than 100 °C were also desirable to enable easy isolation of the product *via* distillation of the solvent. The chosen solvents and the reaction conversion are summarised in Table 2-4. It is worth noting here that methyl methacrylate is an industrially useful class of solvent known as a reactive diluent. The diluent is then copolymerised with the product in its application.¹⁷⁰ Reactions were performed as before using a TEGDVE/solvent (1/1 v/v) solution feed rate of 2.5 mol/hr into a vessel containing solvent, pTsOH (0.1 mol %) and HEMA. The conversion upon completion of addition and after 30 minutes of stirring was monitored *via* ¹H NMR spectroscopy.

Table 2-4 - Solvent's properties and effect on conversion of HEMA to A1.

Solvent	Immiscible with H ₂ O	Density < H ₂ O	b.p. < 100 °C	Conversion after addition (%) ^a	Conversion after stirring (%) ^b
2-methyl THF	x	✓	✓	78	95
Acetone	x	✓	✓	98	>99%
DCM	✓	x	✓	>99%	>99%
Dimethyl carbonate	Partially	x	✓	>99%	>99%
Ethyl acetate	✓	✓	✓	98	>99%
Isopropyl acetate	Partially	✓	✓	>99%	>99%
Methyl methacrylate	x	✓	x	>99%	>99%
No solvent	N/A	N/A	N/A	>99%	>99%
THF	x	✓	✓	85	99
Water	N/A	N/A	x	0	0

^aDetermined via ¹H NMR spectroscopy (CDCl₃) relative to the acetal CH at 14 mins and ^b30 mins, samples were quenched with NEt₃, no residual HEMA or TEGDVE were observed.

The average conversion of two repeats are summarised in Table 2-4, after completion of the addition of the TEGDVE solution and stirring, all solvents gave ≥95% conversion except water. The reactions in water were not expected to proceed due to the hydrolysis of the vinyl ether groups and it will be omitted from further discussion. Interestingly, the conversion after addition was lowest when using coordinating solvents, THF and 2-methyl THF, whereas the remaining solvents had near quantitative conversion. The reduced conversion was thought to be due to

the formation of hydrogen bond between the ethereal oxygen of the furan ring and the hydroxyl of HEMA reducing its nucleophilicity.

All solvents used gave near quantitative conversion after stirring for 30 minutes. The choice of solvent could also be performed based on their sustainability, safety, and cost. When considering the solvents from a sustainability standpoint, the E factor and process mass index would be lowest for the reaction using no solvent, however, in the absence of any calorimeter data and the requirement to remove pTsOH from the product *via* aqueous/organic solvent extraction, it was deemed unsuitable. Based upon solvent selection guides of GSK, Pfizer and Sanofi, Byrne et al. have published a comprehensive green solvent selection guide¹⁶⁶ that considers safety and sustainability. Both acetone and ethyl acetate can be sourced renewably and are preferred based upon their safety and environmental scores and were chosen for further scale up work.

2.2.2.3. Optimisation of reaction work up conditions

So far, the reaction optimisation process has been concerned with conversion of the starting materials to A1 and it is understood that quantitative conversion of HEMA is reached within 30 min of completion of the TEGDVE addition when using 0.1 mol % pTsOH. Therefore, a reliable work up process that gave A1 in a high a yield was sought. Initial syntheses of A1 were adapted from a similar process described by Nasanit *et al.*⁹³, in which the purification procedure was column chromatography. The adapted process included removing the reaction solvent (THF), redissolution in DCM and performing a series of aqueous washes (3 × H₂O and 3 × brine) before being dried over Na₂SO₄, this was followed by purification by column chromatography. Problematically, this process was time consuming and produced a lot of aqueous, solvent and silica waste, while achieving 75% yield of pure A1.

Upon examination of the ¹H NMR spectrum of crude A1 after washing it was found that residual HEMA, DCM and water were present. The amount of HEMA was expected to decrease with the optimised pTsOH mol % as less vinyl ether hydrolysis could occur. Also the DCM could

be removed by increasing the duration of concentration *in vacuo* and the water by improved drying, although some is to be expected due to the hygroscopic nature of the tri(ethylene glycol) component in A1. Therefore, the column chromatography purification procedure was deemed unnecessary and liquid-liquid extraction purification of A1 synthesised in ethyl acetate or acetone was investigated.

Table 2-5 - Effect of wash volume (%) on yield of A1 synthesised in acetone or ethyl acetate.

Solvent	Wash volume (wt % of organic phase)	Yield (%)
Acetone	7	97
	10	84
Ethyl acetate	7	92
	10	82

Reactions in acetone and EtOAc were performed at a larger scale with a theoretical yield of 23 g. of A1. Upon completion of the reactions, the crude reaction mixtures were split into two 36 mL portions and the effect of wash volume percent on yield was investigated. For the reactions performed in acetone the wash process was two washes of the organic extract with saturated brine, as acetone is miscible with water. For reactions performed in ethyl acetate the wash process was one wash with deionised H₂O and one wash with saturated brine. For both solvents, the wash volume was either 7 or 10 vol % of the organic phase, the initial preparation by Nasanit *et al.*⁹³ used ~30 vol %, which generated greater waste and also it was likely more product was lost to the discarded phases. A higher yield was observed for both solvents when a lower wash volume % was used, this was thought to be due to loss of A1 into the aqueous and/or brine phase arising from the hydrophilic tri(ethylene glycol) component (Table 2-5). The highest yield achieved was 97% when the wash volume was 7% and acetone was used, however, when performing the washes, a white precipitate formed that made separation of the phases challenging. Therefore, a wash volume of 7% using ethyl acetate as

the solvent was chosen for scale up as it gave a yield of 92%, although some emulsification of the two phases occurred which slowed the separation process.

2.2.2.4. Scale Up of A1 Synthesis

A scaled-up synthesis of A1 was performed using the optimised conditions. The theoretical mass of A1 was 462.5 g and the yield was 90%, which may be improved by further refining the washing procedure. ¹H NMR spectroscopy showed no impurities, but a degree of oligomerisation had occurred as the methylene CH₂ integral at 3.40-3.90 ppm was 16.73, which is greater than the expected 14 and preventing or reducing the oligomerisation is discussed in the future work.

2.2.2.5. Sustainability comparison of start and final protocols of Scaled Up A1 Synthesis

Table 2-6 - Green metrics for initial and optimised synthesis of A1.

Synthetic Procedure	Atom Economy (%)	E Factor	Process Mass Index
Initial	100	5.6	443
Scale up	100	0.42	1.7

The atom economy of the synthesis of A1 is 100% for both the initial and optimised syntheses of A1, however, this provides no insight into the overall wastefulness of the process. The generation of waste was expected to have been significantly reduced when compared to the initial synthesis of A1 that utilised back extraction of the product into DCM, multiple washes, and column chromatography. The E factor for the initial synthesis falls within the expected range for fine chemicals, a large reduction is observed for the scale up synthesis which is within the range for bulk chemicals.¹⁰⁸ A large reduction in waste is shown in the difference in values of the process mass index for both synthetic procedures. They differ by two orders of magnitude highlighting the usefulness in optimising a process to minimise environmental consequences.

2.3. Conclusions

A novel dimethacrylate cross-linker bearing two acetal functional groups was synthesised from HEMA and TEGDVE. The hydrolysis of A1 was probed by ^1H NMR spectroscopy and HPLC-MS revealing the products to be tri(ethylene glycol) and acetaldehyde. Further experiments investigated the effect of acid pK_a on the extent of A1 hydrolysis at 50 °C for 5 hrs in 0.15 M acetone- d_6 / D_2O (9/1 v/v) solutions. It was found that the extent of hydrolysis increased with decreasing pK_a over the course of 5 hrs, however 100 % was only achieved when using acids with a $pK_a < 1.29$. This demonstrated the potential to synthesise pH degradable thermosets *via* the incorporation of A1.

The synthesis of A1 was then optimised and scaled up to reduce batch to batch variation affecting mechanical testing results, reduce the time spent performing and purifying reactions and improve the sustainability. An oligomerisation side reaction related to the pTsOH loading was also identified *via* ^1H NMR spectroscopy and HPLC-MS. Under the reaction conditions residual H_2O in pTsOH monohydrate is capable of partially and fully hydrolysing the TEGDVE vinyl groups to tri(ethylene glycol) which can react further to with TEGDVE to make mono or di HEMA capped oligomers. The pTsOH acid catalyst loading was reduced from 5 to 0.1 mol% with no considerable reduction in conversion at 120 minutes, alternative reaction solvents and purification processes were investigated, and ethyl acetate chosen and the requirement of column chromatography for purification removed. Finally, the reaction was optimised and scaled up to yield 450 g of A1 (90 % yield) *via* a process with both a lower E-factor and process mass index than the original.

2.4. Experimental

2.4.1. Materials

pTsOH hydrate (97%) was purchased from Alfa Aesar. Tri(ethylene glycol)divinyl ether was provided by BASF. Acetone ($\geq 99.0\%$), ethyl acetate ($\geq 99.5\%$), sodium carbonate anhydrous, sodium chloride ($\geq 99.5\%$), sodium sulfate anhydrous ($\geq 99\%$) were purchased from Fisher. 2-MeTHF anhydrous ($\geq 99.0\%$), acetone- d_6 (99.0%), $CDCl_3$ (99.8%), chloroacetic acid (99%), D_2O (99.9%), dichloroacetic acid ($\geq 99\%$), dichloromethane ($\geq 99.9\%$), dimethyl carbonate (99%), HEMA (97%), hexane ($\geq 95.0\%$), isobutyl acetate (natural, $\geq 97.0\%$), 3Å molecular sieves, trichloroacetic acid ($\geq 99\%$), triethylamine ($\geq 99\%$), tri(ethylene glycol) (99%) and trifluoroacetic acid (99%) were purchased from Sigma-Aldrich. Silica gel (40–63 μm) and THF (HPLC grade) were purchased from VWR. All reagents were used as supplied, unless otherwise stated.

2.4.2. Instrumentation

NMR spectra were recorded on a Bruker Avance 400 MHz spectrometer at 25 °C. 1H NMR spectra were recorded at 400 MHz and ^{13}C spectra at 101 MHz. Spectra were processed using the MestreNova software. IR spectra were recorded on a PerkinElmer FTIR Spectrum Two equipped with UATR Two diamond. Size exclusion chromatography was performed on an Agilent PL-GPC50 equipped with a refractive index detector and PLgel Mixed-C (7.8 \times 300 mm, 5 μm bead size) with an integrated PLgel 5 μm guard column, at a flow rate of 1.0 mL min^{-1} . All the samples were measured relative to a set of ten low-dispersity poly(methyl methacrylate) standards (Agilent, UK) with peak molecular weights ranging from 550 to 1,568,000 Da. The eluent system was THF with 0.025 w/v% butyl hydroxytoluene. Elemental microanalysis (CHN) was performed on an Elementar Vario Micro Cube. HPLC-MS was performed on an Agilent 6530 Q-TOF MS, samples were run in electro-spray ionisation

positive mode. Syringe pump additions were performed using a World Precision Instruments AL-1000.

2.4.3. Initial Synthesis of A1

THF (25 mL), tri(ethylene glycol) divinyl ether (2.50 g, 0.012 mol) and hydroxyethyl methacrylate (3.20 mL, 0.025 mol) were added to an oven dried round bottom flask and stirred on an ice bath for 30 min. To this, pTsOH monohydrate (0.120 g, 0.63 mmol) was added in portions and the mixture stirred in an ice bath for a further 6 hrs. The reaction was monitored by TLC in ethyl acetate/hexane (1:1 v/v). Once complete, saturated aqueous Na₂CO₃ (10 mL) was added and mixture stirred for a further 10 min. The reaction mixture was filtered and concentrated *in vacuo* to give a white suspension. H₂O (15 mL) was added and then washed with DCM (3 × 10 mL). The organic extracts were washed with H₂O (3 × 10 mL) and brine (3 × 10 mL) and dried over Na₂SO₄. Solids were removed by filtration and volatiles removed *in vacuo* to give a colourless oil. The crude product was purified *via* column chromatography using solvent gradient elution of ethyl acetate/hexane (40/60, 50/50, 60/40) with NEt₃ (2 vol %) to yield a colourless oil (4.00 g, 8.96 mmol, 75%). δ_{H} (400 MHz, CDCl₃): 6.13 (d, 2H), 5.58 (d, 2H), 4.80 (m, 2H), 4.29 (m, 4H), 3.64(m, 16H), 1.94 (m, 6H), 1.31 (m, 6H). ^{13}C { ^1H } NMR (CDCl₃): δ 167.7, δ 136.6, δ 125.9, δ 99.8, δ 70.7, δ 64.1, δ 62.6, δ 19.6, δ 19.4, δ 18.4. ATR-IR: 2987-2874. cm⁻¹ (C-H), 1716 cm⁻¹ (COO), 1296 cm⁻¹ (COC), 1133 cm⁻¹ (COO), 939.99 cm⁻¹ (C=C). HPLC-MS C₂₂H₃₈O₁₀, [M]⁺ theoretical 462.25 amu, experimental [M+Na]⁺ 485.25.20. CHN calculated (C 59.17%, H 8.58%), observed (C 57.11%, H 8.23%).

2.4.4. Hydrolysis of A1

A1 (0.1 g, 0.2 mmol) was added to an acidic stock solution (1.5 mL, 0.15 M acid) in acetone-d₆/D₂O (9/1 v/v) and heated to 50 °C for 6–48 hours. An aliquot (0.7 mL) was taken and its ¹H NMR spectrum recorded. Hydrolysis (%) was calculated using the integrals of the acetal CH and acetaldehyde CH resonances at 4.80 and 9.79 ppm, respectively, using the following equation:

Equation 2-1

$$\text{Hydrolysis (\%)} = \left(\frac{\text{Acetaldehyde CH (4.80 ppm)}}{\text{Acetaldehyde CH (4.80 ppm)} + \text{Acetal CH (9.79 ppm)}} \right) \times 100$$

2.4.5. Effect of acid on scale up

General procedure

A 50 mL round-bottomed flask was charged with DCM (20 mL), HEMA (6 mL, 0.05 mol) and pTsOH (Table 2-7). The solution was cooled in an ice bath for 30 min. TEGDVE (5.00 g, 0.025 mol) was added to DCM (5 mL) and added dropwise using a syringe pump at a flow rate of 0.025 mol/hr. Aliquots (0.2 mL) were taken periodically, quenched with NEt₃ (2 μL, 0.014 mmol) and diluted with CDCl₃ (0.5 mL). Reactions were quenched by the addition of sat. Na₂CO₃ (5 mL) after 6 hrs. The transparent solution was washed with H₂O (2 × 5 mL) and brine (5 mL), the organic phase was dried over Na₂SO₄, filtered, and concentrated *in vacuo* to yield a colourless oil. Conversion was calculated using the following equation:

Equation 2-2

$$\text{HEMA Conversion (\%)} = \left(1 - \frac{\text{HEMA integral (6.13 ppm)}}{\text{HEMA integral (6.13 ppm)} + \text{A1 integral (6.10 ppm)}} \right) \times 100$$

Table 2-7 - Effect of pTsOH on A1 synthesis experiment formulations.

pTsOH / mol % of TEGDVE	pTsOH / mg (mmol)	HEMA / mL (mmol)	TEGDVE / g (mmol)	DCM / mL
0	0	6 (50)	5.00 (25)	25
0.1	4.7 (0.0246)	6 (50)	5.00 (25)	25
0.5	23.5 (0.123)	6 (50)	5.00 (25)	25
5	235 (1.23)	6 (50)	5.00 (25)	25

2.4.6. Anhydrous Synthesis of A1

Tri(ethylene glycol)divinyl ether was purified *via* azeotropic distillation with toluene three times and stored over 3 Å molecular sieves under nitrogen. HEMA and THF were stored over 3 Å molecular sieves under nitrogen for 24 hours prior to use. To an oven dried Schlenk flask under nitrogen HEMA (3.20 mL, 0.025 mol), pTsOH (0.120 g, 0.63 mmol) and THF (25 mL) were added stirred on an ice bath for 30 minutes. TEGDVE (2.50 g, 0.012 mol) was added dropwise, and the reaction was stirred for six hours. Once complete, saturated aqueous Na₂CO₃ (10 mL) was added and mixture stirred for a further 10 min. The reaction mixture was filtered and concentrated *in vacuo* to give a white suspension. H₂O (15 mL) was added and then washed with DCM (3 × 10 mL). The organic extracts were washed with H₂O (3 × 10 mL) and brine (3 × 10 mL) and dried over Na₂SO₄. Solids were removed by filtration and volatiles removed *in vacuo* to give a colourless oil.

2.4.7. Control Polymerisation of TEGDVE

General Procedure

To a round-bottomed flask pTsOH and DCM (20 mL) were added and cooled on ice for 30 min. Tri(ethylene glycol)divinyl ether (5.0 mL, 0.025 mol) was added to DCM (5 mL) and added dropwise to the reaction mixture using a syringe pump at 0.25 mol/hr. After 30 min. the reaction was quenched with saturated Na₂SO₄ (5 mL) and stirred for 10 min. The reaction mixture was washed with H₂O (3 × 5 mL) and brine (1 × 5 mL) and the organic extract was dried over MgSO₄, filtered, concentrated *in vacuo* and dried in a desiccator yielding an oil*. ¹H NMR spectra recorded in CDCl₃.

*Samples synthesised with 0.5 and 1 mol % pTsOH were yellow

Table 2-8 - Control polymerisation of TEGDVE formulations.

pTsOH / mol % of TEGDVE	pTsOH / g (mmol)	TEGDVE / g (mol)	DCM / mL
0.1	0.0047 (0.0246)	5.00 (0.025)	25
0.5	0.0235 (0.123)	5.00 (0.025)	25
1	0.047 (0.246)	5.00 (0.025)	25

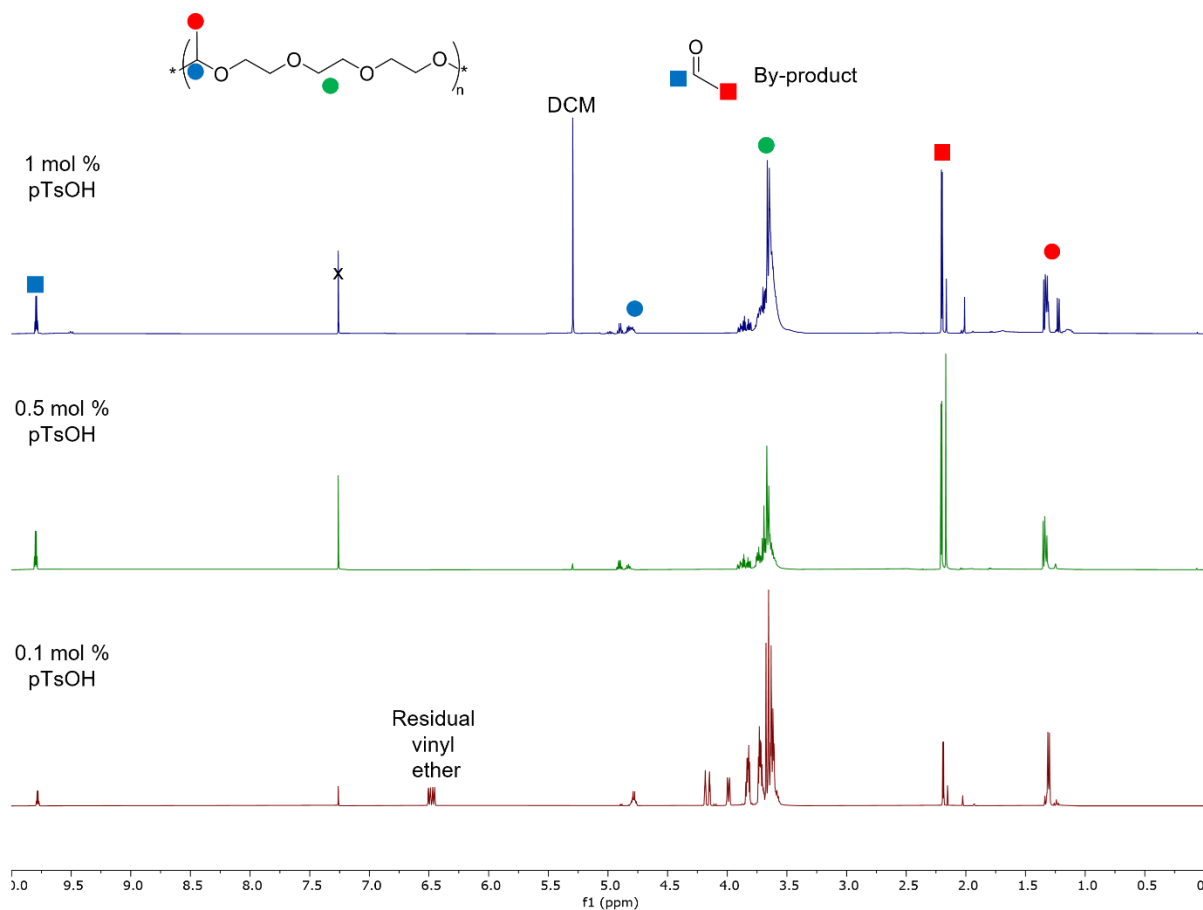


Figure 2-6 – ^1H NMR Spectra (CDCl_3) of reaction products of control polymerisation of TEGDVE.

2.4.8. Control Polymerisation of TEGDVE and TEG

General Procedure

To a round-bottomed flask pTsOH, TEG (3.71 g, 0.025 mol) and DCM (20 mL) were added and cooled on ice for 30 minutes. Tri(ethylene glycol)divinyl ether (5.0 mL, 0.025 mol) was added to DCM (5 mL) and added dropwise to the reaction mixture using a syringe pump at 0.25 mol/hr. After 30 minutes reaction was quenched with saturated Na_2SO_4 (5 mL) and stirred for 10 minutes. The reaction mixture was washed with H_2O (3×5 mL) and brine (1×5 mL) and the organic extract was dried over MgSO_4 , filtered, concentrated *in vacuo* and dried in a desiccator yielding an oil. ^1H NMR spectra recorded in CDCl_3 .

Table 2-9 - Control polymerisation of TEGDVE and TEG formulations.

pTsOH / mol % of TEGDVE	pTsOH / g (mol)	TEG / g (mol)	TEGDVE / g (mol)	DCM / mL
0.1	0.0047 (0.0246)	3.71 (0.025)	5.00 (0.025)	25
0.5	0.0235 (0.123)	3.71 (0.025)	5.00 (0.025)	25
1	0.047 (0.246)	3.71 (0.025)	5.00 (0.025)	25

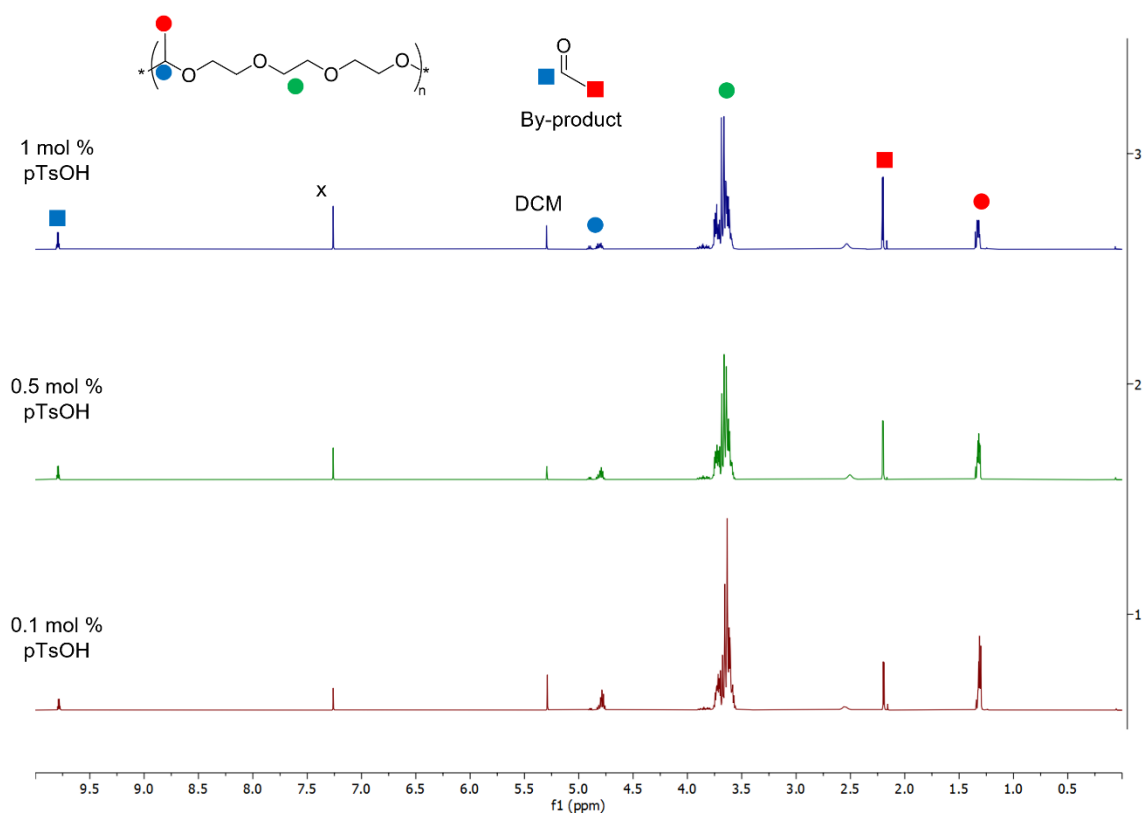


Figure 2-7 - ^1H NMR spectra (CDCl₃) of poly(acetal) synthesised from TEGDVE and TEG.

2.4.9. Effect of TEGDVE Addition Rate

A 50 mL round-bottomed flask was charged with DCM (20 mL), HEMA (6 mL, 0.05 mol) and pTsOH (4.7 mg, 0.247 mmol), and stirred on ice for 30 min. A solution of DCM (5 mL) and TEGDVE (5.00 g, 0.0247 mol) was added to a syringe and added dropwise to the reaction mixture using a syringe pump at 0.5 or 2.5 mol/hr. Aliquots (0.2 mL) were taken periodically and quenched with NEt₃ (2 μL, 0.014 mmol) and diluted with CDCl₃ (0.5 mL) for ¹H NMR spectroscopy analysis. Conversion was calculated using the following equation:

Equation 2-3

$$\text{HEMA Conversion (\%)} = \left(1 - \frac{\text{HEMA integral (6.13 ppm)}}{\text{HEMA integral (6.13 ppm)} + \text{A1 integral (6.10 ppm)}}\right) \times 100$$

2.4.10. Effect of Solvent on Synthesis of A1

A 50 mL round-bottomed flask was charged with DCM (20 mL), HEMA (6 mL, 0.05 mol) and pTsOH (4.7 mg, 0.247 mmol), and stirred on ice for 30 minutes. A solution of DCM (5 mL) and TEGDVE (5.00 g, 0.0247 mol) was added to a syringe and added dropwise to the reaction mixture using a syringe pump at 2.5 mol/hr. Aliquots (0.2 mL) were taken periodically and quenched with NEt₃ (2 μL, 0.014 mmol) and diluted with CDCl₃ (0.5 mL) for ¹H NMR spectroscopy analysis. Conversion was calculated using the following equation:

Equation 2-4

$$\text{HEMA Conversion (\%)} = \left(1 - \frac{\text{HEMA integral (6.13 ppm)}}{\text{HEMA integral (6.13 ppm)} + \text{A1 integral (6.10 ppm)}}\right) \times 100$$

2.4.11. Effect of work up

General procedure

A round-bottomed flask was charged with solvent (50 mL), HEMA (13.0 g, 0.1 mol) and pTsOH (9.5 mg, 0.50 mmol), and stirred on ice for 30 minutes. TEGDVE (10.1 g, 0.05 mol) was added to a syringe and added dropwise to the reaction mixture *via* a syringe pump at 2.5 mol/hr. Aliquots (0.2 mL) were taken periodically and quenched with NEt₃ (2 μL, 0.014 mmol) and

diluted with CDCl_3 (0.5 mL) for ^1H NMR spectroscopy analysis. Samples (36 mL) of the crude reaction mixture were taken and washed as per table below. The organic extracts were collected, dried over Na_2SO_4 , filtered and concentrated *in vacuo*.

Table 2-10 - Wash formulations and yield of A1 recovered.

Solvent	Crude volume / mL	Wash volume / %	H_2O / mL	Brine / mL	Yield / %
Acetone	36	7	0	2 × 2.5	97
	36	10	0	2 × 3.75	84
Ethyl acetate	36	7	2.5	2.5	92
	36	10	3.75	3.75	82

2.4.12. Synthetic scale up

HEMA (236.5 g, 1.95 mols), ethyl acetate (200 mL) and pTsOH (1.902 g, 0.1 mol) were added to a reactor equipped with an overhead stirrer and cooled on ice until the internal temperature reached 0 °C. TEGDVE (202.3 g, 1 mol) was added dropwise while ensuring the internal temperature was <5 °C. After the addition of TEGDVE was complete the reaction was stirred for 1 hr and allowed to reach room temperature before quenching with saturated aqueous Na_2CO_3 (10 mL). The organic phase was then washed with H_2O (20 mL) and brine (20 mL), dried over Na_2SO_4 , filtered and concentrated *in vacuo* to yield a clear oil (416 g, 90 %).

2.4.13. Green Metric Calculations

Atom economy was calculated using the following values and equation:

Equation 2-5

$$\text{Atom economy (\%)} = \frac{2 \times (130.14) + 202.25}{462.53} \times 100$$

E factor was calculated using the following equation:

Equation 2-6

$$E \text{ factor} = \frac{\text{mass of waste}}{\text{mass of product}}$$

For the initial synthesis of A1 the following data was used:

Table 2-11 – E factor waste data for initial synthesis of A1.

Chemical	Mass / g	Reagent	Product	Waste
HEMA	3.424	✓		
TEGDVE	2.5	✓		
pTsOH	0.12	✓		✓
THF	22.23			✓
A1	4 (74.6 % yield)		✓	

For the optimised and scaled up synthesis of A1 the following data was used:

Table 2-12 – E factor waste data for optimised A1 synthesis.

Chemical	Mass / g	Reagent	Product	Waste
HEMA	253.8	✓		
TEGDVE	202.3	✓		
pTsOH	0.190	✓		✓
Ethyl acetate	180.4			✓
A1	425.5 (92 % yield)		✓	

The process mass index was calculated using the following equation:

Equation 2-7

$$\text{process mass index} = \frac{\text{Mass used in process}}{\text{Mass of product}}$$

For the synthesis of A1 the following data was used:

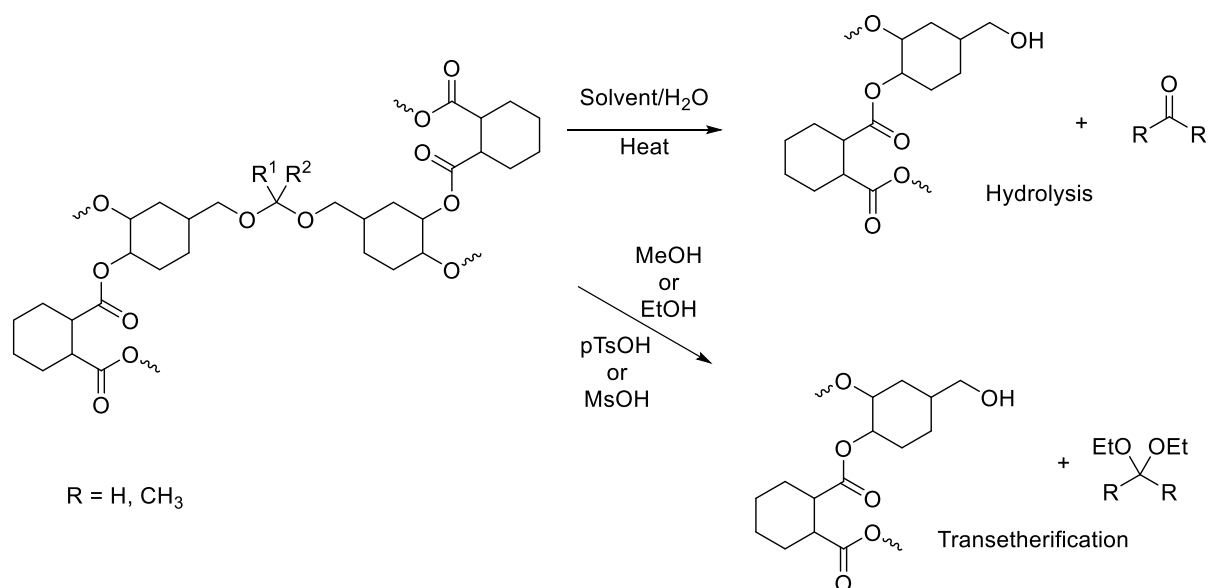
Table 2-13 - Process mass index data for initial and optimised synthesis of A1.

Synthesis	Initial	Optimised
Chemical	Mass / g	
HEMA	3.424	253.8
TEGDVE	2.5	202.3
pTsOH	0.12	0.1902
THF	22.23	180.4
DCM	39.9	0
Sat. Sodium carbonate soln.	13.4	26.8
H ₂ O	55	20
Brine soln.	25	17
Silica gel	50	0
Ethyl acetate	902	0
Hexane	655	0
A1	4 (74.6 % yield)	425.5 (92 % yield)

Chapter 3 – Synthesis and Degradation of Acetal Containing Methacrylate Thermosets

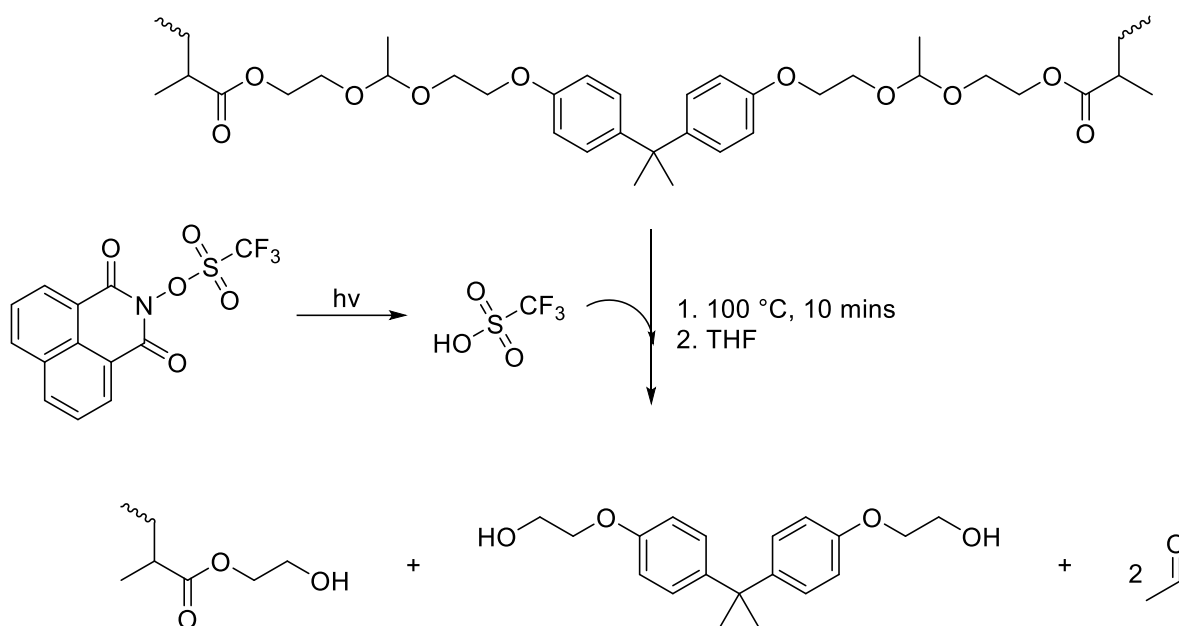
3.1. Introduction

Literature examples of pH degradable thermosets incorporating acetal groups mainly focus on epoxy resins, which are summarised in this introduction with some examples of (meth)acrylate-based acetal resins. Watson *et al.* synthesised a series of acetal containing epoxy resins from *cis*-cyclohexane-1,2-dicarboxylic anhydride, a series of three novel diepoxy monomers and one commercially available cyclic acetal-containing diepoxy monomer, that degraded *via* acetal hydrolysis or transesterification (Scheme 3-1). Samples for degradation were prepared as thin film discs of approximately 1 cm diameter, immersed in solutions of ethanol, water and acetic acid (1:1:1 or 2:1:1 by volume) with acid concentrations of 4.8 or 4.4 M at 88 °C. When R¹ and R² were both CH₃ the resin was degraded and formed a homogeneous solution in 2-3 minutes, however, when R¹ was H and R² was CH₃, only partial degradation was observed over 60 minutes. Furthermore, there was no observed degradation when R¹ and R² were H, or the commercially available cyclic acetal monomer, cyclohexane *meta*-dioxane, was used. The authors do not say which concentration of acetic acid these experiments were performed in. The authors also showed networks could be degraded *via* transesterification in solutions of methane sulfonic acid, or pTsOH (0.026-0.5 M) in ethanol or methanol. The previously degradation resistant resins where, R¹ and R² were both H, degraded within 60 mins under these conditions. When R¹ was H and R² was CH₃ or R¹ and R² were CH₃ was <10 mins.¹⁷¹



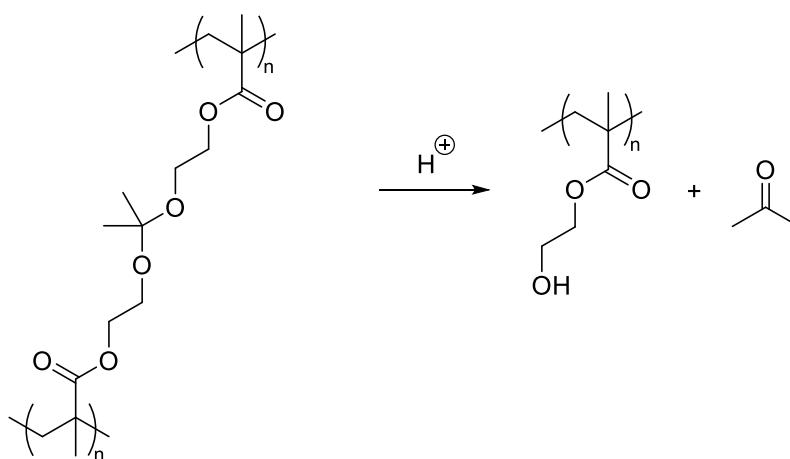
Scheme 3-1 – Early examples of epoxy resin networks with degradable acetal groups.¹⁷¹

Shirai *et al.*, synthesised a series of highly cross-linked (meth)acrylate resins *via* polymerisation of the di or trifunctional monomers using thermal and photo initiators in the presence of a photoacid. The acetal bearing monomers were synthesised *via* a two-step procedure first reacting an aromatic di or triol with 2-chloroethyl vinyl ether and subsequent nucleophilic addition of HEMA or 2-hydroxyethyl acrylate. Thin films containing 1 wt % photoacid generator were irradiated at 366 nm and baked at 100 °C for 10 minutes, after which the films became soluble in THF. The photogenerated triflic acid had catalysed acetal hydrolysis, yielding p(HEMA) or p(2-hydroxyethyl acrylate), an aromatic diol or triol and acetaldehyde (Scheme 3-2).¹⁵¹



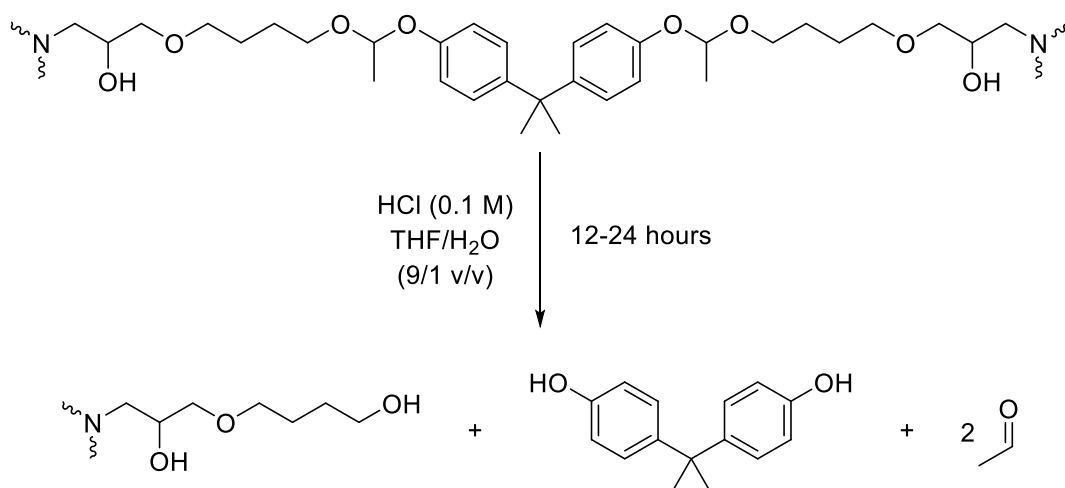
Scheme 3-2 – Highly cross-linked acetal containing (meth)acrylate networks synthesised by Shirai *et al.*¹⁵¹

Heath *et al.*, synthesised an acetal containing diacrylate *via* transacetalisation of 2,2-dimethoxypropanone with 2-hydroxyacrylate. This was polymerised using a photoinitiator. Films of 1 μm thickness were then degraded in acidic THF solutions at room temperature and 60 °C, the concentration, acid species and cosolvents used are not described (Scheme 3-3).¹⁷²



Scheme 3-3 - pH degradable poly(methacrylate) films synthesised by Heath *et al.*¹⁷²

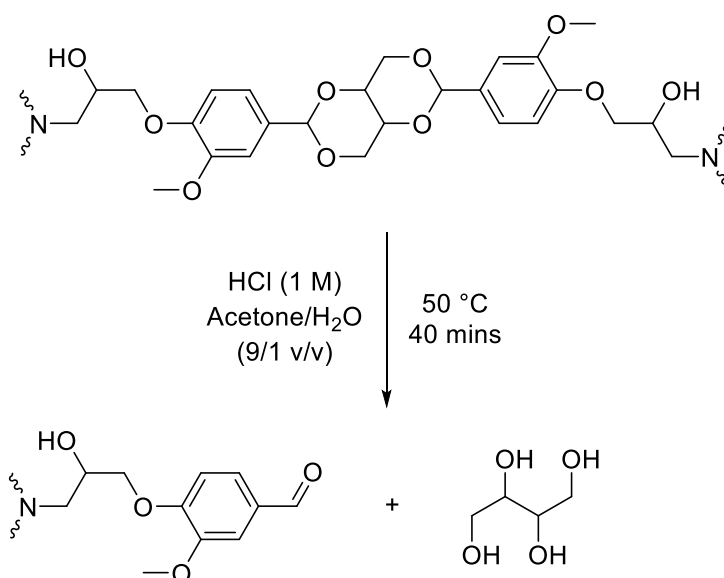
Hashimoto *et al.* synthesised acetal containing epoxy resins and carbon fibre composites using tetraethylenepentamine as a curing agent. The acetal functionality was incorporated *via* reaction between hydroxyl groups on bisphenol A or a phenolic resin and an epoxy functionalised vinyl ether, 4-vinyloxybutyl glycidyl ether or cyclohexane dimethanol vinyl glycidyl ether. They were degraded in 0.1 M HCl THF/water (9/1 v/v) solutions at room temperature over 12-24 hours (Scheme 3-4). The authors collected the degradation products bisphenol A or Cresol Novolak and the carbon fibre resin which may be reused. Bisphenol A and Cresol Novolak were characterised by ¹H NMR and SEC which showed high purity and the Cresol Novolak M_n and M_w/M_n values were similar to those of the virgin material.¹⁷³



Scheme 3-4 – Acetal containing epoxy resins synthesised by Hashimoto *et al.*¹⁷³

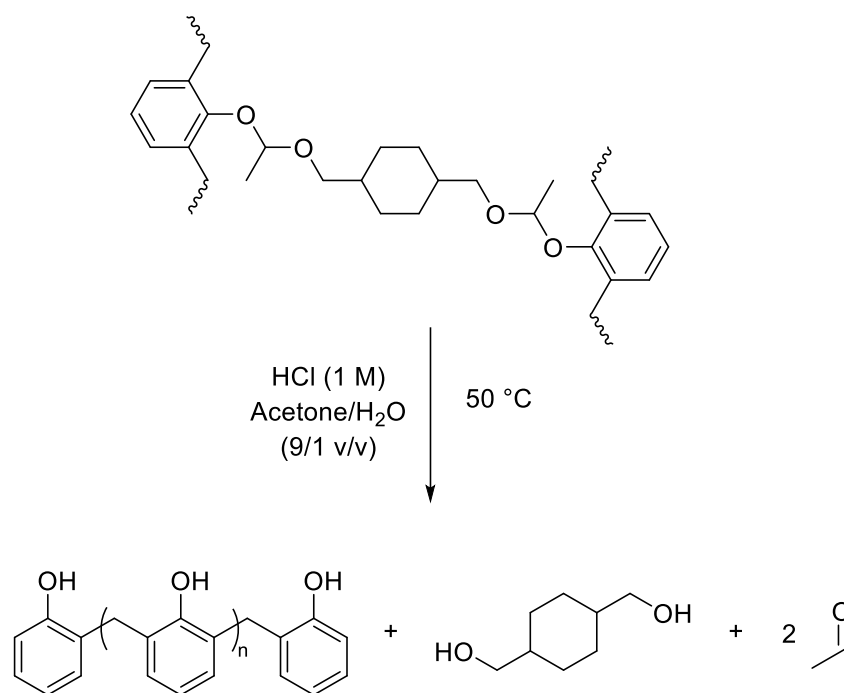
Yuan *et al.* synthesised a dicyclo diacetal degradable component *via* reacting two equivs. of vanillin with erythritol and subsequent functionalisation of this diacetal with epichlorohydrin to yield a diepoxy monomer. This was polymerised with diaminodiphenyl sulfone yielding a pH degradable resin that formed erythritol and vanillin derivatives (Scheme 3-5). Real time ¹H NMR spectra of the degradation process were recorded in 0.1 M HCl DMSO-d₆/H₂O (9/1 v/v) at 50 °C and found to be complete within 5 hrs. The authors found that degradation time decreased from 160 to 55 mins with increasing solvent polarity due to greater ease of hydrogen ion ionisation. Thin film degradation outcome was dependent on the acetone/H₂O ratio in 0.1 M HCl solutions. When using 9/1-5/5 v/v solutions thin films degraded within 2 hrs.

However, when the ratio was 4/6-1/9 no degradation was observed, this was thought to be due to the low acetone content reducing the solubility of degradation products. Lastly degradation time was found to decrease with increasing acid strength in 1 M acetone/H₂O (9/1 v/v) solutions; HCl, H₂SO₄ and H₃PO₄ gave degradation times of 40, 70 and 480 min. respectively.¹⁷⁴



Scheme 3-5 – Bioderived acetal containing epoxy resins synthesised by Yuan *et al.*¹⁷⁴

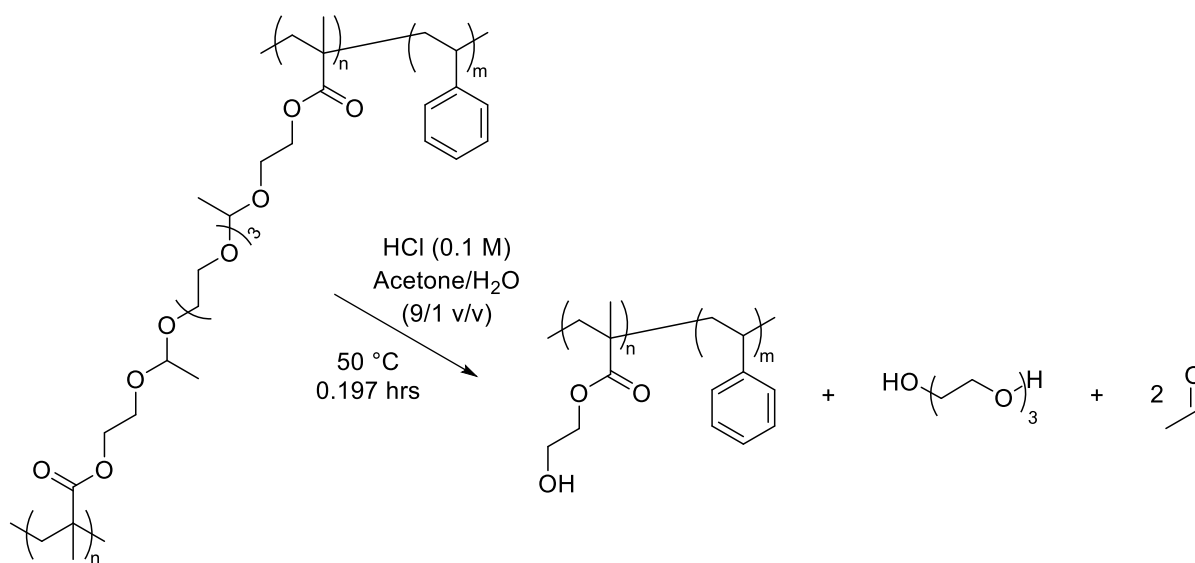
Li *et al.* synthesised acetal resins from phenolic resins and 1,4-cyclohexanedimethanol vinyl ether that degraded to the parent phenolic resin, 1,4-cyclohexanedimethanol and acetaldehyde (Scheme 3-6). The authors characterised the network degradation rate gravimetrically and used solvent contact angle on the surface of thermosets to select suitable solvents for degradation, finding degradation rate was increased when contact angles were low in solutions of acetone/H₂O. Further to this, the authors found that degradation rate was found to increase in solvents that gave a high swelling ratio. The degradation rate decreased with acid strength and no degradation was observed in acetic and phosphoric acids in 0.1 M acetone/H₂O solutions.⁷⁰ Further studies by Wang *et al.*⁹⁹ on acetal containing epoxy resins, Li *et al.*⁷² on resins synthesised from epigallocatechin gallate and tri(ethylene glycol)divinyl ether, and Chen *et al.*⁷³ on phenolic resin and tri(ethylene glycol)divinyl ether derived resins found degradation was dependent on acid concentration and type, temperature and solvent.



Scheme 3-6 – Degradation of phenolic resins with acetal cross-links.⁷⁰

Lu *et al.*⁷¹ synthesised a series of styrene, 2-ethylhexyl methacrylate and HEMA copolymers and terpolymers. During the syntheses, cross-linking was performed *in situ via* reaction of the HEMA hydroxyl and tri(ethylene glycol)divinyl ether to form diacetal cross-links. The acid degradation products yielded linear polymers, tri(ethylene glycol) and acetaldehyde (Scheme 3-7). These cross-links are identical to those generated when cross-linking networks with A1; the cross-links were varied from 0-10 mol %. The authors used swelling ratios to select suitable solvents for degradation. DMF and DMSO gave the greatest swelling ratios for all samples, however, they favoured THF due to its low boiling point. The authors found that the contact angle of various THF/H₂O solutions and neat THF was lowest when the ratio was THF/H₂O 9/1 v/v, which also had the highest degradation rate at 50 °C and complete dissolution was achieved in 0.17 hrs. Cross-link density was found to slow the degradation time in 0.1 M HCl THF/H₂O (9/1 v/v) at 50 °C from 0.17 to 4 hrs when increasing from 2.5 to 10 mol % cross-linker. The authors focussed on styrene copolymers with 5 mol % acetal cross-linker and found that increasing temperature from 25 to 50 °C in 0.1 M HCl THF/H₂O (9/1 v/v) decreased the degradation time from 21.5 to 0.197 hrs. Changing the solvent in 0.1 M HCl

solvent/H₂O (9/1 v/v) solutions was found to have a large effect on degradation, when using acetone, ethanol, methanol, DMF and DMSO the greatest mass loss was 26.86 % after 12 hours in acetone. Having determined THF to be the most efficient solvent for degradation the authors investigated the effect changing the ratio of THF/H₂O in 0.1 M HCl at 50 °C had on degradation. Increasing the H₂O content slowed degradation and, interestingly, decreasing it to 9.5/0.5 THF/H₂O also increased the degradation time from 0.197 to 0.25 hrs. Lastly, the authors also showed that degradation rate decreased when decreasing the acid concentration.



Scheme 3-7 – Degradable thermosets bearing identical cross-links to A1.⁷¹

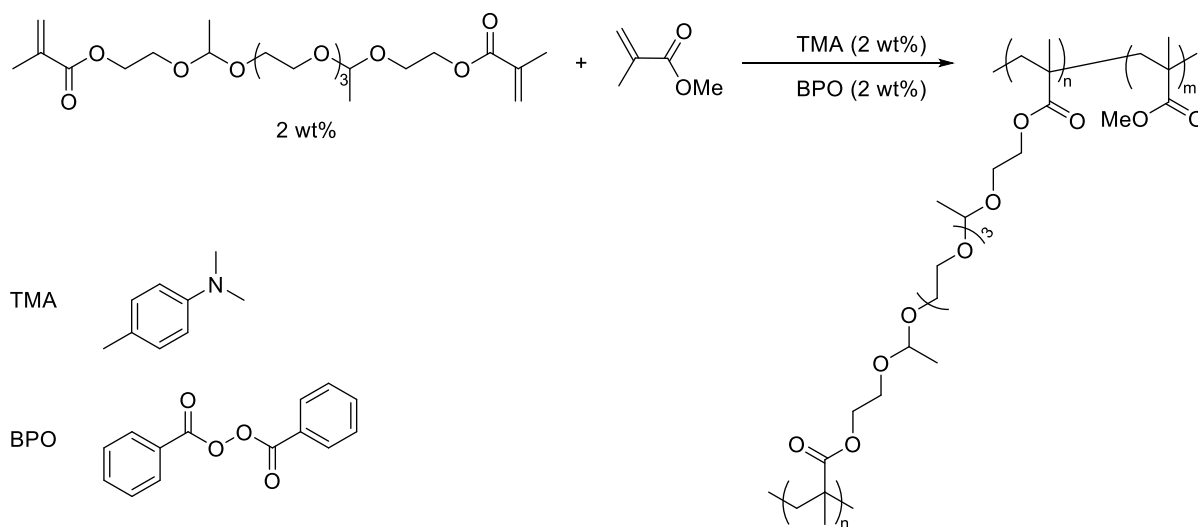
While acetal containing degradable thermosets have been in the literature since Watson *et al.* reported them in 1996,¹⁷¹ it is only recent examples that have begun to characterise their degradation behaviour and products.^{70,174} Lu *et al.* synthesised thermosets with identical cross-links to A1, however the cross-link was produced *in situ* during the polymerisation by reacting HEMA with TEGDVE. Within this chapter free radical curing thermosets of methyl methacrylate cross-linked with A1 are synthesised and characterised. Subsequently their degradation behaviour is characterised and compared to that of A1.

3.2. Results and Discussion

3.2.1. Degradable A1 and methyl methacrylate thermosets

3.2.1.1. Synthesis and Thermal Characterisation of p(MMA-co-A1)

Having synthesised A1 and demonstrated its full hydrolysis in 0.15 M solutions of acids with a $pK_a < 1.29$, it was expected that thermosets cross-linked with A1 would be degradable under acidic conditions. A model thermoset was synthesised by bulk polymerisation of MMA and A1 (2 wt%) using benzoyl peroxide (BPO) and 4,*N,N*-trimethylaniline (4-TMA) as a redox initiator (Scheme 3-8). MMA, BPO and 4-TMA were selected as they are used in commercial adhesive systems,³ although MMA use is less prevalent due to regulations controlling the use of volatile organic compounds (VOCs).¹⁷⁵



Scheme 3-8 Synthesis of acid degradable model adhesive *via* bulk polymerisation.

The networks were characterised by thermogravimetric analysis (TGA) and differential scanning calorimetry (DSC). TGA gives insight into the temperature at which thermal degradation of the thermoset occurs and therefore an understanding of the operating temperatures it can withstand during its processing and application. Furthermore, TGA allows determination of the loss of any volatile components that can indicate residual monomers from the synthesis of the thermoset.¹⁷⁶

DSC allows measurement of the glass transition temperature (T_g), the temperature at which polymers undergo a physical transition from the glassy to rubbery state. For thermosets no further transition is observed due to the chemical cross-links in the network.¹⁷⁷ However, the T_g provides understanding of the degree of cure (extent of reaction) when synthesising thermosets,^{178,179} and is another useful parameter for processing and application temperatures. Failure to understand the thermal properties of polymers prior to their application can have catastrophic failures, such as the Space Shuttle Challenger disaster.¹⁸⁰

TGA revealed a thermal profile inconsistent with that of a cross-linked MMA thermoset (Figure 3-1). Linear poly(MMA) is known to undergo a thermal depolymerisation that gives a rapid loss of mass at temperatures >200 °C, the temperature at which this occurs is influenced by end groups,^{181–183} and the types of linkages present in the backbone (i.e. head-tail, tail-tail, head-head) which each have their own thermal stability and impart the thermal profile with mass loss at different temperatures.^{184–187} Cross-linked p(MMA) exhibits a similar thermal profile to that of its linear equivalent but with a higher thermal stability resulting from the cross-links.¹⁸⁸ However, the TGA profile of A1 cross-linked MMA model adhesives used in preliminary degradation studies displayed a loss of volatile compounds at ~ 100 °C which was attributed to residual MMA from the polymerisation. Following this a gradual loss in mass was observed that dropped sharply at 400 °C. The presence of further volatile species was an indication that low conversion was reached during the polymerisation.

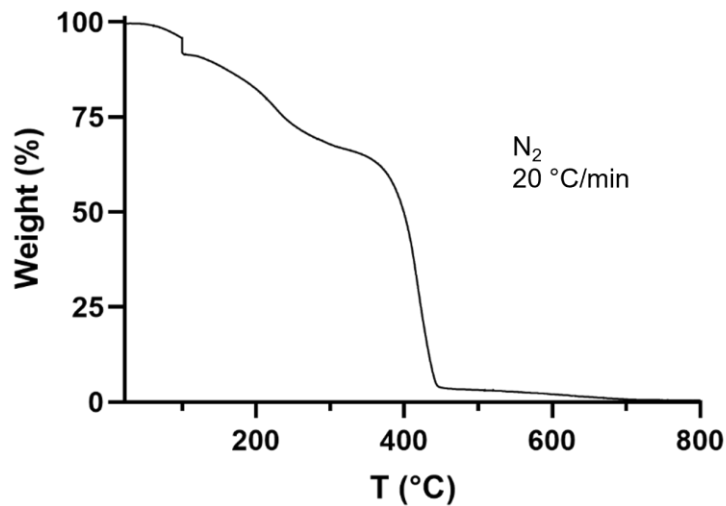


Figure 3-1 TGA thermogram of A1 cross-linked MMA model adhesive.

DSC characterisation of the model adhesive further supported low monomer conversion. Cross-linking is known to increase the T_g ,¹⁸⁹ therefore the T_g was expected to be higher than that of linear p(MMA) which is in the region of 105-120 °C.¹⁹⁰ However, the observed T_g was much lower than expected ~50 °C (Figure 3-2). Such a low T_g is indicative of the presence of unreacted MMA plasticising the thermoset network.¹⁸⁹ The evidence of low conversion when making the model thermosets has implications for the future analysis of degradation. Therefore, a more detailed investigation of the thermoset synthesis was undertaken.

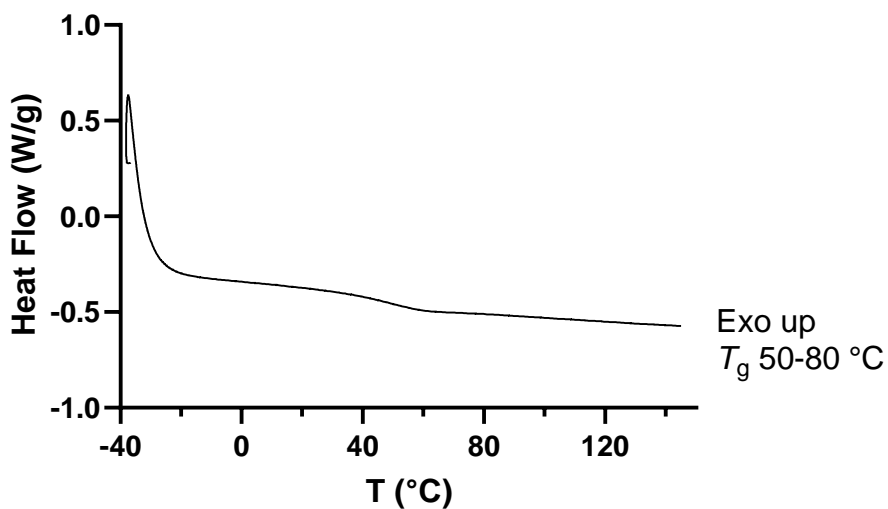
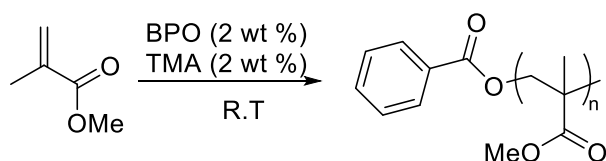


Figure 3-2 DSC thermogram of A1 cross-linked MMA model adhesive, 20 °C/min from -40-150 °C.

3.2.1.2. Effect of Post Curing on glass transition temperature

A bulk polymerisation of MMA to p(MMA) (Scheme 3-9) was used as a model into the cure kinetics and the effect of thermal post curing treatment on the T_g of p(MMA). p(MMA) was chosen as its T_g is well known, ranging from of 105-120 °C.¹⁹⁰ Furthermore, the synthesis of linear p(MMA) enabled the reaction to be monitored by ¹H NMR spectroscopy, preliminary experiments to track conversion gravimetrically were hindered by experimental error due to the volatility of MMA causing the mass to vary.



Scheme 3-9 Model p(MMA) synthesis.

MMA was polymerised using the same redox initiator system, BPO and 4,*N,N*-trimethylaniline (TMA) at 2 wt %, as initial model thermosets. Initial attempts to study the kinetics of the bulk polymerisation were unsuccessful due to difficulty in sampling the high viscosity reaction mixture.¹⁹¹ The experimental setup was changed to a series of batch bulk polymerisations each corresponding to a time point, this leads to greater experimental error but enables the characterisation of the high viscosity and glassy reaction media. Again, initial experiments were unsuccessful due to inconsistent conversion thought to arise from further polymerisation taking place after quenching by exposure to air. To ensure no further polymerisation could occur in the highly concentrated reaction medium each sample was quenched by the addition of acetone- d_6 /D₂O MEHQ solution and immersion of the reaction vessel into liquid nitrogen. Conversion of MMA to p(MMA) was determined by ¹H NMR spectroscopy (Figure 3-3) and showed the reaction reached ~90 % conversion after 6 hrs. Upon leaving the reaction for 24 hrs no further reaction was observed.

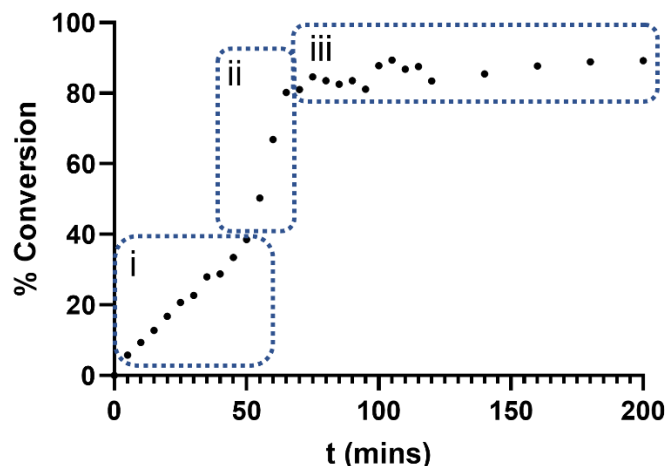


Figure 3-3 - Conversion of MMA during p(MMA) model thermoset synthesis determined by ^1H NMR.

Free radical polymerisation undergoes an auto-acceleration process, also known as the Trommsdorff-Norrish effect, which results from the effect of changing reaction medium on the termination constant k_t of propagating chains, this is observed as three distinct regions (Figure 3-3, labelled i, ii and iii).¹⁹¹ Region i falls between 0-40 % conversion and is a low viscosity mixture of p(MMA) in MMA, termination occurs by chain transfer, combination, disproportionation or inhibition.¹⁹² During this region viscosity increases with conversion leading to a decrease in the segmental and translation diffusion that enables chain ends to meet species capable of terminating the propagating chain end.

As the reaction reaches the gel point k_t decreases leading to an increase in the rate of reaction (region ii) and auto-acceleration is observed. Within this region the diffusion of propagating chain ends by translational and segmental motion and reptation occurs over a timescale that is large with respect to the lifetime of a propagating chain. However, low molar mass species such as monomers can diffuse quickly through the gel-like reaction medium. Further reaction leads to the formation of a glassy matrix (region iii) in which the remaining monomer diffuses slowly and k_t and k_p are low.^{191,192} Under the reaction conditions the polymerisation reached ~90 % conversion. Further reaction is unlikely to occur without elevating the temperature of the glassy p(MMA) matrix above the T_g of 105 °C, such as to 120 °C, in a process known as post-curing.¹⁹¹

Samples of p(MMA) were again synthesised by the bulk polymerisation of MMA (Scheme 3-9) and the effect of post-cure temperature and time on the T_g was investigated by DSC (Figure 3-4). When post-cured for 24 hrs at 60 °C and 80 °C the T_g was much lower than expected at 54 °C and 66 °C, respectively. However, post-curing at 100 °C for 24 hrs and 48 hrs the T_g was found to be 82 °C and 107 °C, respectively. The increase in T_g is likely from a combination of thermally-initiated polymerisation, the increased mobility of MMA in the softened p(MMA) matrix and the evaporation of unreacted MMA. A T_g of 107 °C falls within the expected range for p(MMA), therefore, the reaction conditions in Scheme 3-9 and the post-curing conditions of 100 °C for 48 hrs were chosen for the synthesis of A1 and MMA-based thermoset resins for investigations into thermoset degradation.

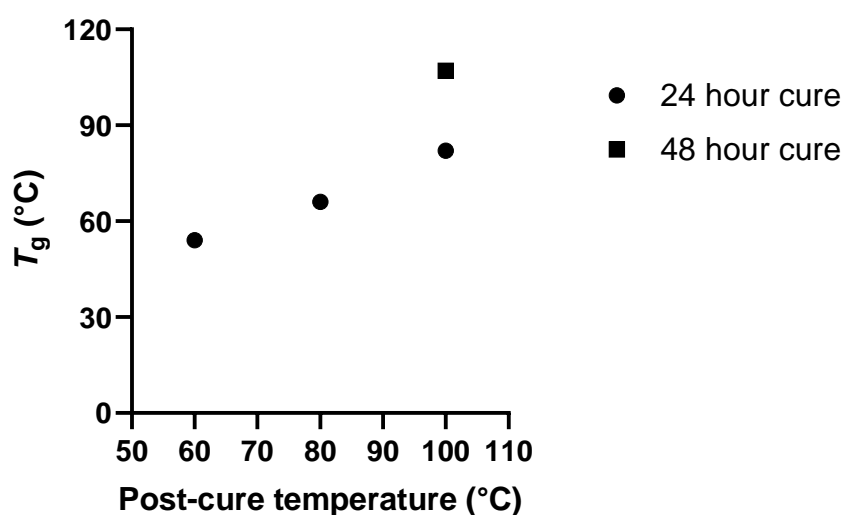
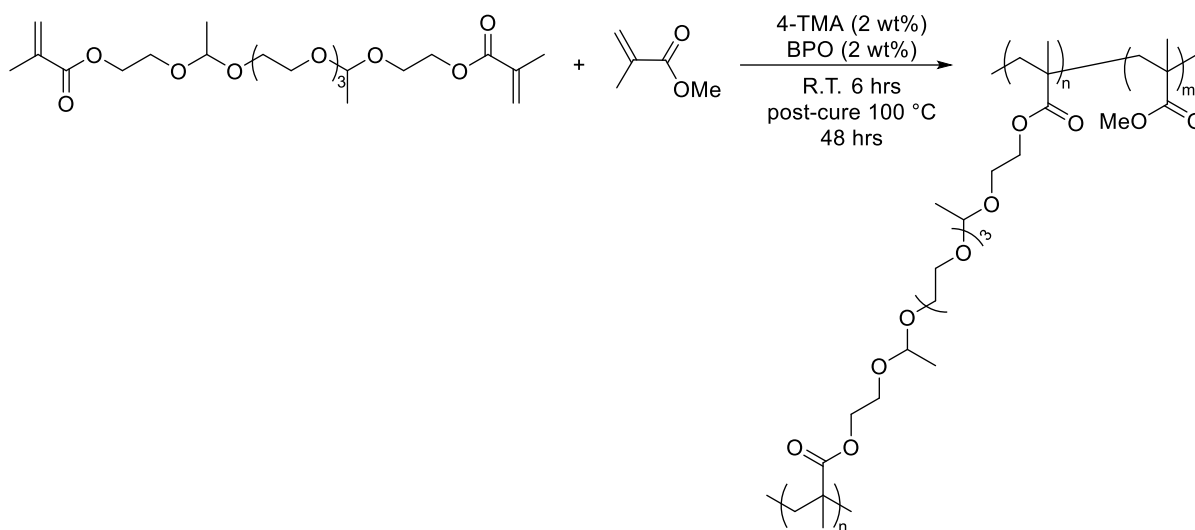


Figure 3-4 Effect of post-cure temperature and time on the T_g of p(MMA).

p(MMA-co-A1) was synthesised using the optimised conditions (Scheme 3-10) yielding a glassy resin. Characterisation by TGA (Figure 3-5) showed a sharp mass loss at temperatures >200 °C consistent with thermal depolymerisation. Unlike previously synthesised p(MMA-co-A1), no observed loss of volatiles was observed. Furthermore, the gel content was determined to be 94% showing a high amount of insoluble material was present, indicating a high degree of cure was achieved. DSC characterisation showed the T_g was 102 °C (Appendices Figure 8-4), higher than the T_g of 50 °C that was previously observed for

p(MMA-co-A1). Having found a suitable method for synthesising p(MMA-co-A1), the degradation properties were re-investigated.



Scheme 3-10 Synthesis of p(MMA-co-A1) using the modified reaction and post-cure conditions.

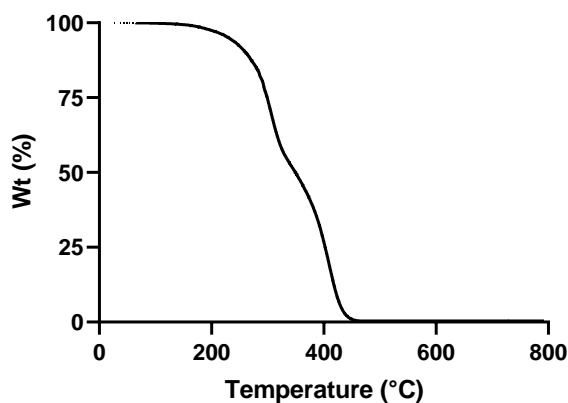
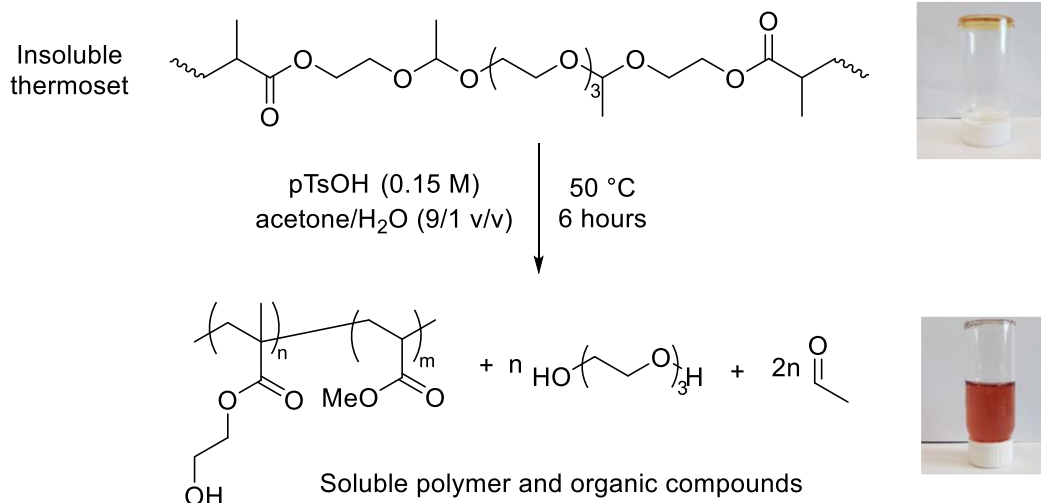


Figure 3-5 TGA thermogram (N₂, 20 °C/min) of p(MMA-co-A1) cured using optimised conditions.

3.2.1.3. Acid Degradation of p(MMA-co-A1)

Based upon previous A1 hydrolysis experiments it was hypothesised that acetal groups in networks cross linked with A1 would be stable under basic and neutral conditions and some weakly acidic solutions. However, when exposed to 0.15 M solutions of acids with a $pK_a < 1.29$ the acetal groups should be hydrolysed, breaking the chemical cross links and yielding a homogeneous solution of p(MMA-co-HEMA), TEG and acetaldehyde (Scheme 3-11). Samples of the cured thermoset p(MMA-co-A1) were soaked in a solution of pTsOH (0.15 M)

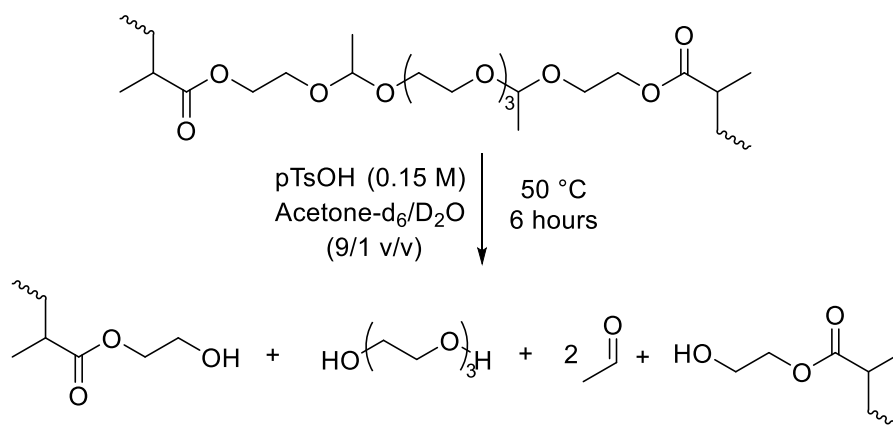
in acetone/H₂O (9/1 v/v) at 50 °C for 6 hrs and visually checked for the formation of a homogeneous solution. Over 6 hrs the glassy thermoset became a swollen gel before forming a homogeneous red solution indicating hydrolysis of the acetal groups. Thus, demonstrating A1 as a suitable cross-linker for acid degradable methacrylate-based thermosets.



Scheme 3-11 Acid degradation pathway of A1 cross-linked adhesives.

3.2.1.4. ¹H NMR Spectroscopic and Gravimetric Study of Thermoset Degradation

Having previously shown the hydrolysis products of the cross-linker A1 were HEMA, acetaldehyde and TEG, an experiment was designed to ensure A1 cross-linked thermosets followed the same hydrolysis pathway. Samples of p(MMA-co-A1) were ground to a powder and degraded in a stock solution of pTsOH (0.15 M) in acetone-d₆/D₂O (9/1 v/v) at 50 °C. Residual insoluble p(MMA-co-A1) was removed by filtration. The filtrate was then characterised by ¹H NMR spectroscopy, and showed the small molecules tri(ethylene glycol) and acetaldehyde were produced with the copolymer p(MMA-co-HEMA). This is consistent with the mechanism of acetal hydrolysis⁹⁴ and shows the hydrolysis of acetal groups in cross-links gives rise to the acid degradation of p(MMA-co-A1).



Scheme 3-12 ^1H NMR spectroscopy study of p(MMA-co-A1) thermoset degradation.

Using the ^1H NMR spectroscopy data the evolution of acetaldehyde over time was monitored and the concentration calculated by comparing with the known analyte pTsOH present in the stock solution (Figure 3-6 and Appendix Figure 8-5). The concentration of acetaldehyde reached a maximum after 135 min. However, previous network degradation experiments took 300 minutes to form homogeneous solutions. This suggests the rate of network degradation is dependent upon the solubilisation of the formed p(MMA-co-HEMA) and acetal hydrolysis. This may also be due to the increased surface area of the ground powder being degraded.

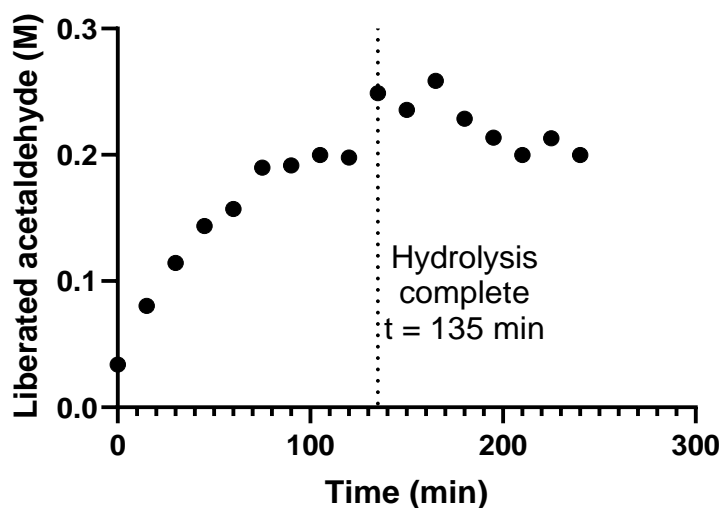


Figure 3-6 Evolution of acetaldehyde during the degradation of p(MMA-co-A1) networks in acetone- $\text{d}_6/\text{D}_2\text{O}$ (9/1 v/v) pTsOH (0.15 M) solutions measured by ^1H NMR spectroscopy.

The degradation kinetics of p(MMA-co-A1) were then followed gravimetrically. Based upon the previous experiment all acetal groups present in p(MMA-co-A1) are hydrolysed after 135 minutes (Figure 3-7). Consequently, any remaining heterogeneous material is p(MMA-co-HEMA) undergoing solubilisation. This was found to be 29 % of the starting mass after 135 minutes. Therefore, polymer dissolution is contributing to the degradation kinetics of p(MMA-co-A1) thermosets.

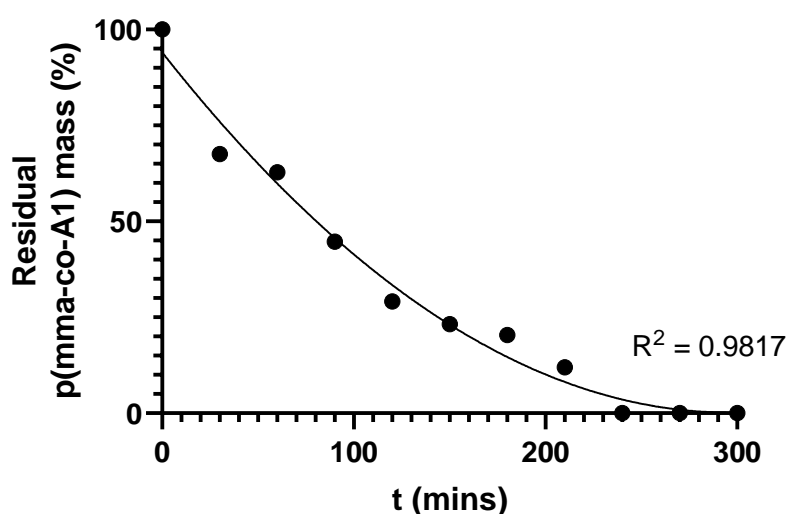


Figure 3-7 Degradation kinetics of p(MMA-co-A1) thermoset in acetone/H₂O (9/1 v/v) pTsOH (0.15 M) at 50 °C for 6 hours.

3.2.1.5. Effect of Solvent on Degradation

The degradation of p(MMA-co-A1) thermosets was then investigated in different solvent/water (9/1 v/v) pTsOH (0.15 M) solutions at 50 °C (Figure 3-8). Acid degradation rates of epoxy resins bearing acetal groups have been shown to increase with the polarity of the solvent used,¹⁷⁴ however, no such relationship was observed for p(MMA-co-A1). The epoxy resins in question degraded to small molecules, whereas p(MMA-co-A1) yields p(MMA-co-HEMA). Homogeneous solutions were formed within 5 hrs in all solvents except DMSO (Figure 3-8). Upon leaving the DMSO experiment to run for 24 hours the system remained heterogeneous. This could be due to poor swelling of the thermoset in DMSO resulting in a low diffusion of pTsOH and H₂O to the acetal groups, meaning hydrolysis occurs exceedingly slowly.

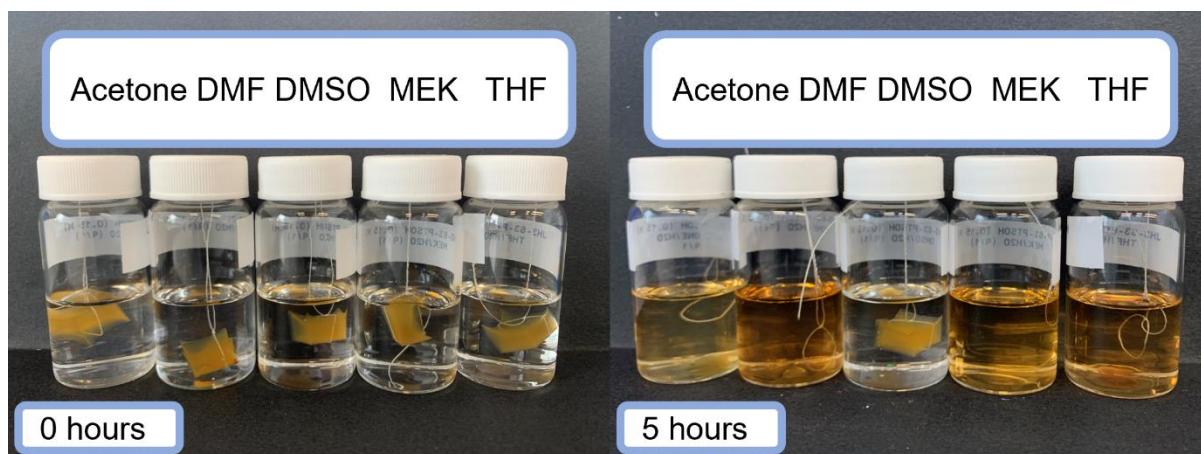


Figure 3-8 Degradation of p(MMA-co-A1) thermosets in different solvent/H₂O (9/1 v/v) pTsOH (0.15 M) solutions.

The swelling ratio of the neat solvents was then determined at room temperature by comparing the initial mass with the swollen mass. In the swollen state the amount of pTsOH and H₂O transported into the thermoset matrix by solvent is expected to be higher. Therefore, it is hypothesised that degradation is more likely to occur in solvents that exhibit a high swelling ratio on p(MMA-co-A1).

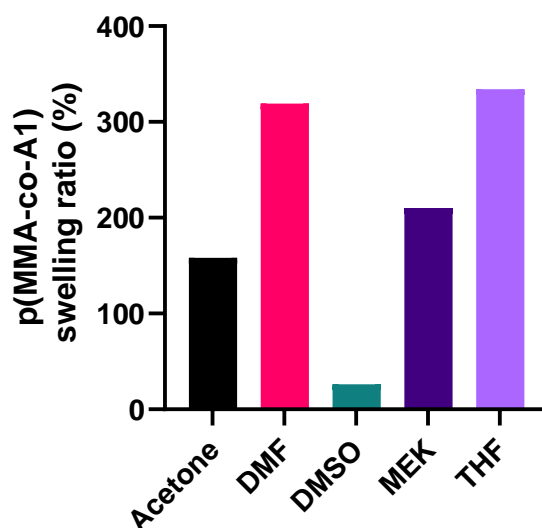


Figure 3-9 Swelling ratio of p(MMA-co-A1) in different solvents.

The swelling ratios were found to be >150 % for all solvents except DMSO which was 26 %. It is therefore plausible that the concentration of pTsOH and H₂O is low in p(MMA-co-A1) when exposed to DMSO and hydrolysis of the acetal groups is zero, low or occurring only at the

surface. A second scenario is also possible whereby hydrolysis of the acetal groups occurs producing p(MMA-co-HEMA); the theoretical amount of the comonomer HEMA present would be very low as only 2 wt% A1 is used to cross-link the thermosets. However, upon taking the remaining sample and drying in a vac oven at 100 °C it was found that 101 % of the starting mass remained suggesting no degradation had occurred. Having observed that a high swelling ratio is required for degradation, further experiments were continued in acetone due to its low toxicity, price and potential to be renewably sourced.¹⁶⁶

3.2.1.6. Effect of Solvent/Water Ratio on Degradation

p(MMA-co-A1) was degraded in acetone/H₂O solutions of varying v/v ratios. The pTsOH concentration was kept constant at 0.15 M and the temperature was held at 50 °C. It was found that increasing the amount of water led to a qualitative decrease in degradation. After 5 hrs residual p(MMA-co-A1) remained in all but the 9/1 v/v acetone/H₂O pTsOH (0.15 M) solution. Samples treated in 8/2 and 7/3 acetone/H₂O solutions were visibly swollen and the solution had taken on the yellow colour of the thermoset. However, samples in the 6/4 and 5/5 acetone/H₂O solutions remained largely unchanged. Upon filtering and drying *in vacuo* at 100 °C the residual thermoset samples it was found that >80 % of the starting mass remained for all but the 9/1 v/v acetone/H₂O pTsOH (0.15 M) solution (Figure 3-11).

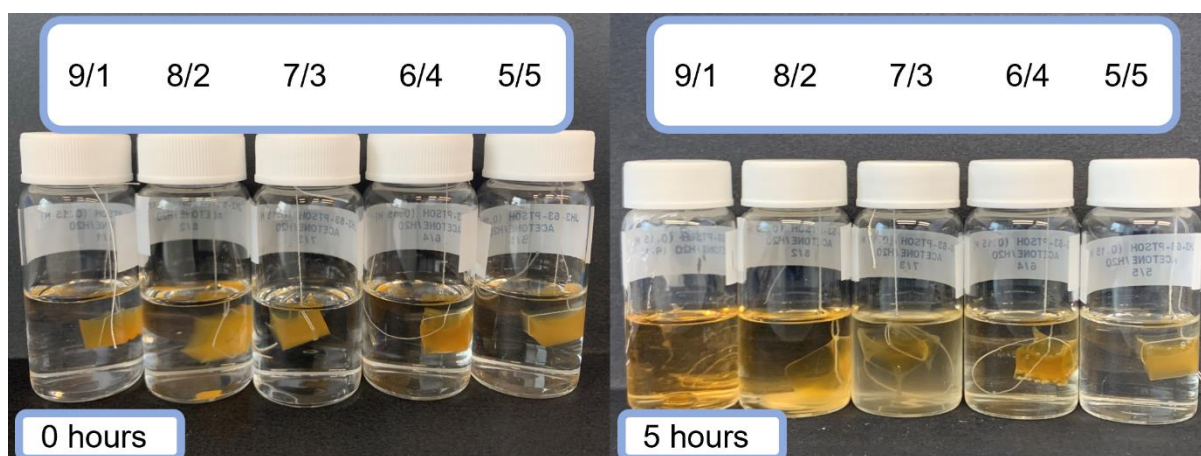


Figure 3-10 Degradation of p(MMA-co-A1) in acetone/H₂O pTsOH (0.15 M) solutions at 50 °C.

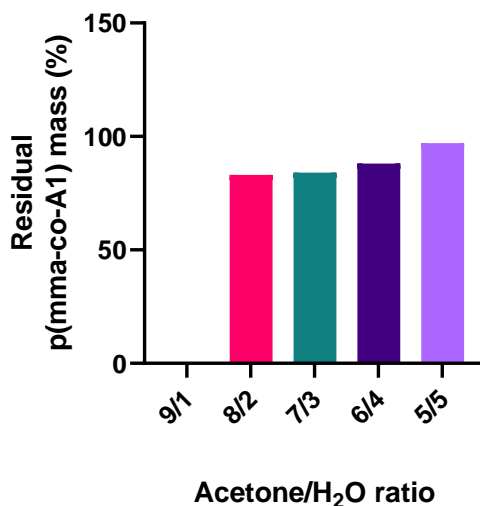


Figure 3-11 Effect of acetone/H₂O ratio of swelling ratio of p(MMA-co-A1) (left) and remaining mass after exposure to different acetone/H₂O pTsOH (0.15 M) solutions (right).

The swelling ratios of p(MMA-co-A1) in acetone and acetone/H₂O solutions ranging from 9/1 to 5/5 v/v show a large decrease upon increasing the H₂O content of the solutions (Figure 3-11). Coupling this with the degradation experiments, there is further support that the ability of the solution to swell the thermoset has a direct impact on the degradation of p(MMA-co-A1) to a homogeneous solution.

3.2.1.7. Effect of Acid Species on Degradation

Previously, the effect of pK_a on the extent of hydrolysis on the cross-linker A1 was investigated (2.2.1.3) and the extent of hydrolysis was found to decrease with increasing pK_a . In those experiments, the hydrolysis was monitored by ¹H NMR spectroscopy. However, the degradation of p(MMA-co-A1) thermosets by acetal hydrolysis is a complex multistep process involving chemical reactions and physical processes which occur on different timescales. Therefore, the effect of pK_a on p(MMA-co-A1) thermoset degradation was investigated to see if the same trend was observed.

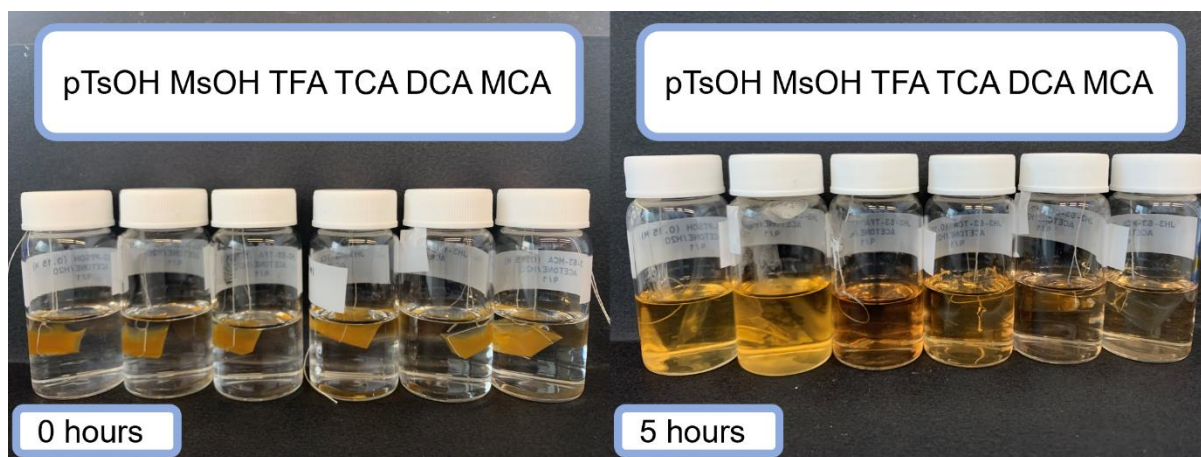


Figure 3-12 Effect of acid on degradation of p(MMA-co-A1).

It was found previously that complete hydrolysis of A1 occurred in acetone- d_6 /D₂O 0.15 M solutions of pTsOH, MsOH, TFA and TCA after 5 hrs at 50 °C. Samples of p(MMA-co-A1) were soaked in 0.15 M acetone/H₂O solutions of pTsOH, MsOH, TFA, TCA, DCA and MCA for 5 hrs at 50 °C to compare the thermoset degradation behaviour to A1. The degradation of p(MMA-co-A1) in the pTsOH, MsOH and TFA solutions was complete within 5 hrs, as was the hydrolysis of A1. However, in the case of TCA it was found that 65 % of the starting mass remained after 5 h, which previously gave complete hydrolysis of A1 (Figure 3-13). This shows the acidic degradation of p(MMA-co-A1) is different to the hydrolysis of A1.

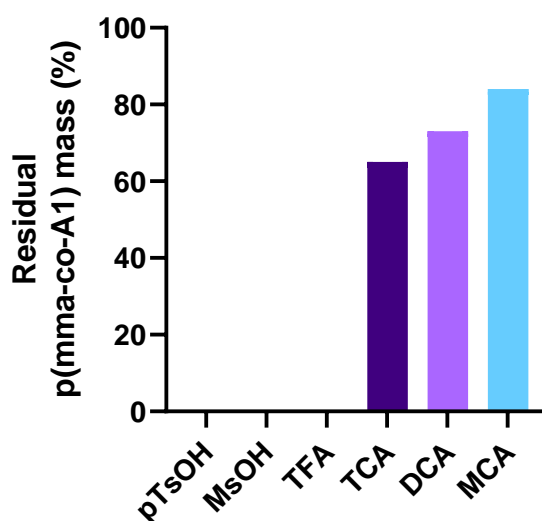


Figure 3-13 Residual weight of p(MMA-co-A1) thermosets after degradation in acetone/H₂O (9/1) acid (0.15 M) solutions.

3.2.2. Degradation Mechanism

From the degradation experiments it is clear the mechanism of p(MMA-co-A1) degradation is dependent on a series of physical and chemical processes. Although there is little literature devoted to the degradation process of pH responsive thermosets, the individual processes thought to be involved, (solvent induced swelling of the thermoset, diffusion of active species throughout the network and polymer dissolution) have been subject to theoretical and experimental investigation. Early on in degradation these processes may occur simultaneously but ^1H NMR spectroscopy has shown the evolution of acetaldehyde reaches a maximum after 135 mins suggesting the final step in p(MMA-co-A1) degradation is dissolution of the produced p(MMA-co-HEMA).

Based upon the experimental findings and available literature, the following mechanism of p(MMA-co-A1) degradation is proposed (Figure 3-14). The physical state of the polymer component of the system transitions from glassy polymer to swollen gel and finally solvated 'free' polymer as the system becomes homogeneous. On a molecular scale the process is more complicated as will be discussed. At $t=0$, or prior to immersion in a pTsOH (0.15 M) acetone/ H_2O (9/1 v/v) solution, the thermoset is a glassy network. Upon immersion solvent diffuses into the thermoset at the interface (i, Figure 3-14). As it diffuses new interfaces are created between solvent and swollen gel, and glassy matrix and swollen gel. Within the swollen gel region hydrolysis of the acetal groups can now occur as pTsOH and H_2O diffuse with the solvent. The network composition of this region is complex with cross-linked chains, partially cross-linked chains and newly formed linear p(MMA-co-HEMA) the result of full cross-link hydrolysis. The latter of these can then undergo dissolution once chain entanglements are overcome by movement of the chain, the rate of which is likely to increase as more cross-links are hydrolysed leading to a net increase in mobility. It is assumed the system becomes a swollen gel (ii, Figure 3-14) before $t=135$ minutes (Figure 3-6) when all acetal groups have been hydrolysed as the accompanying pTsOH and H_2O , that diffuse into the network with acetone, are required for hydrolysis to occur. The true structure of the network at this point is

a mixture of hydrolysed and cross-link chains, some of the former will have begun to undergo dissolution into the solvent which is observed qualitatively in experiments as a reduction in size of the gel. After 135 mins. the acetal groups are consumed leaving only p(MMA-co-HEMA) to undergo dissolution (iii, Figure 3-14) in the remaining 280 mins, it is therefore clear that the rate of p(MMA-co-A1) degradation is dependent on swelling and diffusion, acetal hydrolysis and dissolution of the formed p(MMA-co-HEMA).

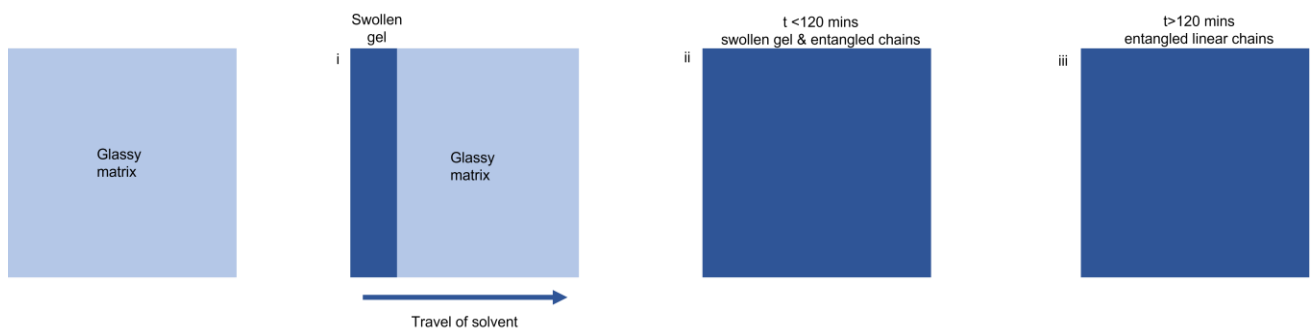


Figure 3-14 Proposed mechanism of p(MMA-co-A1) degradation.

3.3. Conclusions

p(MMA-co-A1) thermosets were used as a model system for degradation experiments, synthesised *via* bulk polymerisation initiated by the redox system BPO/TMA. However, initial characterisation *via* TGA and DSC showed loss of low molecular weight species and an unexpectedly low T_g indicating a low degree of cure. To circumnavigate challenges associated with characterising cross-linked networks the curing of a model p(MMA) system was followed by ^1H NMR spectroscopy using the same reaction conditions. Conversions of MMA were around 80 % which is characteristic of bulk free radical polymerisations. Therefore, the effect of post curing in an oven at different temperatures and durations was investigated. The highest p(MMA) T_g was obtained after post-curing for 48 hrs at 100 °C and p(MMA-co-A1) cured under the same conditions had a T_g of 102 °C.

p(MMA-co-A1) was found to form homogeneous solutions when soaked in pTsOH (0.15 M) acetone/H₂O (9/1 v/v) solutions at 50 °C for 6 hrs, this was then repeated and monitored gravimetrically revealing degradation was complete at 5 hrs. However, ^1H NMR spectroscopy of degradation filtrates showed acetaldehyde was no longer produced at 2 hrs suggesting the degradation process was dependent on a variety of factors. The effect of solvent, solvent water ratio and acid pK_a on degradation were investigated. The solvent swelling ratio was found to be related whether thermoset samples degraded, and acetone was chosen for further studies. The ratio of acetone/H₂O had to be kept at 9/1 v/v for degradation to occur within 5 hrs at 50 °C and was also thought to be due to the lower swelling ratio when using 8/2 v/v or lower. Lastly, the effect of acid pK_a in 0.15 M acid in acetone/H₂O (9/1 v/v) solutions at 50 °C over 5 hrs on degradation was investigated using the same acid series in Chapter 2. Interestingly the cross-linker A1 was fully hydrolysed by trichloroacetic acid within 5 hrs, however, only 35 % mass loss was observed in the p(MMA-co-A1) thermosets after 5 hrs further suggesting the degradation kinetics are dependent on physical and chemical factors that we propose a mechanism for.

3.4. Experimental

3.4.1. Materials

A1 was synthesised as described in chapter two. Methyl methacrylate (99.0 %) was purchased from Acros Organics. Basic alumina and DMF (≥ 99.0 %) were purchased from Fisher. Methyl ethyl ketone (laboratory reagent grade) was purchased from Scientific Laboratory Supplies. 4-methoxy phenol (99 %), 4-*N,N*-trimethylaniline (99%), benzoyl peroxide (Luperox, 25 % H₂O), DMSO (≥ 99.9 %), isobutyl acetate (natural, ≥ 97.0 %) and methane sulfonic acid (≥ 99 %), were purchased from Sigma-Aldrich. All reagents were used as supplied, unless otherwise stated. Details of other materials can be found in Chapter 2.4.

3.4.2. Instrumentation

DSC was performed on a TA Instruments DSC25, 5-10 mg of sample was placed in an aluminum Tzero pan that was sealed with a Tzero Hermetic lid. Samples were equilibrated at -40 °C for five minutes before the following program, 20 °C/min ramp to 200 °C, 20 °C/min ramp to -40 °C and a final 10 °C/min ramp to 200 °C. The T_g was determined using the TA Instruments Trios software. TGA was performed on a TA Instruments Q500, ~10 mg of sample was placed in a flame cleaned platinum pan and heated under N₂ from 25-800 °C at a ramp rate of 20 °C/min. Details of other instrumentation can be found in Chapter 2.4.

3.4.3. Model Adhesive Synthesis

The following stock solutions were prepared. Methyl methacrylate (82.8 g, 0.83 mol), A1 (1.8 g, 4.0 mmol) and benzoyl peroxide (25 % H₂O, 4.8 g, 15 mmol) were mixed. Methyl methacrylate (86.4 g, 0.86 mol) and 4-*N,N*-trimethylaniline (3.6 g, 26 mmol) were mixed. The two solutions were added to a 200 mL dual syringe equipped with a static mixer. Adhesives were then dispensed into moulds (0.5 cm³) and cured at room temperature for 48 hrs before being placed in an oven preheated to 40 °C oven overnight. The product was a glassy orange cube.

3.4.4. Adhesive Degradation Study

To poly(MMA-co-A1) (~500 mg) a solution of acid (10 mL, 0.15 M) in acetone/water (9/1 v/v) was added and heated to 50 °C for 24 hours. If no solubilisation was observed acetone (40 mL) was added and left for 48 hours at 50 °C.

3.4.5. ¹H NMR spectroscopy kinetic study of bulk polymerisation of p(MMA)

Methyl methacrylate was purified by passing over a column of basic alumina. BPO (1.49 g, 4.49 mmol) was added to methyl methacrylate (28.2 g, 0.281 mol) and 4,*N,N*-trimethylaniline (0.575 g, 0.423 mmol) was added to methyl methacrylate (28.2 g, 0.281 mol). Both solutions were degassed with N₂ for 30 minutes. 0.5 mL of each solution was added to a sample *vial* sealed with a septum and mixed on a vortex. The reaction proceeded at room temperature for a fixed time. Reactions were quenched by the addition of an acetone-d₆/MEHQ stock solution (1 mL, 0.15 M) followed by immersion of the *vial* in liquid N₂. Samples were diluted with CDCl₃ and their ¹H NMR spectrum recorded. Conversion was calculated using the following equation:

Equation 3-1

$$MMA \text{ conversion } (\%) = \left(1 - \frac{I_{3.55 \text{ ppm}}}{I_{3.55 \text{ ppm}} + I_{3.44}}\right) \times 100$$

3.4.6. Post-curing study of p(MMA)

Methyl methacrylate was purified by passing over a column of basic alumina. BPO (1.49 g, 4.49 mmol) was added to methyl methacrylate (28.2 g, 0.281 mol) and 4,*N,N*-trimethylaniline (0.575 g, 0.423 mmol) was added to methyl methacrylate (28.2 g, 0.281 mol). Both solutions were degassed with N₂ for 30 minutes. 0.5 mL of each solution was added to a sample *vial* sealed with a septum and mixed on a vortex. The reaction proceeded at room temperature for 6 hours. *Vials* were then placed in an oven preheated to 60-100 °C for 24 or 48 hours.

3.4.7. Synthesis and post curing of p(MMA-co-A1)

The following stock solutions were made up. Methyl methacrylate (82.8 g, 0.83 mol), acetal cross-linker (1.8 g, 4.0 mmol) and benzoyl peroxide (25 % H₂O, 4.8 g, 15 mmol) were mixed. Methyl methacrylate (86.4 g, 0.86 mol) and 4,*N,N*-trimethylaniline (3.6 g, 26 mmol) were mixed. The two solutions were added to a 200 mL dual syringe equipped with a static mixer. Adhesives were then dispensed into moulds (0.5 cm³) and cured at room temperature for 6 hours. before being placed in an oven preheated to 100 °C for 48 hours. The product was a glassy orange cube.

3.4.8. ¹H NMR spectroscopy study of p(MMA-co-A1) degradation

Samples of p(MMA-co-A1) (0.05 g) were ground to a fine powder and added to a pTsOH (1.5 mL, 0.15 M) acetone-d₆/D₂O (9/1 v/v) solution and heated to 50 °C for up to 24 hours. The insoluble fraction of adhesive was removed *via* filtration through cotton wool and the ¹H NMR spectrum of the filtrate recorded. The relative concentration of acetaldehyde was calculated from ¹H NMR spectra using the integrals of the following peaks pTsOH at δ 7.68 ppm and acetaldehyde at δ 2.07 ppm. The following equation was used:

Equation 3-2

$$Conc_{acetaldehyde} (M) = \frac{I_{2.07 \text{ ppm}}}{I_{7.68}} \times \frac{No. \text{ of protons}_{pTsOH}}{No. \text{ of protons}_{acetaldehyde}} \times conc_{pTsOH}$$

3.4.9. Gravimetric degradation study of p(MMA-co-A1)

To samples of poly(MMA-co-A1) (~500 mg) acetone/water (9/1 v/v) pTsOH (10 mL, 0.15 M) was added and heated to 50 °C for a fixed time between 0-300 minutes. At pre-determined time intervals, the insoluble fraction was collected by filtration and dried in a vacuum oven at 100 °C for 48 hours and the mass recorded. The remaining weight % was calculated using the following equation:

Equation 3-3

$$Weight (\%) = \left(\frac{initial \ mass - final \ dry \ mass}{initial \ mass} \right) \times 100$$

3.4.10. Degradation Studies

General procedure

To poly(MMA-co-A1) (~500 mg) a solution of acid (10 mL, 0.15 M) in solvent/water (9/1 v/v) was added and heated to 50 °C for 24 hours. If no solubilisation was observed solvent (40 mL) was added and left for 48 hours at 50 °C.

3.4.11. Determination of swelling ratios

General procedure

p(MMA-co-A1) (400 mg) was added to a sample *vial* containing solvent or a solvent/H₂O (9/1 v/v) solution (10 mL). Samples were left at room temperature for 48 hours, removed dried with paper towel and weighed. The swelling ratio was determined using the following equation:

Equation 3-4

$$\text{Swelling ratio (\%)} = \left(\frac{\text{mass of swollen gel} - \text{dry mass}}{\text{dry mass}} \right) \times 100$$

3.4.12. Determination of gel content

p(MMA-co-A1) (200 mg) was added to a Soxhlet thimble and extracted with refluxing THF (300 mL) for 24 hours. Sample placed in a vacuum oven at 70 °C for 48 hours and weighed. The gel content was determined using the following equation:

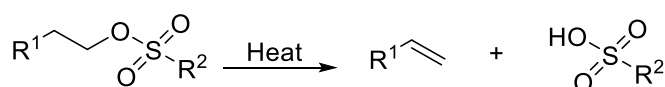
Equation 3-5

$$\text{gel content (\%)} = \left(\frac{\text{initial mass} - \text{final mass}}{\text{initial mass}} \right) \times 100$$

Chapter 4 – Acid Generators

4.1. Introduction

Having demonstrated that methyl methacrylate networks cross-linked with acetal crosslinker A1 could undergo acid-catalysed degradation to form homogeneous solutions of p(MMA-co-HEMA), the use of thermal acid generators (TAGs) and photoacid generators (PAGs) as internal acid sources was investigated. From the results in Chapter 3, the generated acid would need a $pK_a \leq 0.25$, corresponding to trifluoroacetic acid, the weakest acid that fully degraded p(MMA-co-A1) at 0.15 M in acetone/H₂O (9/1 v/v) solutions within 5 hours at 50 °C. Several strategies for the photo release of sulfonic and carboxylic acids exist in the literature.^{116,117,193} The focus of this chapter is largely the thermally-driven intramolecular elimination (E_i) of sulfonates, the products of which are a sulfonic acid and an alkene (Scheme 4-1).¹⁹⁴



Scheme 4-1 – Intramolecular elimination of sulfonate forming an alkene and sulfonic acid.

The mechanism of elimination is debated and may be concerted, proceeding *via* 5 or 6 membered transition states,¹⁹⁵ meaning multiple pathways are possible in the same substrates.^{194,195,204,196–203} Corey *et al.*¹⁹⁴ synthesised a series of 8-quinolyl sulfonates and 2-pyridyl sulfonates from the corresponding sulfonyl chlorides and alcohol using NEt₃, pyridine or ⁿbutyl lithium in yields of 65-91% (Figure 4-1). Interestingly the pyrolysis products were not consistent with a concerted pathway, suggesting the amine group was acting as an internal base leading to an E₂ type elimination. The highest temperatures of E_i (T_{E_i}) were observed for the 1-octanol sulfonates of 8-quinoline and 2-pyridine, 220 °C and 225 °C respectively, and the olefin yields were <50%. T_{E_i} was greatly reduced for the 2-octanol sulfonates of 8-quinoline and 2-pyridine, 150 °C and 115 °C respectively, and the olefin yields were >85 %. The temperature of sulfonate elimination was affected by the ester structure showing there is scope

for tuning the temperature, which needs to be above the post-cure of 100 °C and below the onset of p(MMA-co-A1) thermal degradation at 250 °C. T_{Ei} is used within this text to refer specifically to the temperature at which cleavage of the sulfonate C-O bond occurs. Within the literature several examples are seen where T_d is incorrectly used to describe temperature of acid generation where it is actually describing the temperature at which mass loss is observed via TGA.

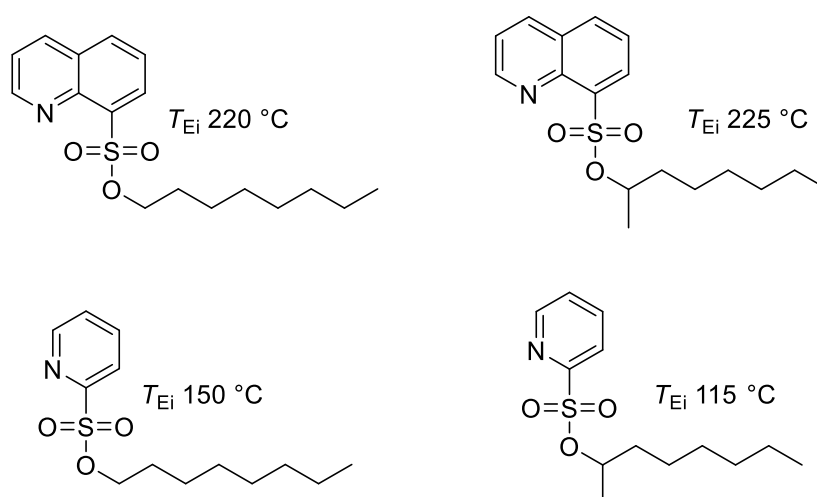


Figure 4-1 – 8-quinolyl and 2-pyridyl sulfonates and their elimination temperatures.¹⁹⁴

Lee *et al.*¹²³ synthesised three aryl cyclohexyl sulfonates with differing substituents in the *para* position on the arene ring (Figure 4-2). Only the nitro derivative's thermal properties were studied, ¹H NMR spectroscopy showed it underwent full thermolysis at 90 °C after 128 minutes in C₆D₆, to yield cyclohexene and *para*-nitrobenzene sulfonic acid. The TAGs were used as latent thermal initiators in the bulk cationic polymerisation of isobutyl vinyl ether. No polymerisation was observed below 50 °C and as thermolysis generated the initiator species this can be taken as the minimum T_{Ei} . Furthermore, at $T > 60$ °C the rate of polymerisation increased, when R was NO₂. When R was H, a significant increase in polymerisation rate was observed at $T > 80$ °C, whereas the rate was low when R was CH₃ indicating that the electron donating and withdrawing properties of the arene substituents have a direct impact on T_{Ei} . Of these species only the cyclohexyl *para*-toluenesulfonate may have a T_{Ei} suitable for degradation of p(MMA-co-A1).

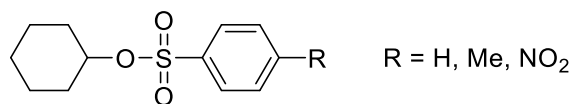


Figure 4-2 – Cyclohexyl sulfonates.¹²³

Shin *et al.*²⁰⁵ synthesised a series of thermally cleavable di-epoxide cross-linkers (Figure 4-3) by reacting disulfonyl chlorides with 3-cyclohexene-1-methanol and subsequent formation of the epoxide by reacting the alkene groups with potassium peroxymonosulfate. These cross-linkers were partially thermolyzed to generate free acid species that catalysed the reaction between poly(vinyl phenol) and the remaining epoxy groups to generate a resin. TGA revealed the onset temperature of E_i for Figure 4-3 a, b and c was 157 °C, 162 °C and 183 °C respectively. Interestingly, when the cross-linkers were cast into thin films that contained 30 mol % poly(styrene) and heated to 100 °C for 150 seconds, the disappearance of the sulfonate groups was observed by IR spectroscopy, suggesting a much lower T_{Ei} than observed by TGA. When using the cross-linker Figure 4-3 a as a source of acid catalyst to cross-link poly(vinyl phenol) films, insoluble fractions were observed at temperatures as low as 70 °C. The authors offer no explanation of the origin of the different thermolysis behaviors observed *via* different techniques or when the cross-linkers were in different systems.

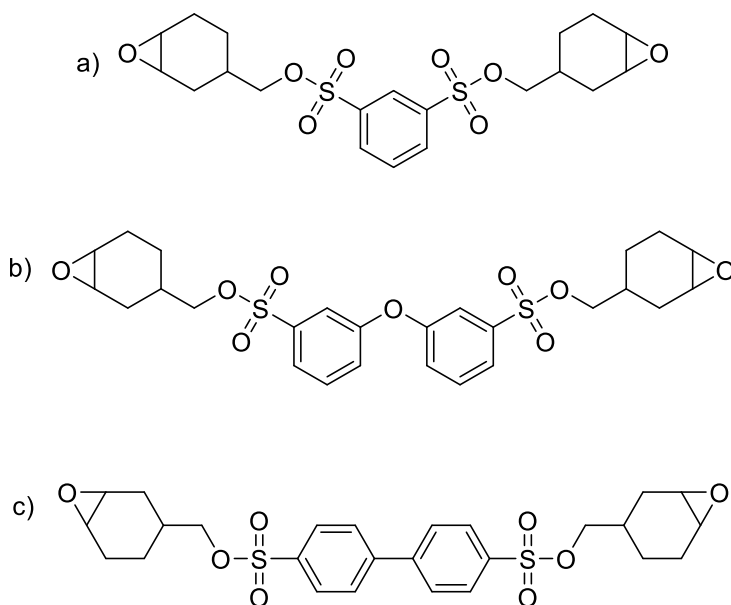


Figure 4-3 – Thermally cleavable sulfonate-based epoxide cross-linkers.²⁰⁵

Kolomanska *et al.*²⁰⁶ synthesised a series 4-styrene sulfonates *via* a multistep route starting with the synthesis of 4-styrene sulfonyl chloride by the reaction of 4-styrene sodium sulfonate with thionyl chloride (Figure 4-4). The 4-styrene sulfonates were synthesised *via* the reaction of 4-styrene sulfonyl chloride with the corresponding alcohol. The corresponding series of polymers were synthesised *via* reversible addition-fragmentation chain-transfer (RAFT) polymerisation and their thermolysis behaviour characterised *via* TGA. It was found that p(styrene sulfonates) bearing branched alkyl pendant groups underwent E_i elimination at lower temperatures than their linear equivalents by temperature sweep TGA, ranging from 190-230 °C. Further characterisation by isothermal TGA at 150 °C for 2 hrs showed that p(styrene sulfonates) bearing branched alkyl pendant groups underwent 10-13% mass loss suggesting that E_i is occurring at lower temperatures.

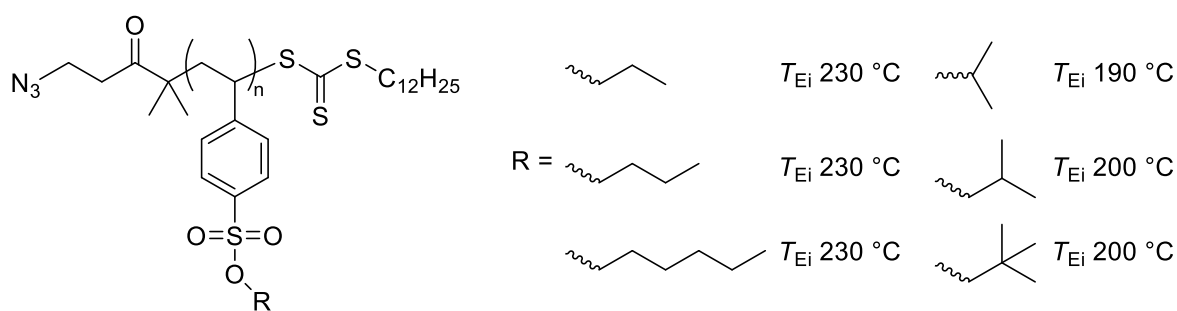
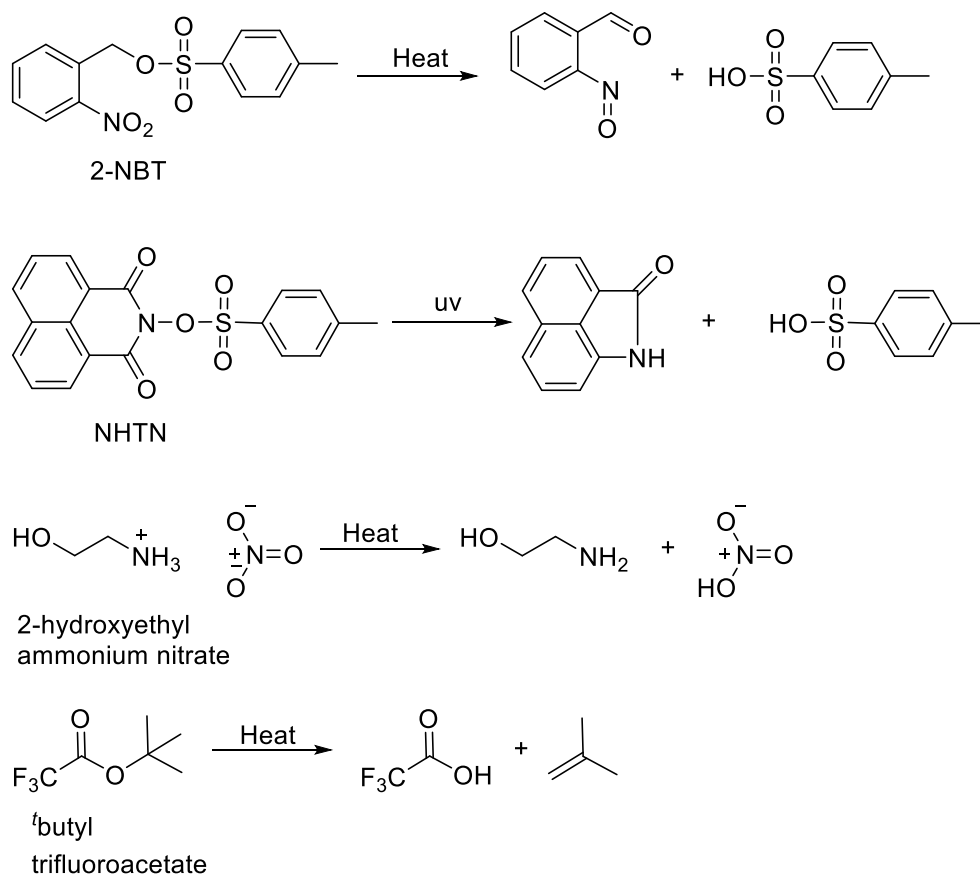


Figure 4-4 – p(styrene sulfonates) synthesised and their T_{Ei} determined *via* temperature sweep TGA.²⁰⁶ Within the literature E_i is used as a method for the preparation of olefins,¹⁹⁴ latent initiators,¹²³ thermally degradable thermosets²⁰⁵ and thermally labile polymers for organic photovoltaics.²⁰⁶ The latter reported by Kolomanska *et al.*²⁰⁶ is the most relevant to the aims of this chapter, the authors synthesise and polymerise 4-styrene sulfonate monomers which produce a polymer bound sulfonic acid group upon heating. The work in this chapter aims to reverse this by creating monomers capable of generating a sulfonic acid *via* E_i that is released and able to diffuse through A1 cross-linked polymer networks and catalyse the hydrolysis of acetal cross-links.

4.2. Results and Discussion

4.2.1. Preliminary Investigations of Acid Generations

Initially, four types of TAGs were investigated as *in situ* acid catalysts: 2-nitrobenzyl tosylate (2-NBT), *N*-hydroxytosylate-1,8-naphthalimide (NHTN), hydroxyethyl ammonium nitrate and *t*-butyl trifluoroacetate (Scheme 4-2). 2-NBT and NHTN were chosen as they generate pTsOH and *t*-butyl trifluoroacetate generates TFA, both acids have previously been shown to catalyse the hydrolysis of A1 and A1 cross-linked networks. Hydroxyethyl ammonium nitrate was chosen as it thermally generates nitric acid which has a pK_a of -1.3^{155} in water. This is within the experimentally determined pK_a that appear optimal for A1 hydrolysis.



Scheme 4-2 - Preliminary acid generators 2-NBT, NHTN, 2-hydroxyethyl ammonium nitrate and *t*-butyl trifluoroacetate thermal/photo acid generation schemes.

Nitrobenzyl esters are well known photo and thermoacid generators^{127,207} and 2-NBT was synthesised following literature preparations¹³⁰ from 2-nitrobenzyl alcohol and *para*-toluene sulfonyl chloride (pTsCl) and characterised *via* ¹H NMR spectroscopy (Appendix Figure 8-6). Interestingly 2-NBT synthesis requires dicyclohexylamine rather than the commonly employed, but weaker, bases pyridine and NEt₃. Their use led to the formation of 2-nitrobenzyl chloride as the major product.²⁰⁸ Thermolysis of 2-NBT yields pTsOH and 2-nitrosobenzaldehyde.¹²⁷

NHTN was synthesised by a two-step process, the intermediate product being *N*-hydroxy-1,8-naphthalimide that was subsequently reacted with pTsCl, the products were characterised *via* ¹H NMR and IR spectroscopy (Appendix Figure 8-7 to Figure 8-10).²⁰⁹ Naphthalimide esters are photoacid generators proceeding through a radical based mechanism followed by proton abstraction to yield pTsOH, the non-acid product is determined by the reaction solvent.²¹⁰ NHTN was synthesised to probe the *viability* of thermal acid generation from naphthalimide esters.

Hydroxyethyl ammonium nitrate is available commercially as a latent acid catalyst in resin precursor solutions, upon heating the salt degrades producing ethanolamine and nitric acid which catalyses the resin formation. Finally, ^tbutyl trifluoroacetate was sought due to the thermally-labile nature of ^tbutyl esters that undergo a thermal rearrangement *via* a six membered transition state that liberates trifluoroacetic acid and isobutylene.^{211–213} However, ^tbutyl trifluoroacetate could not be synthesised *via* Steglich or Fischer esterification methods. This was thought to be due to degradation of the product during purification.

4.2.2. TGA Analysis of Acid Generators

Previous work has shown to achieve a good degree of curing in p(MMA-co-A1) thermosets a post curing step at 100 °C is required. Therefore, acid generators present in p(MMA-co-A1) thermosets should be stable at 100 °C. 2-NBT has been shown by TGA to undergo thermolysis to pTsOH from 150 °C onwards.^{126,127,214} NHTN and hydroxyethyl ammonium nitrate were characterised by TGA to ensure they underwent thermolysis above 100 °C to prevent prematurely hydrolysing acetal cross-links (Figure 4-5). The TGA traces of NHTN and hydroxyethyl ammonium nitrate both showed a mass loss at 280 °C and 210 °C, respectively, these were assigned as the temperature of thermolysis. Both underwent thermolysis above 100 °C meaning they are suitable for use in p(MMA-co-A1) thermosets.

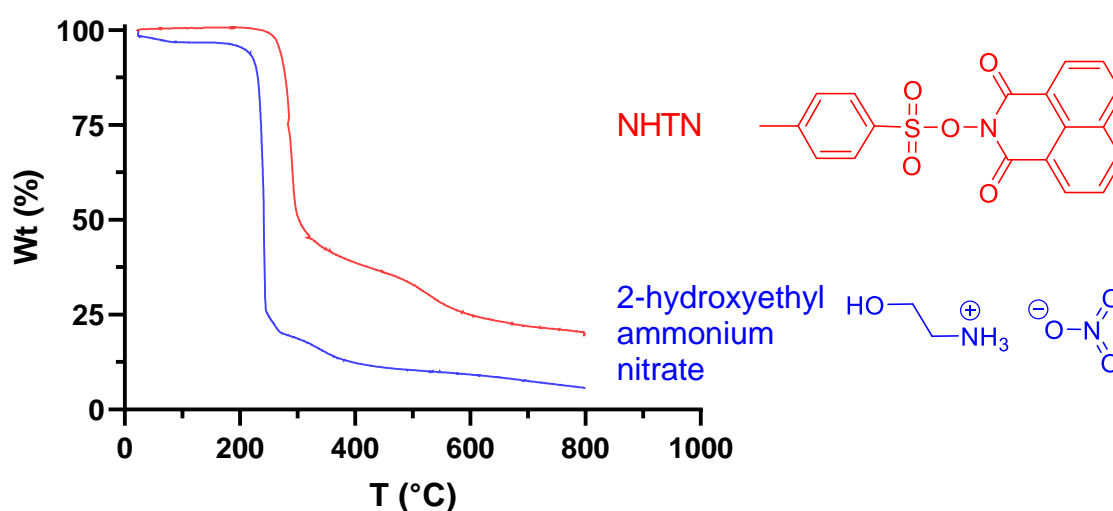


Figure 4-5 - TGA thermograms (N₂, 20 °C/min) of NHTN and hydroxyethyl ammonium nitrate.

A further criterion is that the temperature of acid generation is prior to the onset of p(MMA-co-A1) network thermal degradation, previously shown to occur from 250 °C onwards. Based upon the TGA data 2-hydroxyethyl ammonium is suitable, however, NHTN generates acid above this temperature meaning networks containing it may thermally degrade when generating acid. Despite this, NHTN was used to gauge whether its thermolysis properties varied in networks.

4.2.3. Addition of TAGs to Networks

To assess whether 2-NBT, NHTN and hydroxyethyl ammonium nitrate were suitable *in situ* acid sources, model thermoset networks were synthesised. Networks were synthesised *via* bulk polymerisation of MMA, methacrylic acid (MAA), A1 and TAG (1 wt%) using BPO and 4-TMA as a redox initiator system. MAA was incorporated as it is commonly used in adhesives to promote adhesion to metal substrates.³ Thermosets were be heated above the TAGs T_{Ei} generating acid *in situ* and forming soluble thermoplastics. Initially 2-NBT was investigated as the acid source, however, it was found that adhesives doped with 2-NBT would not cure when using the redox initiator (Figure 4-6).

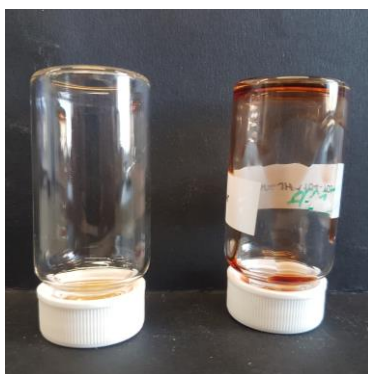


Figure 4-6 - Inverted vials of adhesives doped with 2-NBT, free flowing fluids suggested poor curing.

Radical curing thermosets commonly use redox systems such as BPO and 4-TMA supplied as a two pot system that separates the components until dispensing, ensuring a long shelf life.^{215,216} However, in the presence of 2-NBT, a solid thermoset was not formed. Inversion of vials containing 2-NBT doped adhesives revealed free flowing liquids, suggesting 2-NBT interacted unfavourably with the initiator system. Previously; Gill & Williams demonstrated the catalytic effect of nitrobenzene on the thermal decomposition of benzoyl peroxide in solutions of benzene and nitrobenzene, favouring the formation of the benzoic acid *via* a radical pathway.²¹⁷ Therefore, the rate of termination may be higher in the presence of 2-NBT *via* a similar pathway accounting for the low conversion.

Subsequent attempts to add NHTN or hydroxyethyl ammonium nitrate to the same adhesive formulation were unsuccessful. Both TAGs were insoluble in the adhesive precursor solution and cured adhesives (Figure 4-7). To overcome the challenges of cure inhibition, solubility and potential leaching²¹⁸ when using additive TAGs, a monomeric TAG was sought.

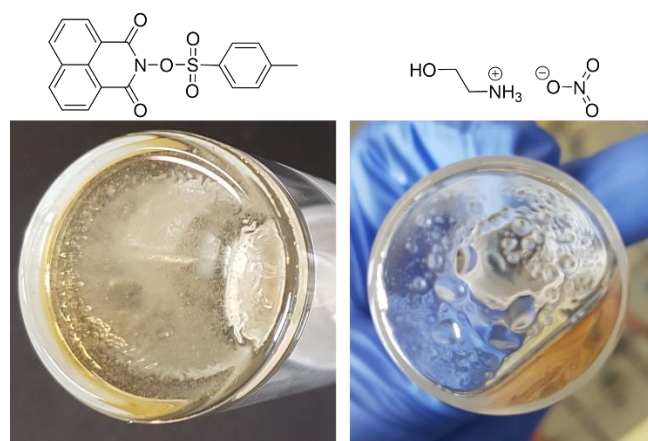
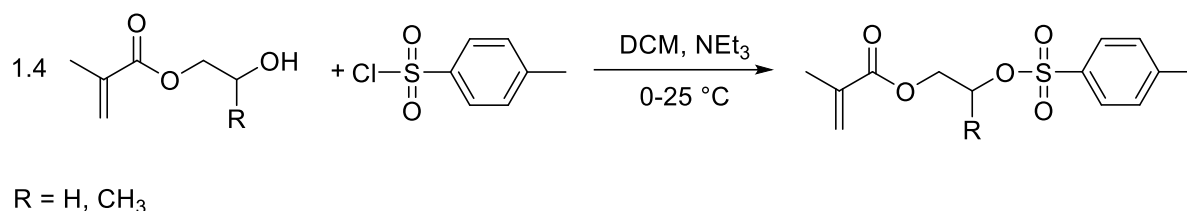


Figure 4-7 – Vials of NHTN (left) and 2-hydroxyethyl ammonium nitrate (right) doped p(MMA-co-MAA-co-A1) adhesives prior to curing.

4.2.4. HPMA and HEMA Tosylates

The desired TAG would need to be capable of undergoing copolymerisation with methacrylates such as A1 and MMA in the thermoset formulation. Commercially available 2-hydroxyethyl methacrylate (HEMA) and 2-hydroxypropyl methacrylate (HPMA) were utilised for their reactive alcohol group (Scheme 4-3). HEMA and HPMA were chosen to investigate the effect of substitution on the α -carbon relative to the sulfonate on T_{Ei} . The tosylates of these monomers were synthesised by reaction with pTsCl using NEt₃ as a HCl trap and purified *via* column chromatography achieving yields of 32 % and 37% for the HPMA and HEMA tosylates, respectively. The products were characterised by ¹H and IR spectroscopy, demonstrating the targeted products had been synthesised (Appendix Figure 8-11 to Figure 8-14). Commercially available HPMA is a mixture of the regioisomers 2-hydroxypropyl methacrylate and 2-hydroxyisopropyl methacrylate, the ratio of which was determined *via* ¹H NMR spectroscopy to be 0.7:0.3 (Appendix Figure 8-15). The ratio of the corresponding tosylates was 0.6:0.4; the decrease in the 2-hydroxypropyl methacrylate derivative was hypothesised to be due to the

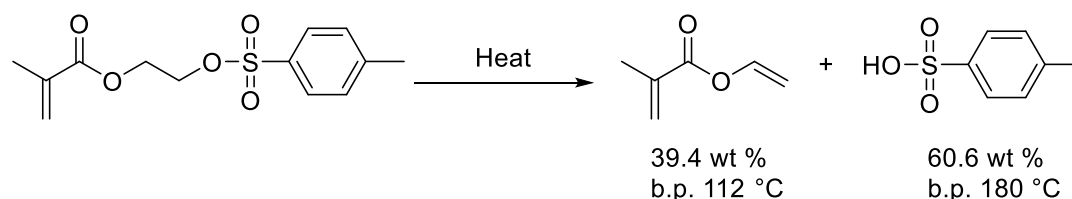
lower reactivity of secondary alcohols due to steric hindrance or greater solubility in the aqueous phase used during purification.⁷⁷



Scheme 4-3 - Synthesis of HPMA and HEMA tosylates by reaction with pTsCl.

4.2.5. Thermal Characterisation of HEMA Tosylate

The tosylates were hypothesised to undergo intramolecular elimination to vinyl methacrylate and pTsOH which has already been shown to have a suitable pK_a to catalyse acetal hydrolysis (Scheme 4-4).^{194,206,219,220} Further to this pTsCl is a cheap and commonly used starting material. The mechanism of intramolecular elimination reaction is known to proceed *via* 5 and 6 membered transition states depending on the substrate.^{118,122,123,131–133,194,206,219,221}



Scheme 4-4 - Intramolecular elimination of HEMA tosylate to vinyl methacrylate and pTsOH.

HEMA tosylate (HEMATos) was initially characterised by differential scanning calorimetry (DSC) and thermal gravimetric analysis (TGA). DSC showed that an exothermic thermal event took place at 120 °C, with a shoulder peak at 160 °C (Figure 4-8). It was expected that TGA would show a 40 % mass loss at 120 °C corresponding to the volatilisation of vinyl methacrylate generated *via* E_i of HEMAtos. However, TGA showed the onset of mass loss at 200 °C and then a sharp drop at 300 °C. In both the DSC and TGA pans a residue was present and it was hypothesised that the DSC peaks may be the thermal initiated polymerisation of HEMAtos or some other thermally driven side reaction that is preventing E_i from occurring.

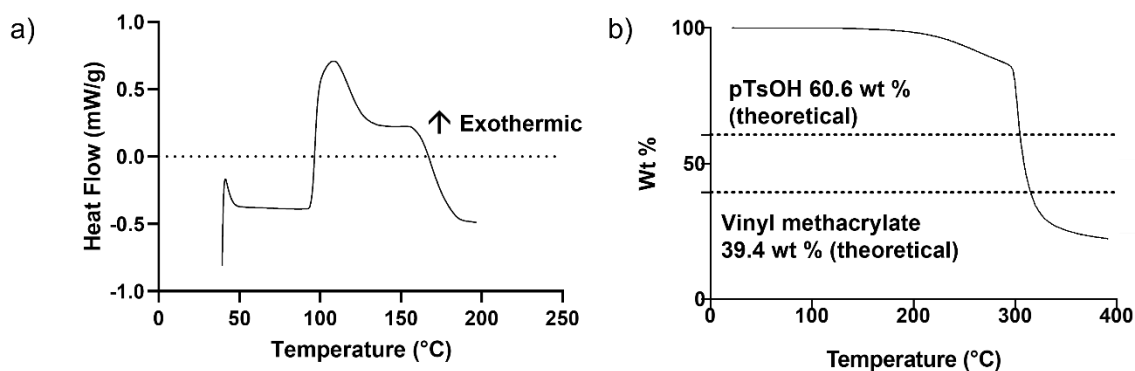
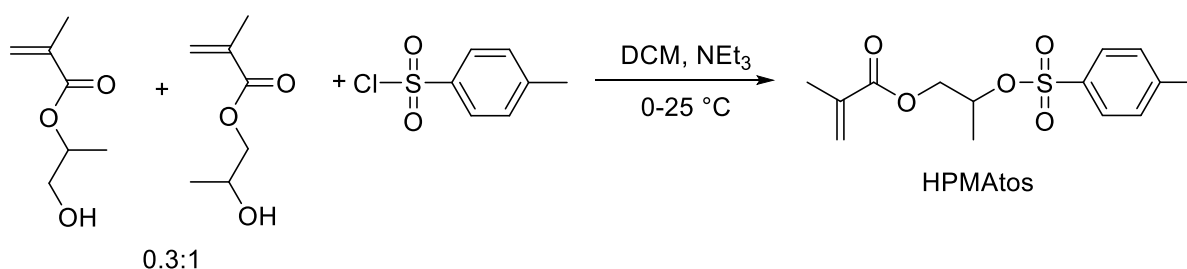


Figure 4-8 – a) DSC (25-200 °C at 10 °C/min) of HEMA Tos showing exotherm that was attributed to homopolymerisation. b) TGA (25-400 °C at 20 °C/min, N₂) of HEMA Tos monomer showing wt % didn't follow expected pattern.

4.2.6. Optimisation and Scale Up of HPMA and HEMA Tosylate Syntheses

The synthesis of HEMA and HPMA tosylates was optimised and scaled up for further studies of the E_i reactions of the corresponding polymers and model thermosets. The reaction between HPMA and pTsCl was chosen (Scheme 4-5) as the secondary alcohol reacts more slowly. Furthermore, the initial synthesis had a yellow impurity that seemed to form prior to the addition of the alcohol functional monomer. A survey of the literature of tosylation reactions was performed to identify alternative bases, catalysts, order of reagent additions and the stoichiometry of reagents (Table 4-1).



Scheme 4-5 - Synthesis of HPMAtos.

Table 4-1 – Literature conditions of tosylation reactions.

Authors	Base	Catalyst	Feed ^a	[OH]:[Cl]:[Base] ^b
Tipson <i>et al.</i> ²²²	Pyridine	-	pTsCl	1:1:1
Kabalka <i>et al.</i> ²²³	Pyridine	-	pTsCl	1:2:3
Yoshida <i>et al.</i> ²²⁴	NEt ₃	NEt ₃ .HCl	pTsCl	1:1.5:2.5
Morita <i>et al.</i> ²²⁵	<i>N,N</i> -dimethylbenzylamine	KOH	pTsCl	1:1.5:0.1
Kazemi <i>et al.</i> ²²⁶	K ₂ CO ₃		None	1:1.5:36
Ding <i>et al.</i> ²⁰⁸	NEt ₃	4-(dimethylamino)pyridine	pTsCl	1:1.5:1.5

^aSpecies fed into the reaction mixture, ^bratio that authors claim give fastest reaction conditions

Based upon the conditions reported in the literature (Table 4-2) a series of HPMAtos syntheses were performed to improve the yield (32%) and suspected low conversion of the secondary alcohol isomer present in commercial HPMA. The majority of tosylations reported in the literature added pTsCl to a solution of alcohol and base so the initial synthesis of HPMAtos was modified to a pTsCl feed. ¹H NMR spectroscopy was used to monitor the conversion of both isomers, the primary alcohol was found to reach >99 % conversion after 27 hrs, after which the secondary alcohol reached only 32 % which increased to 38 % at 72 hrs (Appendix Figure 8-16 to Figure 8-19). When using pyridine, the primary and secondary alcohols were found to reach >99 % and 40 %, respectively (Appendix Figure 8-20 to Figure 8-23). When using DMAP in reactions with pyridine the primary and secondary alcohols were found to reach >99 % and 35 %, respectively (Appendix Figure 8-24 to Figure 8-27). However, Kabalka *et al.*²²³ reported the rate of tosylation is improved by using a [OH]:[pTsCl]:[pyridine]

molar ratio of 1:2:3. Upon repeating the synthesis of HPMAtos under these conditions an increase in secondary alcohol conversion to 98 % in 72 hrs was observed (Appendix Figure 8-28 to Figure 8-30).

Table 4-2 – Experimental conditions of HPMAtos synthesis optimisation experiments.

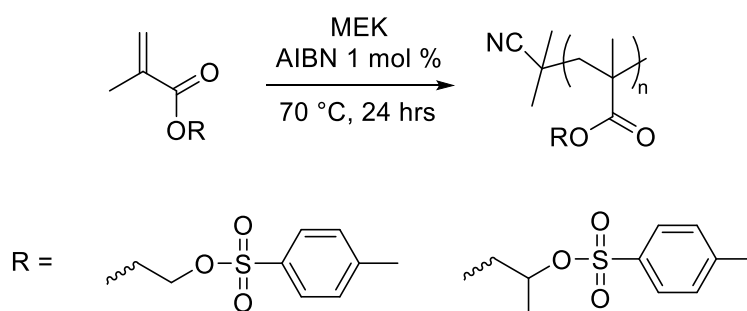
Experiment	Base	Catalyst	Feed	[OH]:[Cl]:[Base]	1° OH Conversion (%) ^a	2° OH Conversion (%) ^a
1	NEt ₃		pTsCl	1:1.5:1.5	>99	38
2	Pyridine		pTsCl	1:1.5:1.5	>99	40
3	Pyridine	DMAP	pTsCl	1:1.5:1.5:0.2 (DMAP)	>99	35
4	Pyridine		pTsCl	1:2:3	>99	98

^aDetermined via ¹H NMR spectroscopy

However, under these conditions there was a large excess of pTsCl and pyridine to be removed from HPMAtos. Therefore, a series of experiments investigating reactive work up procedures were performed on portions of the crude reaction mixture and monitored *via* TLC. Propylamine, ^tBuOH, poly(vinyl alcohol) and sat. sodium bicarbonate were added to the reaction crude mixture and stirred²²⁷⁻²²⁹. It was found that after one hour of stirring with sat. sodium bicarbonate no pTsCl was present.

4.2.7. FRP Polymerisation of HPMAtos and HEMAtos

HPMAtos and HEMAtos were polymerised to their corresponding polymers *via* free radical polymerisation initiated by 2,2'-azobis(2-methylpropionitrile) (AIBN) at 70 °C in methyl ethyl ketone (MEK) (Scheme 4-6). After 24 hrs the conversion of HPMAtos to p(HPMAtos) and HEMAtos to p(HEMAtos) was determined *via* ¹H NMR spectroscopy to be 90 and 80 %, respectively. The crude polymers were purified by precipitation into methanol and centrifugation prior to characterisation by SEC. The M_w was 42800 and 65600 g/mol for p(HPMAtos) and p(HEMAtos) respectively, indicating the formation of polymeric species (Table 4-3, Appendices Figure 8-31). The dispersity (\mathcal{D}) was determined to be 1.33 and 1.72 for p(HPMAtos) and p(HEMAtos) respectively (Table 4-3), which are expected for uncontrolled free radical polymerisation where termination of propagating chains is uncontrolled leading to broad molecular weight distributions.^{191,192}



Scheme 4-6 – Free radical polymerisation of HPMAtos and HEMAtos.

Table 4-3 – ¹H NMR spectroscopy conversion and SEC data for the polymerisations of HPMAtos and HEMAtos.

Polymer	Conversion (%) ^a	M_w (g/mol) ^b	\mathcal{D} ^b
p(HPMAtos)	90	42800	1.33
p(HEMAtos)	80	65600	1.72

^aDetermined *via* ¹H NMR spectroscopy after 18 hrs, ^bdetermined by SEC in THF relative to p(MMA) standards.

4.2.8. Thermolysis of p(HPMATos) and p(HEMATos)

p(HPMATos) and p(HEMATos) synthesised *via* free radical polymerisation were characterised by TGA and DSC to investigate the temperature of E_i . A suitable TAG for p(MMA-co-A1) systems must undergo E_i before the onset of thermal degradation of the network, but not at the post-cure temperature of 100 °C. The TGA thermograms recorded under N_2 for both p(HPMATos) and p(HEMATos) with p(MMA-co-A1) are shown in Figure 4-9. Interpreting these thermograms it is assumed the drop in mass corresponds to the generation of pTsOH as the remaining mass is non-volatile polymer. p(HEMATos) undergoes 60 % mass loss, corresponding to pTsOH, at $T > 250$ °C and is closely followed by a thermal degradation path similar to poly(MMA-co-A1) therefore it is unsuitable as an internal acid source for the acetal group hydrolysis. The DSC thermogram shows an exothermic peak at 240 °C which was attributed to the E_i reaction, supporting the TGA data.

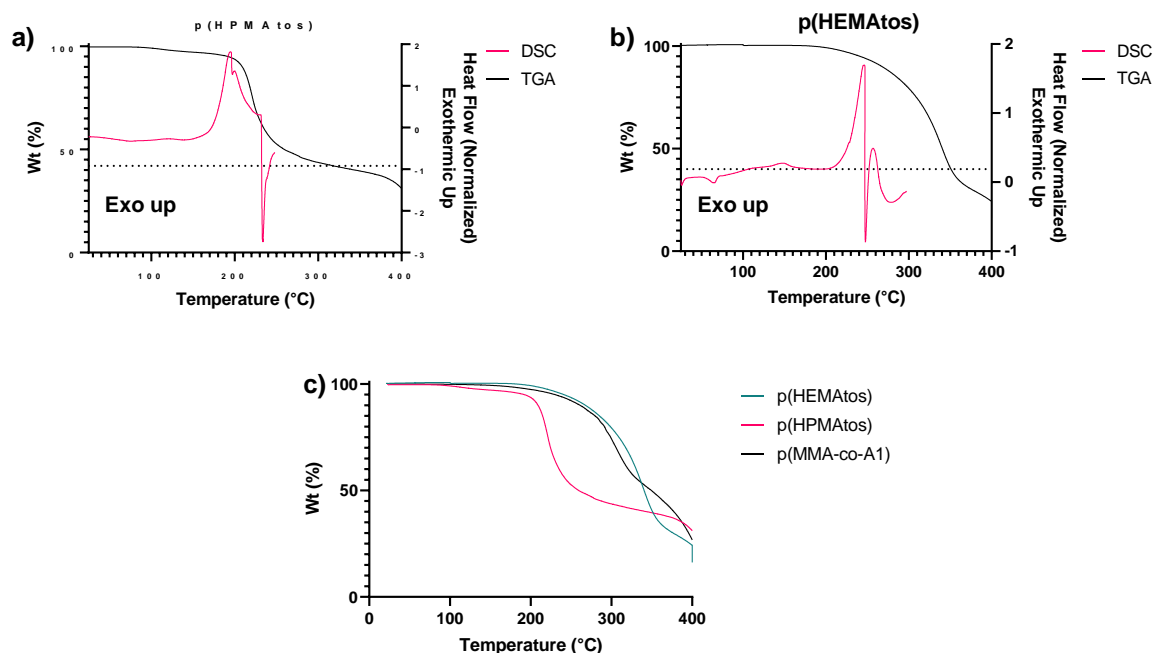
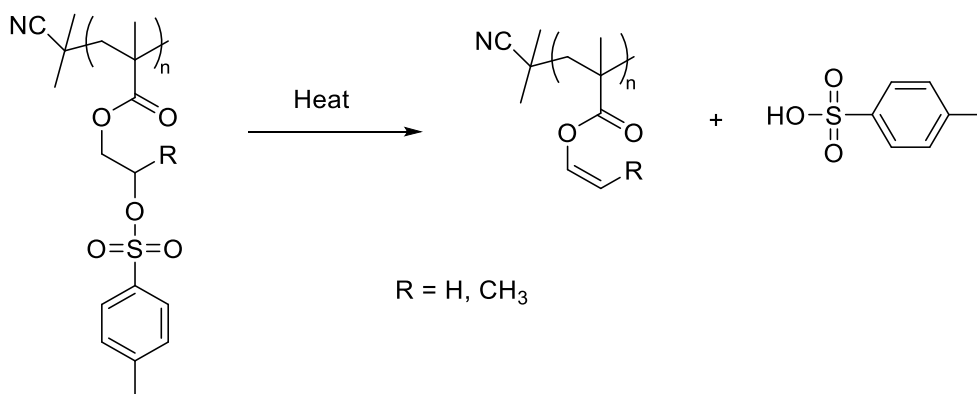


Figure 4-9 – a) DSC and TGA thermograms of p(HPMATos), b) DSC and TGA thermograms of p(HEMATos) and c) TGA thermograms of p(HEMATos), p(HPMATos) and p(MMA-co-A1).

The TGA thermogram of p(HPMATos) showed a 58% mass loss, corresponding to pTsOH, beginning at 200 °C, which is below the onset of p(MMA-co-A1) thermal degradation. The DSC further supports this showing an exothermic peak at 190 °C. Therefore, p(HPMATos) was thought to undergo E_i at a suitable temperature to enable *in situ* acid generation for acetal group hydrolysis in p(MMA-co-A1). The difference in E_i temperature between p(HPMATos) and p(HEMATos) was attributed to the α -methyl group giving a lower energy transition state which will be discussed in detail later.

Having found evidence for a thermally driven process *via* TGA and DSC characterisation, a molecular understanding was sought. The p(HPMATos) and p(HEMATos) residues that remained in the DSC pans were characterised *via* ^1H NMR spectroscopy, HPLC-MS and IR spectroscopy. The E_i reaction products were hypothesised to be pTsOH and p(vinyl methacrylate) or p(methylvinyl methacrylate), corresponding to p(HEMATos) or p(HPMATos), respectively (Scheme 4-7). However, attempts to dissolve the residues were unsuccessful suggesting they had cross-linked; the pendent vinyl groups may react *via* a radical process¹⁹⁶ or Friedel-Crafts type reaction.^{206,230}



Scheme 4-7 - Proposed E_i reaction of p(HPMATos) and p(HEMATos).

The DSC pan residues were washed with DMSO- d_6 and ^1H NMR spectroscopy and HPLC-MS was performed on the extract. ^1H NMR spectroscopy revealed both extracts contained pTsOH, determined by the peaks at 7.48, 7.12 and 2.29 ppm (Figure 4-10 a and b). This was also seen in the HPLC-MS as pTsOH, $[\text{M}+\text{H}]^+$ 170.93 AMU (Appendices Figure 8-32 & Figure

8-33). The insoluble residue was then dried *in vacuo* to remove any residual DMSO- d_6 and characterised by IR spectroscopy. The expected vinyl peak at $\sim 1650\text{ cm}^{-1}$ was not observed, supporting that a cross-linking side reaction involving it was taking place at elevated temperatures (Appendices Figure 8-34 & Figure 8-35).

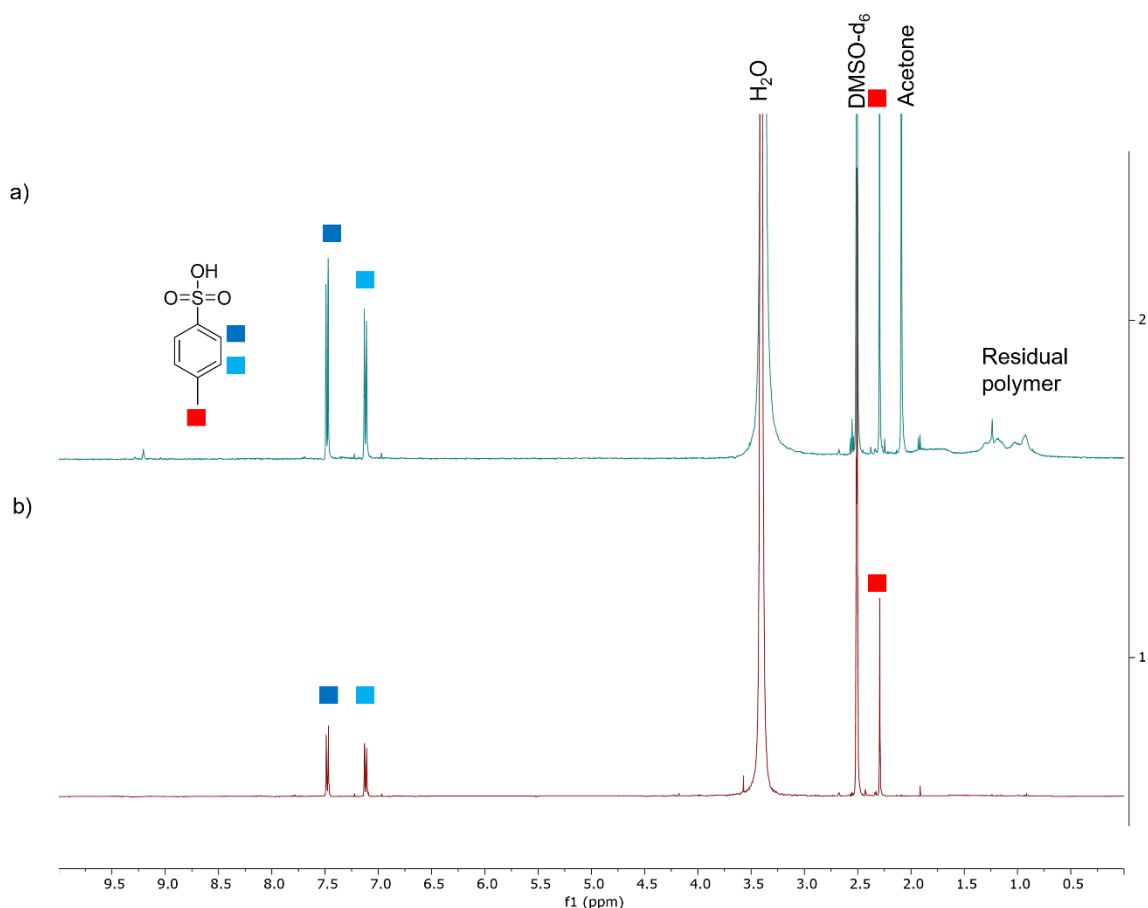


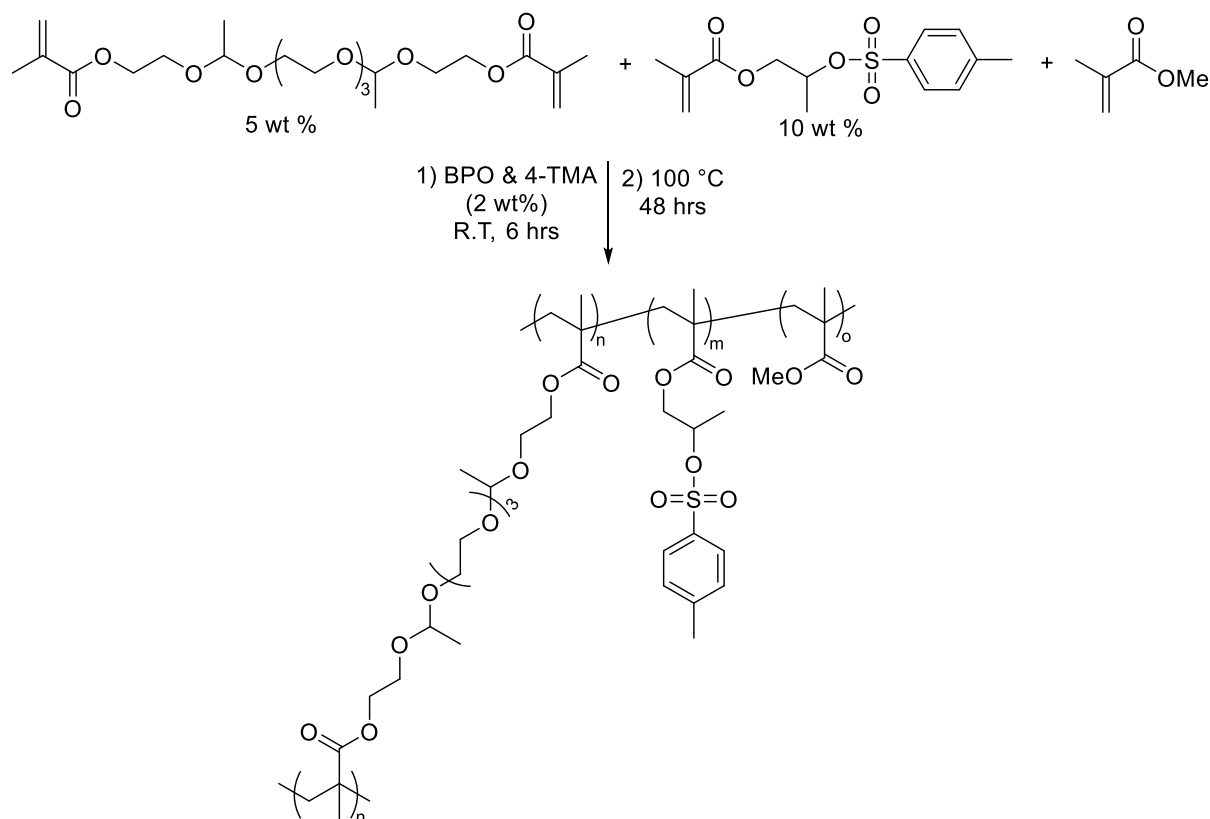
Figure 4-10 - ^1H NMR ($\text{DMSO-}d_6$) spectrum of a) p(HEMATos) and b) p(HPMATos) DSC pan extract, showing heating liberates pTsoH.

Based upon these studies HPMATos was chosen for use as an internal acid source in p(MMA-co-A1) as it underwent E_i at $\sim 200\text{ }^\circ\text{C}$ based upon the TGA data which is suitable for the thermoset post-curing conditions discovered in Chapter 2 and is below the temperature at which p(MMA-co-A1) thermally degrades. However, the overall goal of introducing HPMATos to p(MMA-co-A1) is to internally catalyse acetal hydrolysis, thus breaking cross-links; the cross-linking of p(HPMATos) is orthogonal to this. It is hypothesised that when HPMATos is

present as a comonomer its effective concentration will be reduced meaning the cross-linking side reaction doesn't occur as the reactive species will be sufficiently separated.

4.2.9. HPMAtos and HEMAtos Model Adhesives

Having demonstrated that p(HPMAtos) underwent E_i at ~200 °C it was incorporated into a model thermoset network. The model network was synthesised *via* bulk polymerisation of A1, MMA and HPMAtos at 5 wt %, 81 wt % and 10 wt %, respectively using BPO and 4-TMA as a redox initiator system (Scheme 4-8). A control network comprising A1 and MMA at 5 wt % and 91 wt % was also synthesised. The A1/MMA/HPMAtos networks were cured at room temperature for 6 hrs and post-cured at 100 °C for 48 hrs. Interestingly, the network containing HPMAtos was a brown colour, whereas the control was pale yellow; both were colourless solutions prior to the addition of 4-TMA. Pale yellow was previously observed in networks synthesised using BPO and 4-TMA as the initiator system.



Scheme 4-8 – Synthesis of model MMA, A1 and HPMAtos networks.

Previous TGA of p(HPMAtos) showed that pTsOH was generated *via* E_i at ~200 °C. The A1/MMA/HPMAtos and control networks were characterised *via* TGA to ensure pTsOH was generated (Figure 4-11). As HPMAtos was present at 10 wt % it was calculated that the wt % of pTsOH in the degradable network was 5.8 wt %. This was the expected mass loss that would be observed *via* TGA. However, the TGA thermogram of the 10 wt % HPMAtos network showed no clear mass loss corresponding pTsOH generation when compared with the control; both showed mass loss with an onset around 200 °C. Furthermore, the presence of HPMAtos in the network increased the thermal stability.

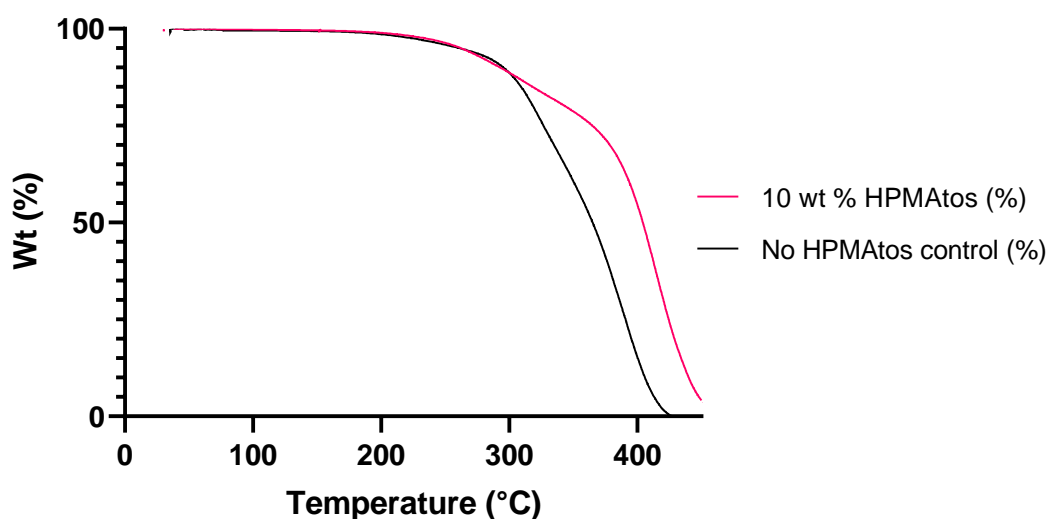
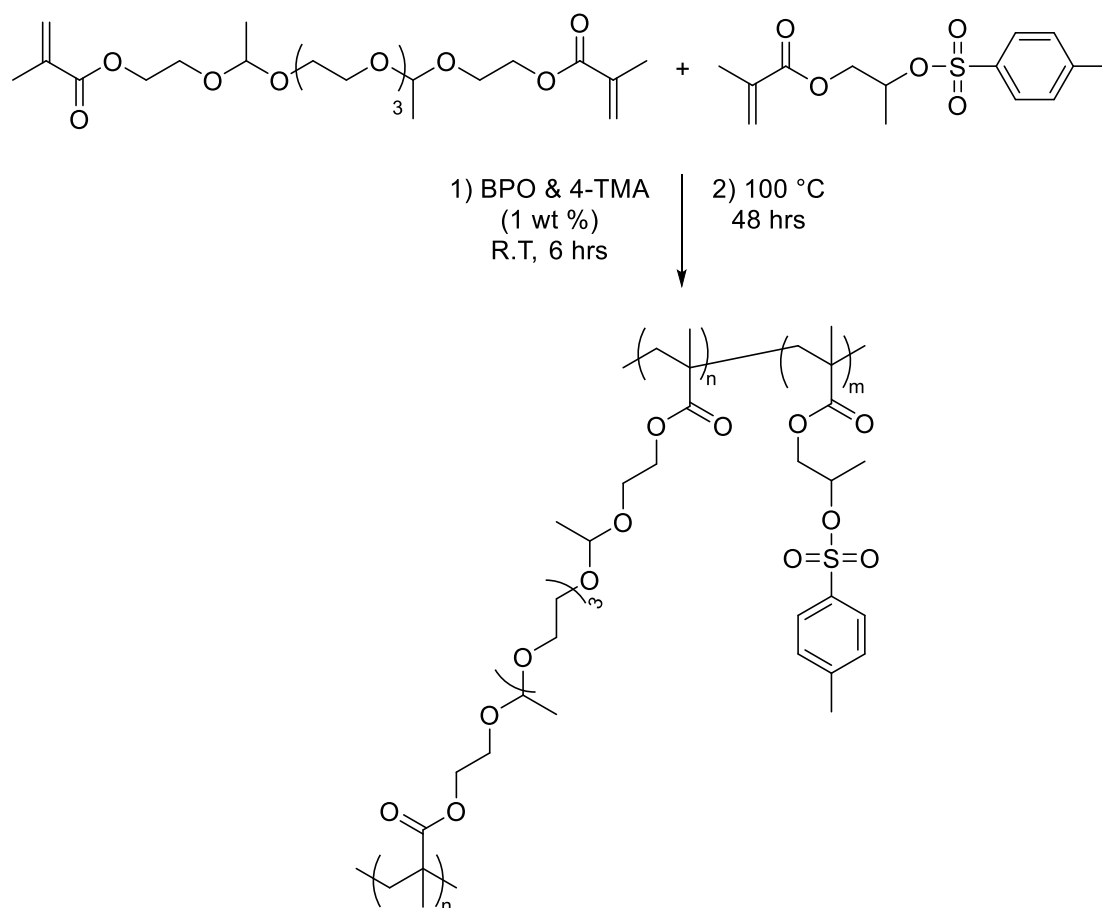


Figure 4-11 – TGA thermogram of HPMAtos network and no HPMAtos control.

An alternative experiment was designed to observe the generation of pTsOH. The 10 wt % HPMAtos containing network was heated at 180 °C for 3 hours in an oven, soaked in acetone, filtered and the filtrate was concentrated *in vacuo*. The resultant residue was then characterised by ¹H NMR spectroscopy and HPLC-MS. The ¹H NMR spectrum showed the residue contained pTsOH, confirmed by the aromatic CH peaks at 7.89 and 7.45 ppm and the CH₃ peak at 2.54 ppm; this was further supported by the HPLC-MS data (Appendices Figure 8-36 & Figure 8-37).

A second set of networks was synthesised without MMA to ease the analysis of the E_i reaction products and investigate whether the *in situ* generated pTsOH could catalyse the hydrolysis of acetal links in A1 (Scheme 4-9). p(A1-co-HPMAtos) was synthesised by polymerising A1 and HPMAtos at 48 wt % each using 1 wt % of BPO and 4-TMA for 6 hours at R.T., followed by post-curing at 100 °C for 48 hrs. A non-degradable control network using ethylene glycol dimethacrylate (EGDMA) instead of A1 was also synthesised. Samples of the networks were heated to 180 °C in an oven for 18 hrs and the small molecules extracted by Soxhlet extraction and concentrated *in vacuo*, and was analysed by ¹H NMR spectroscopy. Control samples of the networks were not heated and underwent Soxhlet extraction to ensure no pTsOH was generated prematurely.



Scheme 4-9 – Synthesis of A1/HPMAtos networks.

The ¹H NMR spectra of the Soxhlet extract residues of EGDMA and A1 networks that weren't heated in the oven had peaks corresponding pTsOH. These were also present in the heated

samples; meaning it could not be determined if this was generated prior to or during the heating in the oven. Premature generation of pTsOH is problematic as it may cause unwanted degradation of thermoset network during application.

To probe this further a final series of networks composed of A1, HPMAtos, and MMA was synthesised. A1 was fixed at 2 wt % in all samples and HPMAtos was varied from 5 to 50 wt % and are referred to as HAM-X, where x denotes the wt % of HPMAtos present. (Table 4-4). MMA was used to ensure solubility of HPMAtos in the polymerisation starting mixture. The networks were synthesised as before and characterised by IR spectroscopy. The expected aromatic stretches were observed at 3000-2800 cm^{-1} , the strong ester stretch from the methacrylates at 1725 cm^{-1} , and a strong aliphatic ether stretch at 1160 cm^{-1} (Figure 4-12). In the HAM-25 and HAM-50 networks spectra an alkene peak at 1600 cm^{-1} was observed suggesting residual monomer was present.

Table 4-4 – A1/MMA/HPMAtos network formulations.

Network	A1 / wt %	MMA / wt %	HPMAtos / wt %	BPO / wt %	4-TMA / wt %
HAM-5	2	89	5	2	2
HAM-10	2	84	10	2	2
HAM-25	2	69	25	2	2
HAM-50	2	44	50	2	2

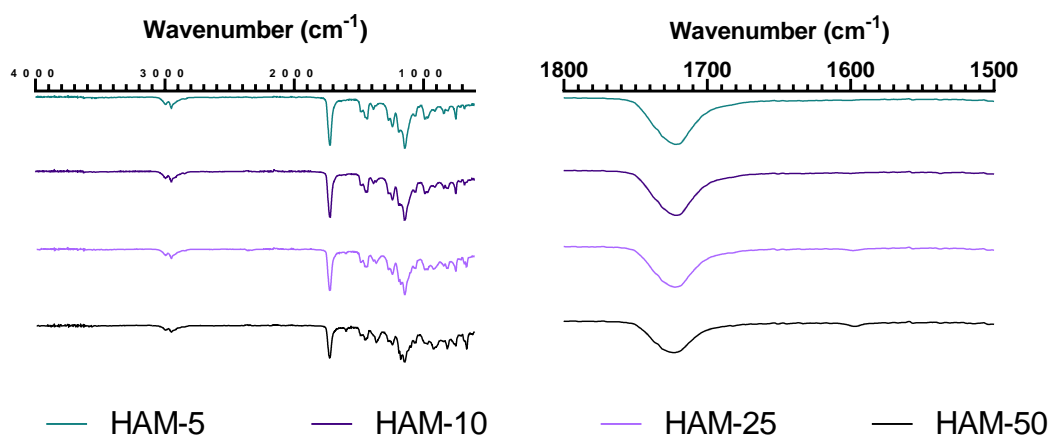


Figure 4-12 – IR spectra of A1/MMA/HPMAtos networks.

The generation of pTsOH within the networks was characterised by TGA. An isothermal step was (180 °C for 3 hrs) added to improve the observation of the E_i reaction. The theoretical mass loss resulting from the generation of pTsOH was calculated using the wt % of pTsOH in the HPMAtos monomer, was calculated as 58 %. It was hypothesized that the mass loss during the 180 °C isothermal step should match the theoretical pTsOH wt % and these are marked on Figure 4-13 with dashed lines.

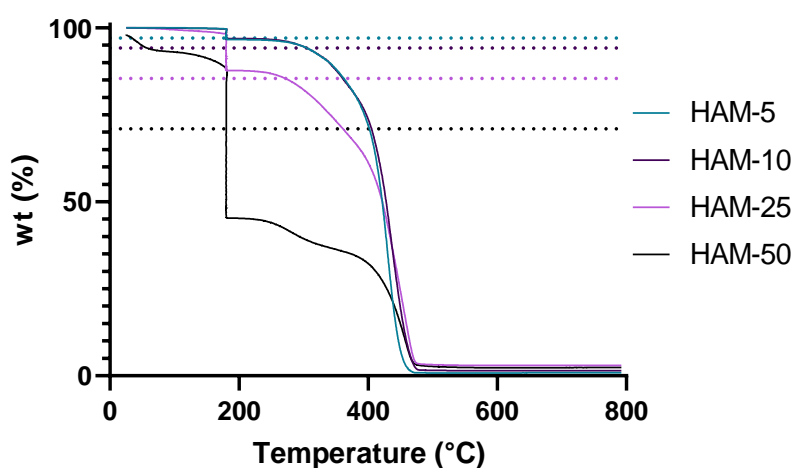


Figure 4-13 – TGA thermogram of A1/MMA/HPMAtos networks obtained *via* heating from 25-180 °C at 20 °C/min, with an isothermal step at 180 °C for 3 h and heating to 800 °C at 20 °C/min.

For the networks HAM-5, HAM-10, and HAM-25 no mass loss was observed until the isothermal step, at which a sharp drop was observed thought to arise from the generation of pTsOH. The observed mass loss was equal to or less than the calculated theoretical amount of pTsOH, supporting that this step was pTsOH generation. However, the TGA thermogram for HAM-50 exhibited unexpected mass loss during the initial temperature ramp from 25-180 °C suggesting the presence of unreacted monomer which was supported by the IR spectrum. Furthermore, the isothermal stage exhibited a greater mass loss than the theoretical amount of pTsOH generated *via* E_i, further supporting that this network was not fully cured.

Lastly, the TGA thermogram for the temperature ramp from 180-800 °C for HAM-5, HAM-10 and HAM-25 are consistent with cured methacrylate networks, showing a sharp drop in mass from 300 °C onward. However, the HAM-50 outline has a broad and multistep mass loss suggesting that the network has residual unreacted species. Alternatively, the TGA of HAM-50 may arise from the premature generation of pTsOH which subsequently catalysed the hydrolysis of the acetal groups, however, this would only account for an unexpected mass loss of <2 wt %. A detailed understanding of the E_i reaction of p(HPMA_{tos}) was then sought before returning to any model network studies to ensure premature E_i was not taking place.

4.2.10. Isothermal TGA Characterisation of p(HPMATos)

To gain a further understanding of the solid-state E_i reaction of p(HPMATos), isothermal TGA studies were performed at 140, 160 and 180 °C. Samples were initially heated to the isothermal target temperature at 10 °C/min and held for 18 hrs before a final 10 °C/min ramp to 800 °C. It was hypothesized that if p(HPMATos) was undergoing E_i at lower temperatures then mass loss would be observed during the isothermal stage.

The TGA thermograms of the isothermal step at 140, 160 and 180 °C are shown in Figure 4-14. Previous temperature sweep TGA has shown that p(HPMATos) undergoes E_i at ~200 °C to high conversion; this was also observed under isothermal conditions at 180 °C. Rapid mass loss from 100 to 50 % was observed from 0-210 mins attributed to the generation of pTsOH. The residual mass was 45 wt %, the theoretical maximum residual mass of 42 wt % was not reached, this was thought to be due to experimental error and potential generation of pTsOH during the initial temperature ramp to 180 °C.

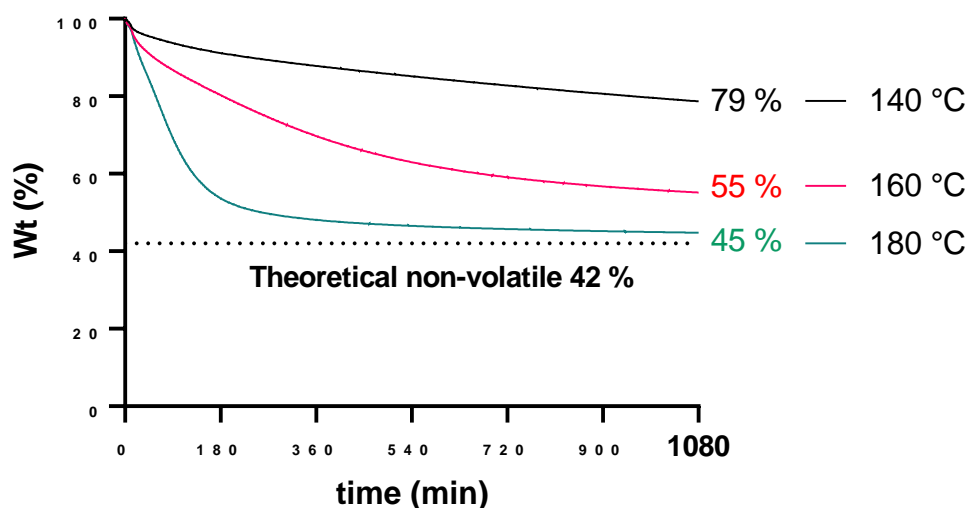


Figure 4-14 – Isothermal TGA thermogram of p(HPMATos) at 140-180 °C.

Unexpectedly, the isothermal TGA at 140 and 160 °C both showed considerable mass loss over 18 hrs indicating E_i was occurring at lower temperatures than previously observed when performing temperature sweep TGA. The residual mass was 79% and 55% at 140 °C and

160 °C, respectively. As previously discussed, a post-cure step was required when synthesising p(MMA-co-A1) networks, the conditions of which were heating at 100 °C for 48 hrs. Based on the isothermal TGA results, it is plausible that when post-curing networks containing HPMAtos, pTsOH is being generated which may be interfering with the post-cure and prematurely degrading the network.

Ideally p(HPMAtos) would have been characterised using isothermal TGA at 120 and 100 °C however, the 18 hrs experimental duration of the isothermal step would probably need to be extended meaning the residence time in the TGA was very long. Therefore, kinetic analysis of the isothermal data was performed to obtain an Arrhenius plot from which the data at 120 and 100 °C could be estimated *via* extrapolation.²³¹⁻²³³ This is possible by plotting a linear version of the Arrhenius equation using the natural log:

Equation 4-1

$$k = Ae^{-\frac{E_a}{RT}}$$

Equation 4-2

$$\ln k = \frac{-E_a}{RT} + \ln A$$

Where k is the rate constant at a given temperature, E_a is the activation energy, R is the gas constant, T is the temperature in Kelvin and A is the pre-exponential factor. By analysing the data from the isothermal TGA it is possible to determine the rate constants of the E_i reaction of p(HPMAtos) at 140 °C, 160 °C and 180 °C. The remaining unknown terms in the linear Arrhenius equation can then be determined by plotting $\ln(k)$ versus $1/T$ where $-E_a/R$ is the gradient and $\ln(A)$ is the y-intercept.²³⁴ As E_i is an intramolecular reaction the reaction is 1st order. Therefore, to determine the k at 140 °C, 160 °C and 180 °C, $\ln(x)$, where x was the fractional conversion, was plotted versus t of the isothermal steps, the gradient of which is $-k$.²³⁴

When plotting $\ln(x)$ versus t of the isothermal step what appeared to be linear plots were obtained for 140 and 160 °C with R^2 values of 0.99 and 0.97, respectively (Figure 4-15). However, these plots are likely non-linear and no relationship is observed due to the low conversion of the E_i reaction. At 180 °C the relationship between $\ln(x)$ and t was non-linear with an R^2 value of 0.80 indicating that the mass loss during the isothermal heating was either incorrectly attributed to conversion of p(HPMAtos) to pTsOH or E_i was occurring alongside another process. To gain an understanding of what the TGA was revealing zero and second order kinetic plots were produced. The zero order plots were non-linear for all temperatures (Appendices Figure 8-38). Interestingly, in the second order plots ($1/x$ versus t) a linear relationship was observed with an R^2 value of 0.99 for all temperatures (Figure 4-16), this would suggest that the reaction is second order which is inconsistent with the proposed E_i mechanism.^{219,220}

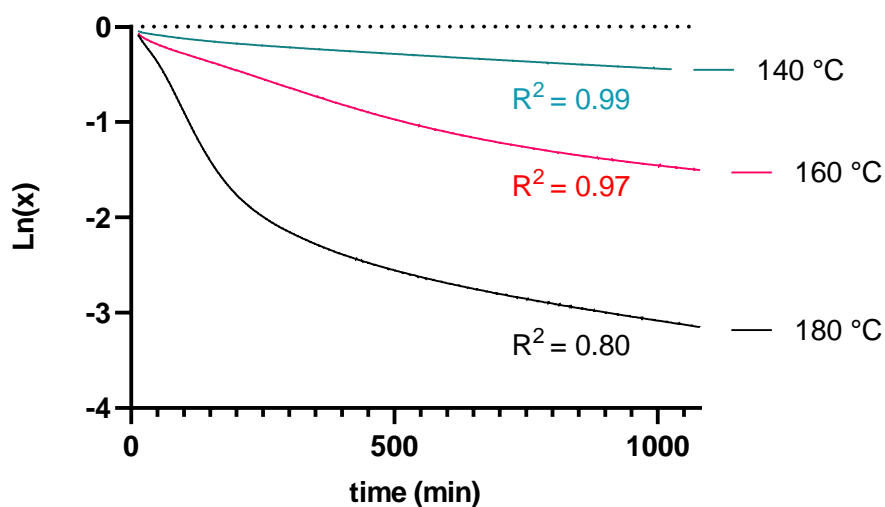


Figure 4-15 – First order kinetic plots of isothermal TGA of p(HPMAtos), where x is the fractional conversion determined from mass loss.

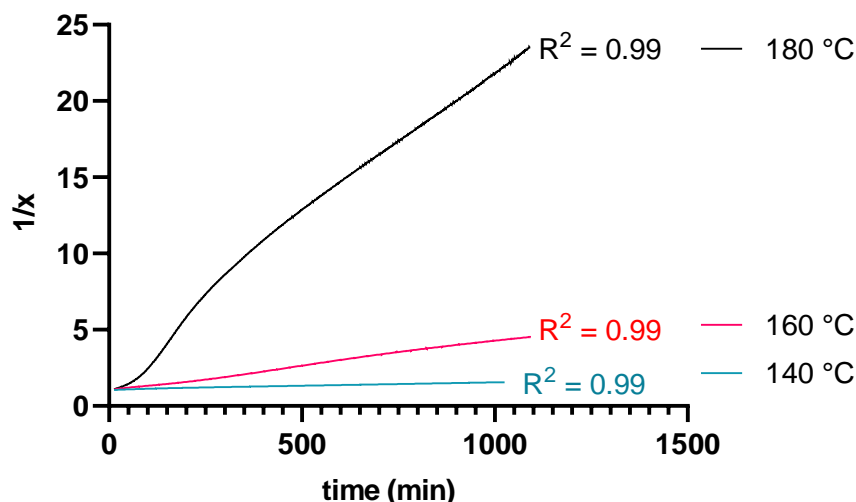


Figure 4-16 – Second order kinetic plots of isothermal TGA of p(HPMATos) , where x is the fractional conversion determined from mass loss.

Upon examining the literature covering TAGs,^{116,117} and specifically E_i of sulfonates,^{133,206} it was clear that TGA is the standard technique for characterising thermolysis. However, there is an important criterion for a TGA being suitable, if the E_i takes place at a temperature below the boiling points of the products then it is unsuitable for that system. This is because the temperature at which mass loss is observed is most likely due to the volatilisation of a small molecule product of E_i and not the true temperature at which E_i occurs.

It was hypothesised that p(HPMATos) and p(HEMATos) both meet this criterion. This was confirmed by comparing the TGA traces of p(HPMATos) and pTsOH monohydrate (Figure 4-17). pTsOH exhibited a mass loss at 100 °C due to H₂O in the sample, however, a sharp decrease in mass began at ~180 °C that was attributed to the evaporation of pTsOH. This matched well with the trace of p(HPMATos) which had a sharp decrease in mass with an onset at 180 °C and ended at ~42 % residual mass, corresponding to the loss of all pTsOH in the system. Therefore, previous TGA of p(HPMATos) and p(HEMATos) that had been used to characterise the temperature of E_i were showing the evaporation of pTsOH instead. Therefore, an alternative technique was sought to gain a true understanding of the temperature of E_i and insight into the reaction mechanism.

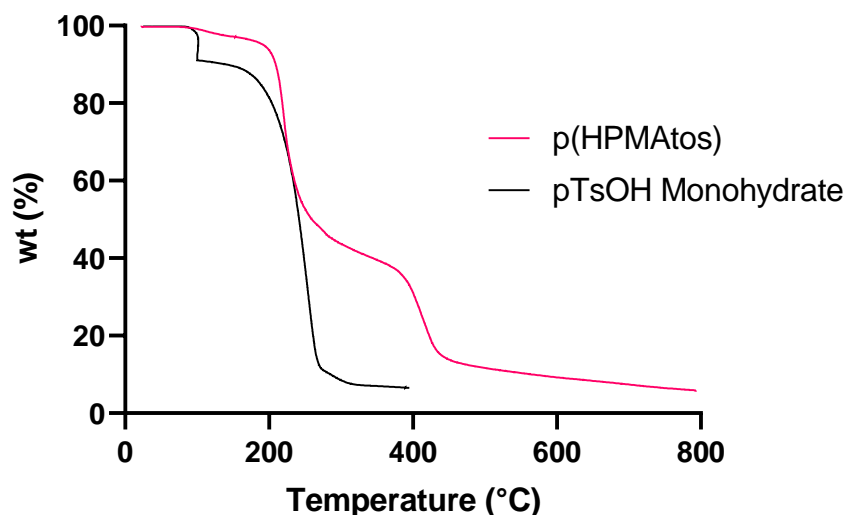
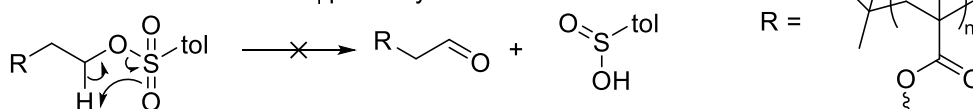


Figure 4-17 – Comparison TGA thermograms of p(HPMAtos) and pTsOH monohydrate.

4.2.11. Variable Temperature NMR Spectroscopy Study of p(HEMATos) and p(HPMAtos) E_i Mechanism

E_i can proceed *via* 5- or 6-membered transition states depending on the functional groups.^{219,235} The reaction products of sulfonate elimination are an alkene and sulfonic acid (Figure 4-18), therefore, they proceed *via* a 6-membered transition state. Variable temperature ¹H NMR (vtNMR) spectroscopy was used to gain insight into the reaction mechanism and products of solution phase E_i of p(HEMATos) and p(HPMAtos). p(HEMATos) is discussed first for simplicity as p(HPMAtos) is a mixture of isomers.

a) 5-membered transition state E_i pathway



b) 6-membered transition state E_i pathway

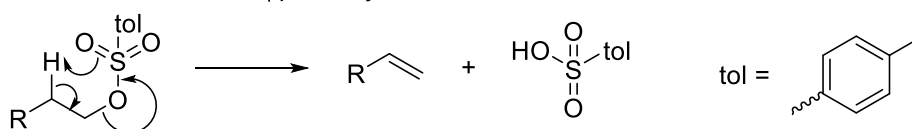
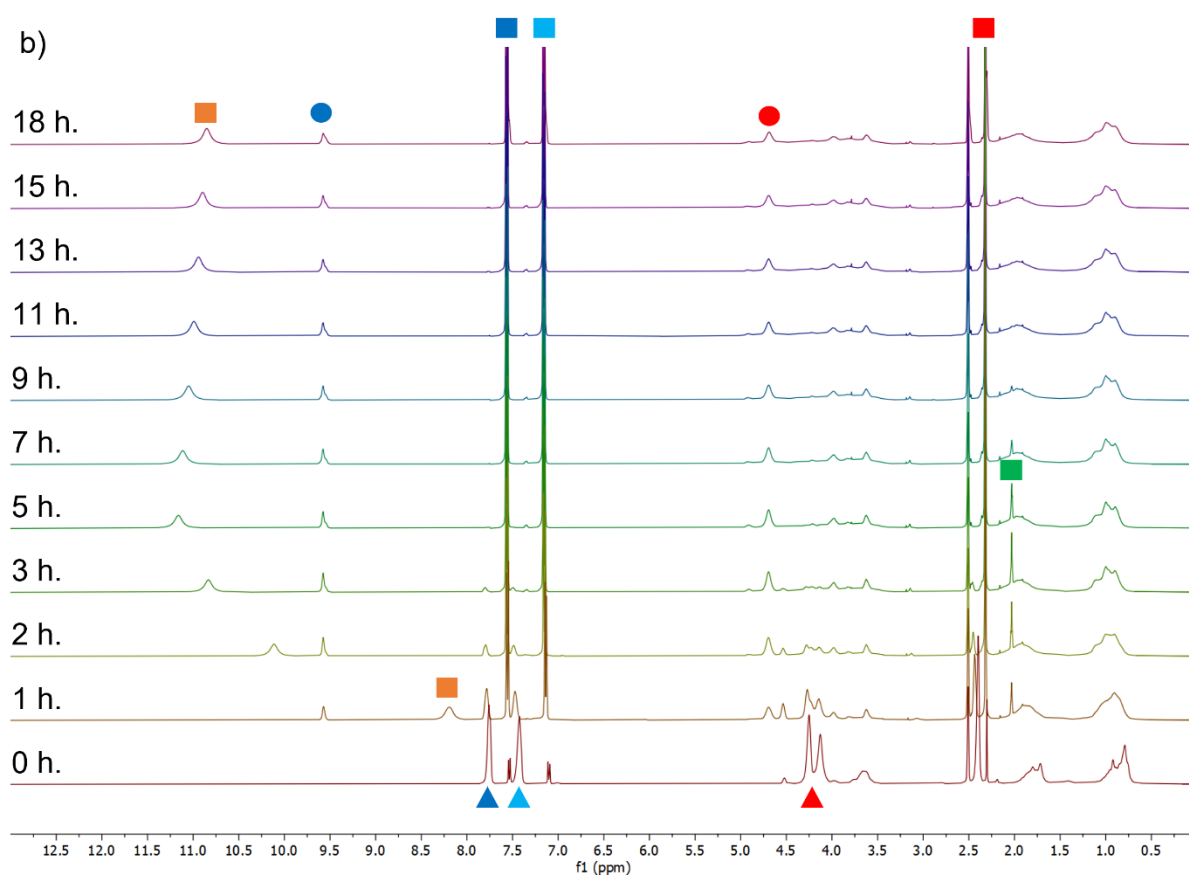
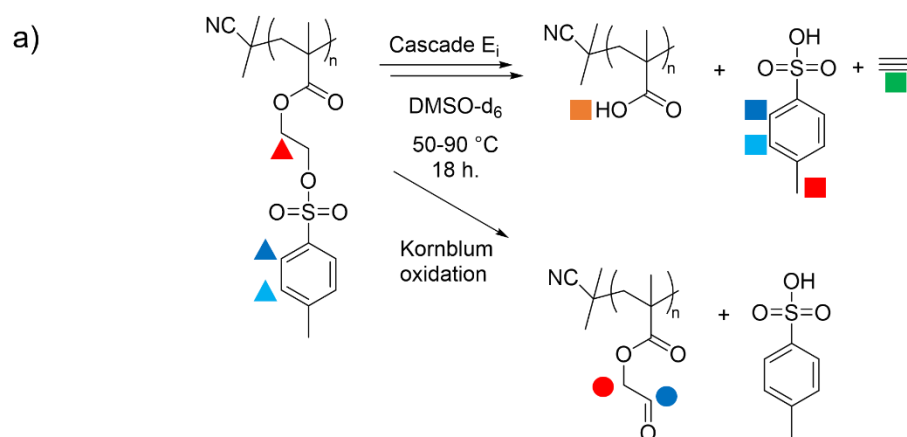


Figure 4-18 – a) 5-membered transition state E_i pathway and b) 6-membered transition state E_i pathway of p(HEMATos).

The predicted E_i reaction products for p(HEMATos) were p(vinyl methacrylate) and pTsOH. From the NMR spectra recorded at different times (0-18 hrs) at 90 °C, a reduction in intensity of the p(HEMATos) aromatic ring CH peaks at 7.76 and 7.42 ppm and increase in the intensity of pTsOH aromatic ring CH doublet peaks at 7.55 and 7.16 ppm was observed, confirming that E_i was occurring (Scheme 4-10 b). The presence of pTsOH in the $t=0$ spectrum is due to the experimental setup as the sample enters the spectrometer preheated to the target temperature resulting in an unavoidable delay between heating and the first spectrum being recorded. Furthermore, the peak corresponding to the CH_2 in the α -position to the sulfonate at 4.25 ppm disappears over time indicating cleavage of the ester group. However, the expected p(vinyl methacrylate) peaks at 7.5, 5 and 4.5 ppm²³⁶ were not observed (Scheme 4-10 b).

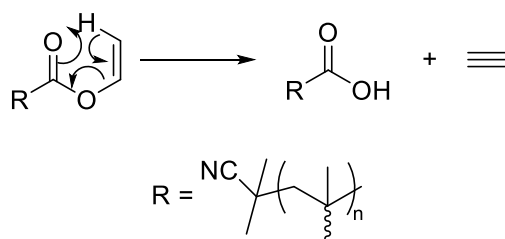


Scheme 4-10 - a) Proposed cascade E_i and Kornblum oxidation reaction pathways of p(HEMATos) and b) 1H NMR (DMSO- d_6) spectra of p(HEMATos) at 90 °C for 18 hrs.

An unexpected broad peak was observed that shifted downfield throughout the experiment to 10.85 ppm, this was assigned to a $COOH$ proton. The downfield shift of this peak with time was attributed to the generation of pTsOH as the experiment proceeded. As the dissociation constant of pTsOH is higher the increase in its concentration overtime leads to an increase in the protonated form of $COOH$. The equilibrium shifts to reduce the amount of free hydronium

ions in the system, leading to the observation of a previously exchangeable proton.^{153,154,237} Allan *et al.* reported that the gas phase pyrolysis of vinyl benzoate at 400-550 °C resulted in the formation of ethyne and benzoic acid. This is the only example of the synthesis of an alkyne *via* ester pyrolysis^{238,239}. It is proposed that the production of the experimentally observed COOH_H peaks proceeded *via* a similar pathway, consuming the pendent alkene groups of vinyl methacrylate units to produce the observed poly(methacrylic acid) components and ethyne (Scheme 4-10 a). Furthermore, ethyne has a boiling point of -84 °C²⁴⁰ and consequently the majority would be present in the headspace of the NMR tube and therefore not easily observed. However, the peak at 2.03 ppm was assigned as the alkyne CH_H proton as it appeared and decreased over time as it moved to the vapour/gas phase.

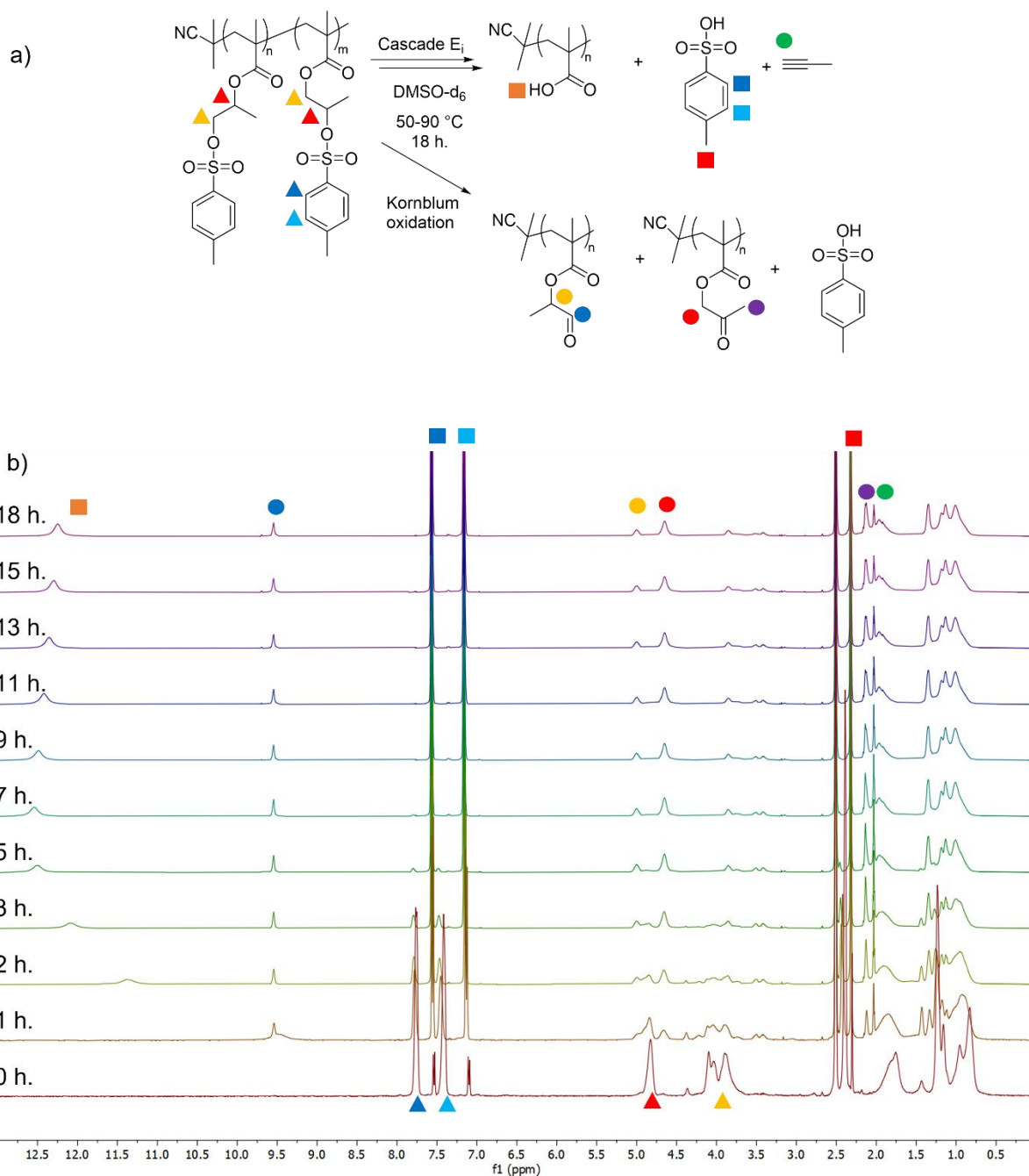
Interestingly, a peak at 9.56 ppm was observed indicating the presence of an aldehyde (Scheme 4-10 b). The intensity of this peak increased with time suggesting it was a by-product of the thermolysis. It was hypothesised that this was the product of vinyl methacrylate hydrolysis due to residual water, the product of which would be the enol derivative of acetaldehyde that would tautomerise to acetaldehyde and p(methacrylic acid). Initially, the peak at 2.02 ppm was assigned as the acetaldehyde CH₃. However, this peak decreased over time whereas the aldehyde CH_H remained. Furthermore, no H₂O peak at 3.33 ppm¹⁵⁹ was observed in the *t*=0 spectrum. It was also considered that the aldehyde could be formed *via* the 5-membered E_i pathway (Scheme 4-11), and that the produced para-toluene sulfinic acid was oxidised to pTsOH.²⁴¹ However, there is little evidence in the literature of sulfonates undergoing this type of E_i.^{194,195,197,219,235,239,242–245}



Scheme 4-11 - Proposed further E_i of p(vinyl methacrylate) to p(MAA).

Kornblum *et al.* and Nace *et al.* both described the synthesis of aldehydes and ketones from aliphatic and aromatic tosylates *via* an oxidation reaction with DMSO, typically in the presence of NaHCO₃ as a catalyst.^{246–249} This reaction proceeds slowly under neutral and weakly acidic conditions. It was hypothesised that any aldehyde in the reaction mixture was formed *via* this reaction.

It was expected that p(HPMATos) would also undergo E_i *via* the same pathway as p(HEMATos), however, the products would be dependent on the isomer. The majority isomer, poly(2-tosylpropyl methacrylate), would produce a ketone pendent group and the minority isomer, poly(tosylisopropyl methacrylate), would produce an aldehyde functional group (Scheme 4-12 a) *via* the 5-membered pathway. For the 6-membered pathway it was expected that a further reaction producing methacrylic acid components would be observed alongside the product propyne. The ratio of these isomers in the monomer HPMATos was determined *via* ¹H NMR spectroscopy, to be 3:1; however, when polymerised the CH₂ peaks used to calculate this coalesced due to the peak broadening in polymeric products (4.00 ppm). Therefore, the two isomers were treated as one when monitoring the reaction, however, their reactivities may be different.



Scheme 4-12 - a) Proposed cascade E_i and Kornblum oxidation reaction pathways of p(HEMATos) and b) 1H NMR (DMSO- d_6) spectra of p(HEMATos) at 90 °C for 18 hrs.

Again, the generation of pTsOH was observed by the presence of the pTsOH aromatic CH doublet peaks at 7.55 and 7.16 ppm which increased in intensity from 0-18 hrs. (Scheme 4-12 b). A reduction in the CH peak at 4.90 ppm and CH_2 peak at 4.00 ppm and was observed corresponding to the cleavage of the sulfonate ester bond in both the minor and major isomers. Evidence of the aldehyde forming pathway was observed as the peak at 9.53 ppm assigned

as the CH proton in the pendant aldehyde group. Furthermore, the peak at 2.02 ppm was assigned as the CH proton in propyne. Lastly, an exchangeable COOH peak that shifted downfield overtime to 12.5 ppm was observed suggesting the 6-membered pathway was also taking place. Again, the majority of propyne was thought to be present in the headspace of the NMR tube due to its low boiling of $-23.2\text{ }^{\circ}\text{C}$. The COOH peak was shifted further downfield than in the p(HEMATos) experiment due to p(HPMATos) having a lower amount of pTsOH per unit mass due to the extra methyl group.

4.2.12. Variable Temperature ^1H NMR Spectroscopy Study of p(HPMATos) and p(HEMA-tos) E_i

To probe the temperature of E_i , p(HPMATos) and p(HEMATos) were characterised *via* ^1H variable temperature NMR spectroscopy. Both polymers were characterised to verify the previously observed effect of CH_3 and H substitution alpha to the sulfonate ester group on the temperature of E_i where p(HPMATos) was found to undergo E_i at a lower temperature *via* TGA. The samples were heated to $50\text{ }^{\circ}\text{C}$, $70\text{ }^{\circ}\text{C}$ or $90\text{ }^{\circ}\text{C}$ for 18 hrs in DMSO-d_6 , spectra were recorded at 30-minute intervals, and the conversion was monitored using the ring CH peak at 7.75 ppm.

The conversion of tosylate to pTsOH determined by vtNMR at 50 , 70 and $90\text{ }^{\circ}\text{C}$ for p(HEMATos) and p(HPMATos) are shown in Figure 4-19. Interestingly E_i was observed at much lower temperatures than previously observed *via* TGA, and p(HEMATos) was more labile than p(HPMATos) based on conversion. For both polymers 100 % conversion of the tosylate to pTsOH was observed after 8 hrs at $90\text{ }^{\circ}\text{C}$ with high conversion observed at $70\text{ }^{\circ}\text{C}$ (93 % and 79 % for p(HEMATos) and p(HPMATos) respectively). E_i was observed in both polymers at $50\text{ }^{\circ}\text{C}$ which may mean that the pTsOH observed in networks previously was generated prematurely by the exotherm during the cure and when heating to $100\text{ }^{\circ}\text{C}$ during the post-cure step.

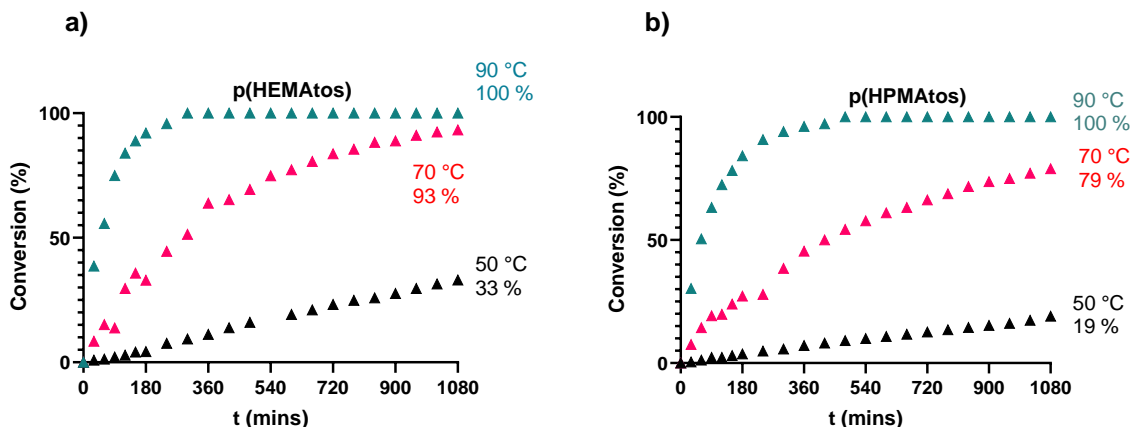


Figure 4-19 – Conversion of tosylate to pTsOH versus time of a) p(HEMATos) and b) p(HPMATos) via vtNMR spectroscopy at 50, 70 or 90 °C in DMSO-d₆.

To ensure that the generation of pTsOH was taking place *via* E_i, the conversion data was used to generate 1st order kinetic plots. Unlike the isothermal TGA data of p(HPMATos), a linear relationship was observed for all temperatures indicating the reaction followed the expected pathway (Figure 4-20). As expected, the k_{obs} for both p(HEMATos) and p(HPMATos) increased with temperature.²³⁴ However, rates were higher for p(HEMATos) at all temperatures which contradicts the TGA data that suggested p(HEMATos) was less reactive than p(HPMATos).

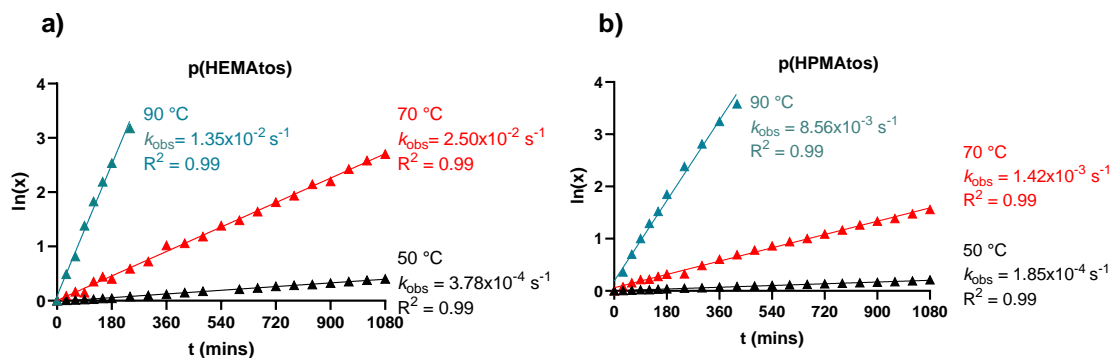


Figure 4-20 – First order kinetic plots of conversion of tosylate to pTsOH at 50 °C, 70 °C, and 90 °C of a) p(HEMATos) and b) p(HPMATos) obtained *via* vtNMR spectroscopy (DMSO-d₆).

Due to the high R^2 values for all values of k_{obs} , it was assumed that p(HEMATos) and p(HPMATos) were reacting *via* the same pathway. If they were undergoing E_i by a combination of 5 and 6-membered transition states then the rate of reaction would vary for both pathways.

This is particularly interesting in p(HPMATos) as it is a mixture of isomers, but the high R^2 values indicate they are both reacting *via* the same pathway.

4.2.13. The Effect of the R Group and the determination of the E_i

Mechanism

As both p(HEMATos) and p(HPMATos) were found to undergo E_i at lower temperatures than expected and *via* an unexpected pathway, a structure-property investigation was undertaken to aid the future design of TAGs and particularly those that undergo E_i at higher temperatures. Using the first order rate constants obtained from the vtNMR spectroscopy experiments at 50, 70 and 90 °C for both p(HEMATos) and p(HPMATos), the activation energy (E_a) for both polymers was determined from their Arrhenius plots (Figure 4-21). The vtNMR spectroscopy experiments demonstrated that p(HEMATos) was more reactive than p(HPMATos) and this was supported by the calculated E_a of 87 kJ/mol versus 94 kJ/mol. However, what causes the higher energy barrier is unclear.

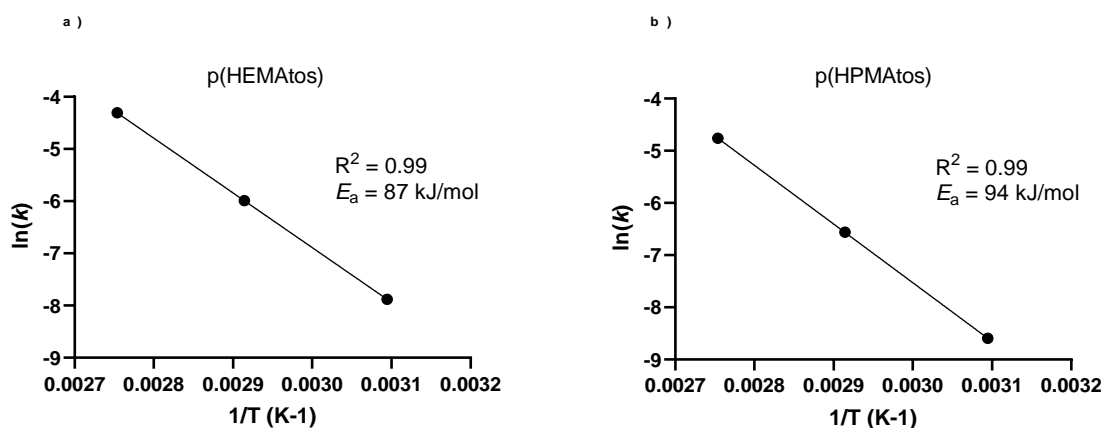


Figure 4-21 – Arrhenius plots of a) p(HEMATos) and b) p(HPMATos).

The mechanism of E_i is known to proceed *via* a concerted mechanism through a 5- or 6-membered cyclic transition state (Figure 4-18).²¹⁹ Reaction with a hydrogen atom on the α carbon leads to a 5-membered transition state. Alternatively reaction with the hydrogen on the β carbon leads a 6-membered transition state. Of the two pathways the 5-membered transition

state proceeds *via* the more readily abstractable proton, due to its proximity to the strongly electron withdrawing tosylate group. However, gas phase experiments and computational models have shown abstraction of this proton leads to a more energetically unstable transition state, due to the poor charge separation.^{196–204,219} From the vtNMR experiments of p(HEMATos) and p(HPMATos) it was determined that both polymers reacted preferentially *via* the 6-membered pathway due to the small amount of aldehyde observed compared to free pTsOH. A disparity in these values suggests that the alkene is preferentially formed and undergoes further reaction to p(methacrylic acid). However, determining the ratio of products was challenging due to the exchangeable nature of the COOH proton. Coupling this with the high R^2 values for both k_{obs} and E_a it is assumed both polymers react *via* the 6-membered transition state.

Therefore, it was assumed that the difference in E_a between p(HPMATos) and p(HEMATos) was due to unfavourable interactions in the transition states arising from the methyl branch point in p(HPMATos). First, the conformation of the 6-membered transition state of p(HEMATos) is considered (Figure 4-22). As the transition state is 6-membered it will adopt a chair-like conformation to minimise strain and thus forcing substituents into pseudo-equatorial or pseudo-axial positions about the ring.^{250,251}

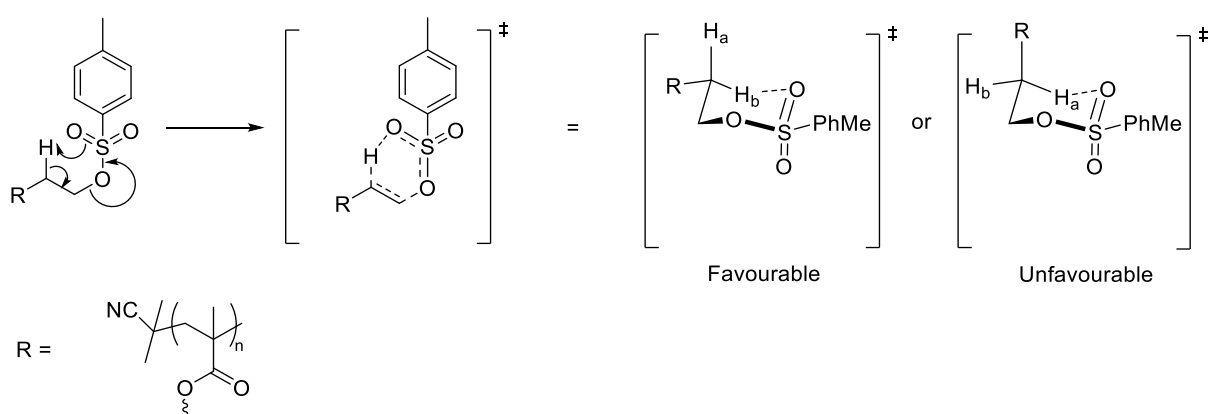


Figure 4-22 – Conformational analysis of p(HEMATos) E; 6-membered transition states.

When reacting *via* the 6-membered pathway there are two possible conformers that may be adopted to give rise to a chair-like transition state (Figure 4-22). However, these conformers

are not equal in stability, in the lowest energy conformation, the R group (polymer backbone) is positioned pseudo-equatorial. In the unfavourable conformation, the R group occupies a pseudo-axial position where it encounters an unfavourable 1,3-diaxial interaction with the pseudo-axial sp^3 -hybridised sulfonate oxygen lone pair orbital.

In the majority isomer of p(HPMAtos), the 6-membered transition states have two favourable conformers, one for each of the enantiomers, *S* and *R*, arising from the chiral centre (Figure 4-23). In the energetically unfavourable transition state conformer for both *S* and *R* enantiomers, both the R and methyl groups occupy pseudo-axial positions. The R group clashes sterically with the aromatic ring of the tosyl group and the methyl group encounters an unfavourable 1,3-diaxial interaction with the pseudoaxial sp^3 hybridised sulfonate oxygen lone pair orbital. The more favourable conformers position both the R and methyl group in pseudo-equatorial positions. However, unlike the p(HEMATos) 6-membered transition state, these groups both encounter 1,2-steric clash which raises the relative E_a of the p(HPMAtos) major isomer conformer.

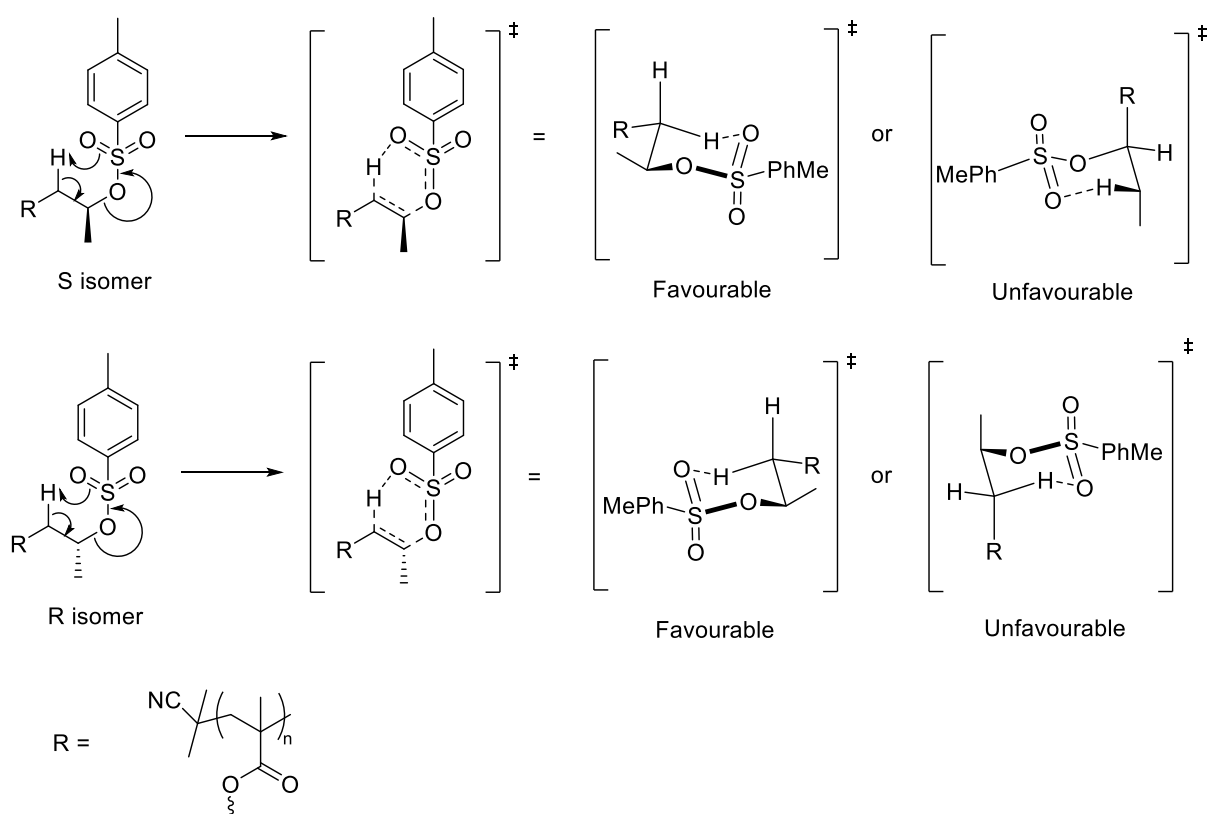


Figure 4-23 Conformational analysis of p(HPMAtos) majority isomer E_i 6-membered transition states.

Lastly, the minority regioisomer of p(HPMAtos) also exists as a pair of stereoisomers, S and R, however, the position of the R and methyl group are on the same carbon meaning the higher E_a in these conformers relative to those of p(HEMATos) cannot be due to 1,2-steric interactions. The unfavourable conformers are destabilised by the R group in the pseudo-axial position which has greater steric bulk than the methyl group, therefore the steric interaction with the tosyl group aromatic ring destabilises the transition state. Therefore, the lowest energy conformers position the bulkier R group in the pseudo-equatorial position. To summarise the lower E_a of p(HEMATos) is due to there being fewer destabilising interactions in the 6-membered transition state compared to p(HPMATos).

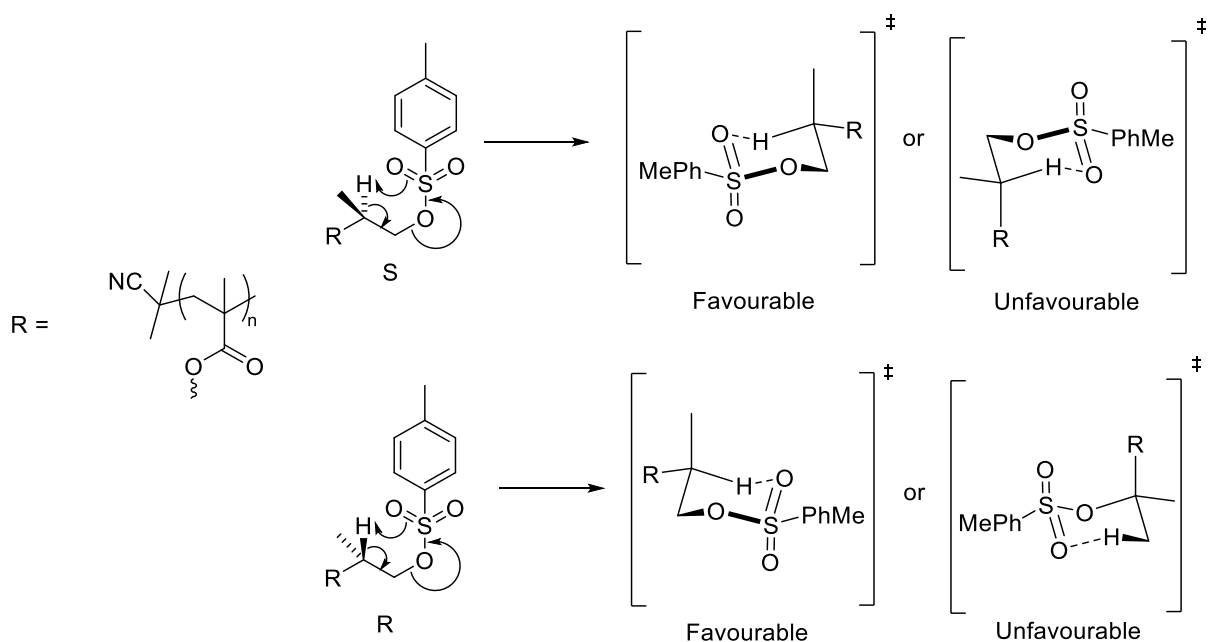


Figure 4-24 Conformational analysis of p(HPMATos) minority isomer E_i 6-membered transition states.

4.2.14. p(HEMATos) solid state E_i ¹H NMR spectroscopy study

The vtNMR studies found that p(HEMATos) was more labile towards E_i than pHPMATos which contradicts the solid state (TGA and DSC) results. Furthermore, E_i occurred at lower temperatures than expected and the reaction products were soluble in DMSO-d₆, whereas solid state studies produced insoluble resins after heating at 140-180 °C.

To investigate the effect of the physical state on the temperature of E_i in p(HEMATos) a series of experiments were performed. p(HEMATos) was heated in vials for 18 hrs over a temperature range of 50-130 °C before DMSO- d_6 was added to allow determination of the conversion of p(HEMATos) to pTsOH via 1H NMR spectroscopy. However, upon heating the samples became discoloured and formed a swollen gel when DMSO- d_6 was added, indicating that the samples had cross-linked and therefore the conversion could not be determined.

The extracts were characterised via 1H NMR spectroscopy (Figure 4-25) to gain insight into the structures of any soluble products and therefore, the cross-linking mechanism. The extracts of the samples heated to 50 and 60 °C contained mostly p(HEMATos) as confirmed by the ring CH peaks at 7.76 and 7.42 ppm, methylene CH_2 peak at 4.25 ppm, aromatic CH_3 peak at 2.33 ppm, the backbone CH_3 at 1.63 ppm and the backbone CH_2 at 0.66 ppm. pTsOH was also present as confirmed by the aromatic CH doublet peaks at 7.47 and 7.11 ppm and the CH_3 peak at 2.28 ppm. However, samples heated to 70 °C or higher contained pTsOH and no polymer, suggesting the remaining sample had cross-linked. Consequently, this means p(HEMATos) undergoes E_i in the solid state at much lower temperatures than previously thought and is unsuitable for use in A1 cross-linked networks due to the temperatures at which they are post-cured. Furthermore, the unwanted cross-linking will mean A1 cross-linked networks cannot be removed by solvent washing at the end of lifetime.

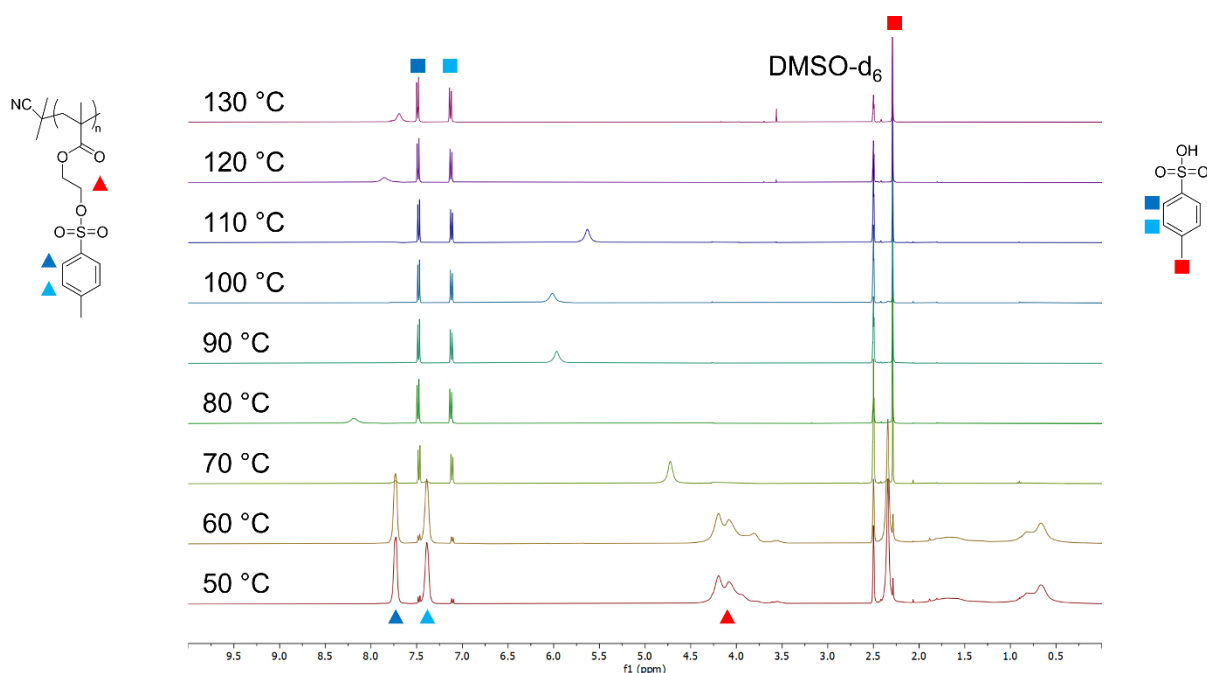
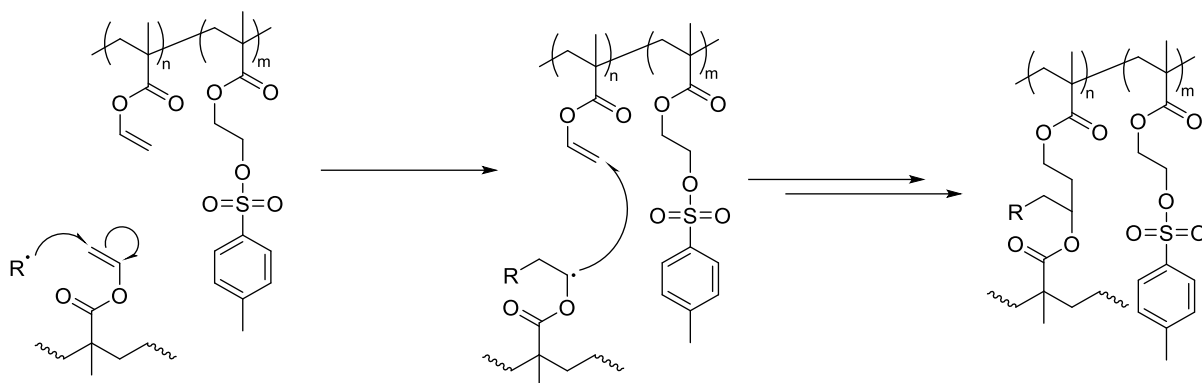
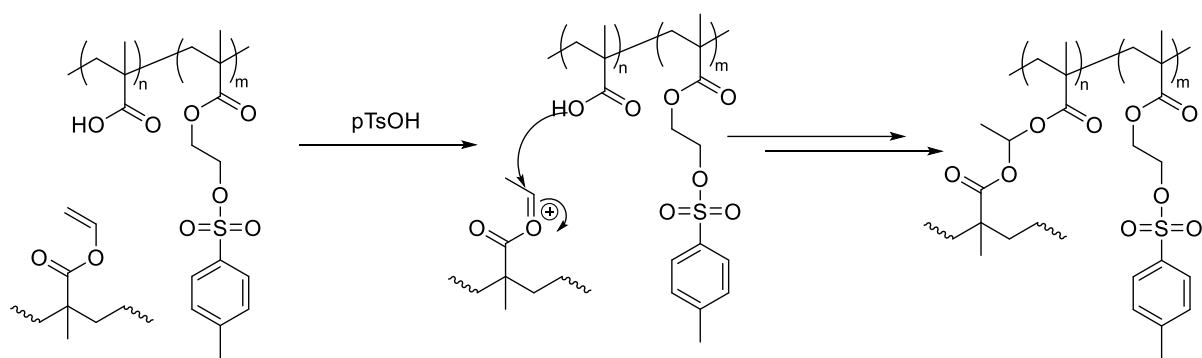


Figure 4-25 – ^1H NMR (DMSO-d_6) spectra of residue extracts after heating.

The cross-linking pathway is unknown; however, four possible mechanisms are proposed. Thermally generated radicals may react with the pendent vinyl groups between two chains creating a cross-link (Scheme 4-13).^{236,252} Another potential pathway is *via* the reaction between methacrylic acid units created by the further elimination of *in situ* formed vinyl esters previously discussed, which may undergo acid catalysed nucleophilic addition to a charged carbonyl derivative created by the tautomerisation of the vinyl pendant group, producing a hemiacetal ester type species (Scheme 4-14). However, hemiacetal esters are known to be thermally labile at temperatures $>100\text{ }^\circ\text{C}$ ¹ so cross-links formed *via* this process are likely to undergo thermolysis forming a soluble product that was not observed in the ^1H NMR spectra of extracts of reactions performed at $>100\text{ }^\circ\text{C}$.



Scheme 4-13 - Proposed free radical cross-linking mechanism of p(HEMATos).



Scheme 4-14 – Proposed nucleophilic addition cross-linking pathway of p(HEMATos).

It is proposed in the literature that p(styrene isobornylsulfonates) undergo a Friedel-Crafts type reaction upon cleavage and the norbonyl cation alkylates the resulting polymer bound pTsOH unit in the meta position.^{206,227,228,253,254} However, no mechanism or detailed structural characterisation are given, it is unclear whether this could lead to cross-linking in p(HEMATos) and p(HPMATos) systems as the pTsOH produced is not polymer bound. Mahindaratne and Wimalasena²³⁰ described a pTsOH catalysed alkylation of norbornyl, cyclohexyl and 4-methyl-2-pentyl tosylates with toluene, which could lead to cross-linking in p(HEMATos) and p(HPMATos).

Lastly, the formation of cross-linked samples of p(HEMATos) in the solid state occurs at lower temperatures than expected, vtNMR studies yielded no cross-linked residues at 50-90 °C. It is believed that this is due to concentration effects whereby pendant groups capable of

undergoing cross-linking reactions are sufficiently diluted in solution meaning they do not come within a close enough proximity to react. Whereas in the solid state the effective concentration is high meaning the pendant groups undergo cross-linking reactions.

4.3. Conclusions

Novel methacrylate TAGS, HEMA_{tos} and HPMA_{tos} were synthesised *via* an optimised route reacting pTsCl with HPMA or HEMA. The corresponding polymers were synthesised *via* free radical polymerisation and their thermal E_i reaction characterised *via* DSC and TGA. Initial characterisation suggested p(HPMA_{tos}) generated pTsOH at 180 °C. However, characterisation of solvent extracts from model thermoset networks of A1/HPMA_{tos}/MMA or A1/HPMA_{tos} revealed the presence of pTsOH after the post-curing at 100 °C.

Isothermal TGA characterisation of p(HEMA_{tos}) and p(HPMA_{tos}) at different temperatures was used to determine the reaction kinetics. However, the data showed second order reaction kinetics, when it was expected to be first order. From this it was determined that TGA is only applicable to TAGs that undergo E_i at a temperature greater than the boiling points of one of the products. p(HEMA_{tos}) and p(HPMA_{tos}) were then characterised *via* vtNMR at 50 °C-90 °C in DMSO-d₆. This revealed the polymers underwent high conversion to pTsOH at 70 °C and 90 °C, much lower temperatures than desired for inclusion into A1 networks.

Finally, the reaction was conducted in the solid state and the products characterised *via* ¹H NMR spectroscopy. Cross-linking of the polymers at 50-130 °C was observed, meaning HPMA_{tos} and HEMA_{tos} are unsuitable for this application.

4.4. Experimental

4.4.1. Materials

1,8-naphthalic anhydride, 2-nitrobenzyl alcohol (97 %), 4-dimethylaminopyridine (≥ 99 %), AIBN (98 %), dicyclohexylamine (99 %), DMSO- d_6 (99.8 atom % D), HCl (37 wt %), HPMA (97%, mixture of isomers), hydroxylamine hydrochloride ($\geq 99.9\%$), pTsCl ($\geq 99\%$), pyridine (99.9 %, (anhydrous)), t BuOH (99 %) were purchased from Sigma-Aldrich. MeOH (HPLC grade), $MgSO_4$ anhydrous, sodium carbonate anhydrous, sodium chloride ($\geq 99.5\%$), NaOH (99 %) and toluene (HPLC grade) were purchased from Fisher. All reagents were used as supplied, unless otherwise stated. Other reagents are listed in previous experimental sections.

4.4.2. Instrumentation

All instrumentation is reported in previous experimental chapters.

4.4.3. Synthesis of 2-nitrobenzyl tosylate¹³⁰

2-nitrobenzyl alcohol (6.12 g, 0.040 mol), pTsCl (8.38 g, 0.044 mol) and acetone (20 mL) were added to a round bottom flask and stirred on an ice bath. Dicyclohexylamine (7.95 mL, 0.040 mol) was added dropwise over 30 minutes and the ice bath removed. Mixture stirred for 3 hours and precipitate removed *via* filtration. Filtrate washed with Na_2CO_3 (2x5 mL), H_2O (5 mL) and brine (5 mL). Organic phase dried over $MgSO_4$, filtered and concentrated in vacuo to yield off white crystals (11.0 g, 90 % yield) 1H NMR (400 MHz, $CDCl_3$) δ 8.12 (dd, $J = 8.2, 1.3$ Hz, 1H), 7.87 – 7.83 (m, 2H), 7.80 – 7.73 (m, 1H), 7.68 (td, $J = 7.6, 1.3$ Hz, 1H), 7.55 – 7.46 (m, 1H), 7.39 – 7.34 (m, 2H), 5.47 (s, 2H), 2.46 (s, 3H), 2.17 (s, 3H).

4.4.4. Synthesis of *N*-hydroxy-1,8-naphthalimide²⁰⁹

1,8-naphthalenedicarboxylic acid (15.1 g, 76.2 mmol), hydroxylamine hydrochloride (6.46 g, 93 mmol) and DMF (90 mL) were added to a round bottom flask and stirred. To the suspension 48 wt% NaOH solution (8.06 g, 96.7 mmol) was added dropwise. Mixture heated to 30 °C for

one hour and subsequently cooled on ice. HCl (20 mL, 3 M) was added dropwise and stirred for 30 minutes. Yellow precipitate collected by filtration, washed with H₂O (3x10 mL) and dried *in vacuo* at 100 °C for 96 hours (14.0, 86 %). ¹H NMR (400 MHz, DMSO-d₆) δ 10.76 (s, 1H), 8.50 (dd, J = 14.8, 7.7 Hz, 2H), 7.89 (t, J = 7.3 Hz, 2H). ¹³C {¹H} NMR (101 MHz, DMSO) δ 161.36, 135.09, 131.88, 131.33, 127.79, 126.74, 122.84. ATR-IR: 3066 cm⁻¹ (O-H), 2824 cm⁻¹ (C-H), 1701 cm⁻¹ (C=O). CHN calculated (C 67.61 %, H 3.31 %, N 6.57 %), observed (C 66.83 %, H 3.55 %, N 6.12 %).

4.4.5. Synthesis of *N*-hydroxytosylate-1,8-naphthalimide

N-hydroxy-1,8-naphthalimide (2.5 g, 0.012 mol), NEt₃ (2.45 mL, 0.018 mol) and THF (30 mL). pTsCl (2.35 g, 0.012 mol) was added to THF (5 mL) and added dropwise. The solution was then refluxed for 4 hours and subsequently cooled. Yellow solid was collected by filtration and washed with cold water (3x10 mL) and dried *in vacuo* at 100 °C for 24 hours (2.47 g, 57 %). ¹H NMR (400 MHz, DMSO) δ 8.58 (d, J = 7.4 Hz, 2H), 8.52 (d, J = 7.3 Hz, 2H), 8.00 – 7.89 (m, 4H), 7.55 (d, J = 8.1 Hz, 2H), 2.53 (s, 3H). ¹³C {¹H} NMR (101 MHz, DMSO) δ 160.13, 147.13, 136.13, 132.21, 132.06, 131.90, 130.65, 129.53, 128.02, 127.22, 122.40, 21.82. ATR-IR: 3125-2970 cm⁻¹ (C-H), 1723.3 cm⁻¹ (C=O). [M+H]⁺ theoretical 368.05 amu, experimental 368.1 amu. CHN calculated (C 62.12 %, H 3.57 %, N 3.81 %, S 8.73 %), observed (C 62.22 %, H 3.79 %, N 4.12 %, S 8.98 %).

4.4.6. General procedure for synthesis of TAG doped adhesives

MMA (0.24 g), methacrylic acid (0.17g), A1 (0.02 g), 4-*N,N*-trimethylaniline (0.06 g) and acid generator (0.01 g) were added to sample *vial* and sealed with a septum. MMA (0.48 g) and BPO (0.02 g) were added to a sample *vial* and sealed with a septum. Both mixtures were mixed on a vortex and degassed with N₂ for 30 minutes. The mixtures were mixed under N₂ and left for 6 hours at room temperature and cured at 100 °C for 48 hrs.

4.4.7. Tosylation of HEMA and HPMA

HEMA (4.68 mL, 0.039 mol), NEt_3 (5.85 mL, 0.042 mol) and DCM (20 mL) were added to a round bottom flask and cooled on an ice bath. pTsCl (6.72 g, 0.35 mol) was added to DCM (10 mL) and added dropwise to the reaction mixture. After 18 hours the mixture was filtered and washed with DCM (3x10 mL). The filtrate was concentrated in vacuo to yield a pale-yellow oil. The crude product was purified *via* column chromatography in an eluent of hexane/ethyl acetate (6/4 v/v, 2 vol% NEt_3) to yield a white solid (2.97 g, 37 %) ^1H NMR (400 MHz, CDCl_3) δ 7.85 – 7.78 (m, 2H), 7.37 (dd, $J = 8.1, 2.2$ Hz, 2H), 6.08 (q, $J = 1.2$ Hz, 1H), 5.60 (p, $J = 1.6$ Hz, 1H), 4.37 – 4.23 (m, 4H), 2.47 (s, 3H), 1.92 (t, $J = 1.3$ Hz, 3H). ATR-IR: 2990 cm^{-1} (C-H), 1719 cm^{-1} (C=O), 1363 (S=O).

HPMA (5.88 mL, 0.039 mol), NEt_3 (5.85 mL, 0.042 mol) and DCM (20 mL) were added to a round bottom flask and cooled on an ice bath. pTsCl (6.72 g, 0.35 mol) was added to DCM (10 mL) and added dropwise to the reaction mixture. After 18 hours the mixture was filtered and washed with DCM (3x10 mL). The filtrate was concentrated in vacuo to yield a pale-yellow oil. The crude product was purified *via* column chromatography in an eluent of hexane/ethyl acetate (6/4 v/v, 2 vol% NEt_3) to yield a white solid (3.34 g, 32 %) ^1H NMR (400 MHz, CDCl_3) δ 7.82 – 7.74 (m, 2H), 7.33 (t, $J = 7.8$ Hz, 2H), 6.01 (dt, $J = 9.8, 1.3$ Hz, 1H), 5.54 (dp, $J = 3.2, 1.6$ Hz, 1H), 5.09 (qdd, $J = 6.5, 5.2, 4.0$ Hz, 0H), 4.84 (pd, $J = 6.6, 3.4$ Hz, 1H), 4.21 – 4.03 (m, 2H), 2.44 (d, $J = 4.1$ Hz, 3H), 1.90 – 1.84 (m, 3H), 1.32 (d, $J = 6.5$ Hz, 2H), 1.26 (d, $J = 6.6$ Hz, 1H). ATR-IR: 2986 cm^{-1} (C-H), 1718 cm^{-1} (C=O), 1362 (S=O).

4.4.8. Synthesis of HPMAtos Method Development Experiments

HPMA (1.5 mL, 0.010 mol), base and DCM (25 mL) were added to a round bottom flask and stirred on an ice bath for 30 minutes. pTsCl was added in portions and the reaction stirred. Samples were taken periodically to monitor conversion *via* ¹H NMR in CDCl₃ and TLC in ethyl acetate/petroleum ether (1/3 v/v). The conversion of the isomeric alcohols to the corresponding tosylates was calculated from ¹H NMR spectra using the following equations:

Equation 4-3

$$\text{primary alcohol conversion (\%)} = \left(\frac{i(5.9)}{i(5.93) + i(6.05)} \right) \times 100$$

Equation 4-4

$$\text{secondary alcohol conversion (\%)} = \left(\frac{i(5.95)}{i(5.95) + i(6.07)} \right) \times 100$$

Table 4-5 – Bases and molar ratios used in method development experiments.

Experiment	Base	[HPMA]:[pTsCl]:[Base]:[DMAP]
1	Triethylamine	1:1.5:1.5:0
2	Pyridine	1:1.5:1.5:0
3	Pyridine	1:1.5:1.5:0.2
4	Pyridine	1:2:3:0

4.4.9. Reactive Workup of HPMAtos Synthesis

HPMA (1.5 mL, 0.010 mol), base and DCM (25 mL) were added to a round bottom flask and stirred on an ice bath for 30 minutes. pTsCl was added in portions and the reaction stirred. Aliquots (5 mL) were taken and added to vials, then stirred. A quenching agent was added (Table 4-6) and monitored by TLC in ethyl acetate/petroleum ether (1/3 v/v).

Table 4-6 - Quenching agent and amount.

Quenching agent	Amount
NEt ₃	0.24 g
^t BuOH	0.3 g
Mowiol 8-88	0.5 g
Sat. Na ₂ CO ₃	1 mL

4.4.10. Optimised Synthesis of HPMAtos

HPMA (14.0 mL, 0.1 mol), DCM (100 mL) and pyridine (24.0 mL, 0.3 mol) were added to a round bottom flask and stirred at 0 °C for 30 minutes. pTsCl (38.2 g, 0.2 mol) was added in portions over an hour. Reaction allowed to reach ambient temperature and stirred for 72 hours. As reaction proceeded white precipitate formed. Reaction quenched with sat. Na₂CO₃ (20 mL) and stirred for 20 minutes. Organic phase separated and washed with sat. Na₂CO₃ (2x20 mL), HCl (3x20 mL, 1 M), H₂O (20 mL) and brine (20 mL). Organic phase diluted with toluene (200 mL) and concentrated *in vacuo*, this was repeated twice more to yield a colourless oil (29.8 g, 98 %) that crystallised upon standing. ¹H NMR (400 MHz, CDCl₃) δ 7.82 – 7.74 (m, 2H), 7.33 (t, J = 7.8 Hz, 2H), 6.01 (dt, J = 9.8, 1.3 Hz, 1H), 5.54 (dp, J = 3.2, 1.6 Hz, 1H), 5.09 (qdd, J = 6.5, 5.2, 4.0 Hz, 0H), 4.84 (pd, J = 6.6, 3.4 Hz, 1H), 4.21 – 4.03 (m, 2H), 2.44 (d, J = 4.1 Hz, 3H), 1.90 – 1.84 (m, 3H), 1.32 (d, J = 6.5 Hz, 2H), 1.26 (d, J = 6.6 Hz, 1H). ¹³C NMR (101 MHz, CDCl₃) δ 166.85, 144.83, 135.60, 134.09, 130.02, 129.96, 128.00, 127.83, 126.47, 126.20, 77.48, 77.16, 76.84, 76.69, 71.21, 67.97, 66.10, 21.73, 18.25, 17.60, 16.19. V_{max} (cm⁻¹) 2992

(CH), 1719 (C=O), 1614 (C=C), 1348 (S=O), 1175 (S=O), 896 (C=C). $[M+Na]^+$ theoretical 321.35 amu, experimental 321.1 amu, purity 98 %. Melting point 68 °C.

4.4.11. Free radical polymerization of HEMAtos

To a vial butan-2-one (5 mL, 20 wt %), HEMAtos (1.00 g, 35.0 mmol) and AIBN (5.80 mg, 0.035 mmol) were added and degassed with N_2 on ice for 30 minutes. The reaction was heated to 70 °C for 18 hours. Crude reaction added dropwise to cold MeOH (50 mL, 10-fold excess) and white precipitate formed and collected *via* centrifugation (4500 rpm, 10 minutes). Supernatant decanted and precipitate redissolved in butan-2-one (5 mL) and reprecipitated into MeOH (50 mL, 10-fold excess), collected *via* centrifugation (4500 rpm, 10 minutes). White solid dried in vacuum oven (30 °C) for 1 week.

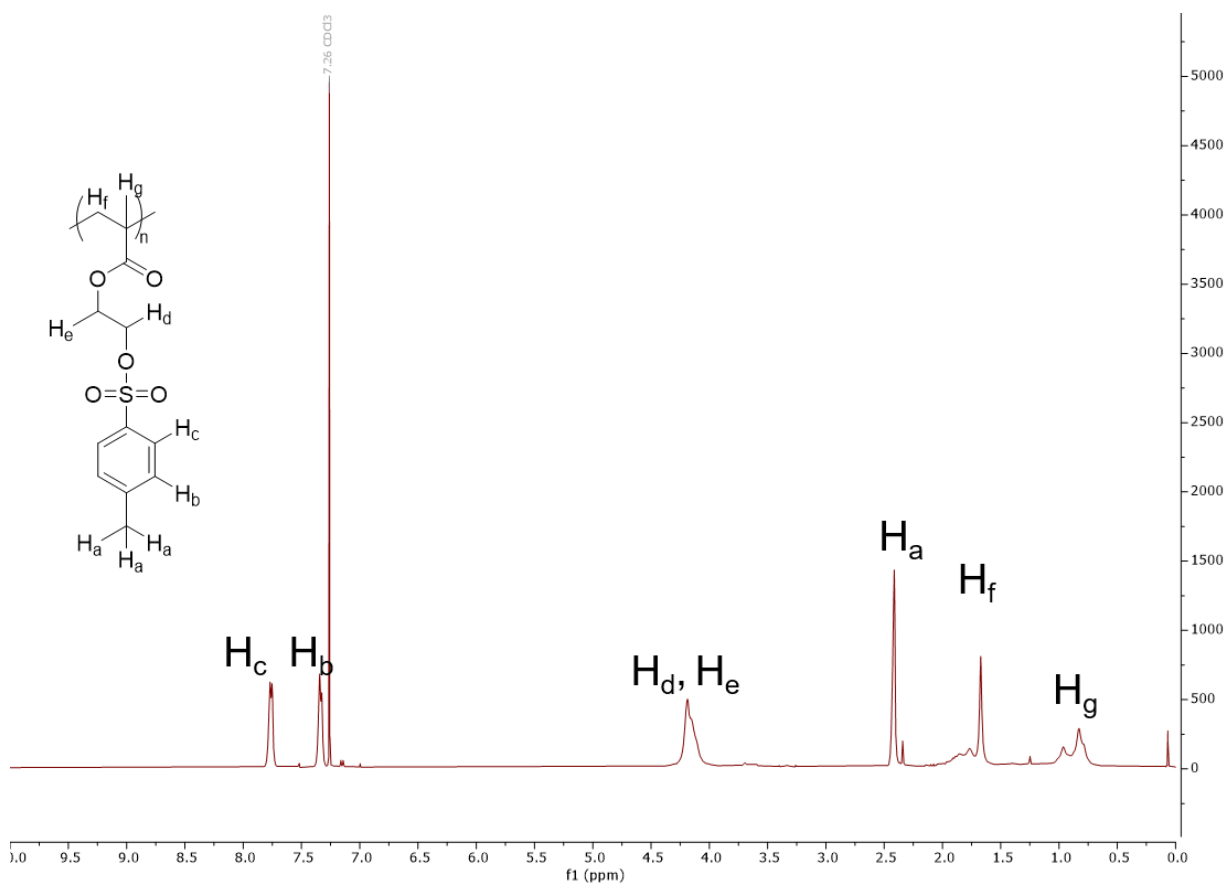


Figure 4-26 - 1H NMR spectrum ($CDCl_3$) of p(HEMAtos).

4.4.12. Free radical polymerization of HPMAtos

To a vial butan-2-one (5 mL, 80 wt %), HPMAtos (1.00 g, 33.5 mmol) and AIBN (5.50 mg, 0.034 mmol) were added and degassed with N₂ on ice for 30 minutes. The reaction was heated to 70 °C for 18 hours. Crude reaction added dropwise to cold MeOH (50 mL, 10-fold excess) and white precipitate formed and collected *via* centrifugation (4500 rpm, 10 minutes). Supernatant decanted and precipitate added to butan-2-one (5 mL) and reprecipitated into MeOH (50 mL, 10-fold excess) collected *via* centrifugation (4500 rpm, 10 minutes). Orange solid added dried in vacuum oven (30 °C) for 1 week.

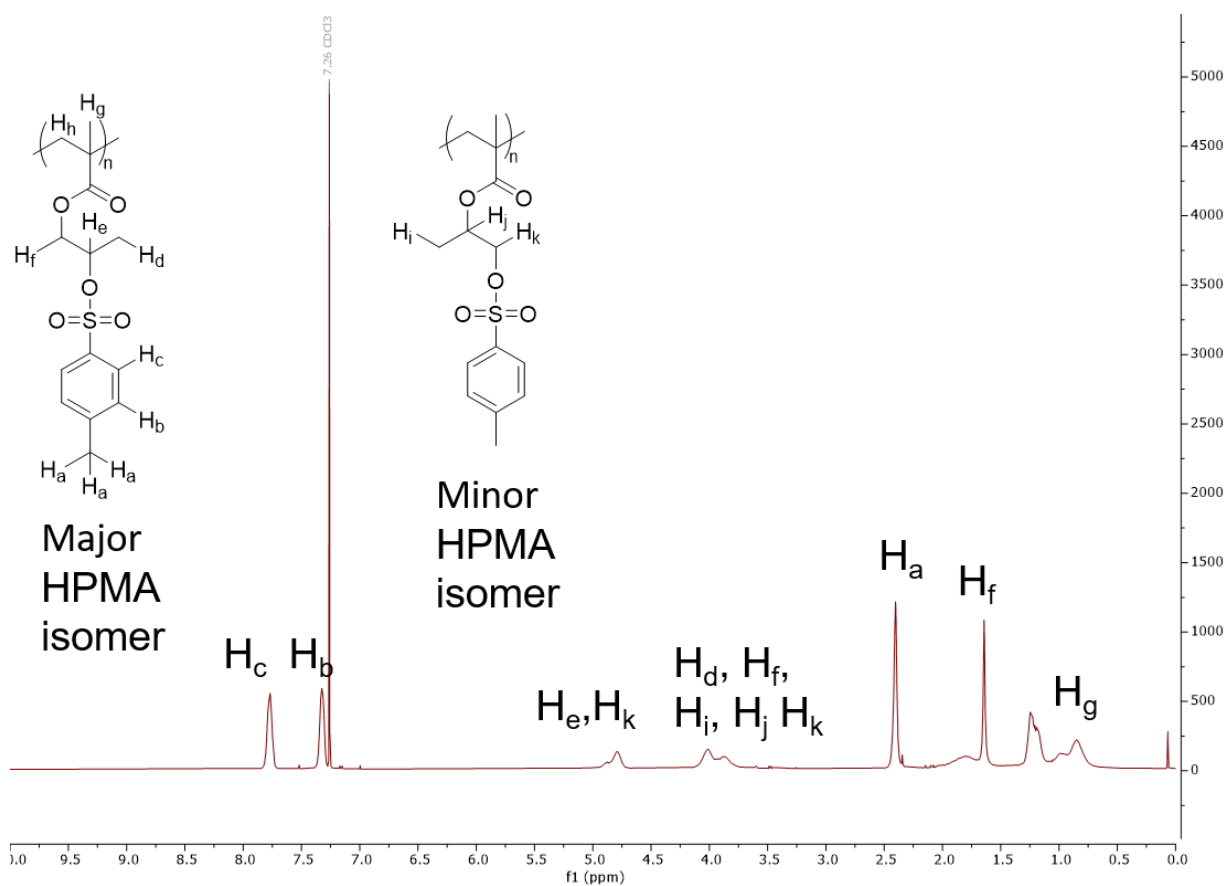


Figure 4-27 - ¹H NMR spectrum (CDCl₃) of p(HPMAtos).

4.4.13. Synthesis of Model Networks

General procedure:

To a sample vial cross-linker, monomer and BPO (0.02g, 2 wt %) were added to a vial following the amounts in Table 4-7, Table 4-8 and Table 4-9 and stirred for 15 mins. 4-TMA (0.02 g, 2 wt %) was added and mixed on a vortex mixer. Samples were left at room temperature for 6 hrs and post-cured in an oven preheated to 100 °C for 48 hrs.

Table 4-7 – Initial A1/MMA/HPMAtos network formulations.

Sample	A1 / g	MMA / g	HPMAtos / g	BPO / g	4-TMA / g
Degradable	0.05	0.81	0.1	0.02	0.02
Control	0.05	0.91	0	0.02	0.02

Table 4-8 - A1/HPMAtos and EGDMA/HPMAtos network formulations.

Sample	A1 / g	EGDMA / g	HPMAtos / g	BPO / g	4-TMA / g
Degradable	0.49	0	0.49	0.01	0.01
Control	0	0.49	0.49	0.01	0.01

Table 4-9 – HAM network formulations.

Network	A1 / g	MMA / g	HPMAtos / g	BPO / g	4-TMA / g
HAM-5	0.02	0.89	0.05	0.02	0.02
HAM-10	0.02	0.84	0.10	0.02	0.02
HAM-25	0.02	0.69	0.25	0.02	0.02
HAM-50	0.02	0.44	0.50	0.02	0.02

4.4.14. Heating of A1/MMA/HPMAtos networks

Samples of network (0.40 g) were placed in a vial, sealed and added to an oven preheated to 180 °C for 3 hrs. Samples were removed and allowed to cool, acetone (10 mL) was added and left for 30 mins. The network was removed by filtration and the filtrate concentrated *in vacuo*. ¹H NMR spectra recorded in CDCl₃.

4.4.15. Heating and Soxhlet extraction of A1/HPMAtos

Samples of network (0.5 g) were heated to 180 °C in an oven for 18 hrs. Samples were then placed in a Soxhlet extraction setup and THF at 70 °C for 24 hrs. The Soxhlet extract was concentrated *in vacuo*, the residue dissolved in DMSO-d₆.

4.4.16. Isothermal TGA characterisation of p(HPMAtos) and p(HEMAtos)

Samples (10 mg) were added to a flame cleaned platinum TGA pan. Samples were then heated at 10 °C/min to 140-180 °C and held for 18 hrs. A further temperature ramp from 140-180 °C to 800 °C was performed at 10 °C/min under N₂. Conversion was determined using the following equations:

Equation 4-5

$$Conversion (\%) = \left(1 - \left(\frac{M_0 - \frac{M_w pTsOH}{M_w HEMAtos}}{M_0}\right)\right) \times 100$$

Equation 4-6

$$Conversion (\%) = \left(1 - \left(\frac{M_0 - \frac{M_w pTsOH}{M_w HPMAtos}}{M_0}\right)\right) \times 100$$

4.4.17. ¹H vtNMR spectroscopy studies of p(HPMAtos) and p(HEMAtos)

Samples (40 mg) were added to DMSO-d₆ (0.6 mL) and inserted into a Bruker Avance 400 MHz spectrometer at preheated to 50-90 °C. ¹H NMR spectra were recorded at 400 MHz. Conversion was determined using the following equation:

Equation 4-7

$$\text{Conversion (\%)} = \left(1 - \frac{\text{integral (7.75 ppm)}_t}{\text{integral (7.75 ppm)}_{t_0}}\right) \times 100$$

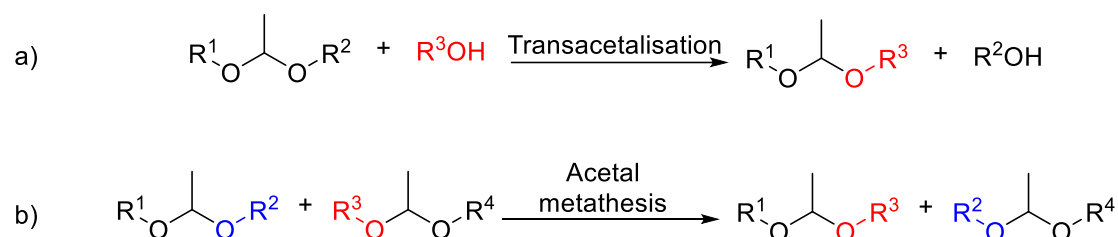
4.4.18. p(HEMAtos) solid state E_i ¹H NMR spectroscopy study

p(HEMAtos) (40 mg) was added to a *vial* and sealed. *Vials* were immersed in an oil bath preheated to 50-130 °C and left for 18 hrs. Samples were cooled to room temperature, DMSO-d₆ was added, insoluble residues were removed *via* filtration and the ¹H NMR spectrum of the filtrate recorded.

Chapter 5 – Acetal Methacrylate CANs

5.1. Introduction

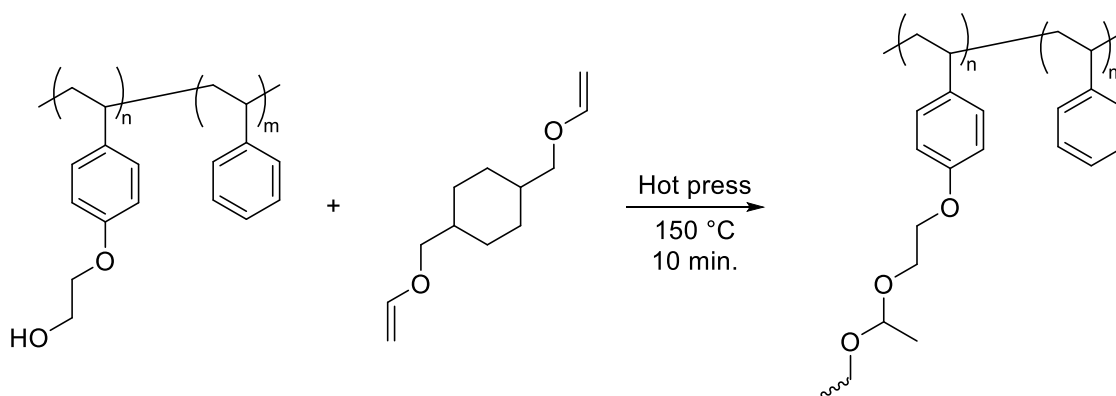
The use of acetals as dynamic covalent groups in covalently adaptable networks (CANs) is a relatively recent discovery.¹⁷⁴ Acetals can undergo exchange reactions *via* two pathways: transacetalisation and acetal metathesis. Transacetalisation is the exchange reaction between an alcohol and an acetal, producing a different acetal and alcohol (Scheme 5-1 a).⁸³ In acetal metathesis two acetals undergo an exchange reducing producing two new acetals (Scheme 5-1 b).⁸¹ A benefit of these reactions is neither require the presence of a catalyst to impart a network with adaptable properties.^{70-76,99-101} Furthermore, the acetal group enables acid degradation of the networks for material recovery and reuse.^{70,99,101}



Scheme 5-1 - a) Transacetalisation and acetal b) metathesis schemes.

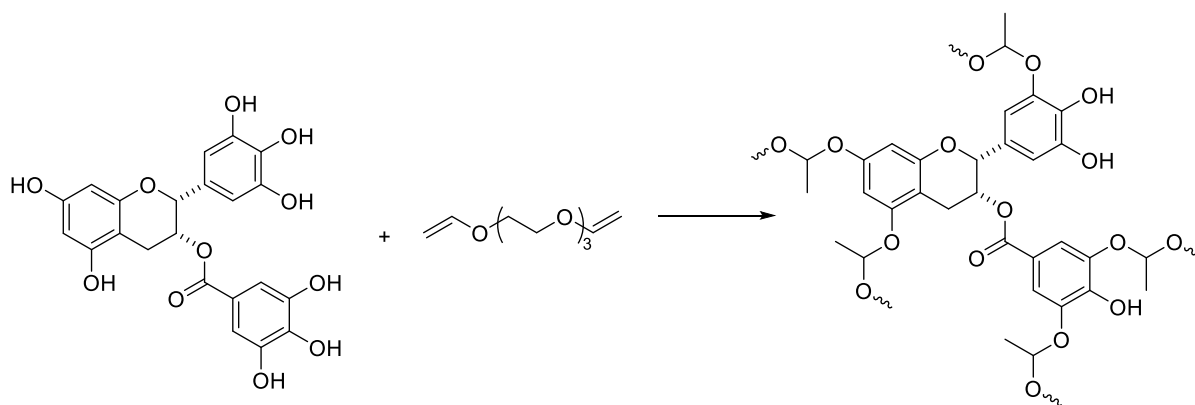
Ma and co-workers synthesised the first example of an acetal-based CAN *via* the thermal addition reaction of a hydroxy-functional poly(styrene) copolymer to 1,4-cyclohexanedimethanol divinyl ether (Scheme 5-2). They found malleability could be controlled *via* the hydroxyl to acetal ratio and samples could be reprocessed in a hot press at 150 °C for 10 mins; the authors do not mention the pressure used. The tensile properties of the reprocessed materials were similar to the starting material, and they could be chemically recycled *via* acetal hydrolysis.¹⁰¹ Further work by Ma and co-workers used this reaction to cross-link other networks such as phenolic resins,⁷⁰ p(HEMA-*co*-styrene) and p(HEMA-*co*-styrene-*co*-2-ethylhexyl methacrylate)⁷¹ with 1,4-cyclohexanedimethanol divinyl ether. Further examples in the literature include the cross-linking of HEMA modified p(styrene-

butadiene) with 1,4-cyclohexanedimethanol divinyl ether,¹⁰⁰ phenolic resin⁷³ or lignin with TEGDVE⁷⁴.



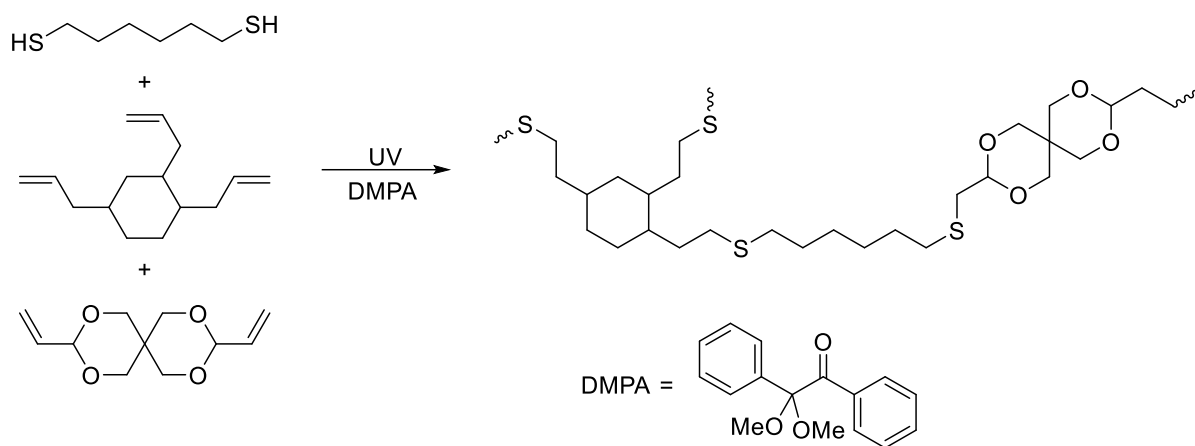
Scheme 5-2 - First literature example of an acetal-based CAN.¹⁵²

Ma and co-workers also showed neighbouring group participation is possible during transacetalisation, altering the reprocessing properties of acetal CANs.⁷² The presence of a hydroxyl group neighbouring the acetal group in 2-(1-butoxyethoxy)phenol lowered the activation energy from $68.5 \pm 3.5 \text{ kJ mol}^{-1}$ for (1-butoxyethoxy)benzene to $43.7 \pm 1.4 \text{ kJ mol}^{-1}$. This was then used in epigallocatechin gallate and TEGDVE networks (Scheme 5-3).



Scheme 5-3 - Acetal CAN utilising β -hydroxy neighbouring groups to lower the activation energy of transacetalisation.⁷²

Lastly, Shuangjian *et al.*²⁵⁵ synthesised a spirocyclic acetal containing CAN *via* a photoinitiated radical thiol-ene reaction (Scheme 5-4). The spirocyclic acetal underwent catalyst-free metathesis to give the network's adaptable properties and improved the thermal stability of the network relative to acyclic acetal examples.



Scheme 5-4 - Radical curing spirocyclic acetal CAN.²⁵⁵

Based upon these reports, we hypothesised that A1 cross-linked networks could undergo transacetalisation and acetal metathesis to create adaptable materials. The research within this chapter focuses on the preliminary synthesis and characterisation of A1 cross-linked network CANs. Focussing on A1/MMA and A1/HEMA/MMA networks to investigate the effect of reaction pathway, metathesis or transacetalisation, on the materials properties.

5.2. Results and Discussion

5.2.1. Lap shears and repressing

Lap shear testing is used to measure the bond strength of an adhesive joining two substrates by pulling them apart.³ It was hypothesised that dynamic bonds could enable two substrates to be re-joined by heating under increased pressure. Aluminium lap shear samples were prepared using a P2 etch, A1 (2 wt%), MMA(94 wt%), BPO (2 wt%) and 4-TMA (2 wt%) and their bond strength determined using a tensometer. Commercially available structural methacrylate-based adhesives contain additives such as elastomers, achieving bond strengths >20 MPa.^{3,4} The initial bond strength of A1 cross-linked and EGDMA cross-linked adhesives was 4.4 ± 0.3 MPa and 5.1 ± 0.2 MPa, respectively (Figure 5-1). These values are both much lower than desired and this was thought to be due to the brittleness of the two networks leading to stress concentration and bond failure. Furthermore, the bond failure method was predominantly adhesive, failing at the interface between adhesive and substrate. Therefore, it was hypothesised that the addition of an adhesion promoter could improve the bond strength. The lower bond strength of A1 may be due to the increased viscosity of the cross-linker compared to EGDMA reducing the surface wetting and therefore, the bond strength.^{256,257}

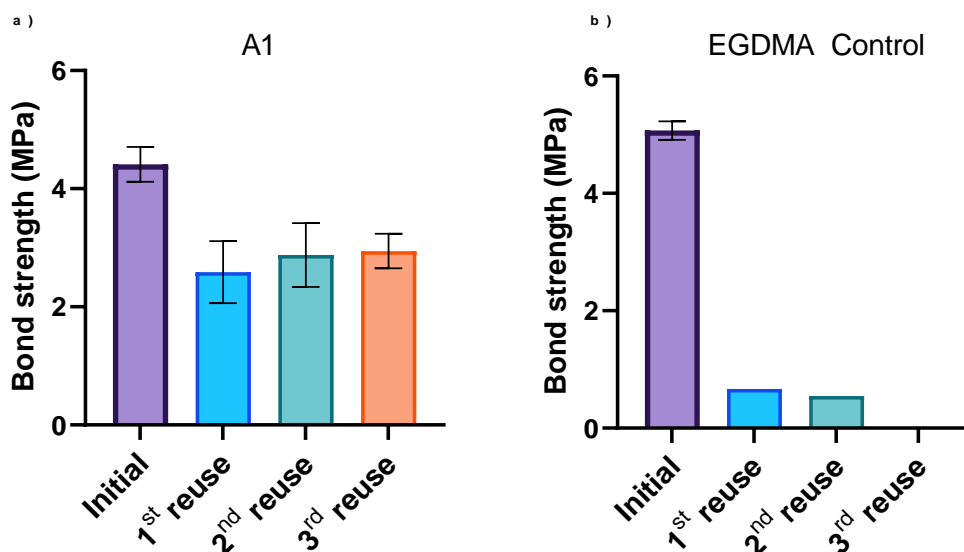


Figure 5-1 - Bond strength data of lap shear testing of a) A1 cross-linked and b) EGDMA crosslinked MMA networks before and after repressing.

Literature reports suggest that networks containing acetal functionality can react *via* acetal metathesis, imparting the network with adaptable behaviour.⁷⁰⁻⁷⁶ To investigate this A1 and EGDMA lap shears were re-joined in a hot press at 150 °C and 1.5 MPa and their bond strengths recorded. EGDMA lap shears were used as a control, although adaptable behaviour can be achieved *via* transesterification, free hydroxyls and a catalyst are required.^{66,258,259} A1 cross-linked networks demonstrated adaptable behaviour, upon re-joining the lap shear samples a first, second and third time, bond strengths of 2.6 ± 0.5 MPa, 2.9 ± 0.5 MPa and 2.9 ± 0.3 MPa were achieved, respectively (Figure 5-1). The large standard deviation was thought to arise from the loss of material when pulling apart the lap shears on the tensometer and material being squeezed from the bond line when repressing. The reuse data for EGDMA networks (Figure 5-1) shows one sample exhibited adaptable behaviour. This was thought to be due to unreacted monomer being polymerised upon heating as opposed to transesterification and the sample could not be re-joined a third time.

To improve the bond strength of A1 networks, further lap shears were synthesised incorporating methacrylic acid (MAA) which promotes adhesion by forming carboxylates with the aluminium surface.³ The formulation was changed to A1 (2 wt %), MAA (7.5 wt %), MMA

(86.5 wt %); BPO (2 wt %) and 4-TMA (2 wt %) were used as the initiator system. The MAA networks had a bond strength of 10 ± 1 MPa, which is over double of those without MAA. This may be further improved to compete with commercial adhesives *via* formulation. Finally, the MAA networks also exhibited adaptable behaviour as shown by the bond strengths after repressing the lap shears (Figure 5-2). It is also possible that the additional MAA units may take part in catalysing the acetal metathesis.^{81,258,260}

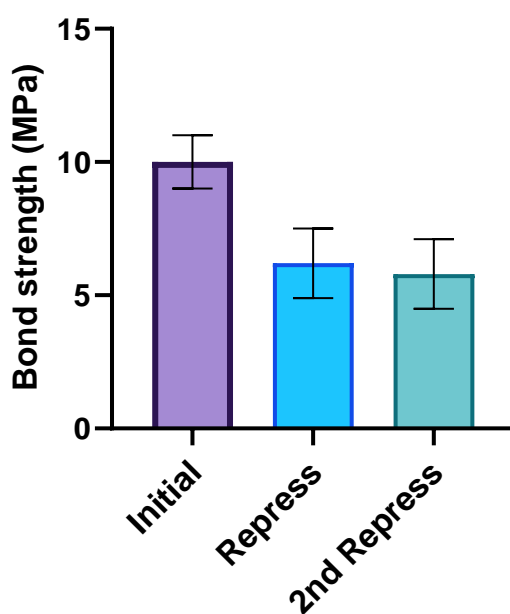


Figure 5-2 - Bond strength of A1/MAA/MMA network after lap shear testing and repressing.

5.2.2. Casting panels and cubes

Having found evidence of adaptable behaviour in A1 cross-linked MMA networks *via* lap shear testing, a series of networks were synthesised for dynamic mechanical analysis, tensile testing, and grinding/reprocessing experiments. The network compositions were varied to investigate the effect of reaction pathway on the reprocessing properties. Networks containing only MMA and A1 were used to probe the metathesis reaction while A1/HEMA/MMA networks were used to probe the transacetalisation reaction and the effect of [OH]:[acetal] group on the macroscopic properties. The formulations of these networks are shown in Table 5-1 and Table 5-2.

Table 5-1 - Formulation of A1/MMA acetal metathesis networks.

A1 mol %	MMA mol %	Benox c-50s ^a mol % ^b	DMA mol % ^b
2	98	0.5	0.25
5	95	0.5	0.25
10	90	0.5	0.25
20	80	0.5	0.25

^aCommercially available blend of BPO (50 wt %) and diethylphthalate, ^bmol % of total vinyl groups

Table 5-2 - Formulation of A1/HEMA/MMA transacetalisation networks.

OH/Acetal ^a	HEMA mol %	A1 mol %	MMA mol %	Benox c-50s ^b mol % ^c	DMA mol % ^c
1	20	10	70	0.25	0.125
0.5	10	10	80	0.5	0.25
0.25	5	10	85	0.5	0.25

^atwo moles of acetal per mole of A1, ^bCommercially available blend of BPO (50 wt %) and diethylphthalate, ^cmol % of total vinyl groups

The networks were synthesised by casting between two glass panels at room temperature (Figure 5-3 a). Upon gelation they were allowed to cool and then post-cured at 100 °C for 48 hrs. Due to the low viscosity of the mixture, glass panels were sealed with silicone sealant prior to casting to ensure no leakage. Throughout the course of casting panels several panels had rough surfaces due to thermal expansion and subsequent contraction resulting from the exotherm and/or shrinkage (Figure 5-3 b). This was avoided by adjusting the ratio of BPO (Benox c-50s) to *N,N*-dimethylaniline (DMA) to vinyl groups. Tensile bars were then prepared by punching pre-heated panels with a die; samples were obtained for all panels except the 20 mol % metathesis panel (Table 5-1) as the samples crumbled. This was thought to be due to the high cross-linker content making the networks very brittle (Figure 5-3 c).

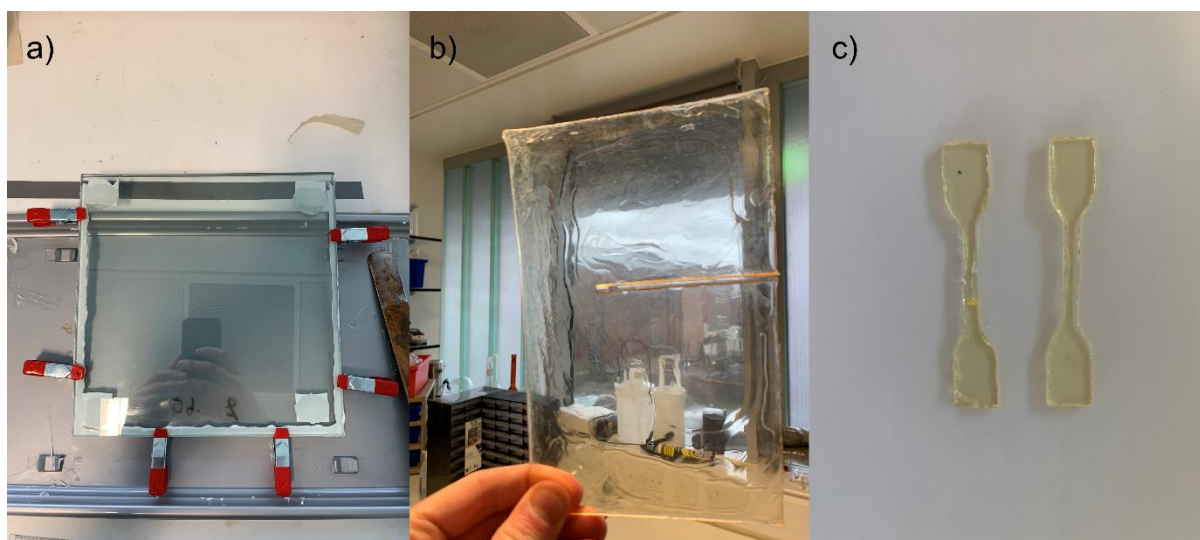


Figure 5-3 - Panel casting setup (a), imperfect panel (b) and damaged tensile samples (c).

5.2.3. TGA Analysis

A1/MMA and A1/HEMA/MMA networks were characterised using TGA (Figure 5-4) to ensure they were cured and that thermal degradation took place well above 150 °C, the temperature at which acetal exchange reactions take place.^{70,71,174,72–76,99–101} The TGA thermograms of A1/MMA and A1/HEMA/MMA networks showed no mass loss at $T < 200$ °C indicating no residual monomer was present. The onset of a sharp mass loss for A1/MMA networks was at 300 °C, well above the expected reprocessing temperature. The order of thermal stability was A1 2 mol % > A1 5 mol % > A1 10 mol %, which was unexpected as cross-linking typically increases thermal stability.²⁶¹ This was thought to arise from the increase in ether and acetal groups at higher A1 mol %, which are less thermally stable than the carbon-carbon bonds in the poly(methacrylate backbone).⁸³ The A1/HEMA/MMA networks had similar thermal stabilities.

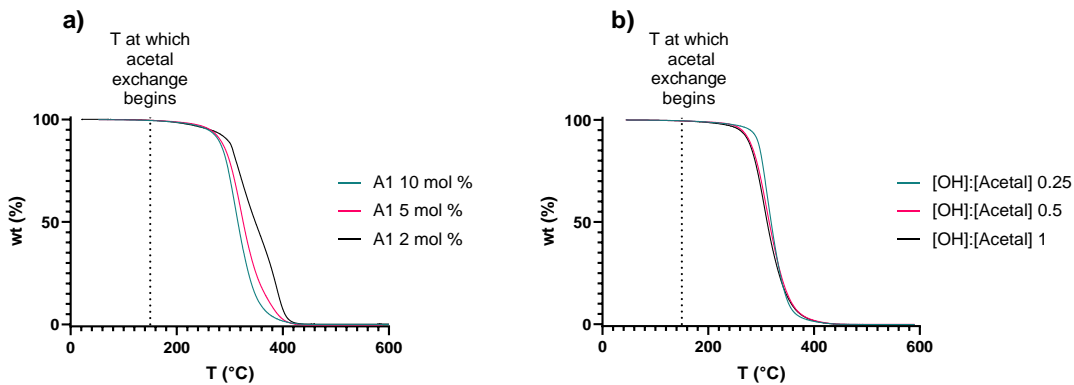


Figure 5-4 - TGA thermograms of a) A1/MMA and b) A1/HEMA/MMA networks, under N₂ from 25-600 °C at 20 °C/min.

5.2.4. Reprocessing by Vacuum Compression Moulding and Hot Press

To determine whether the acetal crosslinkers would enable reprocessing, samples of the A1/MMA (10 mol %) and A1/HEMA/MMA ([OH]:[acetal] = 1) networks were ground into a powder then reformed by vacuum compression moulding at elevated temperatures. The conditions chosen for this were based on those described for acetal CANs in the literature.^{70-76,99,100,174} Samples were heated at 150 °C under vacuum for 15 mins, 30 mins and 60 mins. After reprocessing, the samples were heterogeneous, and particles could be seen within the sample (Figure 5-5). Furthermore, the samples could be easily crumbled by hand and upon immersion in acetone they broke apart whereas a homogeneous network should swell under these conditions. Upon heating to 170 °C and leaving for 15, 30, 60 and 180 min. the same problem was observed. It was hypothesised that this was due to the relatively low pressure exerted on the sample during vacuum compression moulding compared to the hydraulic hot presses used in literature examples. This reduces the interfacial mixing between individual particles and dynamic groups.

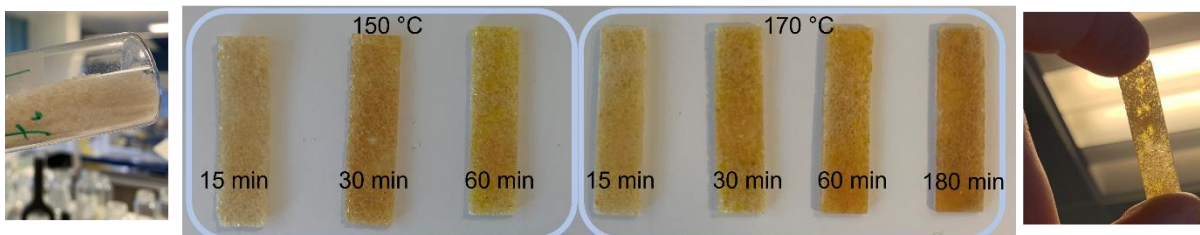


Figure 5-5 - Samples produced from ground network samples by vacuum compression moulding. Ground samples of A1/MMA (10 mol %) and A1/HEMA/MMA ([OH]:[acetal] = 1) were then compressed under 0.5 or 1 MPa of pressure within a PTFE lined aluminium mould at 150-180 °C for 30-180 min (Figure 5-6). Samples became increasingly discoloured with increased heating duration; this was attributed to oxidation of the network. However, heterogeneous samples were recovered suggesting that something was affecting the dynamic behaviour of the networks and preventing the formation of homogeneous panels. This may be due to the lower pressure used compared to the lap shear repressing that was performed at 1.5 MPa and potential thermal gradient that arose from using a mould.



Figure 5-6 - Grinding and hot-press reforming of A1/HEMA/MMA networks.

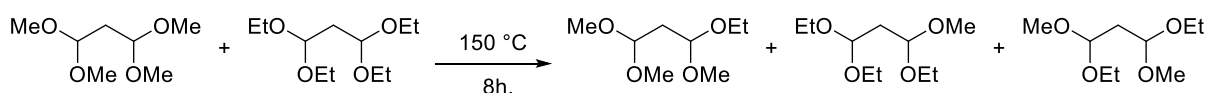
5.2.5. Potential Issues with A1/MMA and A1/HEMA/MMA Networks

The difficulty in reprocessing the A1/MMA and A1/HEMA/MMA networks could have arisen from network effects, such as high T_g , changing the relaxation properties compared to networks described in the literature,^{70-74,76,99,100} side reactions altering the chemical composition of the networks and different synthetic protocols to the networks described in the literature. These will now be discussed.

One possible reason for the network's reluctance to rearrange is the effect of the matrix on the topological freezing temperature, the lower temperature at which CANs may be reprocessed.^{262,263} It may be that the relatively high melting point of p(MMA), 160 °C¹⁷⁷ is resulting in slow conformational rearrangement of the network.

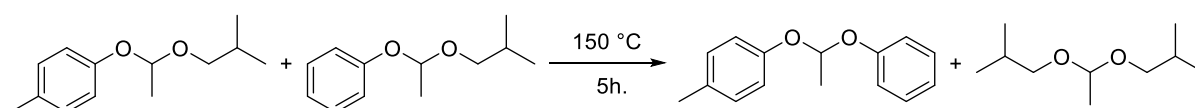
A further reason the A1/MMA networks may not be forming the expected homogeneous networks is that previous reports of acetal metathesis polymerisation^{81,159,260,264,265} have shown that acetal metathesis requires an acid catalyst. Kinetic studies by Pemba and Miller⁸¹ into the transacetalisation reaction show that a protonated acetal acts as the electrophile, driving the transacetalisation reaction, producing products in a statistical mixture. However, conversely to this Zhu and co-workers^{70,101}, Chen *et al.*⁷ and Shuangjian *et al.*²⁵⁵ report acid catalyst free acetal metathesis in CANs.

Zhu and co-workers first reported the acid free reaction of 1,1,3,3-tetraethoxypropane and 1,1,3,3-tetra-methoxypropane at 150 °C for 8 hrs (Scheme 5-5).¹⁰¹ The reaction mixture was characterised by ¹H NMR spectroscopy up to 8hrs during which time new peaks formed at 4.72, 4.85 and 4.99 ppm. These were assigned as the products acetal CH₂proton but were not specifically assigned. Firstly, it is unclear why this proton would shift downfield when none of the products contain a more electron withdrawing group than any of the starting materials. Secondly, the ¹H NMR spectra show these products are very much a minority product, whereas acetal metathesis should yield a statistical mixture of products.^{81,260,265} Lastly, if acetal metathesis was taking place then polymeric products would form as both starting materials are difunctional and capable of reacting with one another and themselves.^{81,83,260,265,266}

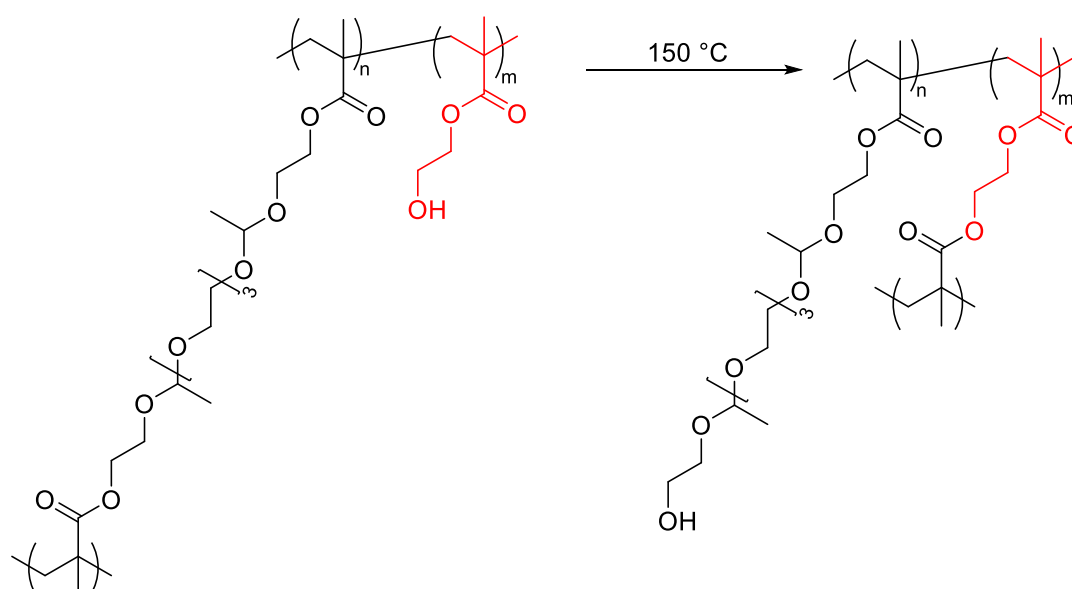


Scheme 5-5 - Zhu *et al.*'s model acetal metathesis reaction and ¹H NMR chemical shifts.¹⁰¹

However, Zhu and co-workers also studied acid free acetal metathesis reactions between 1-(1-isobutoxyethoxy)-4-methylbenzene and (1-isobutoxyethoxy)benzene *via* GC-MS and the results showed a statistical mixture of products (Scheme 5-6). All but one product was correctly identified by mass spectroscopy.⁷⁰ Shuangjian *et al.* report the acid free metathesis of cyclic acetals but suggest that atmospheric water takes part in the reaction. They also highlight the effect acetal R groups have on their reactivity towards metathesis²⁵⁵. Chen *et al.* suggest that metathesis and transacetalisation occur simultaneously in acetal CANs with free hydroxyls⁷. Hydroxyl free CANs synthesised by all authors, however, do show dynamic behaviour, but are synthesised *via* step-growth polymerisation. Consequently unless high conversion is reached,¹⁶⁴ free hydroxyls will remain in the system and may take part in transacetalisation or act as proton sources for the metathesis reaction.



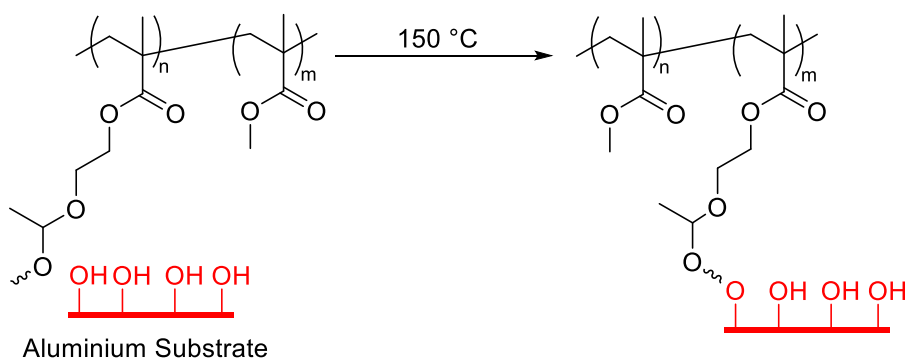
Scheme 5-6 - Zhu and co-workers' model metathesis reaction between 1-(1-isobutoxyethoxy)-4-methylbenzene and (1-isobutoxyethoxy) benzene.⁷⁰



Scheme 5-7 - Potential transesterification cross-linking pathways of A1 cross-linked networks containing HEMA.

In the A1/HEMA/MMA networks, the elevated temperatures may be driving a transesterification reaction between HEMA and MMA or A1 (Scheme 5-7). The product of which is a network containing ester cross-links, which require elevated temperatures and catalysis to impart networks with adaptable properties.^{66,258,259} Thus the formation of ester cross-links prevents the networks from forming homogeneous samples.

The lack of adaptable behaviour in A1/MMA networks led to confusion on the origin of adaptable behaviour observed in A1/MMA lap shears. Rahman *et al.*²⁵⁹ showed that phenylboronic pinacol ester functionalised styrene and styrene copolymers will form pinacol ester bonds with silica nanoparticles and hydroxyl functionalised lap shear substrates such as steel and aluminium. It is hypothesised that A1/MMA adhesives may form acetal bonds with the aluminium substrate OH bonds during the repressing step *via* transacetalisation (Scheme 5-8).



Scheme 5-8 - Transacetalisation between aluminium substrate and A1.

5.3. Conclusions

Recent work has shown acetal containing thermosets are examples of covalently adaptable networks. A1/MMA and A1/MAA/MMA model adhesives exhibited adaptable behaviour, lap shear samples were hot pressed at 1.5 MPa and 150 °C for 15 minutes and found to retain 50-60 % of their original bond strength up to three times. A series of A1/HEMA/MMA and A1/MMA networks were synthesised and characterised *via* TGA to ensure they were stable at 150 °C, the reprocessing temperature found in the literature. The networks were thermally stable to ~300 °C.

Samples of the networks were ground, and reprocessing was attempted *via* vacuum compression moulding and hot pressing the samples in a mould. However, these samples did not form the expected homogeneous networks. Multiple potential causes were identified such as lower pressure than previously used, the effect of the p(MMA) components on the network, the disputed metathesis mechanism, and the potential for cross-linking *via* transesterification in the HEMA networks. However, due to time constraints these questions remain open.

5.4. Experimental

5.4.1. Materials

Iron (III) sulfate hydrate (97 %) and sulfuric acid (95-98 %) were purchased from Sigma-Aldrich. Aluminium strips 26.5x10x1.5 mm were provided by Scott Bader. BENOX-C50s (BPO, phthalates 50 wt %) was purchased from United Initiators. All other reagents are reported in previous chapters.

5.4.2. Instrumentation

Vacuum compression moulding was performed using a MeltPrep VCM with a 10x40 mm bar insert on ground samples (1 g). Hot press moulding was performed using an in-house press, ground samples (5-10 g) were placed into a PTFE lined aluminium mould (80x60 mm) and the press was pre-heated to a target temperature. The charged mould was heated for 15 minutes prior to applying pressure, after which pressure was applied. The mould was cooled prior to opening. Lap shear testing was performed on a Tinius Olsen H5K at a crosshead speed of 1 mm/min, a minimum of five repeats were performed.

5.4.3. Etching aluminium substrates

P2 preparation is described elsewhere²⁶⁷. P2 etch solution was added to a vessel and heated to 60-68 °C. Aluminium substrates were degreased by rubbing with propan-2-ol and allowing to dry. Substrates ~5 cm were immersed in the stirred solution for 12 min. Samples were immersed in a deionised water bath, then placed into a second deionised water bath for 5 mins. Substrates were then placed into an oven preheated to 40 °C for 20-30 mins and used within one hr of being removed from the P2 etch solution.

5.4.4. Synthesis of Lap Shears

The following stock solutions were prepared. Methyl methacrylate (82.8 g, 0.83 mol), A1 (1.8 g, 4.0 mmol) and benzoyl peroxide (25 % H₂O, 4.8 g, 15 mmol) were mixed. Methyl methacrylate (86.4 g, 0.86 mol) and 4,*N,N*-trimethylaniline (3.6 g, 26 mmol) were mixed. The two solutions were added to a 200 mL dual syringe equipped with a static mixer. Adhesives were made up as before and dispensed into a disposable cup, glass beads (212-300 micrometres) were added as spacers and applied to substrates held in a mould that gave a bond area of 25x12 mm. Samples were cured at ambient for 6 hrs before being placed in a preheated 100 °C oven overnight.

5.4.5. Synthesis of Panels

General procedure:

Monomers and BENOX C-50s were added (see Table 5-3 and Table 5-4) to a beaker and stirred until a homogeneous solution had formed. DMA was added and the mixture was stirred until it began to thicken. Solution was poured between to sealed glass plates set to 3 mm apart and left overnight. Glass plates were separated and resulting resin panel cured at 40 °C for 3 hrs then 100 °C for 24 hrs.

Table 5-3 - A1/MMA network formulations.

A1 mol %	A1 / g (mol)	MMA / g (mol)	BENOX C-50s / g (mmol of BPO)	DMA / g (mmol)
2	8.50 (0.018)	90.1 (0.89)	2.27 (9.4)	0.284 (2.4)
5	19.3 (0.042)	79.4 (0.79)	2.12 (8.8)	0.266 (2.2)
10	33.5 (0.072)	65.3 (0.65)	1.93 (8.0)	0.241 (2.0)
20	53.0 (0.12)	45.9 (0.46)	1.67 (6.9)	0.208 (1.7)

Table 5-4 - A1/HEMA/MMA Network Formulations.

[OH]:[acetal]	HEMA / g (mol)	A1 / g (mol)	MMA / g (mol)	BENOX c-50s / g (mmol of BPO)	DMA / g (mmol)
1	12.2 (0.094)	43.4 (0.094)	43.8 (0.43)	0.871 (1.8)	0.109 (0.9)
0.5	5.70 (0.044)	40.5 (0.088)	52.6 (0.52)	1.80 (3.7)	0.226 (1.9)
0.25	2.67 (0.0205)	38.0 (0.082)	58.2 (0.58)	1.86 (3.8)	0.232 (1.9)

Chapter 6 - Concluding Remarks

Thermosets are a broad class of polymers with excellent thermal and mechanical properties used in a range of applications in industries. However, chemical cross-links create challenges for their recycling and reuse. Two potential solutions to this are chemically recyclable thermosets and covalently adaptable networks, the acetal functional group is suitable for both.

A novel dimethacrylate cross-linker bearing two acetal functional groups was synthesised from 2-hydroxyethyl methacrylate and tri(ethylene glycol)divinyl ether. The extent of acetal hydrolysis was found to increase with decreasing pK_a in 0.15 M acetone- d_6 /D₂O (9/1 v/v) solutions at 50 °C for 5 hrs. However, 100 % hydrolysis was observed only when using acids with a $pK_a < 1.29$. There is scope to create a library of diacetal cross-linkers by changing the divinyl ether and alcohol components for use in (meth)acrylate thermosets and more such as urethane-acrylates.

Model thermosets were synthesised from the acetal cross-linker and methyl methacrylate. Their degradation properties in acidic solvent/H₂O solutions at 50 °C for 5 hours. were investigated and compared to the neat cross-linker. Homogeneous solutions formed indicating acetal group hydrolysis, however, lower pK_a acids were required for full degradation within 5 hours than compared to the cross-linker. It was hypothesised that the mechanism of degradation was a complex mixture of chemical and physical processes that effect the kinetics.

Structural characterisation of hydrolysis experiments solutions showed the degradation products were p(methyl methacrylate-co-2-hydroxyethyl methacrylate) and the commodity chemicals tri(ethylene glycol) and acetaldehyde. There is scope for synthesis of chemically identical networks from p(methyl methacrylate-co-2-hydroxyethyl methacrylate) and tri(ethylene glycol)divinyl ether which is to be investigated in the future. Furthermore, recovery of tri(ethylene glycol) and acetaldehyde from the degradation solution may enable a synthetic route to tri(ethylene glycol)divinyl ether, heading towards a circular system. Lastly, the long-term stability of acetal containing thermosets will need to be assessed in a variety of

environments to ensure their suitability for application and prevent unwanted release of degradation products to the environment.

The concept of internalising the acid source for hydrolysis was then researched using conventional acid generators such as 2-nitrobenzyl tosylate, the selection of which was guided by previous investigations of the effect of pK_a on hydrolysis. However, attempts to incorporate acid generators as additives to the prepolymer solution were unsuccessful due to acid generators acting as inhibitors or having poor solubility. To circumnavigate this novel tosylates of 2-hydroxyethyl methacrylate and 2-hydroxypropyl methacrylate were synthesised. The homopolymers were characterised by the field favoured technique of thermogravimetric analysis, however, it was found that the unique structure of these tosylates meant this technique was unsuitable.

Variable temperature nuclear magnetic resonance spectroscopy was used to characterise the thermal elimination of the poly(tosylates) in the solution phase at various temperatures. The poly(tosylates) generated pTsOH however, the expected poly(vinyl methacrylate) product was not observed, this was attributed to further reactions such as ester pyrolysis and Kornblum oxidation. It was also found that elimination of *para*-toluene sulfonic acid occurred at $<100\text{ }^\circ\text{C}$ for both poly(tosylates) meaning they were unsuitable for use in model acetal thermosets. Furthermore, elimination in the solid state formed insoluble residues *via* hypothesised cross-linking reactions, rendering the tosylates unsuitable for their desired applications. Further work is required to determine the nature of the cross-linking reactions by synthesising model tosylates and investigating alternative acid chemistries such as oxime sulfonates.

Finally preliminary research into the use of the novel dimethacrylate cross-linker in covalently adaptable networks was undertaken, acetal/HEMA/MMA and acetal/MMA networks were synthesised to investigate the acetal metathesis and transacetalisation pathways. Thermogravimetric analysis revealed acetal/HEMA/MMA and acetal/MMA networks were thermally stable to $\sim 300\text{ }^\circ\text{C}$.

Acetal/MMA and acetal/MAA/MMA model adhesives exhibited adaptable behaviour, lap shear samples were hot pressed at 1.5 MPa and 150 °C for 15 minutes and were found to retain 50-60 % of their original bond strength up to three times. However, ground samples of the networks didn't show any reprocessible behaviour under vacuum compression moulding or in a hot press, the causes of which should be the focus of future work.

References

- (1) Ma, S.; Webster, D. C. Degradable Thermosets Based on Labile Bonds or Linkages: A Review. *Prog. Polym. Sci.* **2018**, *76*, 65–110. <https://doi.org/10.1016/j.progpolymsci.2017.07.008>.
- (2) IUPAC - thermosetting polymer (TT07168) <https://goldbook.iupac.org/terms/view/TT07168> (accessed Sep 29, 2022).
- (3) Comyn, J. *Adhesion Science*; RSC Publishing, 1998.
- (4) Guo, Q. Overview of Thermosets: Present and Future. In *Thermosets structure, properties and applications*; Elsevier, 2017; pp 3–29.
- (5) Geyer, R.; Jambeck, J. R.; Law, K. L. Production, Use, and Fate of All Plastics Ever Made. *Sci. Adv.* **2017**, *3* (7), e1700782. <https://doi.org/10.1126/sciadv.1700782>.
- (6) Thompson, D. L.; Hartley, J. M.; Lambert, S. M.; Shiref, M.; Harper, G. D. J.; Kendrick, E.; Anderson, P.; Ryder, K. S.; Gaines, L.; Abbott, A. P. The Importance of Design in Lithium Ion Battery Recycling-a Critical Review. *Green Chem.* **2020**, *22* (22), 7585–7603. <https://doi.org/10.1039/d0gc02745f>.
- (7) Mulcahy, K. R.; Kilpatrick, A. F. R.; Harper, G. D. J.; Walton, A.; Abbott, A. P. Debondable Adhesives and Their Use in Recycling. *Green Chem.* **2022**, *24* (1), 36–61. <https://doi.org/10.1039/d1gc03306a>.
- (8) Li, H.; Aguirre-Villegas, H. A.; Allen, R. D.; Bai, X.; Benson, C. H.; Beckham, G. T.; Bradshaw, S. L.; Brown, J. L.; Brown, R. C.; Castillo, M. A. S.; Cecon, V. S.; Curley, J. B.; Curtzwiler, G. W.; Dong, S.; Gaddameedi, S.; Garcia, J. E.; Hermans, I.; Kim, M. S.; Ma, J.; Mark, L. O.; Mavrikakis, M.; Olafasakin, O. O.; Osswald, T. A.; Papanikolaou, K. G.; Radhakrishnan, H.; Sánchez-Rivera, K. L.; Tumu, K. N.; Lehn, R. C. Van; Vorst, K. L.; Wright, M. M.; Wu, J.; Zavala, V. M.; Zhou, P.; Huber, G. W. Expanding Plastics Recycling Technologies: Chemical Aspects, Technology Status and Challenges.

ChemRxiv **2022**. <https://doi.org/10.1039/d2gc02588d>.

- (9) Pickering, S. J. Recycling Technologies for Thermoset Composite Materials-Current Status. *Compos. Part A Appl. Sci. Manuf.* **2006**, *37* (8), 1206–1215. <https://doi.org/10.1016/j.compositesa.2005.05.030>.
- (10) Petrie, E. M. Adhesion & Bonding: Adhesives-Enablers of Sustainability. *Met. Finish.* **2010**, *108* (5), 20–22. [https://doi.org/10.1016/S0026-0576\(10\)80102-3](https://doi.org/10.1016/S0026-0576(10)80102-3).
- (11) Schenzel, A. M.; Klein, C. O.; Rist, K.; Moszner, N.; Barner-Kowollik, C. Reversing Adhesion: A Triggered Release Self-Reporting Adhesive. *Adv. Sci.* **2016**, *3* (3), 1–5. <https://doi.org/10.1002/advs.201500361>.
- (12) Wind Turbine Blades Can't Be Recycled, So They're Piling Up in Landfills - Bloomberg <https://www.bloomberg.com/news/features/2020-02-05/wind-turbine-blades-can-t-be-recycled-so-they-re-piling-up-in-landfills?leadSource=uverify> wall (accessed Sep 29, 2022).
- (13) Yang, Y.; Boom, R.; Irion, B.; van Heerden, D. J.; Kuiper, P.; de Wit, H. Recycling of Composite Materials. *Chem. Eng. Process. Process Intensif.* **2012**, *51*, 53–68. <https://doi.org/10.1016/j.cep.2011.09.007>.
- (14) Post, W.; Susa, A.; Blaauw, R.; Molenveld, K.; Knoop, R. J. I. A Review on the Potential and Limitations of Recyclable Thermosets for Structural Applications. *Polym. Rev.* **2020**, *60* (2), 359–388. <https://doi.org/10.1080/15583724.2019.1673406>.
- (15) Liu, Y.; Yu, Z.; Wang, B.; Li, P.; Zhu, J.; Ma, S. Closed-Loop Chemical Recycling of Thermosetting Polymers and Their Applications: A Review. *Green Chem.* **2022**, *24* (15), 5691–5708. <https://doi.org/10.1039/d2gc00368f>.
- (16) Khalid, M. Y.; Arif, Z. U.; Ahmed, W.; Arshad, H. Recent Trends in Recycling and Reusing Techniques of Different Plastic Polymers and Their Composite Materials. *Sustain. Mater. Technol.* **2022**, *31*, e00382.

<https://doi.org/10.1016/j.susmat.2021.e00382>.

- (17) Vollmer, I.; Jenks, M. J. F.; Roelands, M. C. P.; White, R. J.; van Harmelen, T.; de Wild, P.; van der Laan, G. P.; Meirer, F.; Keurentjes, J. T. F.; Weckhuysen, B. M. Beyond Mechanical Recycling: Giving New Life to Plastic Waste. *Angew. Chemie - Int. Ed.* **2020**, *59* (36), 15402–15423. <https://doi.org/10.1002/anie.201915651>.
- (18) Ragaert, K.; Delva, L.; Geem, K. Van. Mechanical and Chemical Recycling of Solid Plastic Waste. *Waste Manag.* **2017**, *69*, 24–58. <https://doi.org/10.1016/j.wasman.2017.07.044>.
- (19) Fortman, D. J.; Brutman, J. P.; De Hoe, G. X.; Snyder, R. L.; Dichtel, W. R.; Hillmyer, M. A. Approaches to Sustainable and Continually Recyclable Cross-Linked Polymers. *ACS Sustain. Chem. Eng.* **2018**, *6* (9), 11145–11159. <https://doi.org/10.1021/acssuschemeng.8b02355>.
- (20) Shen, M.; Cao, H.; Robertson, M. L. Hydrolysis and Solvolysis as Benign Routes for the End-of-Life Management of Thermoset Polymer Waste. *Annu. Rev. Chem. Biomol. Eng.* **2020**, *11* (June), 183–201. <https://doi.org/10.1146/annurev-chembioeng-120919-012253>.
- (21) Zhao, Y. B.; Lv, X. D.; Ni, H. G. Solvent-Based Separation and Recycling of Waste Plastics: A Review. *Chemosphere* **2018**, *209*, 707–720. <https://doi.org/10.1016/j.chemosphere.2018.06.095>.
- (22) Helmer Pedersen, T.; Conti, F. Improving the Circular Economy via Hydrothermal Processing of High-Density Waste Plastics. *Waste Manag.* **2017**, *68*, 24–31. <https://doi.org/10.1016/j.wasman.2017.06.002>.
- (23) Jensen, J. P.; Skelton, K. Wind Turbine Blade Recycling: Experiences, Challenges and Possibilities in a Circular Economy. *Renew. Sustain. Energy Rev.* **2018**, *97* (August), 165–176. <https://doi.org/10.1016/j.rser.2018.08.041>.

- (24) Raquez, J. M.; Deléglise, M.; Lacrampe, M. F.; Krawczak, P. Thermosetting (Bio)Materials Derived from Renewable Resources: A Critical Review. *Prog. Polym. Sci.* **2010**, *35* (4), 487–509. <https://doi.org/10.1016/J.PROGPOLYMSCI.2010.01.001>.
- (25) Ghosh, K.; Jones, B. H. Roadmap to Biodegradable Plastics-Current State and Research Needs. *ACS Sustain. Chem. Eng.* **2021**, *9* (18), 6170–6187. <https://doi.org/10.1021/acssuschemeng.1c00801>.
- (26) Yardley, R. E.; Kenaree, A. R.; Gillies, E. R. Triggering Depolymerization: Progress and Opportunities for Self-Immolative Polymers. *Macromolecules* **2019**, *52* (17), 6342–6360. <https://doi.org/10.1021/acs.macromol.9b00965>.
- (27) Sirianni, Q. E. A.; Gillies, E. R. The Architectural Evolution of Self-Immolative Polymers. *Polymer (Guildf)*. **2020**, *202* (March), 122638. <https://doi.org/10.1016/j.polymer.2020.122638>.
- (28) Wang, H. S.; Truong, N. P.; Pei, Z.; Coote, M. L.; Anastasaki, A. Reversing RAFT Polymerization: Near-Quantitative Monomer Generation Via a Catalyst-Free Depolymerization Approach. *J. Am. Chem. Soc.* **2022**, *144* (10), 4678–4684. <https://doi.org/10.1021/jacs.2c00963>.
- (29) Wang, H. S.; Truong, N. P.; Jones, G. R.; Anastasaki, A. Investigating the Effect of End-Group, Molecular Weight, and Solvents on the Catalyst-Free Depolymerization of RAFT Polymers: Possibility to Reverse the Polymerization of Heat-Sensitive Polymers. *ACS Macro Lett.* **2022**, *11* (10), 1212–1216. <https://doi.org/10.1021/acsmacrolett.2c00506>.
- (30) Jehanno, C.; Pérez-Madrigal, M. M.; Demartean, J.; Sardon, H.; Dove, A. P. Organocatalysis for Depolymerisation. *Polym. Chem.* **2019**, *10* (2), 172–186. <https://doi.org/10.1039/c8py01284a>.
- (31) Conk, R. J.; Hanna, S.; Shi, J. X.; Yang, J.; Ciccio, N. R.; Qi, L.; Bloomer, B. J.; Heuvel, S.; Wills, T.; Su, J.; Bell, A. T.; Hartwig, J. F. Catalytic Deconstruction of Waste

- Polyethylene with Ethylene to Form Propylene. *Science*. **2022**, 377 (6614), 1561–1566.
<https://doi.org/10.1126/science.add1088>.
- (32) Yoshida, S.; Hiraga, K.; Takehana, T.; Taniguchi, I.; Yamaji, H.; Maeda, Y.; Toyohara, K.; Miyamoto, K.; Kimura, Y.; Oda, K. A Bacterium That Degrades and Assimilates Poly(Ethylene Terephthalate). *Science*. **2016**, 351 (6278), 1196–1199.
<https://doi.org/10.1126/science.aad6359>.
- (33) Banea, M. D.; Da Silva, L. F. M.; Campilho, R. D. S. G.; Sato, C. Smart Adhesive Joints: An Overview of Recent Developments. *J. Adhes.* **2014**, 90 (1), 16–40.
<https://doi.org/10.1080/00218464.2013.785916>.
- (34) Hutchinson, A.; Liu, Y.; Lu, Y. Overview of Disbonding Technologies for Adhesive Bonded Joints. *J. Adhes.* **2017**, 93 (10), 737–755.
<https://doi.org/10.1080/00218464.2016.1237876>.
- (35) Cingil, H. E.; Balmer, J. A.; Armes, S. P.; Bain, P. S. Conducting Polymer-Coated Thermally Expandable Microspheres. *Polym. Chem.* **2010**, 1 (8), 1323–1331.
<https://doi.org/10.1039/c0py00108b>.
- (36) Ciardiello, R.; Belingardi, G.; Martorana, B.; Brunella, V. Physical and Mechanical Properties of a Reversible Adhesive for Automotive Applications. *Int. J. Adhes. Adhes.* **2019**, 89, 117–128. <https://doi.org/10.1016/j.ijadhadh.2018.12.005>.
- (37) Banea, M. D.; da Silva, L. F. M.; Carbas, R. J. C.; de Barros, S. Debonding on Command of Multi-Material Adhesive Joints. *J. Adhes.* **2017**, 93 (10), 756–770.
<https://doi.org/10.1080/00218464.2016.1199963>.
- (38) Schmid, A.; Sutton, L. R.; Armes, S. P.; Bain, P. S.; Manfrè, G. Synthesis and Evaluation of Polypyrrole-Coated Thermally-Expandable Microspheres: An Improved Approach to Reversible Adhesion. *Soft Matter* **2009**, 5 (2), 407–412.
<https://doi.org/10.1039/b811246k>.

- (39) Kawate, K.; Kanki, T. WO0040648A1, 2000.
- (40) Kolbe, J.; Kowalik, T.; Popp, M.; Sebald, M.; Schorsch, O.; Heberer, S.; Pridohl, M.; Zimmermann, G.; Hartwig, A.; Born, E. US 2004249037 A1, 2004.
- (41) Xue, Y.; Bai, H.; Peng, B.; Fang, B.; Baell, J.; Li, L.; Huang, W.; Voelcker, N. H. Stimulus-Cleavable Chemistry in the Field of Controlled Drug Delivery. *Chem. Soc. Rev.* **2021**, *50* (8), 4872–4931. <https://doi.org/10.1039/D0CS01061H>.
- (42) Binauld, S.; Stenzel, M. H. Acid-Degradable Polymers for Drug Delivery: A Decade of Innovation. *Chem. Commun.* **2013**, *49* (21), 2082–2102. <https://doi.org/10.1039/c2cc36589h>.
- (43) Seidi, F.; Jenjob, R.; Crespy, D. Designing Smart Polymer Conjugates for Controlled Release of Payloads. *Chem. Rev.* **2018**, *118* (7), 3965–4036. <https://doi.org/10.1021/acs.chemrev.8b00006>.
- (44) Sangermano, M.; Tonin, M.; Yagci, Y. Degradable Epoxy Coatings by Photoinitiated Cationic Copolymerization of Bisepoxide with ϵ -Caprolactone. *Eur. Polym. J.* **2010**, *46* (2), 254–259. <https://doi.org/10.1016/j.eurpolymj.2009.10.023>.
- (45) Tomuta, A. M.; Fernández-Francos, X.; Ferrando, F.; Ramis, X.; Serra, À. Enhanced Chemical Reworkability of DGEBA Thermosets Cured with Rare Earth Triflates Using Aromatic Hyperbranched Polyesters (HBP) and Multiarm Star HBP-b-Poly(ϵ -Caprolactone) as Modifiers. *Polym. Adv. Technol.* **2013**, *24* (11), 962–970. <https://doi.org/10.1002/pat.3171>.
- (46) Trullemans, L.; Koelewijn, S. F.; Scodeller, I.; Hendrickx, T.; Van Puyvelde, P.; Sels, B. F. A Guide towards Safe, Functional and Renewable BPA Alternatives by Rational Molecular Design: Structure-Property and Structure-Toxicity Relationships. *Polym. Chem.* **2021**, *12* (41), 5870–5901. <https://doi.org/10.1039/d1py00909e>.
- (47) Swan, S. H.; Colino, S. *Count down: How Our Modern World Is Threatening Sperm*

- Counts, Altering Male and Female Reproductive Development, and Imperiling the Future of the Human Race*; Scribner, 2021.
- (48) Zhang, Y.; Ying, H.; Hart, K. R.; Wu, Y.; Hsu, A. J.; Coppola, A. M.; Kim, T. A.; Yang, K.; Sottos, N. R.; White, S. R.; Cheng, J. Malleable and Recyclable Poly(Urea-Urethane) Thermosets Bearing Hindered Urea Bonds. *Adv. Mater.* **2016**, *28* (35), 7646–7651. <https://doi.org/10.1002/adma.201601242>.
- (49) Ying, H.; Cheng, J. Hydrolyzable Polyureas Bearing Hindered Urea Bonds. *J. Am. Chem. Soc.* **2014**, *136* (49), 16974–16977. <https://doi.org/10.1021/ja5093437>.
- (50) Ying, H.; Zhang, Y.; Cheng, J. Dynamic Urea Bond for the Design of Reversible and Self-Healing Polymers. *Nat. Commun.* **2014**, *5* (3218), 1–9. <https://doi.org/10.1038/ncomms4218>.
- (51) Silva, A. L.; Bordado, J. C. Recent Developments in Polyurethane Catalysis: Catalytic Mechanisms Review. *Catalysis Reviews - Science and Engineering*. Taylor & Francis Group February 2004, pp 31–51. <https://doi.org/10.1081/CR-120027049>.
- (52) Schellekens, Y.; Van Trimpont, B.; Goelen, P. J.; Binnemans, K.; Smet, M.; Persoons, M. A.; De Vos, D. Tin-Free Catalysts for the Production of Aliphatic Thermoplastic Polyurethanes. *Green Chem.* **2014**, *16* (9), 4401–4407. <https://doi.org/10.1039/c4gc00873a>.
- (53) Guan, J.; Song, Y.; Lin, Y.; Yin, X.; Zuo, M.; Zhao, Y.; Tao, X.; Zheng, Q. Progress in Study of Non-Isocyanate Polyurethane Progress in Study of Non-Isocyanate Polyurethane. *Ind. Eng. Chem.* **2011**, *50*, 6517–6527. https://doi.org/10.1021/IE101995J/ASSET/IMAGES/LARGE/IE-2010-01995J_0019.JPEG.
- (54) Endo, T.; Suzuki, T.; Sanda, F.; Takata, T. A Novel Approach for the Chemical Recycling of Polymeric Materials: The Network Polymer \rightleftharpoons Bifunctional Monomer

- Reversible System. *Macromolecules* **1996**, *29* (9), 3315–3316. <https://doi.org/10.1021/ma951850f>.
- (55) Chikaoka, S.; Takata, T.; Endo, T. Synthesis and Reactions of Exo Methylene Containing Poly Cyclic Orthoester. *Macromolecules* **1994**, *27*, 2380–2382.
- (56) Hitomi, M.; Sanda, F.; Endo, T. Reversible Crosslinking-Decrosslinking of Polymers Having Bicyclo Orthoester Moieties in the Side Chains. *Macromol. Chem. Phys.* **1999**, *200* (6), 1268–1273. [https://doi.org/10.1002/\(SICI\)1521-3935\(19990601\)200:6<1268::AID-MACP1268>3.0.CO;2-N](https://doi.org/10.1002/(SICI)1521-3935(19990601)200:6<1268::AID-MACP1268>3.0.CO;2-N).
- (57) Sanda, F.; Yoshida, K.; Endo, T. Cationic Ring-Opening Polymerization of Mono and Bifunctional Spiro Orthoesters Containing Ester Groups, and Depolymerization of the Obtained Polymers. *Am. Chem. Soc. Polym. Prepr. Div. Polym. Chem.* **1999**, *40* (1), 240–241.
- (58) García, J. M.; Jones, G. O.; Virwani, K.; Mccloskey, B. D.; Boday, D. J.; Huurne, G. M.; Horn, H. W.; Coady, D. J.; Bintaleb, A. M.; Alabdulrahman, A. M. S.; Alsewailam, F.; Almegren, H. A. A.; Hedrick, J. L. Recyclable, Strong Thermosets and Organogels via Paraformaldehyde Condensation with Diamines. *Science*. **2014**, *344*, 732–735.
- (59) Christensen, P. R.; Scheuermann, A. M.; Loeffler, K. E.; Helms, B. A. Closed-Loop Recycling of Plastics Enabled by Dynamic Covalent Diketoenamine Bonds. *Nat. Chem.* **2019**, *11* (5), 442–448. <https://doi.org/10.1038/s41557-019-0249-2>.
- (60) Taynton, P.; Yu, K.; Shoemaker, R. K.; Jin, Y.; Qi, H. J.; Zhang, W. Heat- or Water-Driven Malleability in a Highly Recyclable Covalent Network Polymer. *Adv. Mater.* **2014**, *26* (23), 3938–3942. <https://doi.org/10.1002/adma.201400317>.
- (61) Taynton, P.; Ni, H.; Zhu, C.; Yu, K.; Loob, S.; Jin, Y.; Qi, H. J.; Zhang, W. Repairable Woven Carbon Fiber Composites with Full Recyclability Enabled by Malleable Polyimine Networks. *Adv. Mater.* **2016**, *28* (15), 2904–2909.

- <https://doi.org/10.1002/adma.201505245>.
- (62) Taynton, P.; Zhu, C.; Loob, S.; Shoemaker, R.; Pritchard, J.; Jin, Y.; Zhang, W. Re-Healable Polyimine Thermosets: Polymer Composition and Moisture Sensitivity. *Polym. Chem.* **2016**, *7* (46), 7052–7056. <https://doi.org/10.1039/c6py01395c>.
- (63) Kissounko, D. A.; Taynton, P.; Kaffer, C. New Material: Vitrimers Promise to Impact Composites. *Reinf. Plast.* **2018**, *62* (3), 162–166. <https://doi.org/10.1016/j.repl.2017.06.084>.
- (64) Zhao, S.; Abu-Omar, M. M. Recyclable and Malleable Epoxy Thermoset Bearing Aromatic Imine Bonds. *Macromolecules* **2018**, *51* (23), 9816–9824. <https://doi.org/10.1021/acs.macromol.8b01976>.
- (65) Winne, J. M.; Leibler, L.; Du Prez, F. E. Dynamic Covalent Chemistry in Polymer Networks: A Mechanistic Perspective. *Polym. Chem.* **2019**, *10* (45), 6091–6108. <https://doi.org/10.1039/c9py01260e>.
- (66) Montarnal, D.; Capelot, M.; Tournilhac, F.; Leibler, L. Silica-like Malleable Materials from Permanent Organic Networks. *Science*. **2011**, *334* (6058), 965–968. <https://doi.org/10.1126/science.1212648>.
- (67) Worrell, B. T.; McBride, M. K.; Lyon, G. B.; Cox, L. M.; Wang, C.; Mavila, S.; Lim, C. H.; Coley, H. M.; Musgrave, C. B.; Ding, Y.; Bowman, C. N. Bistable and Photoswitchable States of Matter. *Nat. Commun.* **2018**, *9* (1), 1–7. <https://doi.org/10.1038/s41467-018-05300-7>.
- (68) Denissen, W.; Winne, J. M.; Du Prez, F. E. Vitrimers: Permanent Organic Networks with Glass-like Fluidity. *Chem. Sci.* **2016**, *7* (1), 30–38. <https://doi.org/10.1039/c5sc02223a>.
- (69) Zou, W.; Dong, J.; Luo, Y.; Zhao, Q.; Xie, T. Dynamic Covalent Polymer Networks: From Old Chemistry to Modern Day Innovations. *Adv. Mater.* **2017**, *29* (14).

<https://doi.org/10.1002/adma.201606100>.

- (70) Li, Q.; Ma, S.; Wang, S.; Liu, Y.; Taher, M. A.; Wang, B.; Huang, K.; Xu, X.; Han, Y.; Zhu, J. Green and Facile Preparation of Readily Dual-Recyclable Thermosetting Polymers with Superior Stability Based on Asymmetric Acetal. *Macromolecules* **2020**, *53* (4), 1474–1485. <https://doi.org/10.1021/acs.macromol.9b02386>.
- (71) Lu, N.; Li, Q.; Ma, S.; Wang, B.; Xu, X.; Wang, S.; Ye, J.; Qiu, J.; Zhu, J. Scalable and Facile Synthesis of Acetal Covalent Adaptable Networks with Readily Adjustable Properties. *Eur. Polym. J.* **2021**, *147*, 1–8. <https://doi.org/10.1016/j.eurpolymj.2021.110291>.
- (72) Li, Q.; Ma, S.; Li, P.; Wang, B.; Yu, Z.; Feng, H.; Liu, Y.; Zhu, J. Fast Reprocessing of Acetal Covalent Adaptable Networks with High Performance Enabled by Neighboring Group Participation. *Macromolecules* **2021**, *54* (18), 8423–8434. <https://doi.org/10.1021/acs.macromol.1c01046>.
- (73) Chen, J.; Zhang, K.; Zhang, K.; Jiang, B.; Huang, Y. Facile Preparation of Reprocessable and Degradable Phenolic Resin Based on Dynamic Acetal Motifs. *Polym. Degrad. Stab.* **2022**, *196*, 109818. <https://doi.org/10.1016/j.polymdegradstab.2022.109818>.
- (74) Moreno, A.; Morsali, M.; Sipponen, M. H. Catalyst-Free Synthesis of Lignin Vitrimers with Tunable Mechanical Properties: Circular Polymers and Recoverable Adhesives. *ACS Appl. Mater. Interfaces* **2021**, *13* (48), 57952–57961. <https://doi.org/10.1021/acsami.1c17412>.
- (75) Shuangjian Yu,; Siwu Wu,; Chengfeng Zhang, Zhenghai Tang, Yanlong Luo, Baochun Guo, and L. Z. Catalyst-Free Metathesis of Cyclic Acetals and Spirocyclic Acetal Covalent Adaptable Networks. *ACS Macro Lett.* **2020**, *9*, 1143–1148. <https://doi.org/10.1021/acs.macromol.0c02699>.

- (76) Li, Q.; Ma, S.; Li, P.; Wang, B.; Feng, H.; Lu, N.; Wang, S.; Liu, Y.; Xu, X.; Zhu, J. Biosourced Acetal and Diels-Alder Adduct Concurrent Polyurethane Covalent Adaptable Network. *Macromolecules* **2021**, *54* (4), 1742–1753. <https://doi.org/10.1021/acs.macromol.0c02699>.
- (77) Clayden, J.; Greeves, N.; Warren, S. Nucleophilic Substitution at C=O With Loss of Carbonyl Oxygen. In *Organic Chemistry*; Oxford University Press, 2001; pp 222–239.
- (78) D., M. A.; A., W. *LUPAC. Compendium of Chemical Terminology*, second.; Blackwell Scientific Publications, 1997.
- (79) Vogel, A. I.; Furniss, B. S.; Hannaford, A. J.; Smith, P. W. G.; Tatchell, A. R. Aliphatic Compounds. In *Vogel's Textbook of Practical Organic Chemistry*; 1989; pp 605–625.
- (80) Smith, M. B.; March, J. Addition to Carbon–Hetero Multiple Bonds. *March's Adv. Org. Chem.* **2007**, 1251–1476. <https://doi.org/10.1002/9780470084960.CH16>.
- (81) Pemba, A. G.; Miller, S. A. Acetal Metathesis: Mechanistic Insight. *Synlett* **2019**, *30* (17), 1971–1976. <https://doi.org/10.1055/s-0037-1611833>.
- (82) Nasanit, R.; Davies, M. C.; Soliman, M.; Watson, S. A.; Grabowska, A. M.; Preece, J. A.; Allen, S.; Abulateefeh, S. R.; Alexander, C.; Briggs, S. S.; Seymour, L. W.; Nasanit, R.; Abulateefeh, S. R.; Allen, S.; Davies, M. C.; Briggs, S. S.; Seymour, L. W.; Preece, J. A.; Grabowska, A. M.; Watson, S. A.; Alexander, C. Multicomponent Synthetic Polymers with Viral-Mimetic Chemistry for Nucleic Acid Delivery. *Mol. Pharm.* **2011**, *9* (1), 1–13. <https://doi.org/10.1021/mp200108q>.
- (83) Hufendiek, A.; Lingier, S.; Du Prez, F. E. Thermoplastic Polyacetals: Chemistry from the Past for a Sustainable Future? *Polym. Chem.* **2019**, *10* (1), 9–33. <https://doi.org/10.1039/c8py01219a>.
- (84) 1,4-Butanediol divinyl ether 98 3891-33-6
<https://www.sigmaaldrich.com/GB/en/product/aldrich/123315> (accessed Jul 21, 2022).

- (85) 1,4-Cyclohexanedimethanol divinyl ether, mixture of isomers 98 17351-75-6
<https://www.sigmaaldrich.com/GB/en/product/aldrich/406171> (accessed Jul 21, 2022).
- (86) Di(ethylene glycol) divinyl ether 99 764-99-8
<https://www.sigmaaldrich.com/GB/en/product/aldrich/139548> (accessed Jul 21, 2022).
- (87) Poly(ethylene glycol) divinyl ether average Mn 250 50856-26-3
<https://www.sigmaaldrich.com/GB/en/product/aldrich/410195> (accessed Jul 21, 2022).
- (88) Tri(ethylene glycol) divinyl ether 98 765-12-8
<https://www.sigmaaldrich.com/GB/en/product/aldrich/329800> (accessed Jul 21, 2022).
- (89) Okimoto, Y.; Sakaguchi, S.; Ishii, Y. Development of a Highly Efficient Catalytic Method for Synthesis of Vinyl Ethers. *J. Am. Chem. Soc.* **2002**, *124* (8), 1590–1591.
<https://doi.org/10.1021/ja0173932>.
- (90) Winternheimer, D. J.; Shade, R. E.; Merlic, C. A. Methods for Vinyl Ether Synthesis. *Synthesis (Stuttg)*. **2010**, *15*, 2497–2511. <https://doi.org/10.1055/s-0030-1258166>.
- (91) Bosch, M.; Schlaf, M. Synthesis of Allyl and Alkyl Vinyl Ethers Using an in Situ Prepared Air-Stable Palladium Catalyst. Efficient Transfer Vinylation of Primary, Secondary, and Tertiary Alcohols. *J. Org. Chem.* **2003**, *68* (13), 5225–5227.
<https://doi.org/10.1021/jo034376h>.
- (92) Matake, R.; Adachi, Y.; Matsubara, H. Synthesis of Vinyl Ethers of Alcohols Using Calcium Carbide under Superbasic Catalytic Conditions (KOH/DMSO). *Green Chem.* **2016**, *18* (9), 2614–2618. <https://doi.org/10.1039/c5gc02977e>.
- (93) Nasanit, R.; Davies, M. C.; Soliman, M.; Watson, S. A.; Grabowska, A. M.; Preece, J. A.; Allen, S.; Abulateefeh, S. R.; Alexander, C.; Briggs, S. S.; Seymour, L. W. Multicomponent Synthetic Polymers with Viral-Mimetic Chemistry for Nucleic Acid Delivery. *Mol. Pharm.* **2011**, *9* (1), 1–13. <https://doi.org/10.1021/mp200108q>.

- (94) Cordes, E. H.; Bull, H. G. Mechanism and Catalysis for Hydrolysis of Acetals, Ketals, and Ortho Esters. *Chem. Rev.* **1974**, *74* (5), 581–603. <https://doi.org/10.1021/cr60291a004>.
- (95) Fife, T. H. General Acid Catalysis of Acetal, Ketal, and Ortho Ester Hydrolysis. *Acc. Chem. Res.* **1972**, *5* (8), 264–272. <https://doi.org/10.1021/ar50056a002>.
- (96) Liu, B.; Thayumanavan, S. Substituent Effects on the PH Sensitivity of Acetals and Ketals and Their Correlation with Encapsulation Stability in Polymeric Nanogels. *J. Am. Chem. Soc.* **2017**, *139* (6), 2306–2317. <https://doi.org/10.1021/jacs.6b11181>.
- (97) Bulmus, V.; Chan, Y.; Nguyen, Q.; Tran, H. L. Synthesis and Characterization of Degradable p(HEMA) Microgels: Use of Acid-Labile Crosslinkers. *Macromol. Biosci.* **2007**, *7* (4), 446–455. <https://doi.org/10.1002/mabi.200600258>.
- (98) Gillies, E. R.; Goodwin, A. P.; Fréchet, J. M. J. Acetals as PH-Sensitive Linkages for Drug Delivery. *Bioconjug. Chem.* **2004**, *15* (6), 1254–1263. <https://doi.org/10.1021/bc049853x>.
- (99) Wang, B.; Ma, S.; Li, Q.; Zhang, H.; Liu, J.; Wang, R.; Chen, Z.; Xu, X.; Wang, S.; Lu, N.; Liu, Y.; Yan, S.; Zhu, J. Facile Synthesis of “Digestible”, Rigid-and-Flexible, Bio-Based Building Block for High-Performance Degradable Thermosetting Plastics. *Green Chem.* **2020**, *22* (4), 1275–1290. <https://doi.org/10.1039/c9gc04020j>.
- (100) Zhang, G.; Tian, C.; Feng, H.; Tan, T.; Wang, R.; Zhang, L. Thermal Reprocessing and Closed-Loop Chemical Recycling of Styrene-Butadiene Rubber Enabled by Exchangeable and Cleavable Acetal Linkages. *Macromol. Rapid Commun.* **2022**, *43* (15), 1–9. <https://doi.org/10.1002/marc.202100887>.
- (101) Li, Q.; Ma, S.; Wang, S.; Yuan, W.; Xu, X.; Wang, B.; Huang, K.; Zhu, J. Facile Catalyst-Free Synthesis, Exchanging, and Hydrolysis of an Acetal Motif for Dynamic Covalent Networks. *J. Mater. Chem. A* **2019**, *7* (30), 18039–18049.

<https://doi.org/10.1039/c9ta04073k>.

- (102) Anastas, P. T.; Warner, J. C. *Green Chemistry: Theory and Practice*; Oxford University Press, 1998.
- (103) Anastas, P. T.; Williamson, T. C.; American Chemical Society. Division of Environmental Chemistry.; American Chemical Society. Meeting (208th: 1994: Washington, D. C. . *Green Chemistry : Designing Chemistry for the Environment*. **1996**, 251.
- (104) Anastas, P.; Eghbali, N. *Green Chemistry: Principles and Practice*. *Chem. Soc. Rev.* **2010**, 39 (1), 301–312. <https://doi.org/10.1039/b918763b>.
- (105) Winterton, N. Twelve More Green Chemistry Principles. *Green Chem.* **2001**, 3 (6), 73–81. <https://doi.org/10.1039/b110187k>.
- (106) Dicks, A. P.; Hent, A. *Green Chemistry and Associated Metrics*. In *Green Chemistry Metrics: A Guide to Determining and Evaluating Process Greenness*; Springer, 2015; pp 1–15. https://doi.org/10.1007/978-3-319-10500-0_1.
- (107) Anastas, P. T.; Zimmerman, J. B. Design through the 12 Principles of Green Engineering. *IEEE Engineering Management Review*. American Chemical Society March 1, 2007, p 16. <https://doi.org/10.1109/EMR.2007.4296421>.
- (108) Sheldon, R. A. Metrics of Green Chemistry and Sustainability: Past, Present, and Future. *ACS Sustain. Chem. Eng.* **2018**, 6 (1), 32–48. https://doi.org/10.1021/ACSSUSCHEMENG.7B03505/ASSET/IMAGES/MEDIUM/SC-2017-03505Y_0008.GIF.
- (109) Trost, B. M. The Atom Economy—A Search for Synthetic Efficiency. *Science*. **1991**, 254 (5037), 1471–1477. <https://doi.org/10.1126/SCIENCE.1962206>.
- (110) Dicks, A. P.; Hent, A. Atom Economy and Reaction Mass Efficiency. In *Green Chemistry*

- Metrics: A Guide to Determining and Evaluating Process Greenness*; Springer, 2015; pp 17–44. https://doi.org/10.1007/978-3-319-10500-0_2.
- (111) Dicks, A. P.; Hent, A. The E Factor and Process Mass Intensity. In *Green Chemistry Metrics: A Guide to Determining and Evaluating Process Greenness*; Springer, 2015; pp 45–67. https://doi.org/10.1007/978-3-319-10500-0_3.
- (112) Sheldon, R. A. The: E Factor 25 Years on: The Rise of Green Chemistry and Sustainability. *Green Chem.* **2017**, *19* (1), 18–43. <https://doi.org/10.1039/c6gc02157c>.
- (113) Diesendruck, C. E.; Steinberg, B. D.; Sugai, N.; Silberstein, M. N.; Sottos, N. R.; White, S. R.; Braun, P. V.; Moore, J. S. Proton-Coupled Mechanochemical Transduction: A Mechanogenerated Acid. *J. Am. Chem. Soc.* **2012**, *134* (30), 12446–12449. <https://doi.org/10.1021/ja305645x>.
- (114) Nagamani, C.; Liu, H.; Moore, J. S. Mechanogeneration of Acid from Oxime Sulfonates. *J. Am. Chem. Soc.* **2016**, *138* (8), 2540–2543. <https://doi.org/10.1021/jacs.6b00097>.
- (115) Lin, Y.; Kouznetsova, T. B.; Craig, S. L. A Latent Mechanoacid for Time-Stamped Mechanochromism and Chemical Signaling in Polymeric Materials. *J. Am. Chem. Soc.* **2019**, *142*, 99–103. <https://doi.org/10.1021/jacs.9b12861>.
- (116) Shirai, M.; Tsunooka, M. Photoacid and Photobase Generators: Chemistry and Applications to Polymeric Materials. *Prog. Polym. Sci.* **1996**, *21* (1), 1–45. [https://doi.org/10.1016/0079-6700\(95\)00014-3](https://doi.org/10.1016/0079-6700(95)00014-3).
- (117) Zivic, N.; Kuroishi, P. K.; Dumur, F.; Gigmès, D.; Dove, A. P.; Sardon, H. Recent Advances and Challenges in the Design of Organic Photoacid and Photobase Generators for Polymerizations. *Angew. Chemie Int. Ed.* **2019**, *58* (31), 10410–10422. <https://doi.org/10.1002/anie.201810118>.
- (118) Shirai, M. Reworkable UV Curing Materials. *Prog. Org. Coatings* **2007**, *58* (2–3), 158–165. <https://doi.org/10.1016/j.porgcoat.2006.08.022>.

- (119) Reisinger, D.; Kaiser, S.; Rossegger, E.; Alabiso, W.; Rieger, B.; Schlögl, S. Introduction of Photolabile Bases for Locally Controlling Dynamic Exchange Reactions in Thermo-Activated Vitrimers. *Angew. Chemie - Int. Ed.* **2021**, *60* (26), 14302–14306. <https://doi.org/10.1002/anie.202102946>.
- (120) Reisinger, D.; Dietliker, K.; Sangermano, M.; Schlögl, S. Streamlined Concept towards Spatially Resolved Photoactivation of Dynamic Transesterification in Vitrimeric Polymers by Applying Thermally Stable Photolabile Bases. *Polym. Chem.* **2022**, *13* (9), 1169–1176. <https://doi.org/10.1039/d1py01722e>.
- (121) Rossegger, E.; Moazzen, K.; Fleisch, M.; Schlögl, S. Locally Controlling Dynamic Exchange Reactions in 3D Printed Thiol-Acrylate Vitrimers Using Dual-Wavelength Digital Light Processing. *Polym. Chem.* **2021**, *12* (21), 3077–3083. <https://doi.org/10.1039/d1py00427a>.
- (122) Sudo, A.; Yamashita, H.; Endo, T. Ring-Opening Polymerization of 1,3-Benzoxazines by p-Toluenesulfonates as Thermally Latent Initiators. *J. Polym. Sci. Part A Polym. Chem.* **2011**, *49*, 3631–3636. <https://doi.org/10.1002/pola>.
- (123) Lee, S.-D.; Takata, T.; Endo, T. Arenesulfonates as Non-Salt-Type Latent Thermal Initiators for Cationic Polymerization. *Macromolecules* **1996**, *29*, 3317–3319. <https://doi.org/10.1021/ja01348a044>.
- (124) Martin, C. J.; Rapenne, G.; Nakashima, T.; Kawai, T. Recent Progress in Development of Photoacid Generators. *J. Photochem. Photobiol. C Photochem. Rev.* **2018**, *34*, 41–51. <https://doi.org/10.1016/j.jphotochemrev.2018.01.003>.
- (125) Tsuchimura, T. Recent Progress in Photo-Acid Generators for Advanced Photopolymer Materials. *J. Photopolym. Sci. Technol.* **2020**, *33* (1), 15–26. <https://doi.org/10.2494/photopolymer.33.15>.
- (126) Neenan, T. X.; Houlihan, F. M.; Reichmanis, E.; Kometani, J. M.; Bachman, B. J.;

- Thompson, L. F. Photo- and Thermochemistry of Select 2,6-Dinitrobenzyl Esters in Polymer Matrices: Studies Pertaining to Chemical Amplification and Imaging. *Macromolecules* **1990**, *23* (1), 145–150. <https://doi.org/10.1021/ma00203a025>.
- (127) Houlihan, F. M.; Shugard, A.; Gooden, R.; Reichmanis, E. Nitrobenzyl Ester Chemistry for Polymer Processes Involving Chemical Amplification. *Macromolecules* **1988**, *21* (7), 2001–2006. <https://doi.org/10.1021/ma00185a019>.
- (128) Reichmanis, E.; Smith, B. C.; Gooden, R. O-Nitrobenzyl Photochemistry: Solution vs. Solid-State Behavior. *J. Polym. Sci. Polym. Chem. Ed.* **1985**, *23* (1), 1–8. <https://doi.org/10.1002/POL.1985.170230101>.
- (129) Barclay, G. G.; Medeiros, D. R.; Sinta, R. F. Thermal Stability of Sulfonate Ester Photoacid Generators in Phenolic Matrices. *Chem. Mater.* **1995**, *7* (7), 1315–1324. <https://doi.org/10.1021/cm00055a007>.
- (130) Bottorff, E. M. US 3,745,188, 1973.
- (131) Corey, E. J.; Posner, G. H.; Atkinson, R. F.; Wingard, A. K.; Halloran, D. J.; Radzik, D. M.; Nash, J. J. Formation of Olefins via Pyrolysis of Sulfonate Esters. *J. Org. Chem.* **1989**, *54* (2), 389–393. <https://doi.org/10.1021/jo00263a024>.
- (132) Matsumura, S.; Hlil, A. R.; Lepiller, C.; Gaudet, J.; Guay, D.; Shi, Z.; Holdcroft, S.; Hay, A. S. Stability and Utility of Pyridyl Disulfide Functionality in RAFT and Conventional Radical Polymerizations. *J. Polym. Sci. Part A Polym. Chem.* **2008**, *46* (April), 7207–7224. <https://doi.org/10.1002/pola>.
- (133) Hofman, A. H.; Pedone, M.; Kamperman, M. Protected Poly(3-Sulfopropyl Methacrylate) Copolymers: Synthesis, Stability, and Orthogonal Deprotection. *ACS Polym. Au* **2022**, *2* (3), 169–180. <https://doi.org/10.1021/acspolymersau.1c00044>.
- (134) Shirai, M. Photocrosslinkable Polymers with Degradable Properties. *Polym. J.* **2014**, *46* (12), 859–865. <https://doi.org/10.1038/pj.2014.79>.

- (135) Okamura, H.; Terakawa, T.; Shirai, M. Photo- and Thermal Curing of Tri-Functional Methacrylate with Degradable Property. *Res. Chem. Intermed.* **2009**, *35* (8–9), 865–878. <https://doi.org/10.1007/s11164-009-0070-4>.
- (136) Shirai, M.; Mitsukura, K.; Okamura, H. Chain Propagation in UV Curing of Di(Meth)Acrylates. *Chem. Mater.* **2008**, *20* (5), 1971–1976. <https://doi.org/10.1021/cm702965e>.
- (137) Okamura, H.; Yamauchi, E.; Shirai, M. Photo-Cross-Linking and de-Cross-Linking of Modified Polystyrenes Having Degradable Linkages. *React. Funct. Polym.* **2011**, *71* (4), 480–488. <https://doi.org/10.1016/j.reactfunctpolym.2011.01.008>.
- (138) Masamitsu Shirai, Kazuyuki Mitsukura, Haruyuki Okamura, M. M. Multi-Functional Methacrylates Bearing Thermal Degradation Properties - Synthesis, Photo- and Thermal Curing, and Thermolysis. *J. Photopolym. Sci. Technol.* **2005**, *18* (2), 199–202.
- (139) Flory, P. J. The Mechanism of Vinyl Polymerizations. *J. Am. Chem. Soc.* **1937**, *59* (2), 241–253. <https://doi.org/10.1021/ja01281a007>.
- (140) Srinivasan, S.; Lee, M. W.; Grady, M. C.; Soroush, M.; Rappe, A. M. Self-Initiation Mechanism in Spontaneous Thermal Polymerization of Ethyl and n-Butyl Acrylate: A Theoretical Study. *J. Phys. Chem. A* **2010**, *114* (30), 7975–7983. <https://doi.org/10.1021/jp102772v>.
- (141) Srinivasan, S.; Lee, M. W.; Grady, M. C.; Soroush, M.; Rappe, A. M. Computational Evidence for Self-Initiation in Spontaneous High-Temperature Polymerization of Methyl Methacrylate. *J. Phys. Chem. A* **2011**, *115* (6), 1125–1132. <https://doi.org/10.1021/jp107704h>.
- (142) Wang, B.; Ma, S.; Yan, S.; Zhu, J. Readily Recyclable Carbon Fiber Reinforced Composites Based on Degradable Thermosets: A Review. *Green Chem.* **2019**, *21* (21), 5781–5796. <https://doi.org/10.1039/c9gc01760g>.

- (143) Binauld, S.; Stenzel, M. H. Acid-Degradable Polymers for Drug Delivery: A Decade of Innovation. *Chem. Commun.* **2013**, 49 (21), 2082–2102. <https://doi.org/10.1039/c2cc36589h>.
- (144) Shahi, S.; Roghani-Mamaqani, H.; Talebi, S.; Mardani, H. Chemical Stimuli-Induced Reversible Bond Cleavage in Covalently Crosslinked Hydrogels. *Coord. Chem. Rev.* **2022**, 455, 214368. <https://doi.org/10.1016/j.ccr.2021.214368>.
- (145) Chan, Y.; Bulmus, V.; Zareie, M. H.; Byrne, F. L.; Barner, L.; Kavallaris, M. Acid-Cleavable Polymeric Core-Shell Particles for Delivery of Hydrophobic Drugs. *J. Controlled Release* **2006**, 115 (2), 197–207. <https://doi.org/10.1016/j.jconrel.2006.07.025>.
- (146) Burek, M.; Waśkiewicz, S.; Lalik, A.; Wandzik, I. Hydrogels with Novel Hydrolytically Labile Trehalose-Based Crosslinks: Small Changes-Big Differences in Degradation Behavior. *Polym. Chem.* **2018**, 9 (27), 3721–3726. <https://doi.org/10.1039/c8py00488a>.
- (147) Bulmus, V.; Chan, Y.; Nguyen, Q.; Tran, H. L. Synthesis and Characterization of Degradable p(HEMA) Microgels: Use of Acid-Labile Crosslinkers. *Macromol. Biosci.* **2007**, 7 (4), 446–455. <https://doi.org/10.1002/mabi.200600258>.
- (148) Themistou, E.; Patrickios, C. S. Synthesis and Characterization of Polymer Networks and Star Polymers Containing a Novel, Hydrolyzable Acetal-Based Dimethacrylate Cross-Linker. *Macromolecules* **2006**, 39 (1), 73–80. <https://doi.org/10.1021/ma0513416>.
- (149) Heath, W. H.; Palmieri, F.; Adams, J. R.; Long, B. K.; Chute, J.; Holcombe, T. W.; Zieren, S.; Truitt, M. J.; White, J. L.; Willson, C. G. Degradable Cross-Linkers and Strippable Imaging Materials for Step-and-Flash Imprint Lithography. *Macromolecules* **2008**, 41 (3), 719–726. <https://doi.org/10.1021/ma702291k>.
- (150) Kim, S.; Linker, O.; Garth, K.; Carter, K. R. Degradation Kinetics of Acid-Sensitive Hydrogels. *Polym. Degrad. Stab.* **2015**, 121, 303–310.

<https://doi.org/10.1016/j.polymdegradstab.2015.09.014>.

- (151) Shirai, M.; Mitsukura, K.; Okamura, H.; Masahiro, M.; Masamitsu Shirai, Kazuyuki Mitsukura, Haruyuki Okamura, M. M. Multi-Functional Methacrylates Bearing Thermal Degradation Properties - Synthesis, Photo- and Thermal Curing, and Thermolysis. *J. Photopolym. Sci. Technol.* **2005**, *18* (2), 199–202.
- (152) Ma, S.; Wei, J.; Jia, Z.; Yu, T.; Yuan, W.; Li, Q.; Wang, S.; You, S.; Liu, R.; Zhu, J. Readily Recyclable, High-Performance Thermosetting Materials Based on a Lignin-Derived Spiro Diacetal Trigger. *J. Mater. Chem. A* **2019**, *7* (3), 1233–1243. <https://doi.org/10.1039/c8ta07140c>.
- (153) Clayden, J.; Greeves, N.; Warren, S. Equilibria, Rates and Mechanisms. In *Organic Chemistry*, 2012; pp 240–268.
- (154) Clayden, J.; Greeves, N.; Warren, S. Acidity, Basicity, and PKa. In *Organic Chemistry*; Oxford University Press, 2012; pp 163–181.
- (155) Bordwell, F. G. Equilibrium Acidities in Dimethyl Sulfoxide. *Acc. Chem. Res.* **1988**, *21*, 456–463. <https://doi.org/10.1021/ja00725a071>.
- (156) Brown, H. C. *Determination of Organic Structures by Physical Methods*; Braude, E. A., Nachod, F. C., Eds.; Academic Press, 1955; Vol. 11. https://doi.org/10.1524/zpch.1957.11.3_4.275.
- (157) Siggel, M. R. F.; Streitwieser, A.; Thomas, T. D. The Role of Resonance and Inductive Effects in the Acidity of Carboxylic Acids. *J. Am. Chem. Soc.* **1988**, *110* (24), 8022–8028. https://doi.org/10.1021/JA00232A011/ASSET/JA00232A011.FP.PNG_V03.
- (158) THF MSDS <https://www.sigmaaldrich.com/GB/en/sds/sial/401757> (accessed Mar 30, 2022).
- (159) Fulmer, G. R.; Miller, A. J. M.; Sherden, N. H.; Gottlieb, H. E.; Nudelman, A.; Stoltz, B.

- M.; Bercaw, J. E.; Goldberg, K. I. NMR Chemical Shifts of Trace Impurities: Common Laboratory Solvents, Organics, and Gases in Deuterated Solvents Relevant to the Organometallic Chemist. *Organometallics* **2010**, *29* (9), 2176–2179. <https://doi.org/10.1021/om100106e>.
- (160) Fife, T. H. Vinyl Ether Hydrolysis. The Facile General Acid Catalyzed Conversion of 2-Ethoxy-1-Cyclopentene-1-Carboxylic Acid to Cyclopentanone. *J. Am. Chem. Soc.* **1965**, *87* (5), 1084–1089. <https://doi.org/10.1021/ja01083a026>.
- (161) Tomlinson, R.; Klee, M.; Garrett, S.; Heller, J.; Duncan, R.; Brocchini, S. Pendent Chain Functionalized Polyacetals That Display PH-Dependent Degradation: A Platform for the Development of Novel Polymer Therapeutics. *Macromolecules* **2002**, *35* (2), 473–480. <https://doi.org/10.1021/ma0108867>.
- (162) Kresege, A. J.; Chiang, Y. The Hydrolysis of Ethyl Vinyl Ether. Part 1. Reaction Mechanism. *J. Phys. Org. Chem.* **1967**, 53–57.
- (163) Bell, R. P. The Reversible Hydration of Carbonyl Compounds. *Adv. Phys. Org. Chem.* **1966**, *4* (C), 1–29. [https://doi.org/10.1016/S0065-3160\(08\)60351-2](https://doi.org/10.1016/S0065-3160(08)60351-2).
- (164) Cowie, J. M. G.; Arrighi, V. Step-Growth Polymerization. In *Polymers: Chemistry & Physics of Modern Materials*; CRC Press LLC, 2007; pp 29–56.
- (165) Anderson, N. G. Vessels and Mixing. In *Practical process research & development*; Academic Press, 2000; pp 269–288.
- (166) Byrne, F. P.; Jin, S.; Paggiola, G.; Petchey, T. H. M.; Clark, J. H.; Farmer, T. J.; Hunt, A. J.; Robert McElroy, C.; Sherwood, J. Tools and Techniques for Solvent Selection: Green Solvent Selection Guides. *Sustain. Chem. Process.* **2016**, *4* (1), 1–24. <https://doi.org/10.1186/s40508-016-0051-z>.
- (167) Prat, D.; Pardigon, O.; Flemming, H. W.; Letestu, S.; Ducandas, V.; Isnard, P.; Guntrum, E.; Senac, T.; Ruisseau, S.; Cruciani, P.; Hosek, P. Sanofi's Solvent Selection Guide:

- A Step Toward More Sustainable Processes. *Org. Process Res. Dev.* **2013**, *17* (12), 1517–1525. <https://doi.org/10.1021/op4002565>.
- (168) Capello, C.; Fischer, U.; Hungerbühler, K. What Is a Green Solvent? A Comprehensive Framework for the Environmental Assessment of Solvents. *Green Chem.* **2007**, *9* (9), 927–934. <https://doi.org/10.1039/b617536h>.
- (169) Welton, T. Solvents and Sustainable Chemistry. *Proc. R. Soc. A Math. Phys. Eng. Sci.* **2015**, *471* (2183), 1–26. <https://doi.org/10.1098/rspa.2015.0502>.
- (170) Jagtap, A. R.; More, A. Developments in Reactive Diluents: A Review. *Polymer Bulletin*. Springer June 30, 2022, pp 5667–5708. <https://doi.org/10.1007/s00289-021-03808-5>.
- (171) Watson, T. J.; Heights, Y.; Buchwalter, S. L.; Kosbar, L. L. Cleavable Epoxy Resins: Design for Disassembly of a Thermoset. *J. Polym. Sci. Part A Polym. Chem.* **1996**, *34* (2), 249–260. [https://doi.org/10.1002/\(SICI\)1099-0518\(19960130\)34:2<249::AID-POLA11>3.0.CO;2-Q](https://doi.org/10.1002/(SICI)1099-0518(19960130)34:2<249::AID-POLA11>3.0.CO;2-Q).
- (172) Heath, W. H.; Palmieri, F.; Adams, J. R.; Long, B. K.; Chute, J.; Holcombe, T. W.; Zieren, S.; Truitt, M. J.; White, J. L.; Willson, C. G. Degradable Cross-Linkers and Strippable Imaging Materials for Step-and-Flash Imprint Lithography. *Macromolecules* **2008**, *41* (3), 719–726. <https://doi.org/10.1021/ma702291k>.
- (173) Hashimoto, T.; Meiji, H.; Urushisaki, M.; Sakaguchi, T.; Kawabe, K.; Tsuchida, C.; Kondo, K. Degradable and Chemically Recyclable Epoxy Resins Containing Acetal Linkages: Synthesis, Properties, and Application for Carbon Fiber-Reinforced Plastics. *J. Polym. Sci. Part A Polym. Chem.* **2012**, *50* (17), 3674–3681. <https://doi.org/10.1002/pola.26160>.
- (174) Yuan, W.; Ma, S.; Wang, S.; Li, Q.; Wang, B.; Xu, X.; Huang, K.; Chen, J.; You, S.; Zhu, J. Synthesis of Fully Bio-Based Diepoxy Monomer with Dicyclo Diacetal for High-Performance, Readily Degradable Thermosets. *Eur. Polym. J.* **2019**, *117*, 200–207.

<https://doi.org/10.1016/j.eurpolymj.2019.05.028>.

- (175) Brockmann, W.; Geiß, P. L.; Klingen, J.; Schröder, B. Chemistry and Properties of Adhesives and Primers. In *Adhesive Bonding*; Wiley-VCH, 2009; pp 39–100.
- (176) Campbell, D.; White, J. R. Thermal Analysis. In *Polymer Characterization Physical techniques*; Chapman and Hall, 1989; pp 301–326. <https://doi.org/10.1021/a1000003j>.
- (177) Young, R. J.; Lovell, P. A. The Crystalline State. In *Introduction to Polymers*; CRC Press, 2011; Vol. Chapter 17, pp 399–447.
- (178) Wisanrakkit, G.; Gillham, J. K.; Enns, J. B. The Glass Transition Temperature (T_g) as a Parameter for Monitoring the Cure of an Amine/Epoxy System at Constant Heating Rates. *J. Appl. Polym. Sci.* **1990**, *41* (7–8), 1895–1912. <https://doi.org/10.1002/APP.1990.070410743>.
- (179) Hale, A.; Macosko, C. W.; Bair, H. E. Glass Transition Temperature as a Function of Conversion in Thermosetting Polymers. *Macromolecules* **1991**, *24* (9), 2610–2621. <https://doi.org/10.1021/ma00009a072>.
- (180) STS-51L and STS-107 - Challenger and Columbia: A Legacy Honored - NASA Space Flight.com <https://www.nasaspaceflight.com/2010/02/sts-51l-sts-107-challenger-columbia-legacy-honored/> (accessed Jul 5, 2022).
- (181) Katsikas, L.; Avramović, M.; Cortés, R. D. B.; Milovanović, M.; Kalagasidis-Krušić, M. T.; Popović, I. G. The Thermal Stability of Poly(Methyl Methacrylate) Prepared by RAFT Polymerisation. *J. Serbian Chem. Soc.* **2008**, *73* (8–9), 915–921. <https://doi.org/10.2298/JSC0809915K>.
- (182) Bekanova, M. Z.; Neumolotov, N. K.; Jablanović, A. D.; Plutalova, A. V.; Chernikova, E. V.; Kudryavtsev, Y. V. Thermal Stability of RAFT-Based Poly(Methyl Methacrylate): A Kinetic Study of the Dithiobenzoate and Trithiocarbonate End-Group Effect. *Polym. Degrad. Stab.* **2019**, *164*, 18–27.

<https://doi.org/10.1016/j.polymdegradstab.2019.03.017>.

- (183) Hu, Y. H.; Chen, C. Y. The Effect of End Groups on the Thermal Degradation of Poly(Methyl Methacrylate). *Polym. Degrad. Stab.* **2003**, *82* (1), 81–88.
[https://doi.org/10.1016/S0141-3910\(03\)00165-4](https://doi.org/10.1016/S0141-3910(03)00165-4).
- (184) Manring, L. E. Thermal Degradation of Saturated Poly(Methyl Methacrylate). *Macromolecules* **1988**, *21* (2), 528–530.
https://doi.org/10.1021/MA00180A046/ASSET/MA00180A046.FP.PNG_V03.
- (185) Manring, L. E. Thermal Degradation of Poly(Methyl Methacrylate). 2. Vinyl-Terminated Polymer. *Macromolecules* **1989**, *22* (6), 2673–2677.
https://doi.org/10.1021/MA00196A024/ASSET/MA00196A024.FP.PNG_V03.
- (186) Manring, L. E.; Sogah, D. Y.; Cohen, G. M. Thermal Degradation of Poly(Methyl Methacrylate). 3. Polymer with Head-to-Head Linkages. *Macromolecules* **1989**, *22* (12), 4652–4654.
https://doi.org/10.1021/MA00202A048/ASSET/MA00202A048.FP.PNG_V03.
- (187) Manring, L. E. Thermal Degradation of Poly(Methyl Methacrylate). 4. Random Side-Group Scission. *Macromolecules* **1991**, *24* (11), 3304–3309.
https://doi.org/10.1021/MA00011A040/ASSET/MA00011A040.FP.PNG_V03.
- (188) Levchik, G. F.; Si, K.; Levchik, S. V.; Camino, G.; Wilkie, C. A. The Correlation between Cross-Linking and Thermal Stability: Cross-Linked Polystyrenes and Polymethacrylates. *Polym. Degrad. Stab.* **1999**, *65* (3), 395–403.
[https://doi.org/10.1016/S0141-3910\(99\)00028-2](https://doi.org/10.1016/S0141-3910(99)00028-2).
- (189) Cowie, J. M. G. Structure-Property Relations. In *Polymers: Chemistry & Physics of Modern Materials*; CRC Press LLC, 2007; pp 263–291.
- (190) Ali, U.; Karim, K. J. B. A.; Buang, N. A. A Review of the Properties and Applications of Poly (Methyl Methacrylate) (PMMA). *Polym. Rev.* **2015**, *55* (4), 678–705.

<https://doi.org/10.1080/15583724.2015.1031377>.

- (191) Young, R. J.; Lovell, P. A. Radical Polymerization. In *Introduction to Polymers*; Third, Ed.; CRC Press, 2011; pp 82–143. <https://doi.org/10.1201/9781439894156-6>.
- (192) Moad, G.; Solomon, D. H. Termination. In *The Chemistry of Radical Polymerisation*; 2005; pp 233–278.
- (193) Klán, P.; Šolomek, T.; Bochet, C. G.; Blanc, A.; Givens, R.; Rubina, M.; Popik, V.; Kostikov, A.; Wirz, J.; Klač, P.; Bochet, C. G.; Givens, R.; Rubina, M.; Popik, V.; Kostikov, A.; Wirz, J. Photoremovable Protecting Groups in Chemistry and Biology: Reaction Mechanisms and Efficacy. *Chem. Rev.* **2013**, *113* (1), 119–191. <https://doi.org/10.1021/cr300177k>.
- (194) Corey, E. J.; Posner, G. H.; Atkinson, R. F.; Wingard, A. K.; Halloran, D. J.; Radzik, D. M.; Nash, J. J. Formation of Olefins via Pyrolysis of Sulfonate Esters. *J. Org. Chem.* **1989**, *54* (2), 389–393. <https://doi.org/10.1021/jo00263a024>.
- (195) Smith, M. B.; March, J. March's Advanced Organic Chemistry. *March's Adv. Org. Chem.* **2006**. <https://doi.org/10.1002/0470084960>.
- (196) Chuchani, G.; Pekerar, S.; Domínguez, R. M.; Rotinov, A.; Martín, I. Kinetics and Mechanism of Elimination of Primary Alkyl Methanesulfonates in the Gas Phase. Correlation of Alkyl Substituents. *J. Phys. Chem.* **1989**, *93* (1), 201–202. <https://doi.org/10.1021/j100338a042>.
- (197) Chuchani, G.; Domínguez, R. M.; Rotinov, A.; Martín, I.; Alvarez G., J. Neighboring Phenyl Participation in Gas-Phase Pyrolysis Kinetics of ω -Phenylalkyl Methanesulfonates. *J. Phys. Chem.* **1990**, *94* (8), 3341–3343. <https://doi.org/10.1021/j100371a027>.
- (198) Chuchani, G.; Martín, I.; Domínguez, R. M. The Gas-Phase Elimination Kinetics of 3-Buten-1-Methanesulphonate and 3-Methyl-3-Buten-1-Methanesulphonate. *Int. J.*

- Chem. Kinet.* **1995**, *27*, 657–661.
- (199) Chuchani, G.; Dominguez, R. M. Anchimeric Assistance of the CO₂CH₃ Substituent in the Elimination Kinetics of 3-(Methoxycarbonyl)Propyl Methanesulfonate in the Gas Phase. *J. Chem. Soc. Perkin Trans. 2* **1993**, *50* (7), 1295–1298. <https://doi.org/10.1039/p29930001295>.
- (200) Alvarez G., J.; Chuchani, G. Electronic Factors in the Elimination Kinetics of 2-halosubstituted Methanesulphonates in the Gas Phase. *J. Phys. Org. Chem.* **1990**, *3* (7), 456–458. <https://doi.org/10.1002/poc.610030707>.
- (201) Chuchani, G.; Alvarez G, J.; Martín, I. Correlation of Alkyl and Polar Substituents in the Elimination Kinetics of 2-substituted Ethyl Methanesulphonates in the Gas Phase. *J. Phys. Org. Chem.* **1991**, *4* (7), 399–403. <https://doi.org/10.1002/poc.610040702>.
- (202) Martin, I.; Chuchani, G.; Dominguez, R.; Rotinov, A. Participation and Rearrangement in the Gas-Phase Elimination Kinetics of 3-(o-Methoxyphenyl)Propyl-1-Methanesulphonate and 4-(p-Methoxyphenyl)Butyl-1-Methanesulphonate. *J. Phys. Org. Chem.* **1992**, *5* (11), 725–730. <https://doi.org/10.1002/poc.610051103>.
- (203) Kaufmann, D.; de Meijere, A.; Luk, K.; Overton, K.; Stothers, J. B. Mechanism of the “Abnormal” Pyrolytic 1,3-Elimination of 2-Adamantyl Methane Sulphonate. *Tetrahedron* **1982**, *38* (7), 977–989. [https://doi.org/10.1016/0040-4020\(82\)85076-X](https://doi.org/10.1016/0040-4020(82)85076-X).
- (204) Chuchani, G.; Martín, I.; José, A.; Hernández, A.; Rotinov, A.; Fraile, G.; Bigley, D. B. Effects of Polar β Substituents in the Gas-Phase Pyrolysis of Ethyl Acetate Esters. *J. Phys. Chem.* **1980**, *84* (9), 944–948. <https://doi.org/10.1021/j100446a002>.
- (205) Shin, Y. D.; Kawaue, A.; Okamura, H.; Shirai, M. Thermally Crosslinkable-Decrosslinkable System Using Diepoxy Crosslinkers Containing Sulfonate Ester Moiety. *React. Funct. Polym.* **2004**, *61* (2), 293–302. <https://doi.org/10.1016/j.reactfunctpolym.2004.06.008>.

- (206) Kolomanska, J.; Johnston, P.; Gregori, A.; Fraga Domínguez, I.; Egelhaaf, H. J.; Perrier, S.; Rivaton, A.; Dagron-Lartigau, C.; Topham, P. D. Design, Synthesis and Thermal Behaviour of a Series of Well-Defined Clickable and Triggerable Sulfonate Polymers. *RSC Adv.* **2015**, *5* (82), 66554–66562. <https://doi.org/10.1039/c5ra13867a>.
- (207) Cameron, J. F.; Fréchet, J. M. J. Cationic Curing of Polymer Coatings: Evaluation of *o*-Nitrobenzyl Tosylate as a Thermally Labile Acid Precursor. *Polym. Bull.* **1991**, *26* (3), 297–303. <https://doi.org/10.1007/BF00587973>.
- (208) Ding, R.; He, Y.; Wang, X.; Xu, J.; Chen, Y.; Feng, M.; Qi, C. Treatment of Alcohols with Tosyl Chloride Does Not Always Lead to the Formation of Tosylates. *Molecules* **2011**, *16* (7), 5665–5673. <https://doi.org/10.3390/molecules16075665>.
- (209) Barber, D. M.; Crosby, A. J.; Emrick, T. Mesoscale Block Copolymers. *Adv. Mater.* **2018**, *30* (13), 2–7. <https://doi.org/10.1002/adma.201706118>.
- (210) Malval, J. P.; Suzuki, S.; Morlet-Savary, F.; Allonas, X.; Fouassier, J. P.; Takahara, S.; Yamaoka, T. Photochemistry of Naphthalimide Photoacid Generators. *J. Phys. Chem. A* **2008**, *112* (17), 3879–3885. <https://doi.org/10.1021/jp0771926>.
- (211) Hurd, C. D.; Blunck, F. H. The Pyrolysis of Esters. *J. Am. Chem. Soc.* **1938**, *60* (10), 2419–2425. <https://doi.org/10.1021/ja01277a035>.
- (212) Rudy, C. E.; Fugassi, P. The Thermal Decomposition of Tertiary Butyl Acetate. *J. Phys. Colloid Chem.* **1948**, *52* (2), 357–363. <https://doi.org/10.1021/j150458a008>.
- (213) Amin, H. B.; Taylor, R. The Nature of the Transition State in Ester Pyrolysis. Part III. The Hammett Correlation for Pyrolysis of *t*-Butyl Benzoates. *J. Chem. Soc. Perkin Trans. 2* **1975**, No. 15, 1802. <https://doi.org/10.1039/p29750001802>.
- (214) Houlihan, F. M.; Neenan, T. X.; Reichmanis, E.; Kometani, J. M.; Thompson, L. F.; Chin, T.; Nalamasu, O. Chemically Amplified Resists: The Chemistry and Lithographic Characteristics of Nitrobenzyl Benzenesulfonate Derivatives. *J. Photopolym. Sci.*

- Technol.* **2008**, 3 (3), 259–273. <https://doi.org/10.2494/photopolymer.3.259>.
- (215) Achilias, D. S.; Sideridou, I. D. Kinetics of the Benzoyl Peroxide/Amine Initiated Free-Radical Polymerization of Dental Dimethacrylate Monomers: Experimental Studies and Mathematical Modeling for TEGDMA and Bis-EMA. *Macromolecules* **2004**, 37 (11), 4254–4265. <https://doi.org/10.1021/ma049803n>.
- (216) Sideridou, I. D.; Achilias, D. S.; Kostidou, N. C. Copolymerization Kinetics of Dental Dimethacrylate Resins Initiated by a Benzoyl Peroxide/Amine Redox System. *J. Appl. Polym. Sci.* **2008**, 109, 515–524. <https://doi.org/10.1002/app>.
- (217) Gill, G. B.; Williams, G. H. Aryl Peroxides. Part IV. The Decomposition of Benzoyl Peroxide in Nitrobenzene. The Effect of Added Nitrobenzene on the Decomposition of Benzoyl Peroxide in Benzene. *J. Chem. Soc. B Phys. Org.* **1966**, 880–885. <https://doi.org/10.1039/J29660000880>.
- (218) Hahladakis, J. N.; Velis, C. A.; Weber, R.; Iacovidou, E.; Purnell, P. An Overview of Chemical Additives Present in Plastics: Migration, Release, Fate and Environmental Impact during Their Use, Disposal and Recycling. *J. Hazard. Mater.* **2018**, 344, 179–199. <https://doi.org/10.1016/j.jhazmat.2017.10.014>.
- (219) Mcculla, R. D.; Cabbage, J. W.; Jenks, W. S. Pyrolytic Elimination Reactions of Sulfinates and Sulfonate Esters. *J. Phys. Org. Chem.* **2002**, 15, 71–77. <https://doi.org/10.1002/poc.464>.
- (220) Nash, J. J.; Leininger, M. A.; Keyes, K. Pyrolysis of Aryl Sulfonate Esters in the Absence of Solvent: E1 or E2? A Puzzle for the Organic Laboratory. *J. Chem. Educ.* **2008**, 85 (4), 552–554. <https://doi.org/10.1021/ed085p552>.
- (221) Atalla, A. A. Molecular Rearrangements of Sulfur Compounds Thermolysis and Photolysis of Ketoxime Arenesulfonates. *Phosphorus. Sulfur. Silicon Relat. Elem.* **1994**, 90 (1–4), 205–211. <https://doi.org/10.1080/10426509408016403>.

- (222) Tipson, R. S. On Esters of P-Toluenesulfonic Acid. *J. Org. Chem.* **1944**, 9 (3), 235–241. <https://doi.org/10.1021/jo01185a005>.
- (223) Kabalka, G. W.; Varma, M.; Varma, R. S.; Srivastava, P. C.; Knapp, F. F. Tosylation of Alcohols. *J. Org. Chem.* **1986**, 51 (12), 2386–2388. <https://doi.org/10.1021/jo00362a044>.
- (224) Yoshida, Y.; Sakakura, Y.; Aso, N.; Okada, S.; Tanabe, Y. Practical and Efficient Methods for Sulfonylation of Alcohols Using Ts(Ms)Cl / Et₃N and Catalytic Me₃N.HCl as Combined Base: Promising Alternative to Traditional Pyridine. *Tetrahedron* **1999**, 55 (8), 2183–2192.
- (225) Morita, J. I.; Nakatsuji, H.; Misaki, T.; Tanabe, Y. Water-Solvent Method for Tosylation and Mesylation of Primary Alcohols Promoted by KOH and Catalytic Amines. *Green Chem.* **2005**, 7 (10), 711–715. <https://doi.org/10.1039/b505345e>.
- (226) Kazemi, F.; Massah, A. R.; Javaherian, M. Chemoselective and Scalable Preparation of Alkyl Tosylates under Solvent-Free Conditions. *Tetrahedron* **2007**, 63 (23), 5083–5087. <https://doi.org/10.1016/j.tet.2007.03.083>.
- (227) Li, X.; Jiang, Y.; Shuai, L.; Wang, L.; Meng, L.; Mu, X. Sulfonated Copolymers with SO₃H and COOH Groups for the Hydrolysis of Polysaccharides. *J. Mater. Chem.* **2012**, 22 (4), 1283–1289. <https://doi.org/10.1039/c1jm12954f>.
- (228) Baek, K. Y.; Kim, H. J.; Lee, S. H.; Cho, K. Y.; Kim, H. T.; Hwang, S. S. Morphology Control of Highly Sulfonated Block Copolymers by a Simple Thermal Process. *Macromol. Chem. Phys.* **2010**, 211 (6), 613–617. <https://doi.org/10.1002/macp.200900475>.
- (229) Cohen, S. G.; Haas, H. C.; Slotnick, H. Studies on Hydroxyethylpolyvinyl Alcohol. *J. Polym. Sci.* **1953**, 11 (3), 193–201. <https://doi.org/10.1002/POL.1953.120110301>.
- (230) Mahindaratne, M. P. D.; Wimalasena, K. Detailed Characterization of P-Toluenesulfonic

- Acid Monohydrate as a Convenient, Recoverable, Safe, and Selective Catalyst for Alkylation of the Aromatic Nucleus. *J. Org. Chem.* **1998**, 63 (9), 2858–2866. <https://doi.org/10.1021/jo971832r>.
- (231) Gill, P. S.; Sauerbrunn, S. R.; Crowe, B. S. High Resolution Thermogravimetry. *J. Therm. Anal.* **1992**, 38 (3), 255–266. <https://doi.org/10.1007/BF01915490>.
- (232) Flynn, J. H.; Wall, L. A. General Treatment of the Thermogravimetry of Polymers. *J. Res. Natl. Bur. Stand. - A. Phys. Chem.* **1966**, 70A (6), 487–523. <https://doi.org/10.1080/00048407212341221>.
- (233) Sauerbrunn, S.; Gill, P. *Decomposition Kinetics Using TGA*; TA Instruments, 1992.
- (234) Atkins, P. W., de Paula J., K. J. Physical Chemistry, 11th Ed. *Oxford Univ. Press. Oxford* **2017**, 944.
- (235) Kingsbury, C. A. Transition States in Ei Reactions. *J. Phys. Org. Chem.* **2010**, 23 (6), 513–518. <https://doi.org/10.1002/poc.1632>.
- (236) Fukuda, W.; Nakao, M.; Okumura, K.; Kakiuchi, H. Polymerizations of Vinyl Methacrylate and Vinyl Acrylate. *J Polym Sci Part A-1 Polym Chem* **1972**, 10 (1), 237–250. <https://doi.org/10.1002/pol.1972.150100121>.
- (237) Clayden, J.; Greeves, N.; Warren, S. Determining Organic Structures. In *Organic Chemistry*, Oxford, 2001; pp 43–80.
- (238) Allan, R. J. P.; Forman, R. L.; Ritchie, P. D. Studies in Pyrolysis. Part IV. Model Systems for the Pyrolysis of Poly(Ethylene Terephthalate) and Allied Polyesters. *J. Chem. Soc.* **1955**, 2717–2725. <https://doi.org/10.1039/jr9550002717>.
- (239) Maccoll, A. Olefin-Forming Eliminations in the Gas Phase. In *The Chemistry of the Alkenes*; Patai, S., Ed.; John Wiley & Sons, Ltd, 2010; Vol. 1, pp 203–240. <https://doi.org/10.1002/9780470771044.ch3>.

- (240) Furniss, B. S.; Hannaford, A. J.; Smith, P. W. G.; Tatchell, A. R. Physical Constants of Organic Compounds. In *Vogel's Textbook of Practical Organic Chemistry*; Longman Scientific & Technical, 1989; pp 1298–1398.
- (241) Patai, S.; Rappoport, Z. *The Chemistry of Sulphonic Acids, Esters and Their Derivatives*; 2006. <https://doi.org/10.1002/0470034394>.
- (242) DePuy, C. H.; King, R. W. Pyrolytic Cis Eliminations. *Chem. Rev.* **1960**, *60* (5), 431–457. <https://doi.org/10.1021/cr60207a001>.
- (243) Allan, R. J. P.; Jones, E.; Ritchie, P. D. 104. Studies in Pyrolysis. Part VIII. Competitive Routes in the Pyrolysis of Esters: Alkylene and Alkylidene Dibenzoates and Some Related Substances. *J. Chem. Soc.* **1957**, 524–531. <https://doi.org/10.1039/jr9570000524>.
- (244) Bengough, W. I.; Ritchie, P. D.; Steedman, W. Studies in Pyrolysis. Part XXI.1 Reaction Mechanisms in the Vapour-Phase Pyrolysis of Vinyl Benzoate. *J. Chem. Soc.* **1963**, 2784–2787. <https://doi.org/10.1039/jr9630002697>.
- (245) Taylor, R. Pyrolysis of Acids and Their Derivatives. *Suppl. B Chem. Acid Deriv. Part 2* **2010**, *2*, 859–914. <https://doi.org/10.1002/9780470771594.ch4>.
- (246) Kornblum, N.; Jones, W. J.; Anderson, G. J. A New and Selective Method of Oxidation. the Conversion of Alkyl Halides and Alkyl Tosylates to Aldehydes. *Journal of the American Chemical Society*. 1959, pp 4113–4114. <https://doi.org/10.1021/ja01524a080>.
- (247) Nace, H. R. The Preparation of Olefins from Arylsulfonate Esters of Alcohols. *J. Am. Chem. Soc.* **1959**, *81* (20), 5428–5430. <https://doi.org/10.1021/ja01529a044>.
- (248) Nace, H. R.; Monagle, J. J.; Nace, H. R. Reactions of Sulfoxides with Organic Halides. Preparation of Aldehydes and Ketones. *J. Org. Chem.* **1959**, *24* (11), 1792–1793. <https://doi.org/10.1021/jo01093a608>.

- (249) Sweat, F. W.; Epstein, W. W. Dimethyl Sulfoxide Oxidations. *J. Org. Chem.* **1967**, *32* (3), 835–838. <https://doi.org/10.1021/jo01278a081>.
- (250) Clayden, J.; Greeves, N.; Warren, S. Diastereoselectivity. In *Organic Chemistry*; Oxford University Press, 2012; pp 852–876.
- (251) Clayden, J.; Greeves, N.; Warren, S. Conformational Analysis. In *Organic Chemistry*; Oxford University Press, 2012; pp 360–381.
- (252) Kawai, W. Polymerizations of Some Diene Monomers. Preparations and Polymerizations of Vinyl Methacrylate, Allyl Methacrylate, N-Allylacrylamide, and N-Allylmethacrylamide. *J. Polym. Sci. Part A-1 Polym. Chem.* **1966**, *4* (5), 1191–1201. <https://doi.org/10.1002/pol.1966.150040518>.
- (253) Baek, K.-Y. Synthesis and Characterization of Sulfonated Block Copolymers by Atom Transfer Radical Polymerization. *J. Polym. Sci. Part A Polym. Chem.* **2008**, *46* (18), 5991–5998. <https://doi.org/10.1002/pola.22568>.
- (254) Okamura, H.; Takatori, Y.; Tsunooka, M.; Shirai, M. Synthesis of Random and Block Copolymers of Styrene and Styrenesulfonic Acid with Low Polydispersity Using Nitroxide-Mediated Living Radical Polymerization Technique. *Polymer (Guildf)*. **2002**, *43* (11), 3155–3162. [https://doi.org/10.1016/S0032-3861\(02\)00162-3](https://doi.org/10.1016/S0032-3861(02)00162-3).
- (255) Yu, S.; Wu, S.; Zhang, C.; Tang, Z.; Luo, Y.; Guo, B.; Zhang, L. Catalyst-Free Metathesis of Cyclic Acetals and Spirocyclic Acetal Covalent Adaptable Networks. *ACS Macro Lett.* **2020**, *9* (8), 1143–1148. <https://doi.org/10.1021/acsmacrolett.0c00527>.
- (256) Good, R. J. Contact Angle, Wetting, and Adhesion: A Critical Review. *J. Adhes. Sci. Technol.* **1992**, *6* (12), 1269–1302. <https://doi.org/10.1163/156856192X00629>.
- (257) Eliades, G. C.; Caputo, A. A.; Vougiouklakis, G. J. Composition, Wetting Properties and Bond Strength with Dentin of 6 New Dentin Adhesives. *Dent. Mater.* **1985**, *1* (5), 170–176. [https://doi.org/10.1016/S0109-5641\(85\)80012-9](https://doi.org/10.1016/S0109-5641(85)80012-9).

- (258) Guerre, M.; Taplan, C.; Winne, J. M.; Du Prez, F. E. Vitrimers: Directing Chemical Reactivity to Control Material Properties. *Chem. Sci.* **2020**, *11* (19), 4855–4870. <https://doi.org/10.1039/d0sc01069c>.
- (259) Rahman, M. A.; Bowland, C.; Ge, S.; Acharya, S. R.; Kim, S.; Cooper, V. R.; Chelsea Chen, X.; Irle, S.; Sokolov, A. P.; Savara, A.; Saito, T. Design of Tough Adhesive from Commodity Thermoplastics through Dynamic Crosslinking. *Sci. Adv.* **2021**, *7* (42), 1–12. <https://doi.org/10.1126/sciadv.abk2451>.
- (260) Pemba, A. G.; Flores, J. A.; Miller, S. A. Acetal Metathesis Polymerization (AMP): A Method for Synthesizing Biorenewable Polyacetals. *Green Chem.* **2013**, *15* (2), 325–329. <https://doi.org/10.1039/c2gc36588j>.
- (261) Danielsen, S. P. O. O.; Beech, H. K.; Wang, S.; El-Zaatari, B. M.; Wang, X.; Sapir, L.; Ouchi, T.; Wang, Z.; Johnson, P. N.; Hu, Y.; Lundberg, D. J.; Stoychev, G.; Craig, S. L.; Johnson, J. A.; Kalow, J. A.; Olsen, B. D.; Rubinstein, M.; Ouchi, T.; Hu, Y.; Sapir, L.; El-Zaatari, B. M.; Wang, X.; Lundberg, D. J.; Beech, H. K.; Lin, T.; Olsen, B. D.; Jeremiah, A.; Kalow, J. A.; Craig, S. L.; Rubinstein, M. Characterization of Polymer Networks. *Chem. Rev.* **2020**, *121* (8), 5042–5092. <https://doi.org/10.1021/acs.chemrev.0c01304>.
- (262) Yang, Y.; Zhang, S.; Zhang, X.; Gao, L.; Wei, Y.; Ji, Y. Detecting Topology Freezing Transition Temperature of Vitrimers by AIE Luminogens. *Nat. Commun.* **2019**, *10* (1), 1–8. <https://doi.org/10.1038/s41467-019-11144-6>.
- (263) Spiesschaert, Y.; Taplan, C.; Stricker, L.; Guerre, M.; Winne, J. M.; Du Prez, F. E. Influence of the Polymer Matrix on the Viscoelastic Behaviour of Vitrimers. *Polym. Chem.* **2020**, *11* (33), 5377–5385. <https://doi.org/10.1039/d0py00114g>.
- (264) Rajput, B. S.; Gaikwad, S. R.; Menon, S. K.; Chikkali, S. H. Sustainable Polyacetals from Isohexides. *Green Chem.* **2014**, *16* (8), 3810–3818.

<https://doi.org/10.1039/c4gc00543k>.

(265) Hill, J. W.; Carothers, W. H. Cyclic and Polymeric Formals. *J. Am. Chem. Soc.* **1935**, *57* (5), 925–928. <https://doi.org/10.1021/ja01308a045>.

(266) Moreno, A.; Lligadas, G.; Ronda, J. C.; Galià, M.; Cádiz, V. Linear and Branched Acetal Polymers from Castor Oil via Acetal Metathesis Polymerization. *Eur. Polym. J.* **2018**, *108*, 348–356. <https://doi.org/10.1016/j.eurpolymj.2018.09.013>.

(267) Russel, W. J. US4212701, 1980.

Appendices

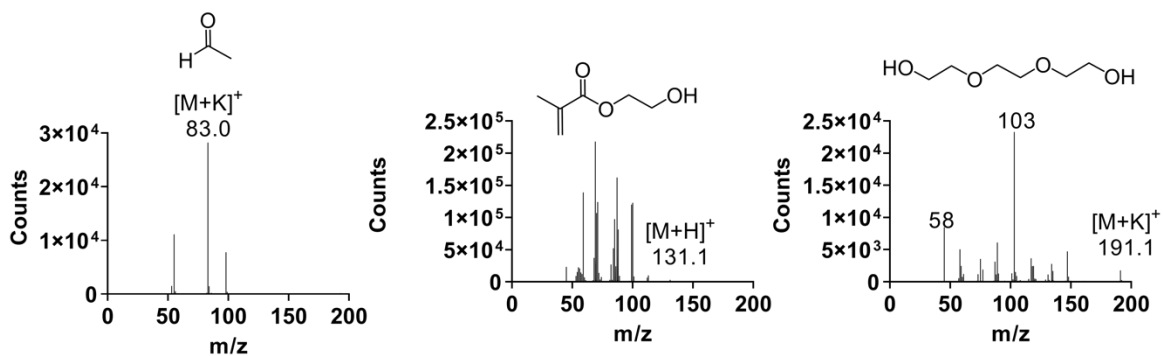
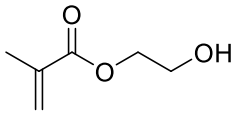
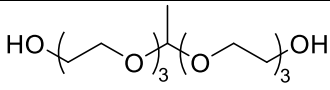
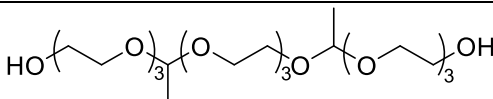
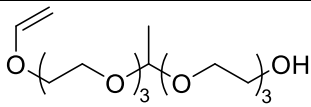
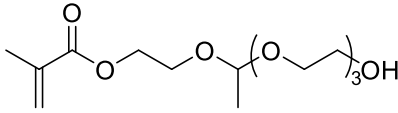
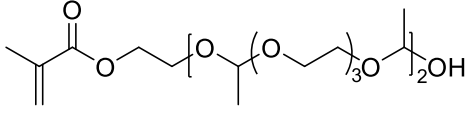
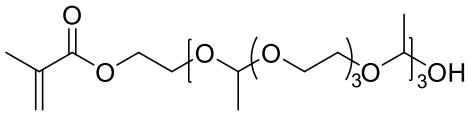
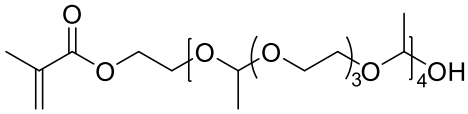
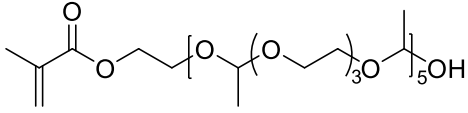
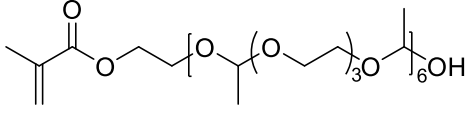
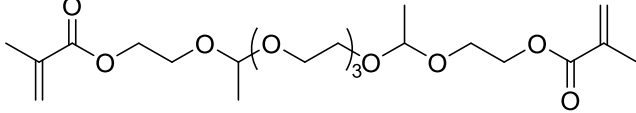


Figure 8-1 - Mass spectra of A1 hydrolysis products separated *via* liquid chromatography.

Table 8-1 - Reaction products determined *via* HPLC-MS when synthesising A1 with 0.5 mol % pTsOH.

Molecule	Retention time (min)	m/z / Experimental (theoretical)
	4.2	[M+Na] ⁺ 153.1 ([M+Na] ⁺ 153.8)
	4.8	[M+Na] ⁺ 349.2 ([M+Na] ⁺ 153.8)
	5.5	[M+Na] ⁺ 525.3 ([M+Na] ⁺ 153.8)
	5.8	[M+Na] ⁺ 375.2 ([M+Na] ⁺ 153.8)
	6.2	[M+Na] ⁺ 329.2 ([M+Na] ⁺ 153.8)
	6.8	[M+Na] ⁺ 505.3 ([M+Na] ⁺ 153.8)

	7.1	[M+Na] ⁺ 681.4 ([M+Na] ⁺ 153.8)
	7.4	[M+Na] ⁺ 857.5 ([M+Na] ⁺ 153.8)
	7.6	[M+Na] ⁺ 1033.6 ([M+Na] ⁺ 153.8)
	7.8	[M+Na] ⁺ 1209.7 ([M+Na] ⁺ 153.8)
	8.9	[M+Na] ⁺ 485.3 ([M+Na] ⁺ 153.8)
Mixture of dimethacrylate cross-linkers	10.2	

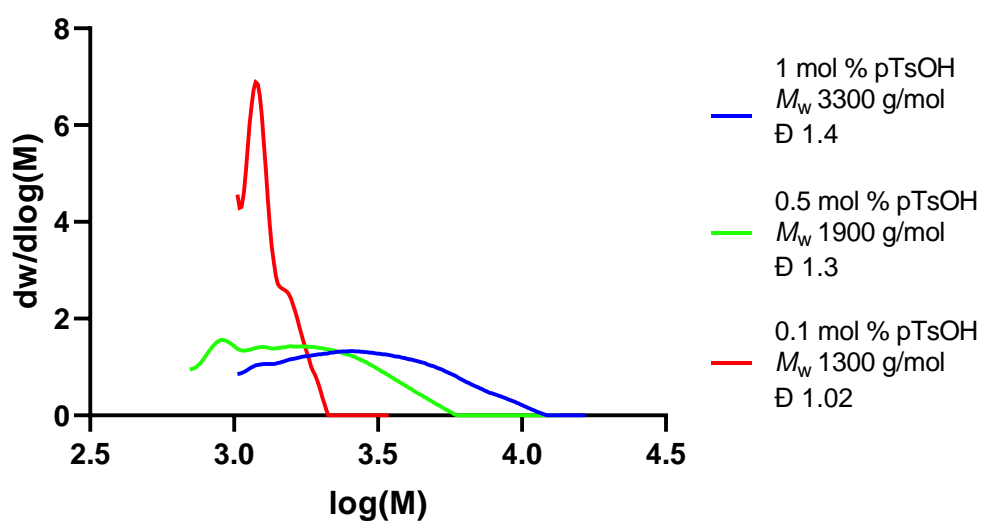


Figure 8-2 - Molar mass distributions for poly(acetal) products synthesised from TEGDVE at different pTsOH loadings.

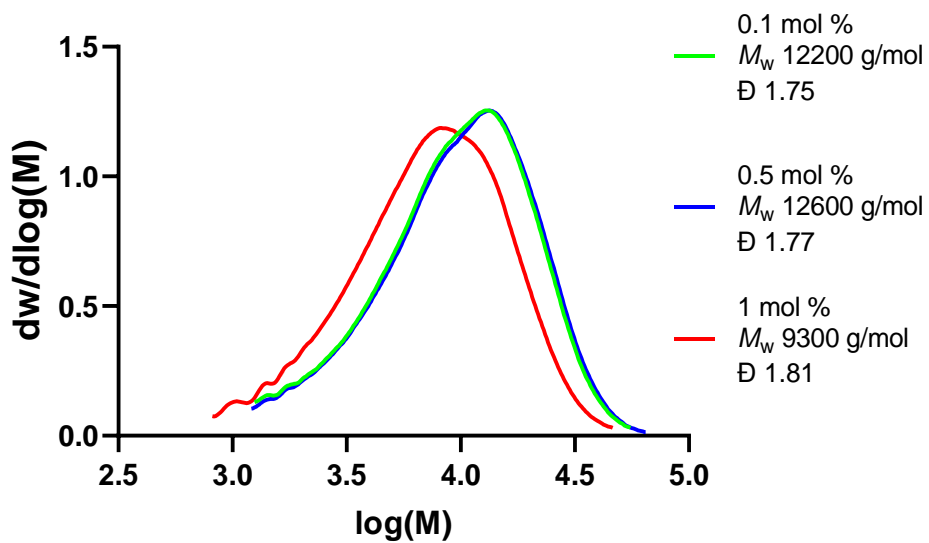


Figure 8-3 - Molar mass distributions for poly(acetal) products synthesised from TEGDVE and TEG at different pTsOH loadings.

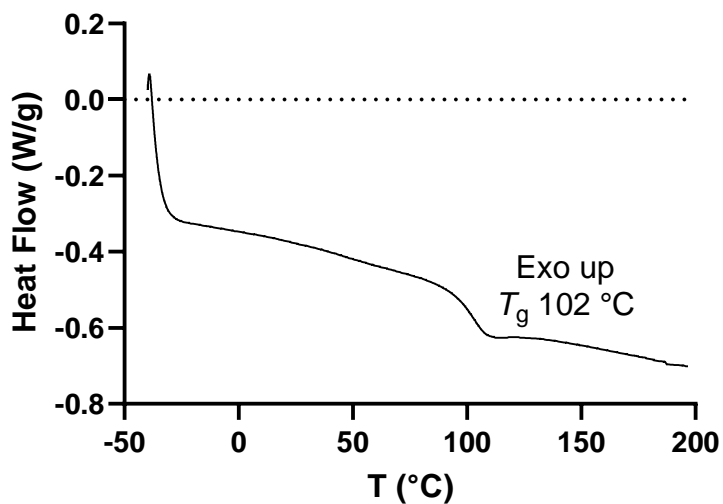


Figure 8-4 - DSC of p(MMA-co-A1) cured at 100 °C for 48 hours.

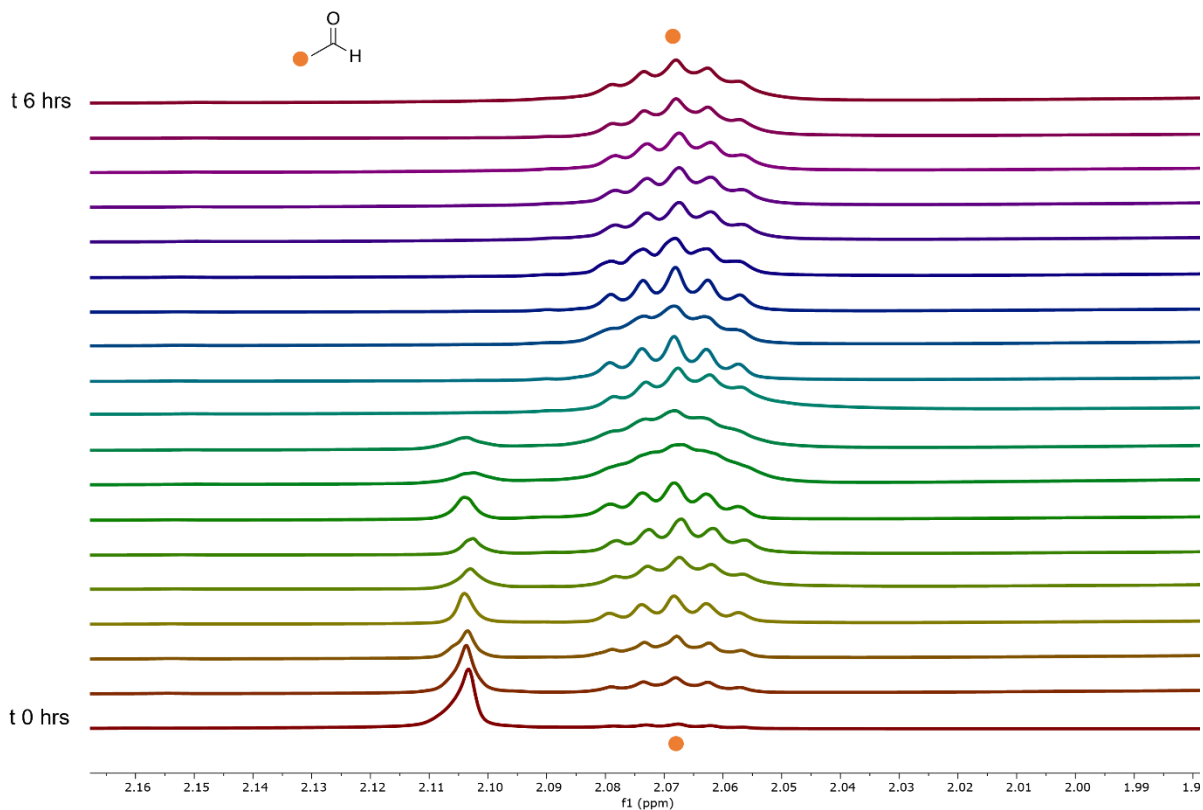


Figure 8-5 - ^1H NMR spectra (acetone- d_6 / D_2O) of p(MMA-co-A1) degradation supernatant.

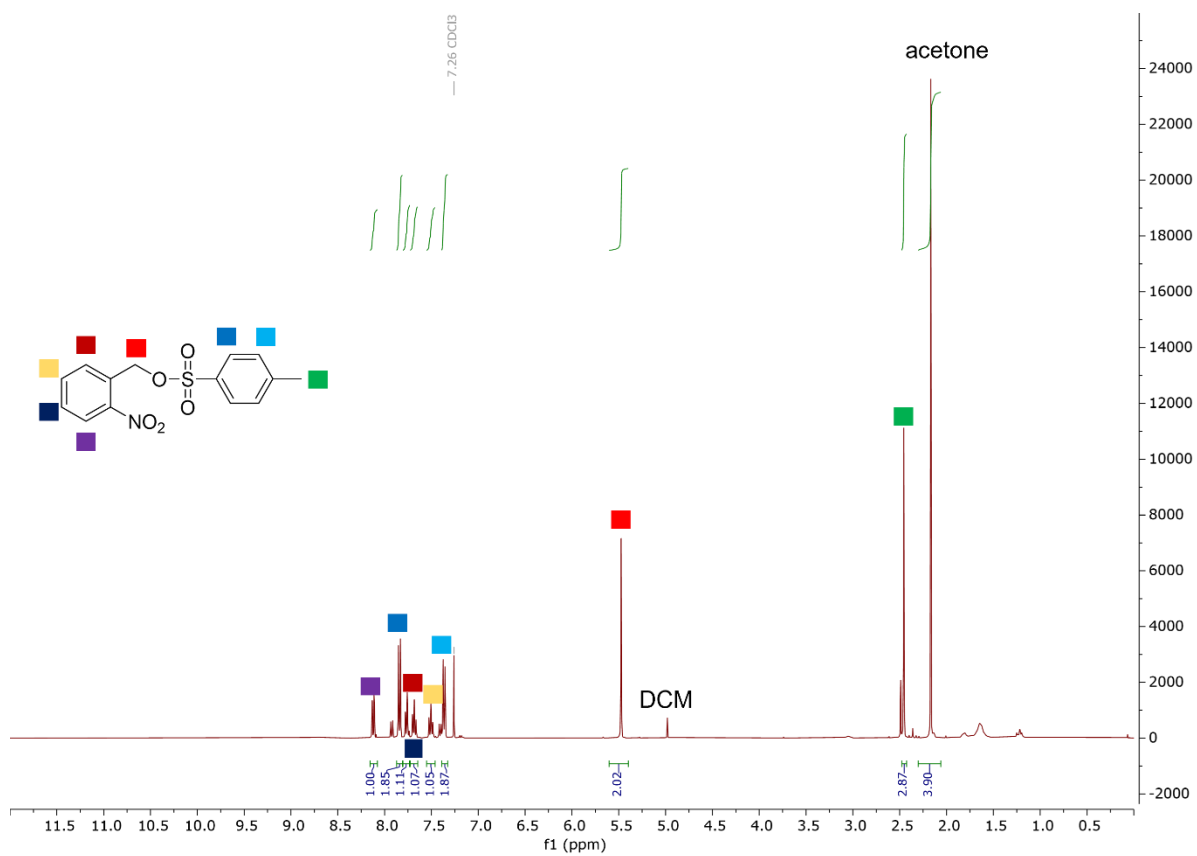


Figure 8-6 - ^1H NMR (CDCl_3) spectrum of *ortho*-nitrobenzyl tosylate.

Magnus_2019_09_10
hydroxy
PROTON.s DMSO {C:\NMRData\Spain_current_year\} chp18jh 3

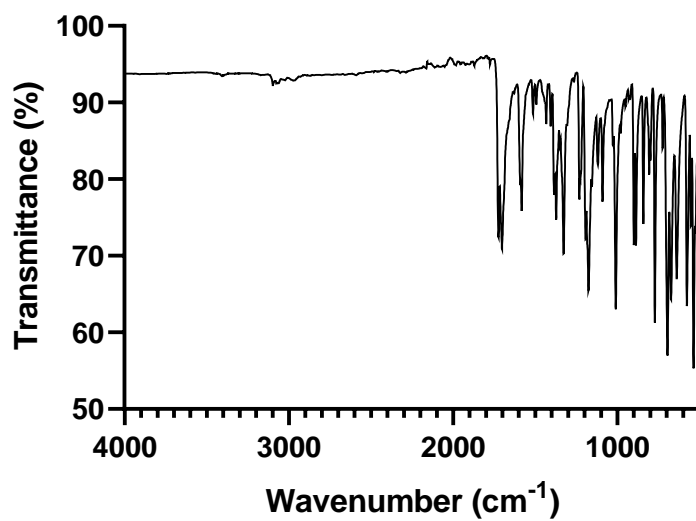
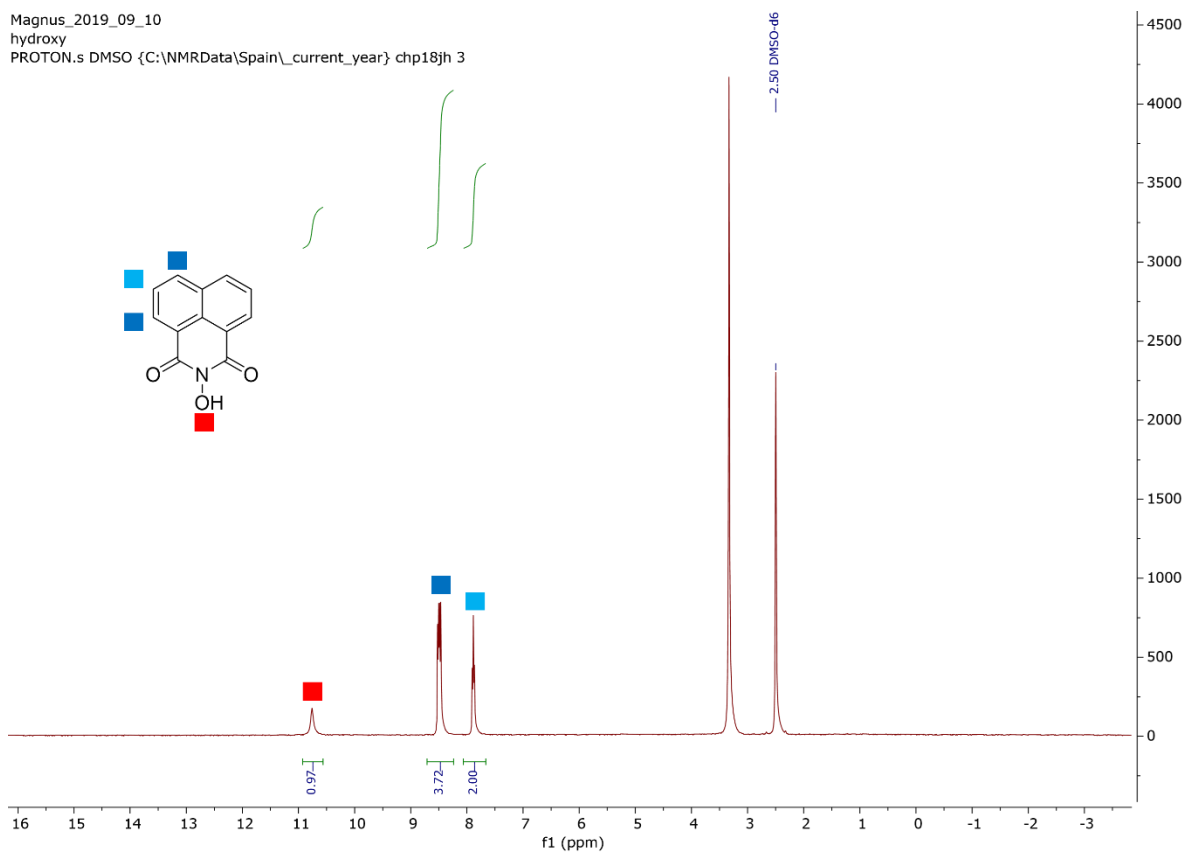


Figure 8-8 - IR spectrum of N-hydroxy-1,8-naphthalimide.

Magnus_2019_09_12
JH1-140
PROTON.s DMSO {C:\NMRData\Spain_current_year\} chp18jh 1

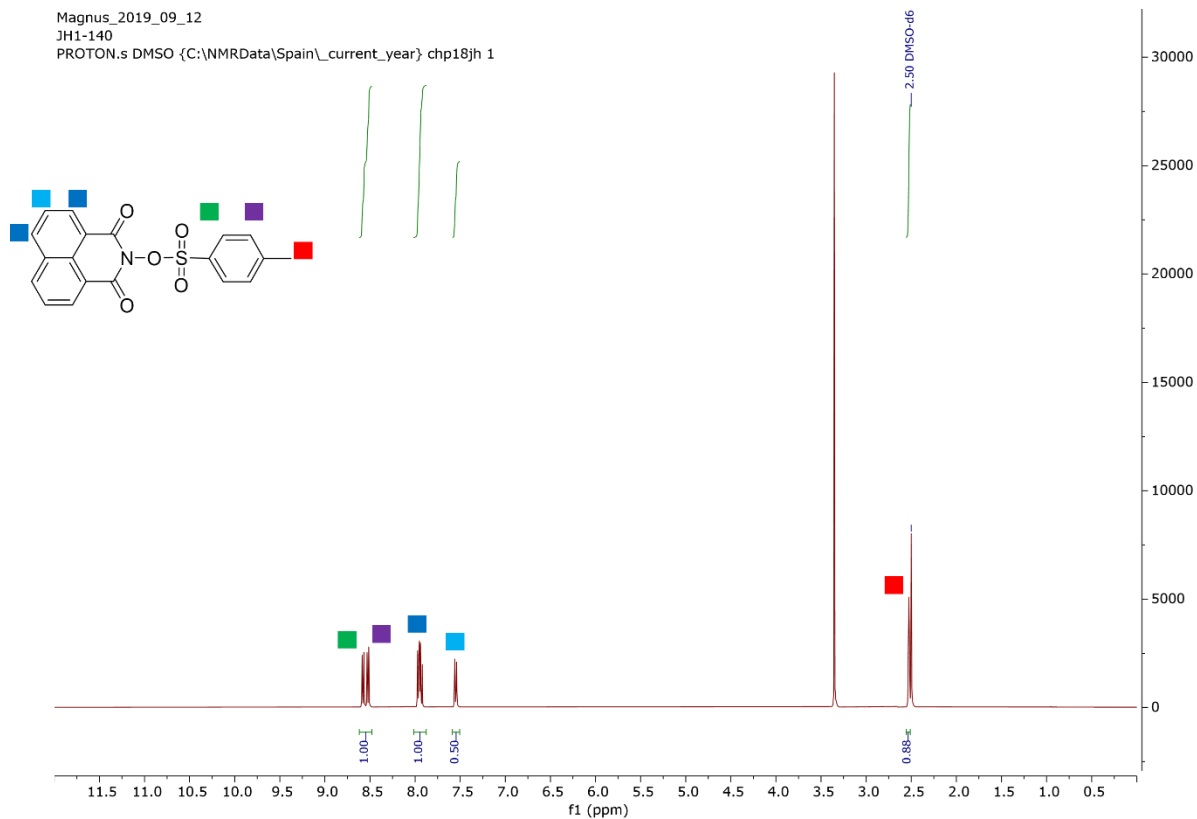


Figure 8-9 - ^1H NMR (CDCl_3) spectrum of NHTN.

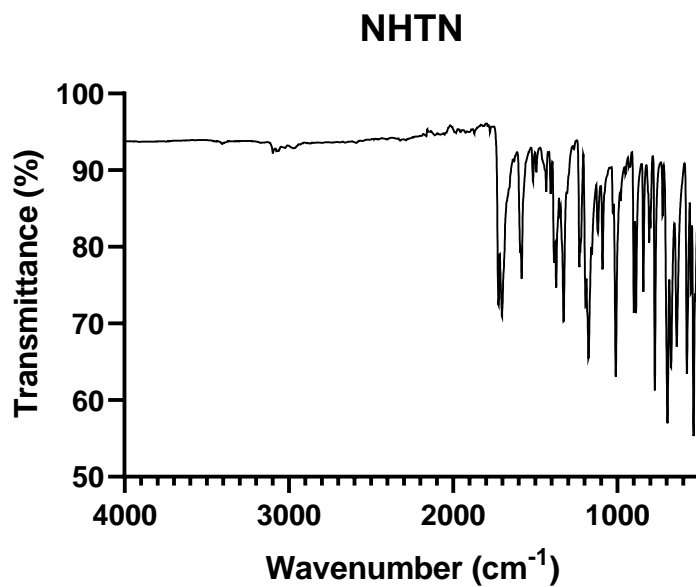
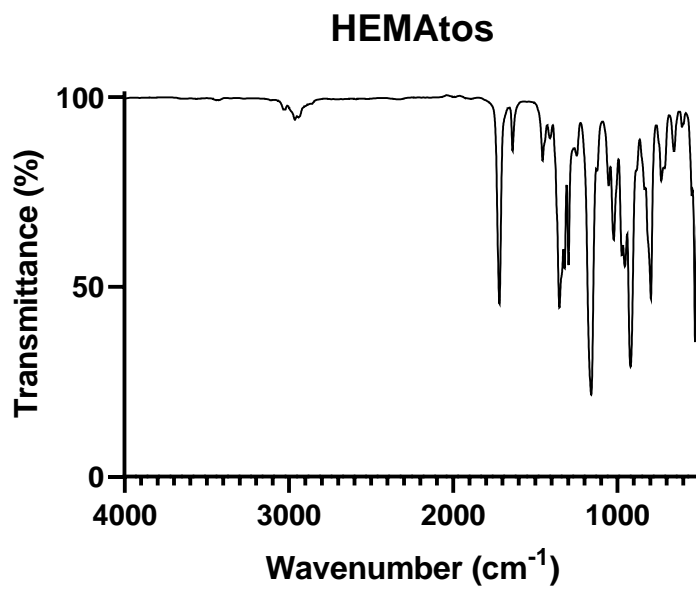
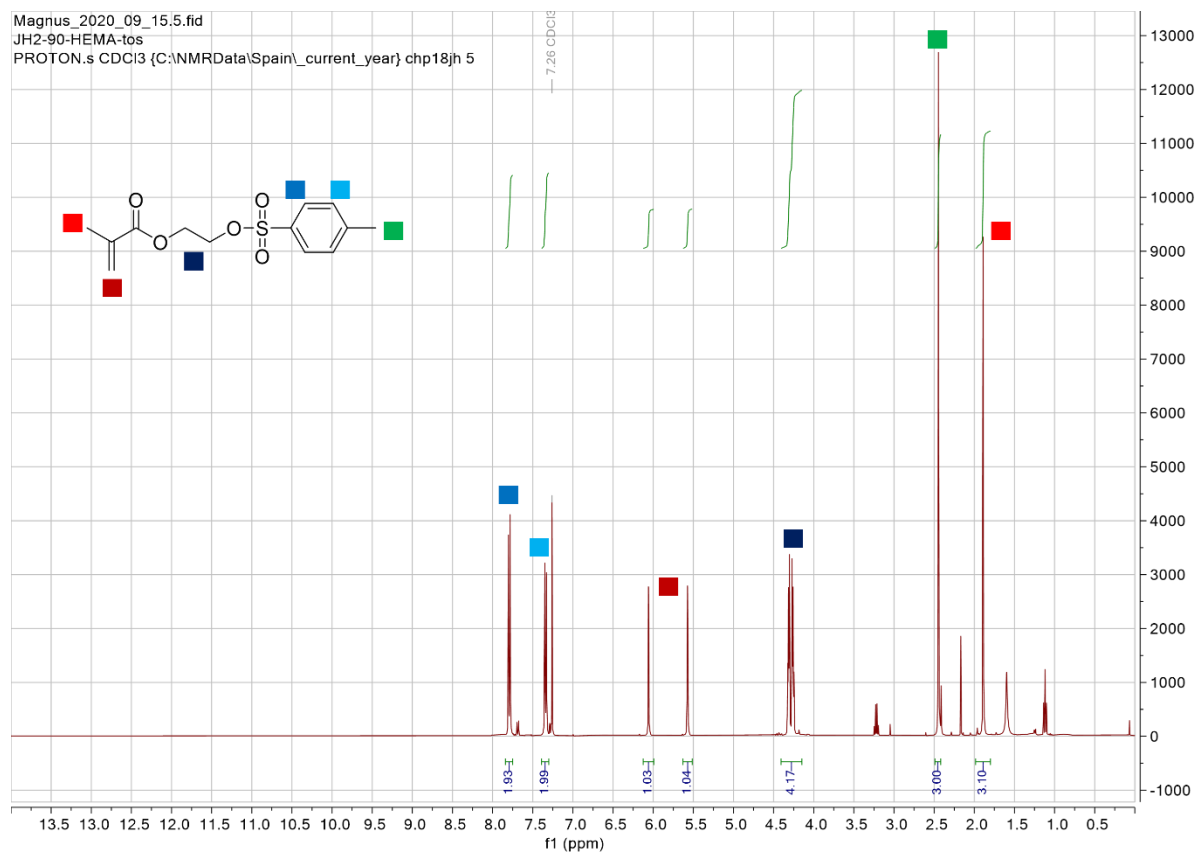


Figure 8-10 - IR spectrum of NHTN.



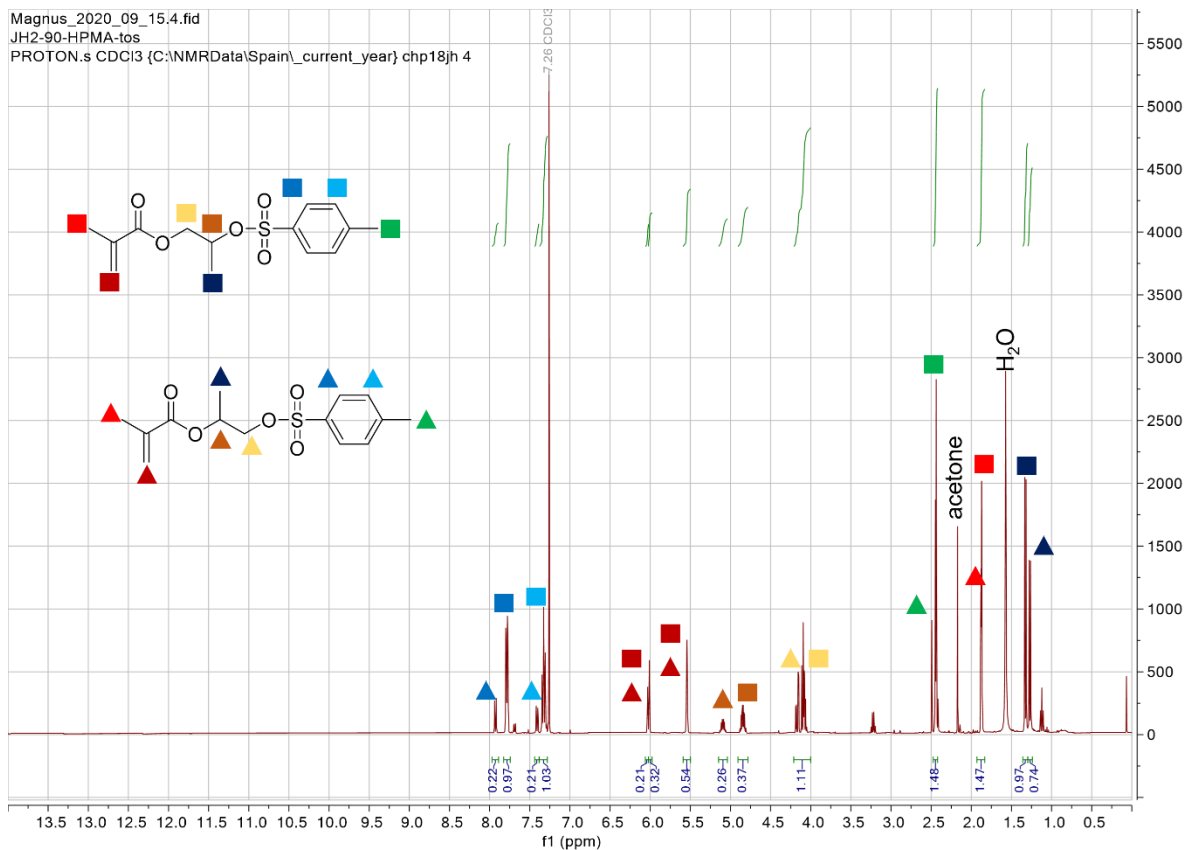


Figure 8-13 ¹H NMR (CDCl₃) spectrum of HPMAtos isomers.

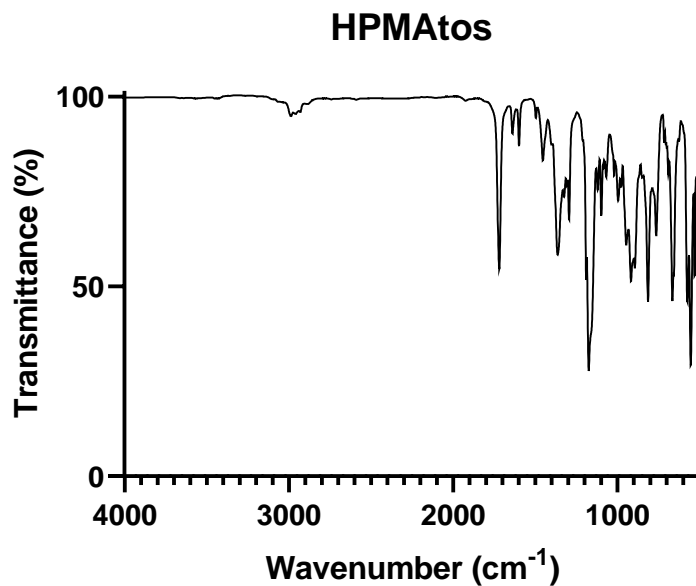


Figure 8-14 - IR spectrum of HPMAtos.

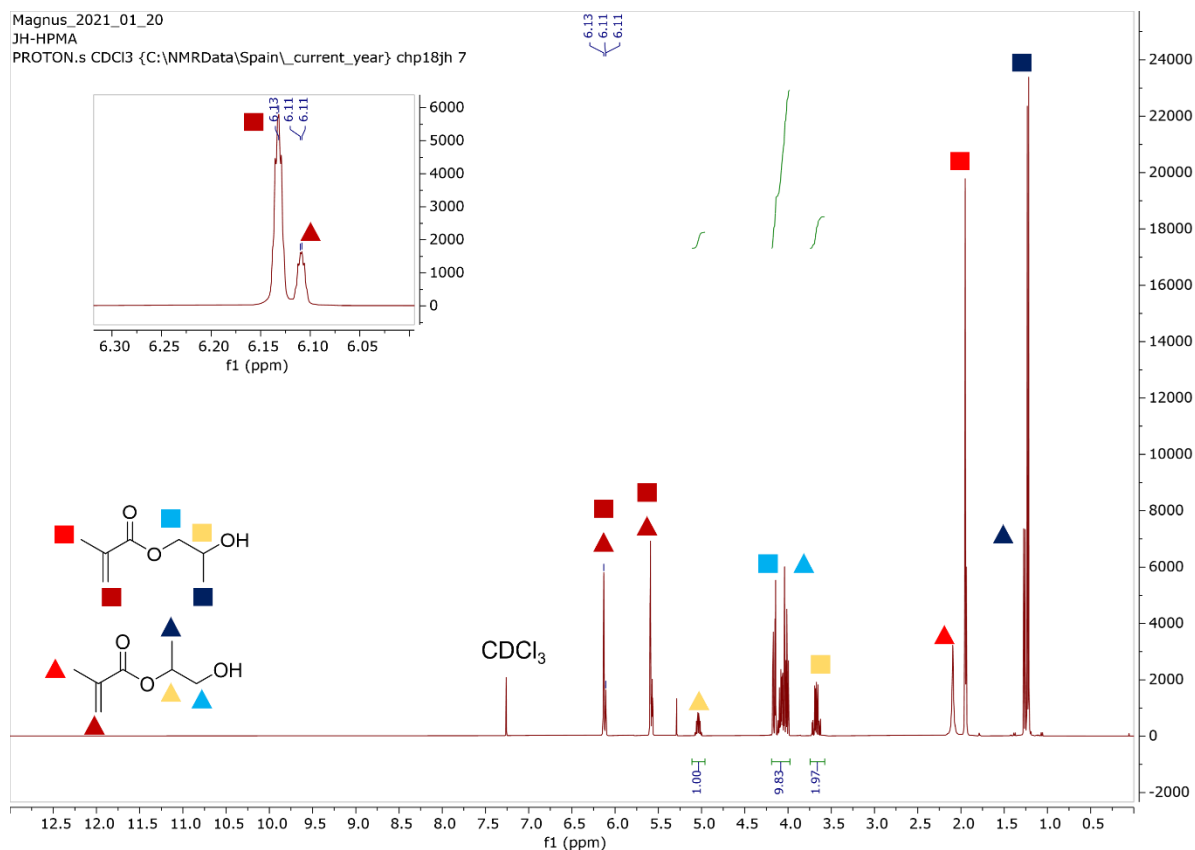


Figure 8-15 - ¹H NMR (CDCl₃) spectrum of HPMA, showing the vinyl peaks at 6.13 ppm and 6.11 ppm used to determine the ratio of the regioisomers.

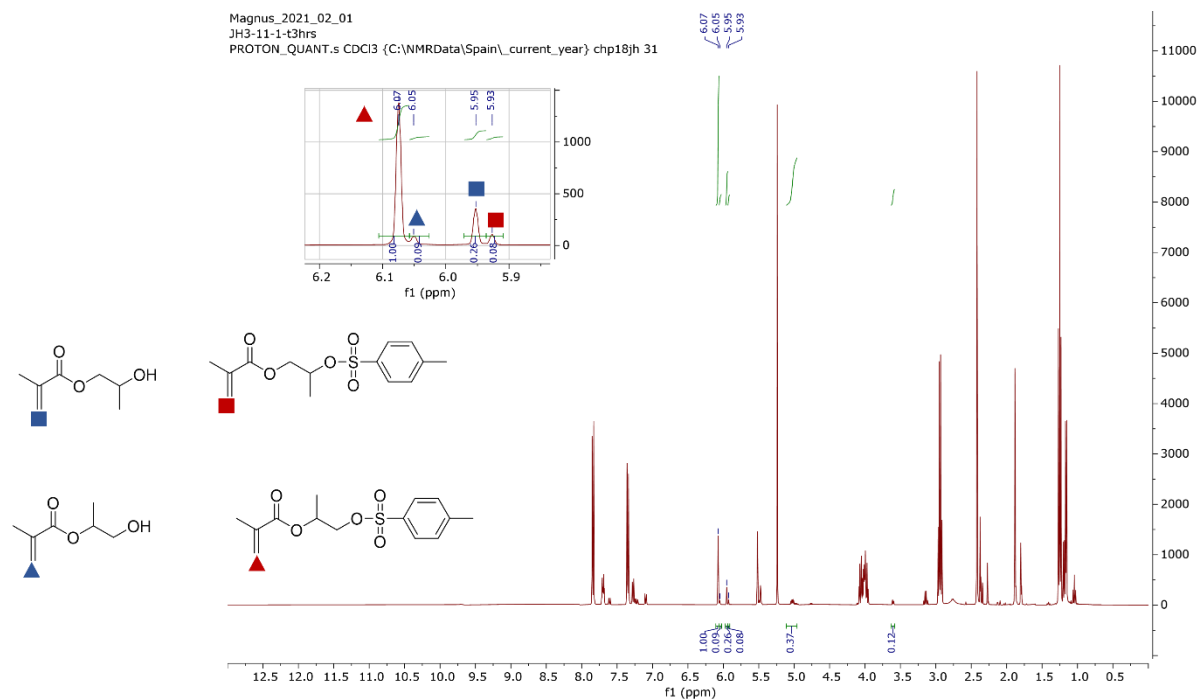


Figure 8-16 - ¹H NMR (CDCl₃) spectrum of HPMA tosylation reaction mixture after 3 hrs, using NEt₃ as the base and the following reagent ratios [OH]:[pTsCl]:[Base] – 1:1.5:1.5. Highlighted vinylic protons were used to monitor the conversion of different HPMA regioisomers.

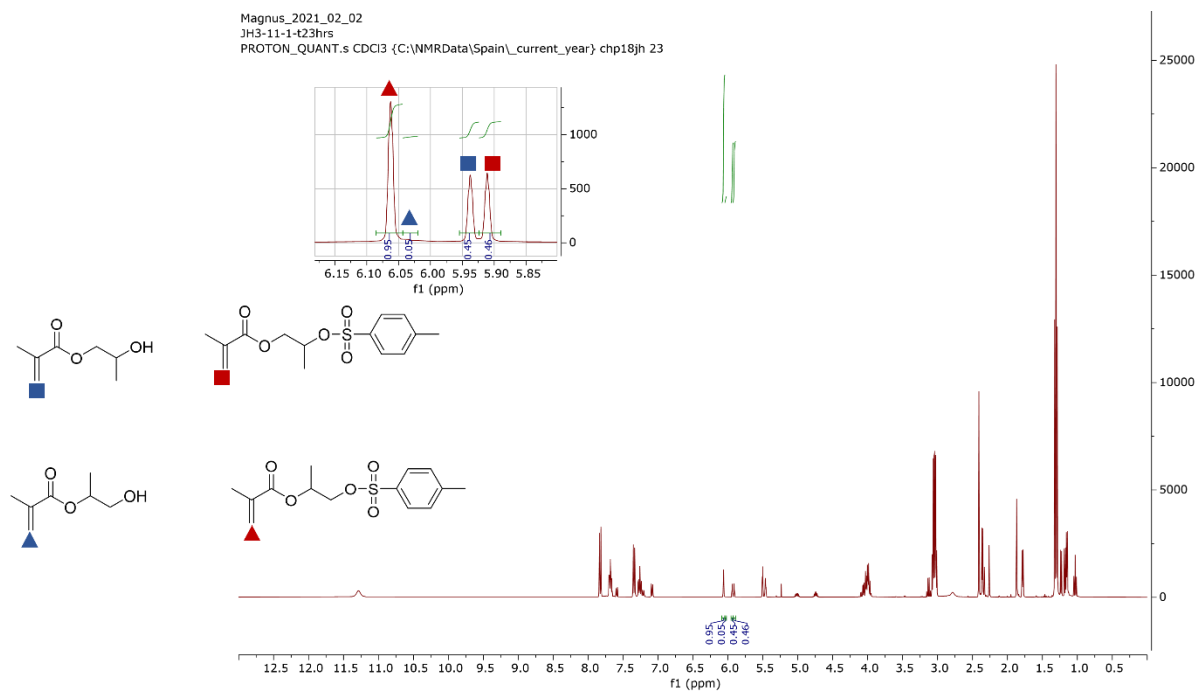


Figure 8-17 - ^1H NMR (CDCl_3) spectrum of HPMA tosylation reaction mixture after w3 hrs, using NEt_3 as the base and the following reagent ratios $[\text{OH}]:[\text{pTsCl}]:[\text{Base}] = 1:1.5:1.5$. Highlighted vinylic protons were used to monitor the conversion of different HPMA regioisomers.

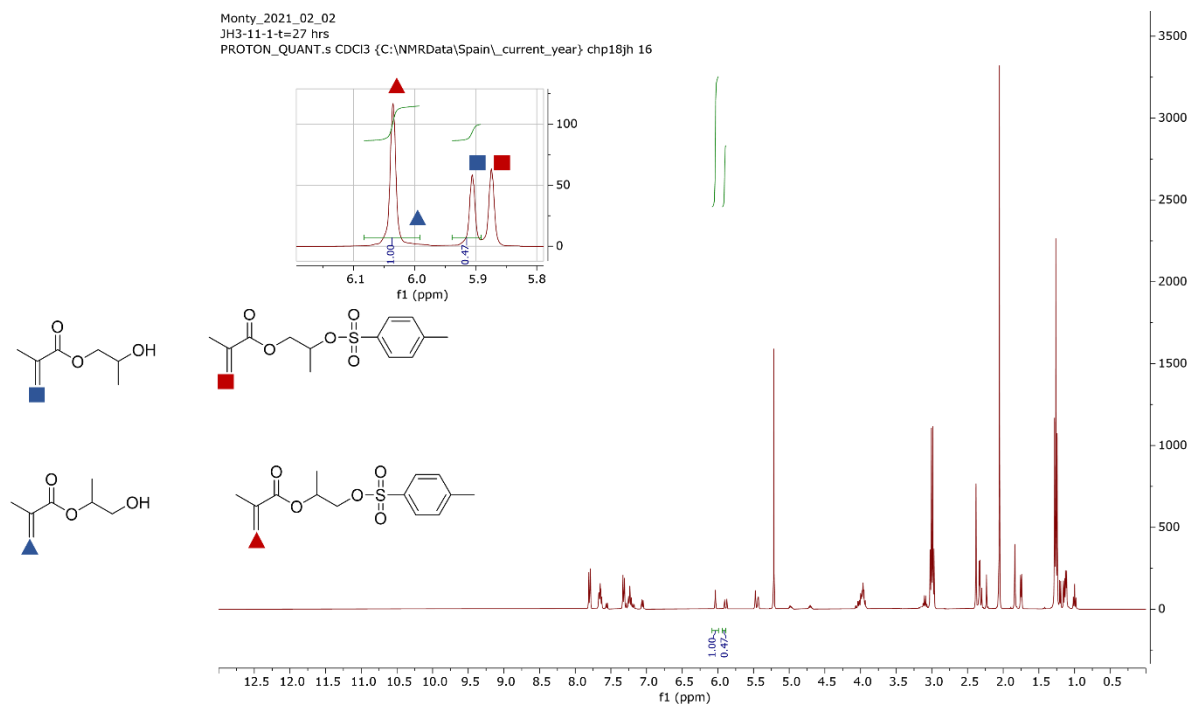


Figure 8-18 - ^1H NMR (CDCl_3) spectrum of HPMA tosylation reaction mixture after 27 hrs, using NEt_3 as the base and the following reagent ratios $[\text{OH}]:[\text{pTsCl}]:[\text{Base}] = 1:1.5:1.5$. Highlighted vinylic protons were used to monitor the conversion of different HPMA regioisomers.

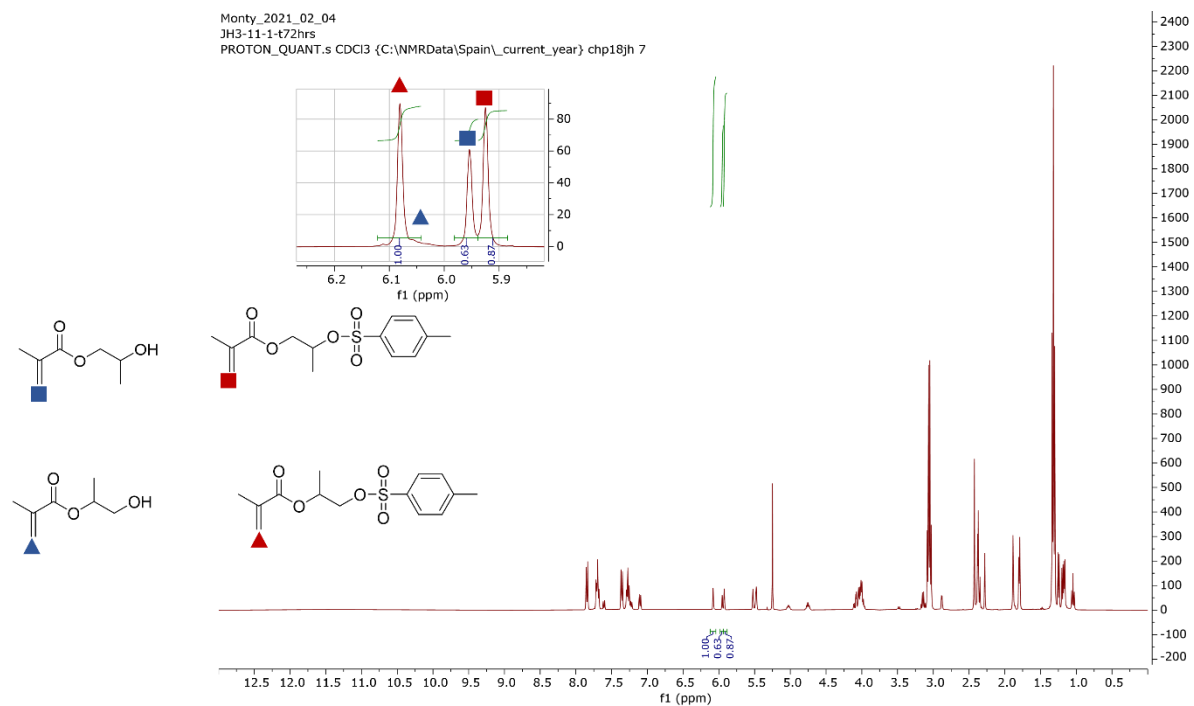


Figure 8-19 - ¹H NMR (CDCl₃) spectrum of HPMA tosylation reaction mixture after 72 hrs, using NEt₃ as the base and the following reagent ratios [OH]:[pTsCl]:[Base] – 1:1.5:1.5. Highlighted vinylic protons were used to monitor the conversion of different HPMA regioisomers.

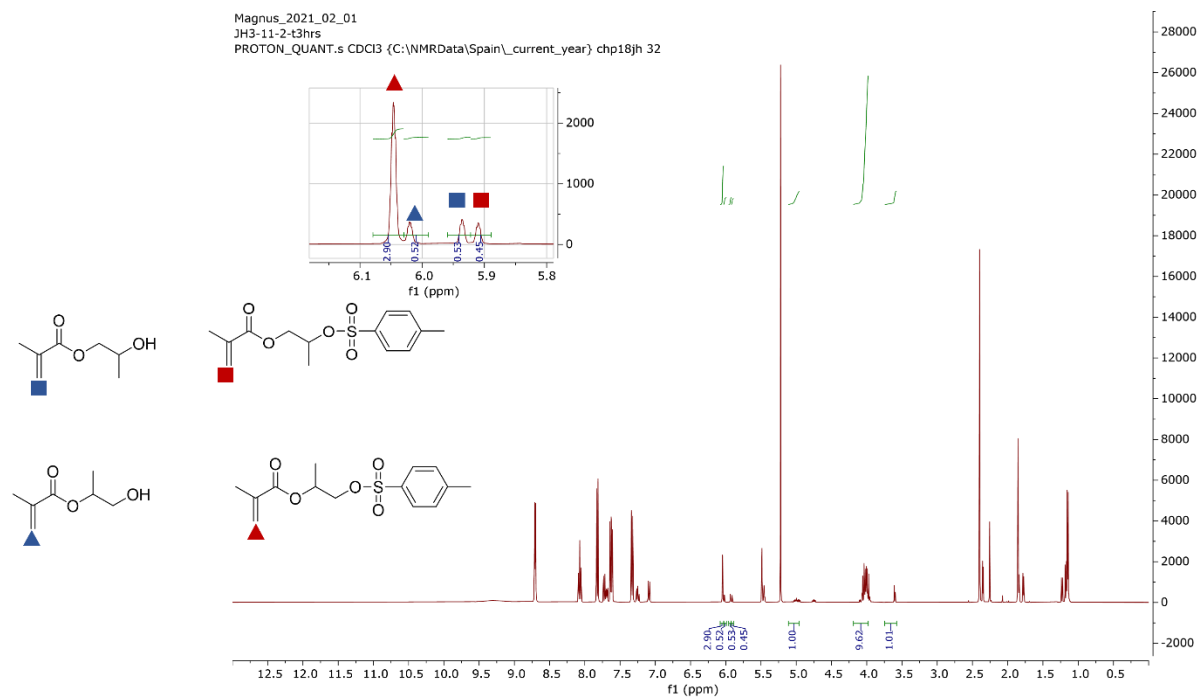


Figure 8-20 - ¹H NMR (CDCl₃) spectrum of HPMA tosylation reaction mixture after 3 hrs, using pyridine as the base and the following reagent ratios [OH]:[pTsCl]:[Base] – 1:1.5:1.5. Highlighted vinylic protons were used to monitor the conversion of different HPMA regioisomers.

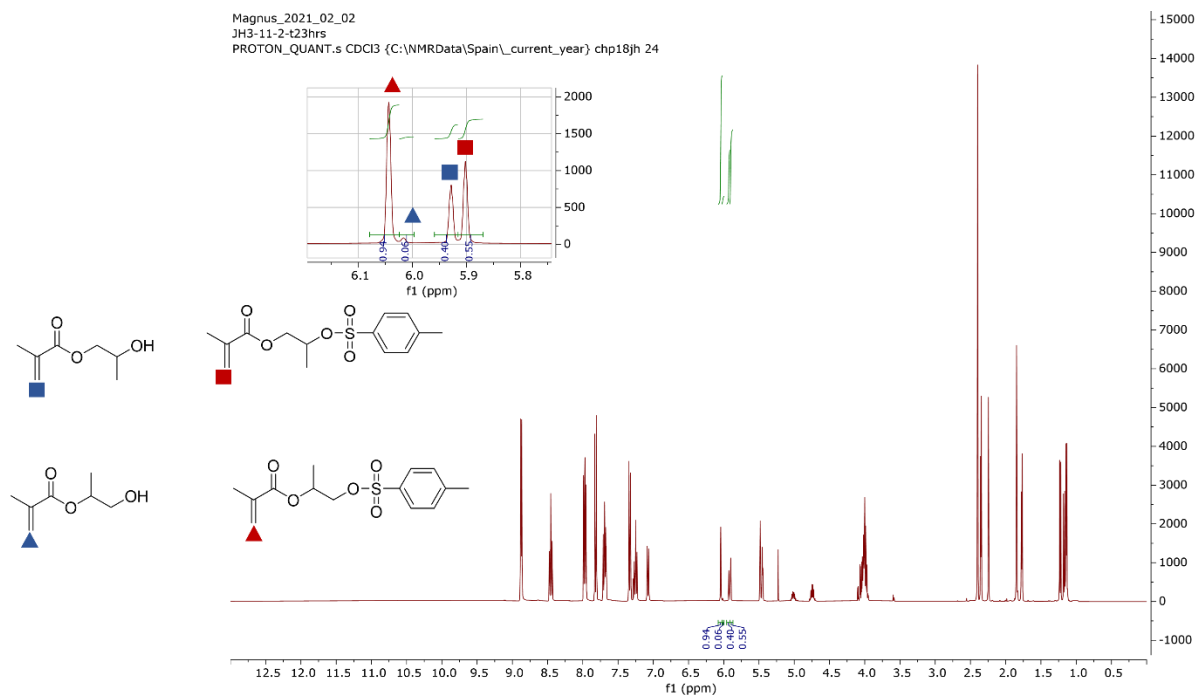


Figure 8-21 - ¹H NMR (CDCl₃) spectrum of HPMA tosylation reaction mixture after 23 hrs, using pyridine as the base and the following reagent ratios [OH]:[pTsCl]:[Base] – 1:1.5:1.5. Highlighted vinylic protons were used to monitor the conversion of different HPMA regioisomers.

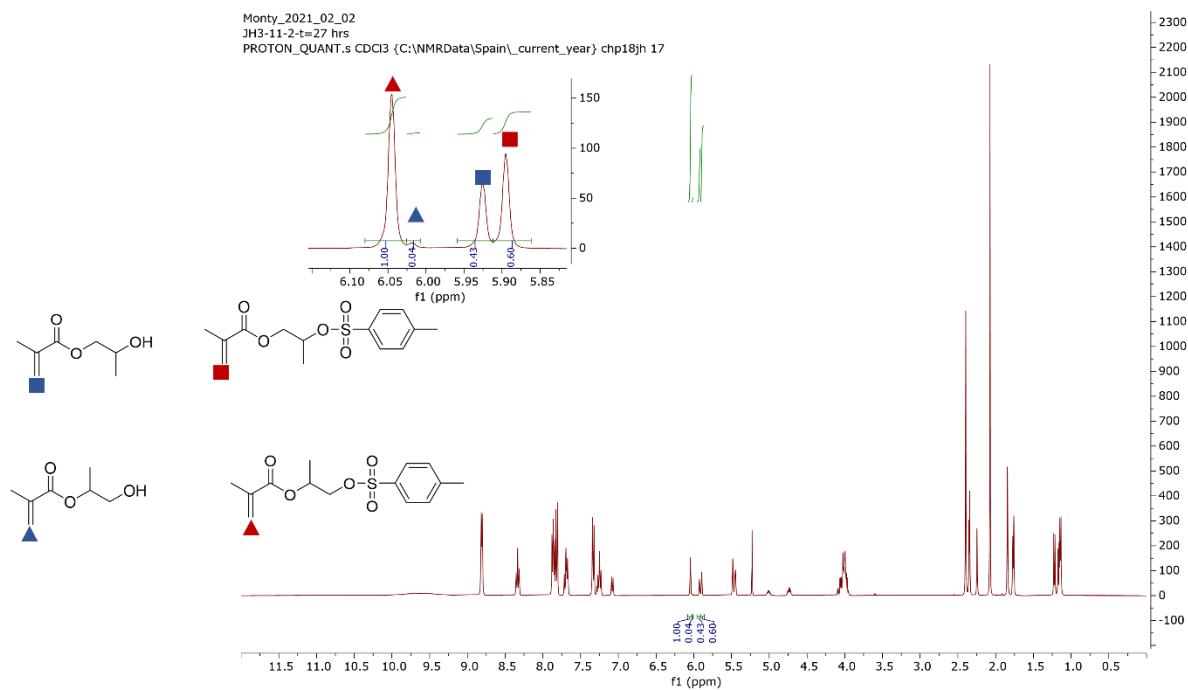


Figure 8-22 - ¹H NMR (CDCl₃) spectrum of HPMA tosylation reaction mixture after 27 hrs, using pyridine as the base and the following reagent ratios [OH]:[pTsCl]:[Base] – 1:1.5:1.5. Highlighted vinylic protons were used to monitor the conversion of different HPMA regioisomers.

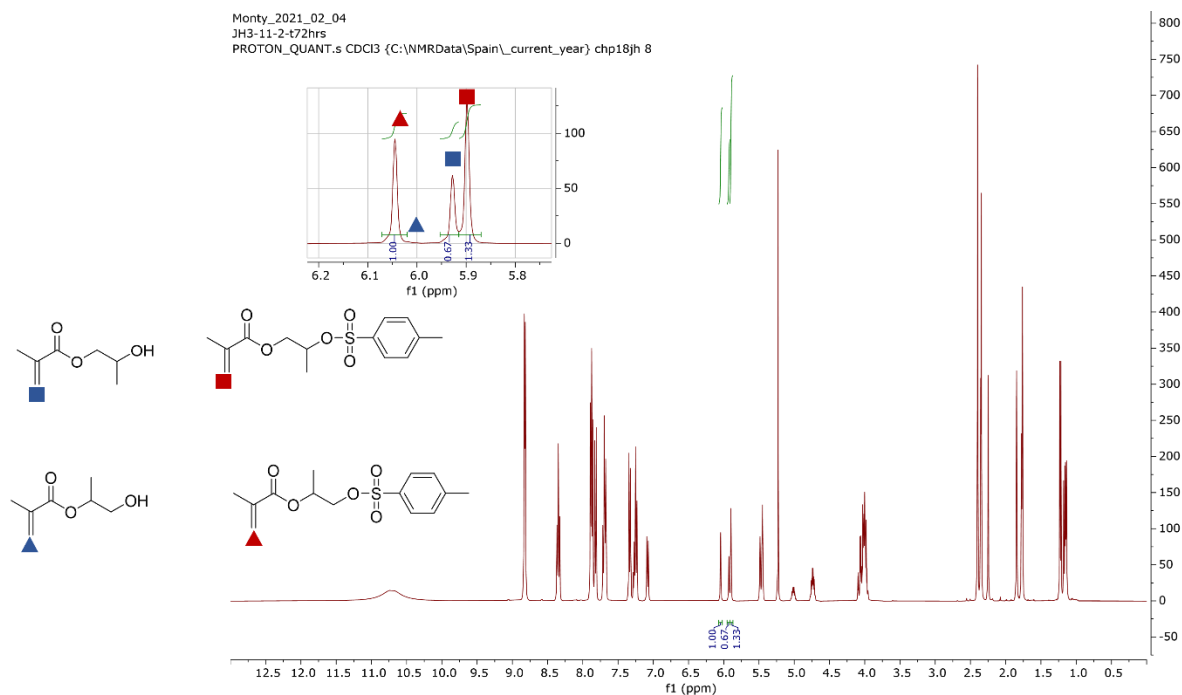


Figure 8-23 - ¹H NMR (CDCl₃) spectrum of HPMA tosylation reaction mixture after 72 hrs, using pyridine as the base and the following reagent ratios [OH]:[pTsCl]:[Base] – 1:1.5:1.5. Highlighted vinylic protons were used to monitor the conversion of different HPMA regioisomers.

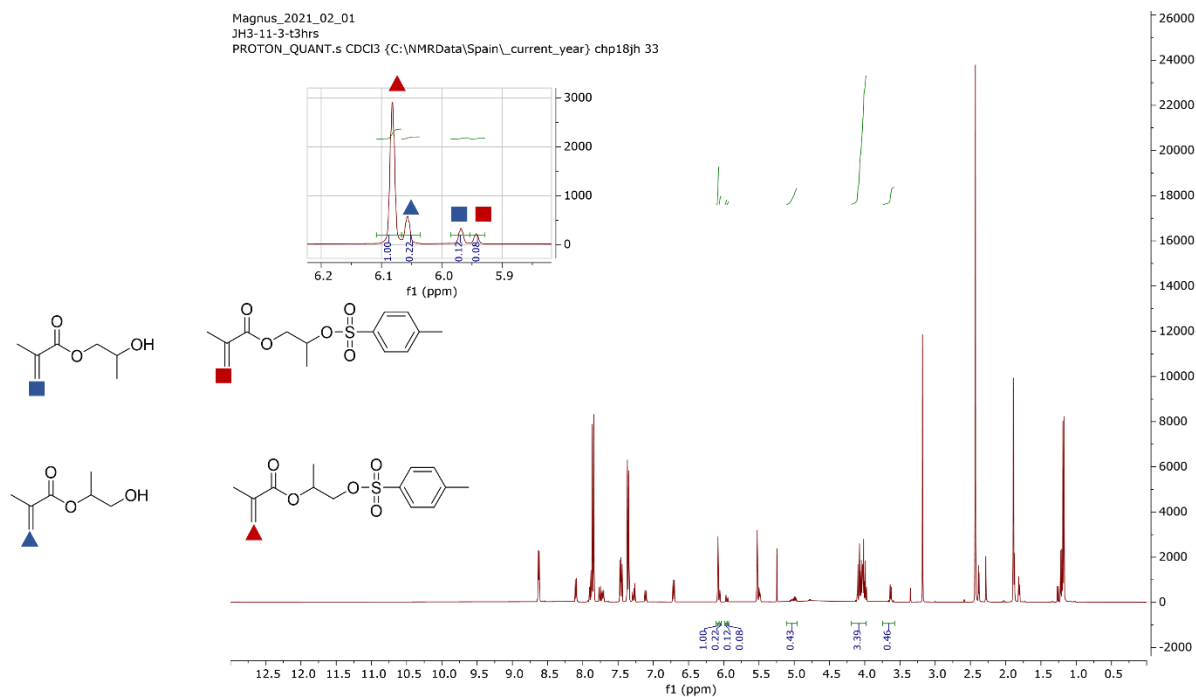
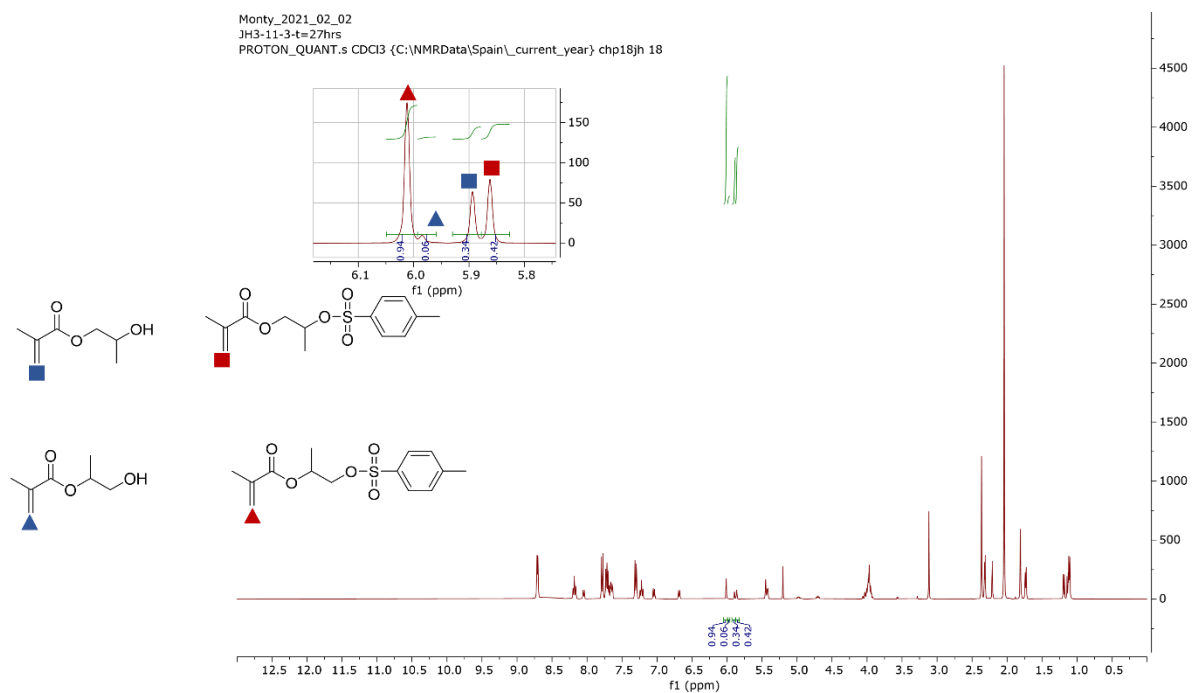
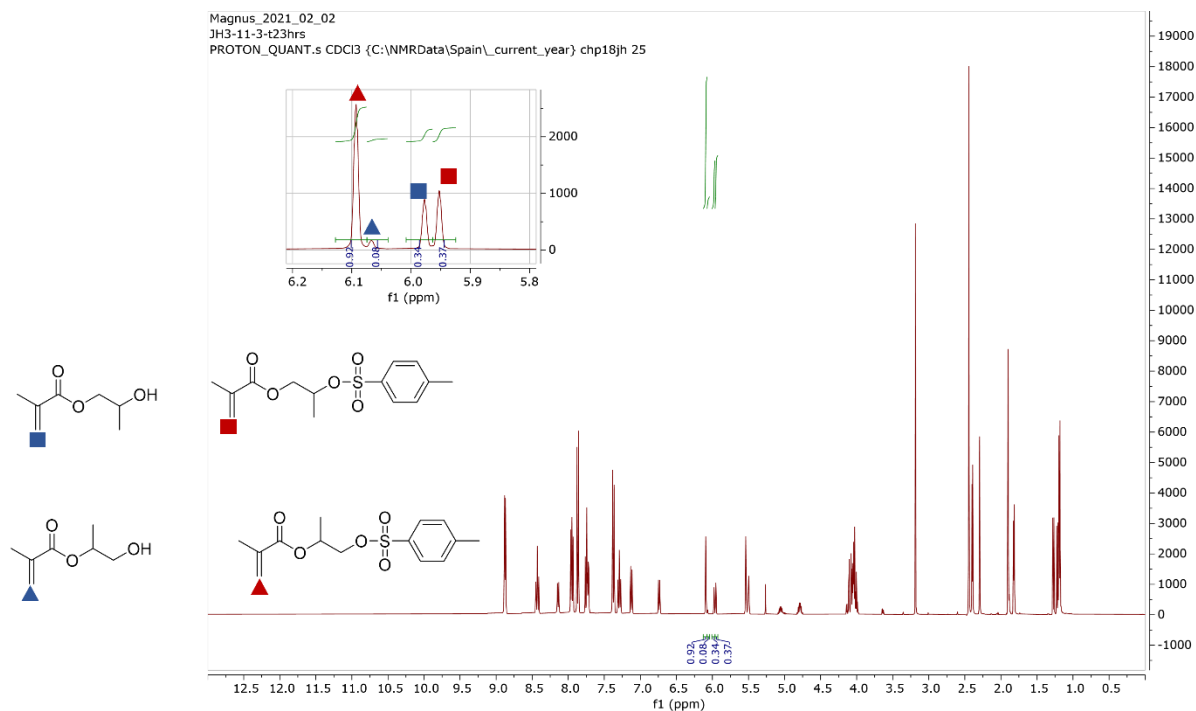


Figure 8-24 - ¹H NMR (CDCl₃) spectrum of HPMA tosylation reaction mixture after 3 hrs, using pyridine as the base with DMAP as a catalyst, and the following reagent ratios [OH]:[pTsCl]:[Base] – 1:1.5:1.5. Highlighted vinylic protons were used to monitor the conversion of different HPMA regioisomers.



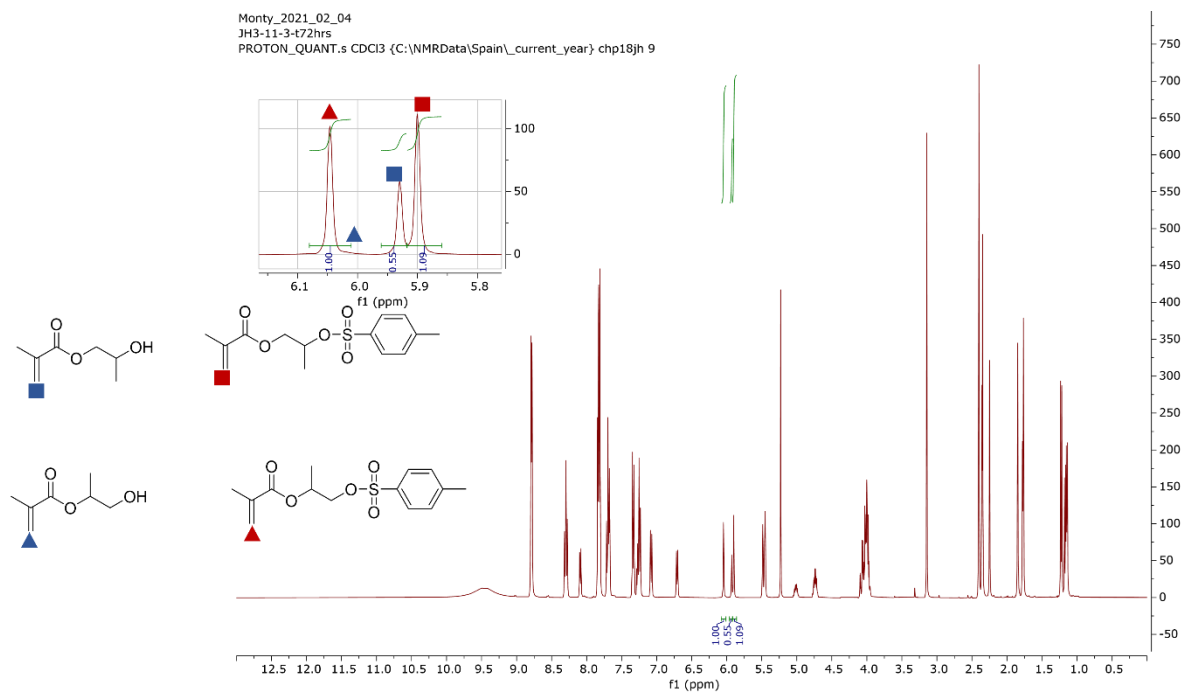


Figure 8-27 - ¹H NMR (CDCl₃) spectrum of HPMA tosylation reaction mixture after 72 hrs, using pyridine as the base with DMAP as a catalyst, and the following reagent ratios [OH]:[pTsCl]:[Base] – 1:1.5:1.5. Highlighted vinylic protons were used to monitor the conversion of different HPMA regioisomers.

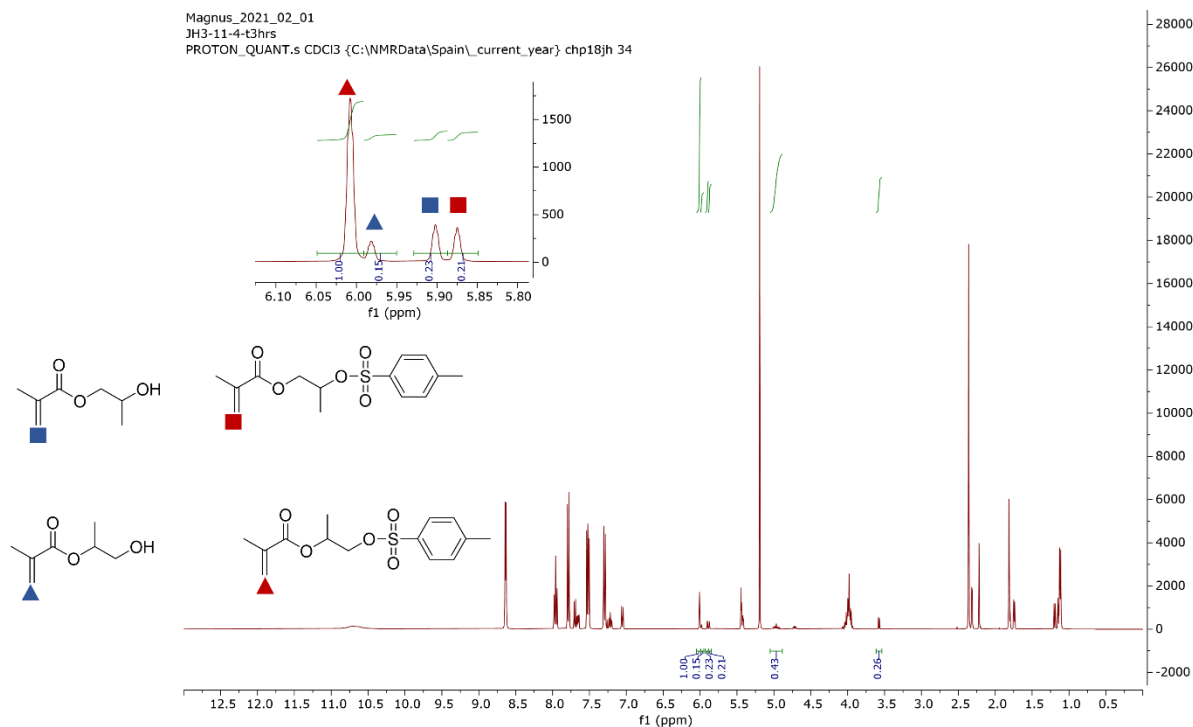


Figure 8-28 - ¹H NMR (CDCl₃) spectrum of HPMA tosylation reaction mixture after 3 hrs, using pyridine as the base and the following reagent ratios [OH]:[pTsCl]:[Base] – 1:2:3. Highlighted vinylic protons were used to monitor the conversion of different HPMA regioisomers.

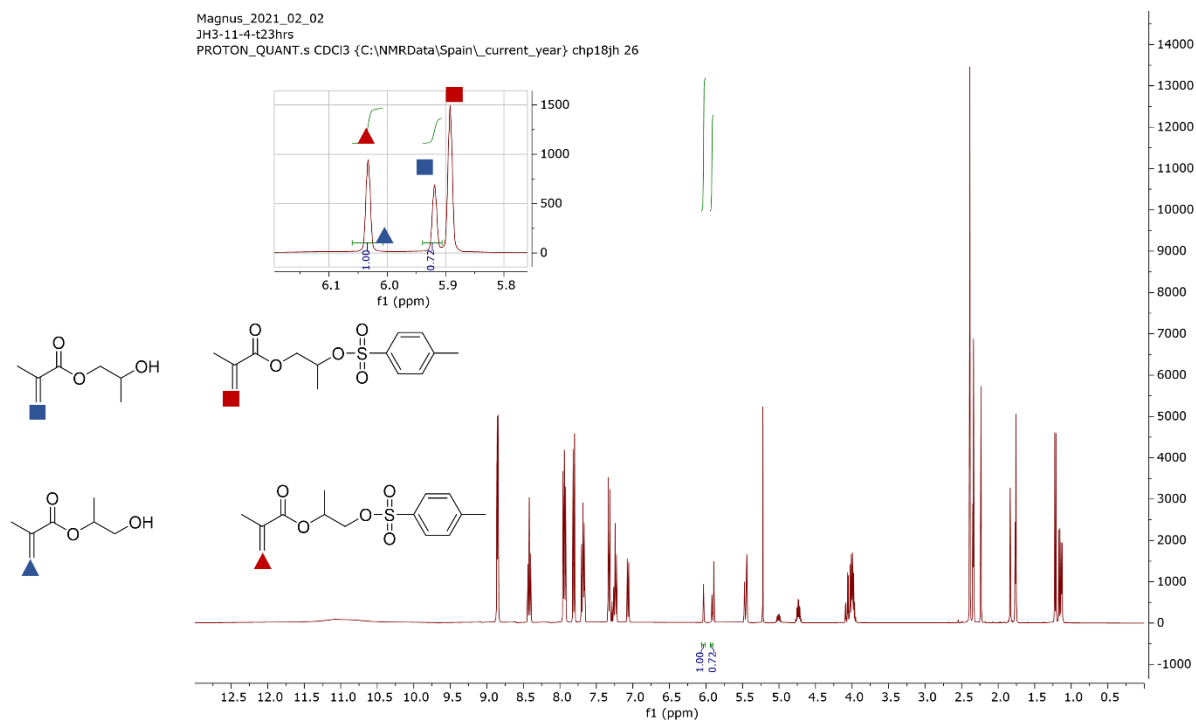


Figure 8-29 - ^1H NMR (CDCl_3) spectrum of HPMA tosylation reaction mixture after 23 hrs, using pyridine as the base and the following reagent ratios $[\text{OH}]:[\text{pTsCl}]:[\text{Base}] - 1:2:3$. Highlighted vinylic protons were used to monitor the conversion of different regioisomers.

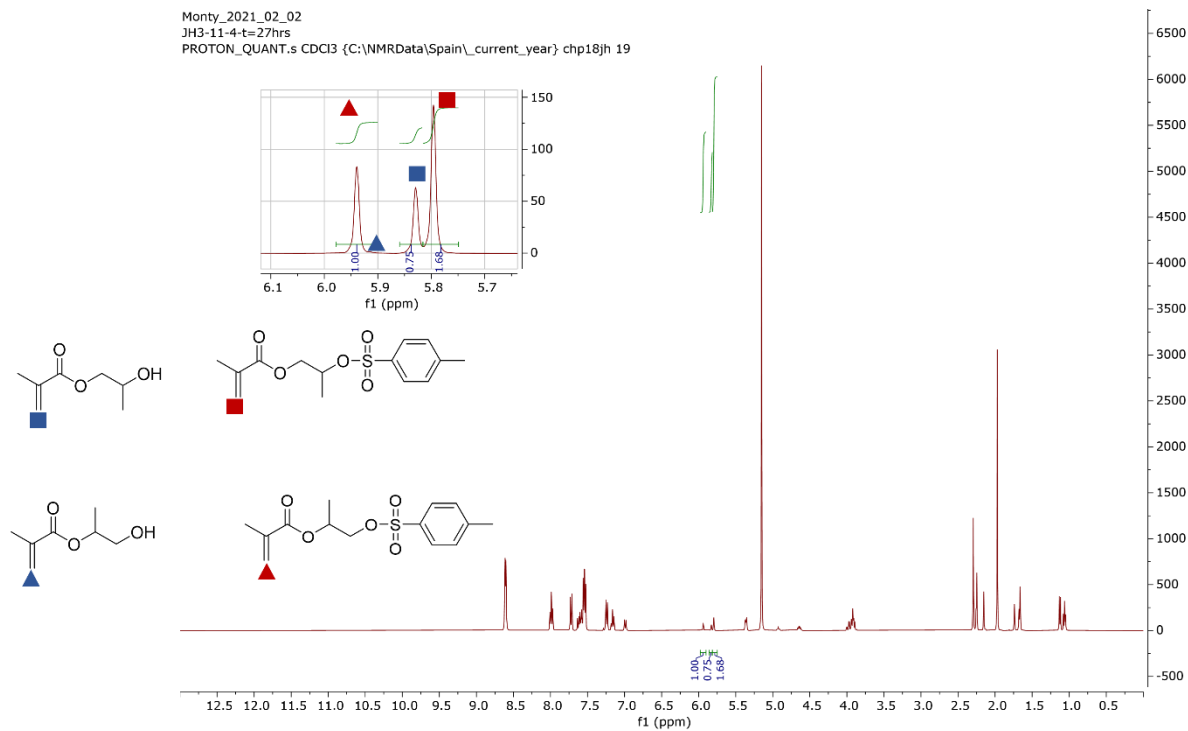


Figure 8-30 - ^1H NMR (CDCl_3) spectrum of HPMA tosylation reaction mixture after 27 hrs, using pyridine as the base and the following reagent ratios $[\text{OH}]:[\text{pTsCl}]:[\text{Base}] - 1:2:3$. Highlighted vinylic protons were used to monitor the conversion of different regioisomers.

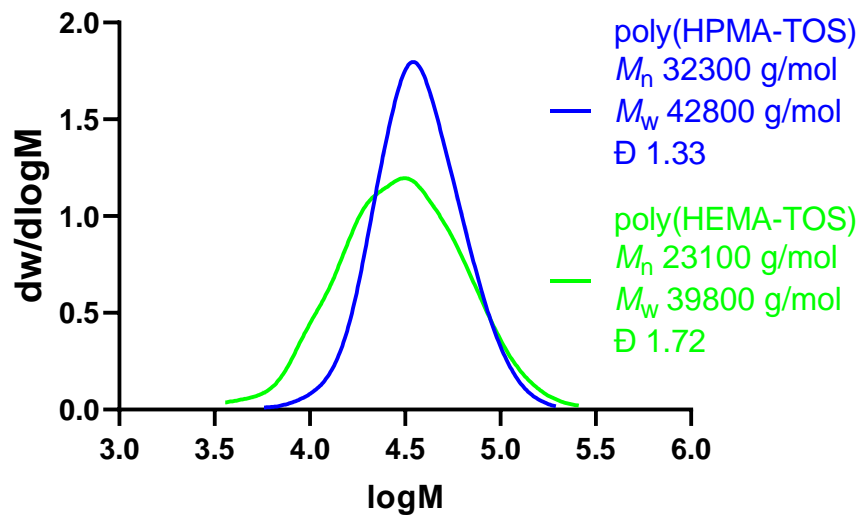


Figure 8-31 - SEC chromatograms for p(HPMA-tos) and p(HEMA-tos)

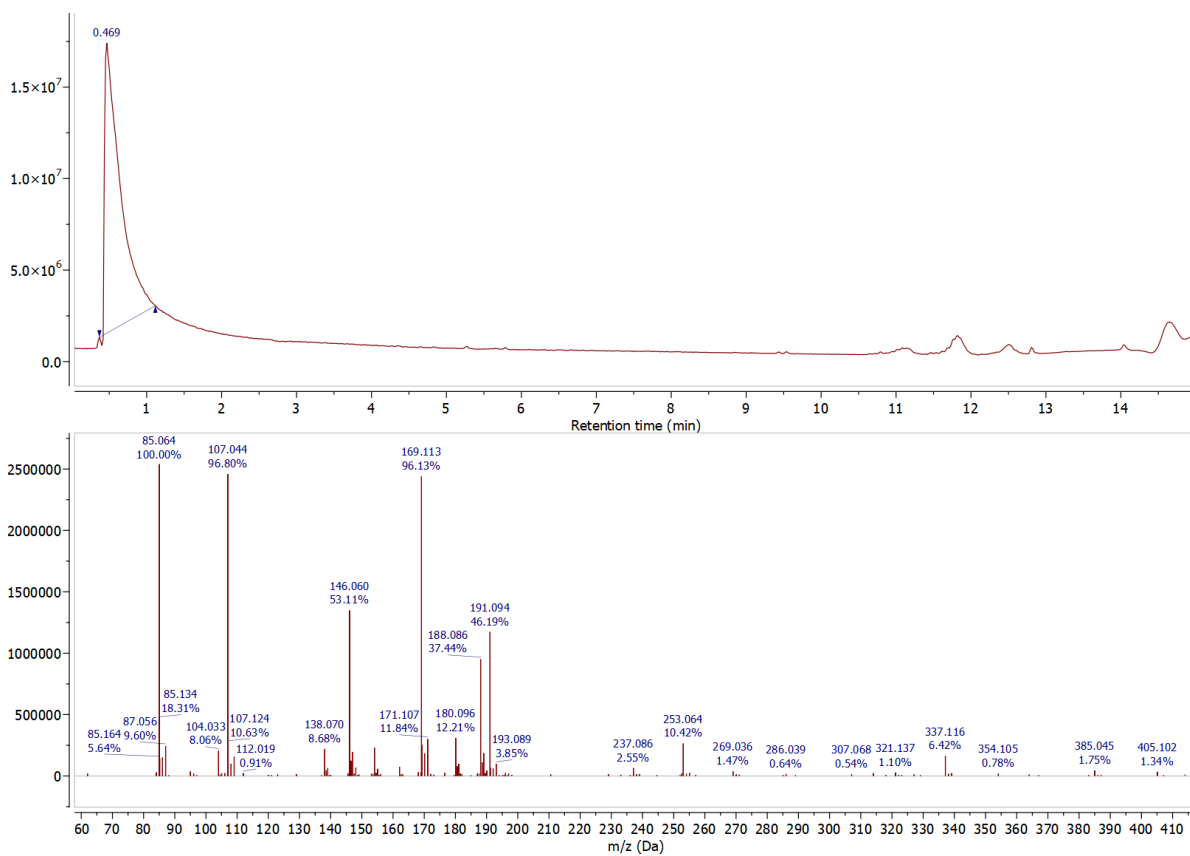


Figure 8-32 - p(HEMATos) DSC pan extract HPLC-MS chromatogram and spectrum.

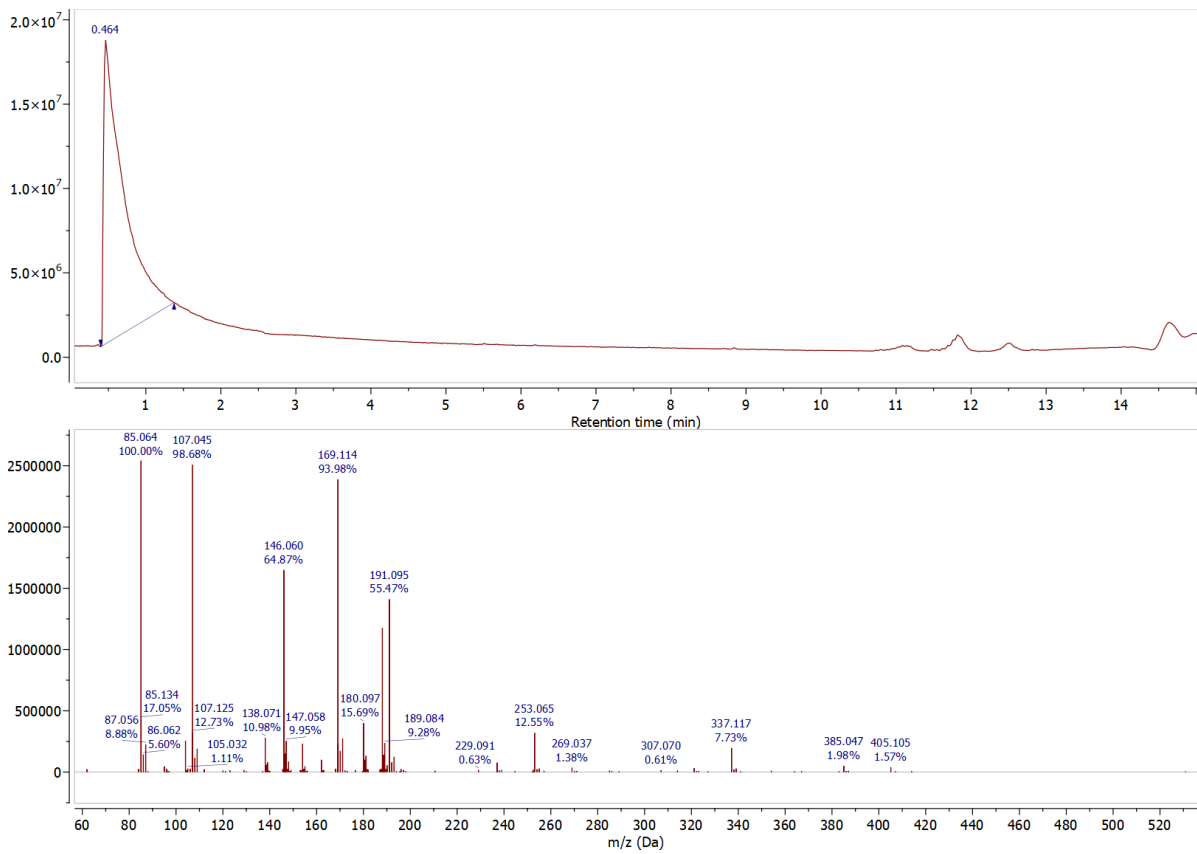


Figure 8-33 - p(HPMAtos) DSC pan extract HPLC-MS chromatogram and spectrum.

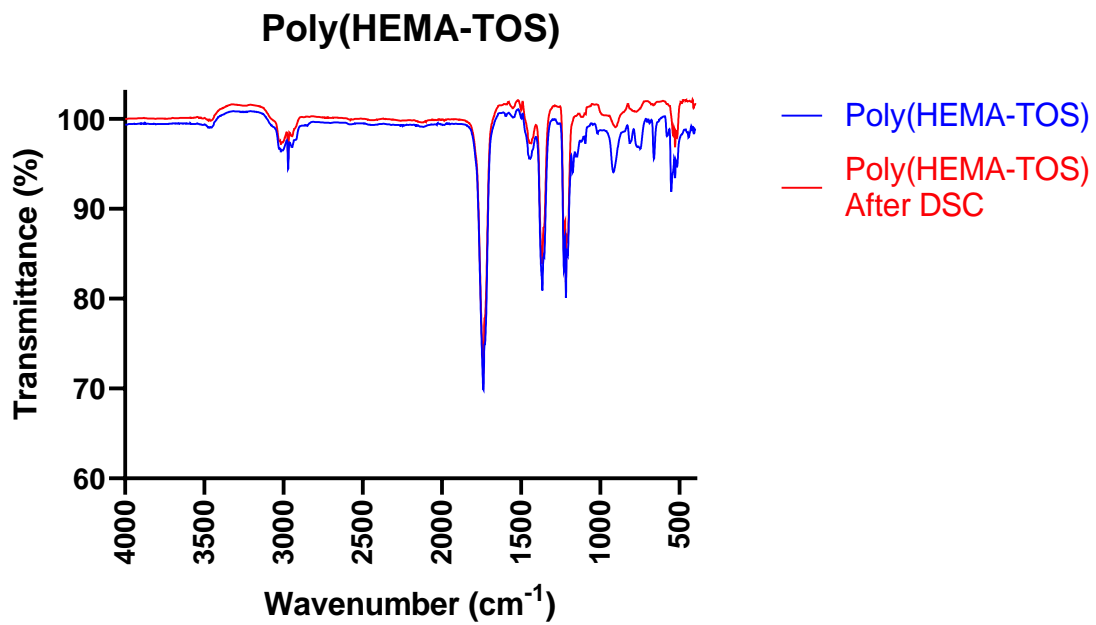


Figure 8-34 - IR spectra of p(HEMAtos) before and after heating.

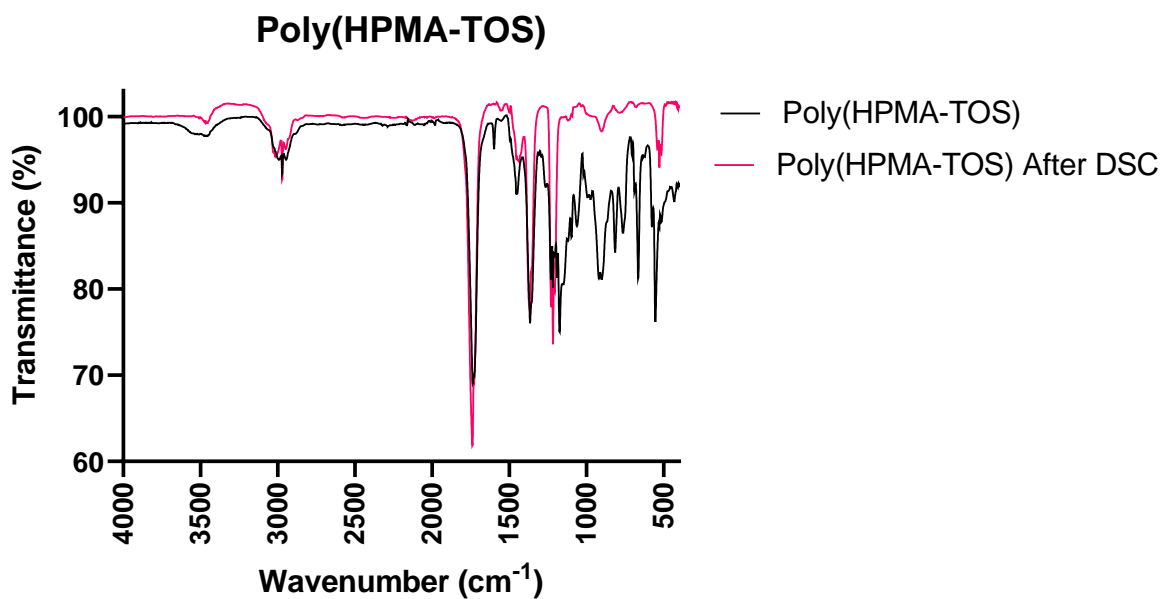


Figure 8-35 - IR spectra of p(HPMAtos) before and after heating.

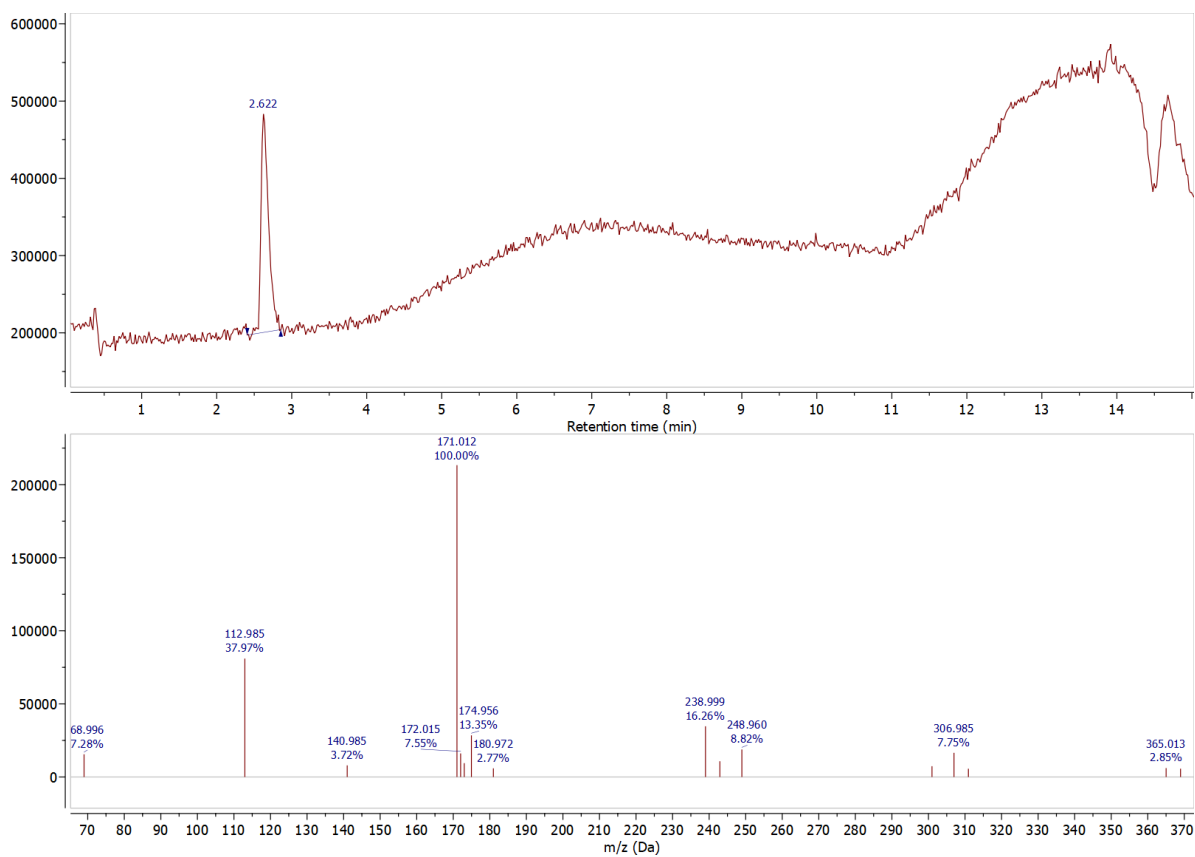


Figure 8-36 - HPLC chromatogram (top) and mass spectrum of 10 wt % HPMAtos/A1/MMA network extract before heating.

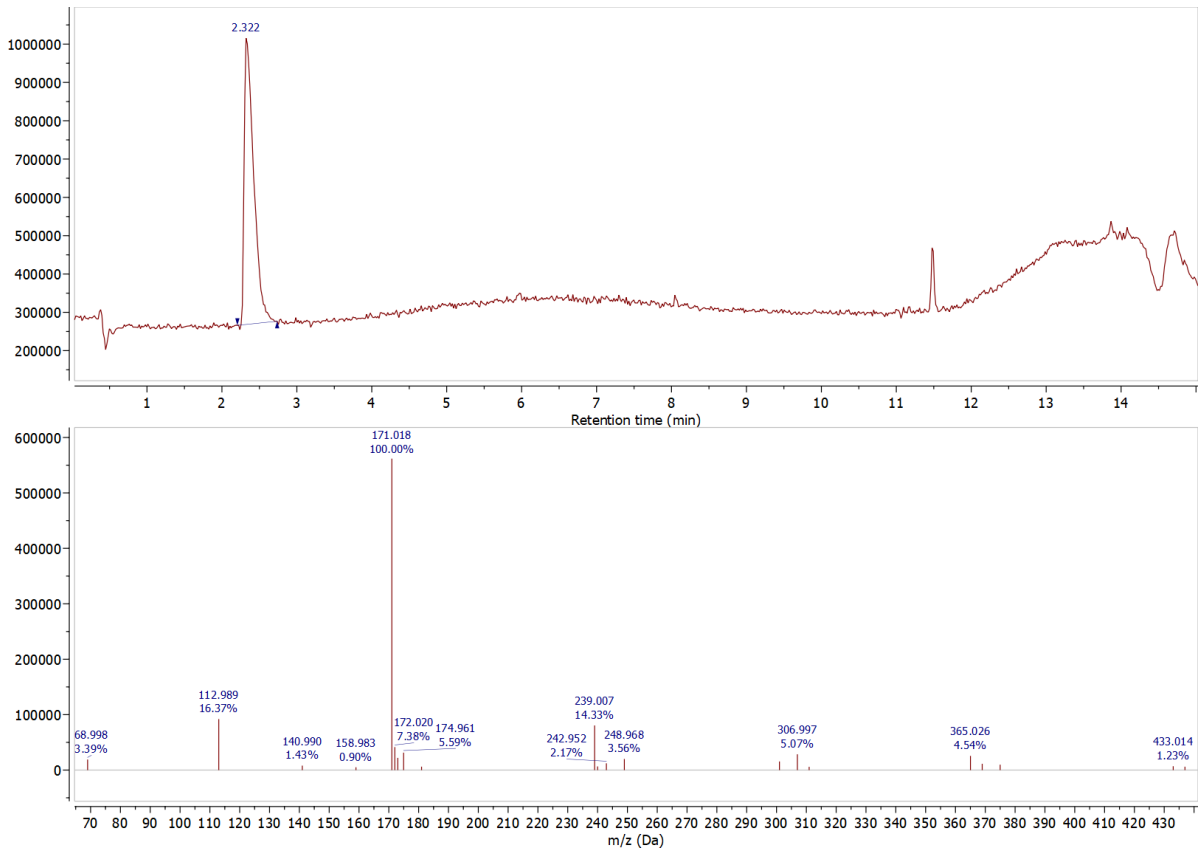


Figure 8-37 - HPLC chromatogram (top) and mass spectrum of 10 wt % HPMAtos/A1/MMA network extract before heating.

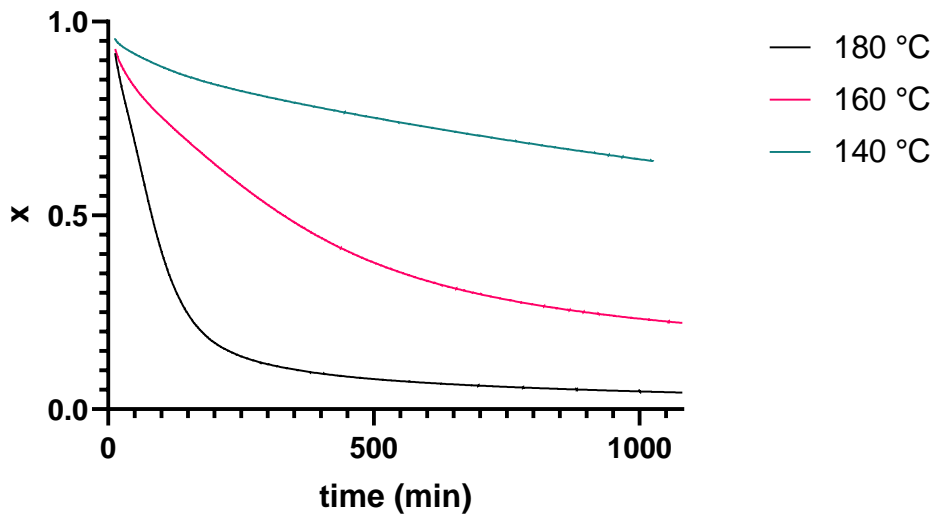


Figure 8-38 - First order kinetic plot of p(HPMAtos) isothermal TGA.

